Mitophagy and the dynamics of mitochondrial DNA inheritance in early development and reproduction

Jordan Marley

BSc, MRes

This thesis is submitted for the degree of doctor of philosophy at Newcastle University

Wellcome Centre for Mitochondrial Research

School of Biosciences

11th May 2021

Author's Declaration

This thesis is submitted for the degree of Doctor of Philosophy at Newcastle University. The research was conducted in the Wellcome Trust Centre for Mitochondrial Research, Institute of Neuroscience, Newcastle University under the supervision of Prof. Mary Herbert, Dr. Gavin Hudson and Dr. Angela Pyle, and is my own work unless stated otherwise.

I certify that none of the material presented here in this thesis has previously been submitted by me for a degree or qualification at this or any other university.

Acknowledgements

Abstract

Inherited heteroplasmic mitochondrial DNA (mtDNA) mutations are a cause of severe disease of adults and children. Thus, methods have been developed to reduce inheritance of pathogenic mtDNA variants; preimplantation genetic diagnosis (PGD) and pronuclear transfer (PNT). However, it is unclear at which stage of development a biopsy better predicts embryo heteroplasmy in PGD. Meanwhile, a small amount of pathogenic variant-harbouring mtDNA is carried over during PNT.

Recent work indicates that embryos undergo mitophagy during late preimplantion development. This coincides with a reported increase in intercellular variation of mtDNA heteroplasmy, raising the question of whether mitophagy contributes to segregation of mtDNA. In addition, manipulation of mitophagy may be applied to reduce carry-over of mtDNA variants during PNT.

To investigate the mechanisms of mitophagy, using a large single cell RNA sequencing data from human embryos, I analysed the expression of key mitophagy genes. *BNIP3* family genes were identified as probable mediators of mitophagy. Overexpression of a phosphomimetic *BNIP3L* protein upregulated mitophagy, which may be useful in preventing survival of carried over mtDNA in PNT. Furthermore, correlations emerged between mitophagy genes and genes driving the establishment of cell lineages in the blastocyst, suggesting lineage-specific regulation of mitophagy.

Using the *tRNAalanine* (*tRNAala*) mouse model carrying a pathogenic mtDNA variant, I verified an increase in intercellular variation of heteroplasmy in the blastocyst. Analysis of the segregation of mtDNA suggested that the 8-cell embryo is the optimal stage for PGD biopsy. Upregulation of mitophagy had no detectable influence on the segregation of mtDNA, suggesting that mitophagy may not be a major source of intercellular variation in heteroplasmy.

I also revealed an accumulation of mtDNA variants in the oocytes of aged *tRNAala* mice. Combined with the presence of a pathogenic mutation, mtDNA variants did not manifest a selection mechanism. This suggests acquired mtDNA variants only modestly impair the health of aged oocytes and age-related loss of fertility is primarily due to other causes.

These findings elucidate mechanisms which may modulate the inheritance of mtDNA in early development. Furthermore, they provide insight into the impact of mitophagy in the preimplantation embryo, and identify an 8-cell embryo biopsy as preferable to that of a

blastocyst in predicting embryo heteroplasmy during PGD. Identification of a method to upregulate mitophagy will help guide the process of preventing the inheritance of mtDNA mutations using PNT.

Contents

Figures

Tables

Abbreviations

6GPL	6-phosphogluconolactonase
6P	Glucose-6-phosphate
6PG	Glucose-6-phosphate isomerase
6PGD	6-Phosphogluconate dehydrogenase
6PGN	6-phosphogluconolactone
ADP	Adenosine 5'-diphosphate
AGM1	Phosphoacetylglucosamine mutase
AGX1	*Alanine*:glyoxylate transaminase 1
AMPK	5' AMP-activated protein kinase
ANCOVA	Analysis of covariance
ANOVA	Analysis of variance
APAF1	Apoptotic protease activating factor 1
ATG	Autophagy-related genes
ATP	Adenosine 5'-triphosphate
ATP6	ATP synthase membrane subunit 6
ATP8	ATP synthase membrane subunit 8
BAD	BCL2 associated agonist of cell death
BAG1	BAG family molecular chaperone regulator 1
BAK1	BCL2 antagonist/killer 1
BAX	BCL2 associated X
BBC3	BCL2 binding component 3
BCL	B-cell lymphoma
BCL2	B-cell lymphoma 2
BCL2A1	BCL2 related protein A1
BCL2L1	BCL2 like 1
BCL2L2	BCL2 like 2
BH3	Bcl-2 homology 3
BID	BH3 interacting domain death agonist
BMP4	Bone morphogenetic protein 4
BNIP3	BCL2 interacting protein 3
BNIP3L	BCL2 interacting protein 3 like
BOK	BCL2 family apoptosis regulator BOK
CA^{2+}	Calcium ion
CASP	Caspase
CCDC2	Calcium-binding and coiled-coil domain-containing protein 2
CDX2	Caudal type homeobox 2
CITED2	Cbp/P300 interacting transactivator with glu/asp rich carboxy-terminal domain 2
CK2	Casein kinase II
COI	Cytochrome oxidase 1
CPM	Counts per million reads mapped
CYCS	Cytochrome c
DE	Differential expression
DIABLO	Diablo IAP-binding mitochondrial protein
DMSO	Dimethyl sulfoxide
DNA	Deoxyribonucleic acid
DNA2	DNA replication helicase/nuclease 2

DNM1L	Dynamin 1 like
DPC	Days post-coitum
EGA	Embryonic genome activation
ETC	Electron transport chain
F6P	Fructose 6-phosphate
FADD	Fas associated via death domain
FADH$_2$	Flavin adenine dinucleotide
FasLG	Fas ligand
FDR	False discovery rate
FGF4	Fibroblast growth factor 4
FGFR	Fibroblast growth factor receptor
FIS1	Fission, Mitochondrial 1
FOXO3	Forkhead Box O3
FUNDC1	FUN14 domain containing 1
G6P	Glucose-6-phosphate
G6PD	Glucose-6-phosphate dehydrogenase
GABARAP	GABA Type A Receptor-Associated Protein
GATA2	GATA Binding Protein 2
GATA3	GATA Binding Protein 3
GATA4	GATA Binding Protein 4
GATA6	GATA Binding Protein 6
GBK	N-Acetylglucosamine kinase
GFAT	Glutamine-fructose-6-phosphate transaminase 1
GLUT	Glucose transporter
GNPNAT	Glucosamine-phosphate N-acetyltransferase 1
GO	Gene ontology
GTP	Guanosine-5'-triphosphate
GV	Germinal Vesicle
H^2	Hydrogen
HBP	Hexose biosynthetic process
HFEA	Human Fertilisation and Embryology Authority
HIF1A	Hypoxia inducible factor 1 subunit alpha
HRK	Activator of apoptosis harakiri
ICM	Inner cell mass
IMM	Inner mitochondrial membrane
IVF	*In vitro* fetilisation
LC3	Microtubule-associated protein 1A/1B-light chain 3
LDH	Lactate dehydrogenase
LIR	LC3 binding region
MAPK	Mitogen-activated protein kinase
MARCHF5	Membrane associated ring-CH-type finger 5
MCL1	Induced myeloid leukemia cell differentiation protein
MFF	Mitochondrial fission factor
MFN1	Mitofusin-1
MFN2	Mitofusin-2
MGAT	Alpha-1,3-mannosyl-glycoprotein 2-neta-N-acetylglucosaminyltransferase
MGME1	Mitochondrial genome maintenance exonuclease 1
MOMP	Mitochondrial outer membrane permeabilization

NADH	Nicotinamide adenine dinucleotide
NADPH	Nicotinamide adenine dinucleotide phosphate
NANOG	Nanog homeobox
ND1/2/3/4/4L/5/6	NADH-ubiquinone oxidoreductase chain 1/2/3/4/4L/5/6
NFE2L2	Nuclear factor erythroid 2 like 2
NGS	Next generation sequencing
NRF1	Nuclear respiratory factor 21
NRF2	Nuclear respiratory factor 2
OGT	O-linked N-acetylglucosamine transferase
OMM	Outer mitochondrial membrane
OPA1	Mitochondrial dynamin-like GTPase
OPTN	Optineurin
OXPHOS	Oxidative phosphorylation
PCA	Principal component analysis
PCR	Polymerase chain reaction
PDH	Pyruvate dehydrogenase
PE	Primitive endoderm
PGAM	Phosphoglycerate mutase 1
PGAM5	PGAM family member 5, mitochondrial serine/threonine protein phosphatase
PGC	Primordial germ cell
PGD	Preimplantation genetic diagnosis
PGM3	Phosphoglucomutase 3
PIK3C3	Phosphatidylinositol 3-kinase catalytic subunit type 3
PINK1	PTEN induced kinase 1
PKM	Pyruvate kinase
PMAIP1	Phorbol-12-myristate-13-acetate-induced protein 1
PN	Pronuclei
PNT	Pronuclear teansfer
POLG	DNA polymerase gamma
POLRMT	RNA polymerase mitochondrial
POU5F1	POU class 5 homeobox 1
PPARGC1A	Peroxisome proliferator-activated receptor gamma coactivator 1-alpha
PPARGC1B	Peroxisome proliferator-activated receptor gamma coactivator 1-beta
PPP	Pentose-phosphate pathway
PPRC1	Peroxisome proliferator-activated receptor gamma coactivator-related protein 1
PRAME	PRAME nuclear receptor transcriptional regulator
PRKN	Parkin RBR E3 ubiquitin protein igase
PTEN	Phosphatase and tensin homolog
R5P	Ribose-5-phosphate
RAD51	RAD51 recombinase
RHEB	Ras homolog enriched in brain
RNA	Ribonucleic acid
ROS	Reactive oxygen species
RPE	Ribulose-5-phosphate-3-epimerase
RPIA	Ribose 5-phosphate isomerase A
SIRT1	NAD-dependent deacetylase sirtuin-1

SLC16A3	Solute carrier family 16 member 3
SOX2	SRY-Box transcription factor 2
SQSTM1	Sequestosome 1
SSBP1	Single stranded DNA binding protein 1
TALDO	Transaldolase 1
TBK1	TANK-binding kinase 1
TE	Trophectoderm
TEAD4	TEA domain transcription factor 4
TFAM	Transcription factor A, mitochondrial
TFAP2A	Transcription factor AP-2 alpha
TFAP2C	Transcription factor AP-2 gamma
TKT	Transketolase
TNFRSF10A	TNF superfamily member 10A
TNFRSF1A	TNF superfamily member 1A
TNFRSF25	TNF receptor superfamily member 25
TNFSF10	TNF superfamily member 10
TNFSF25	TNF superfamily member 25
TOP1MT	DNA topoisomerase I mitochondrial
TOP2B	Topoisomerase (DNA) II beta
TP53	Tumor protein p53
TRADD	TNFRSF1A associated via death domain
tRNA	Transfer ribonucleic acid
tRNAala	Transfer ribonucleic acid *alanine*
t-SNE	t-distributed Stochastic Neighbor Embedding
TUNEL	Terminal deoxynucleotidyl transferase dUTP nick end labeling
TWNK	Twinkle mtDNAhHelicase
UAP1	UDP-N-Acetylglucosamine Pyrophosphorylase 1
UBB	Ubiquitin B
UDP	Uridine-5′-diphosphate
ULK1	Unc-51 like autophagy activating kinase
USP30	Ubiquitin carboxyl-terminal hydrolase 30
UTP	Uridine-5′-triphosphate
VPS13D	Vacuolar protein sorting 13 homolog D
XIAP	X-Linked Inhibitor Of Apoptosis
YAP1	Yes-associated protein 1
ZGA	Zygotic genome actication
ZP	Zona pellucida

1. Introduction

1.1. Mitochondrial function and genetics

Mitochondria are an essential organelle of eukaryotic cells, their primary function being to supply energy to the cell in the form of adenosine triphosphate (ATP) (Figure 1.1). This is primarily achieved using the electron transport chain (ETC), which generates an electrochemical gradient across the mitochondrial membrane. This gradient is vital to a range of the mitochondria's functions but most importantly enables the enzymatic generation of ATP from adenosine diphosphate (ADP) via oxidative phosphorylation (OXPHOS). Mitochondria also mediate a wide range of other metabolic processes such as reaction oxygen species (ROS) management, calcium signalling and apoptosis (Friedman and Nunnari, 2014).
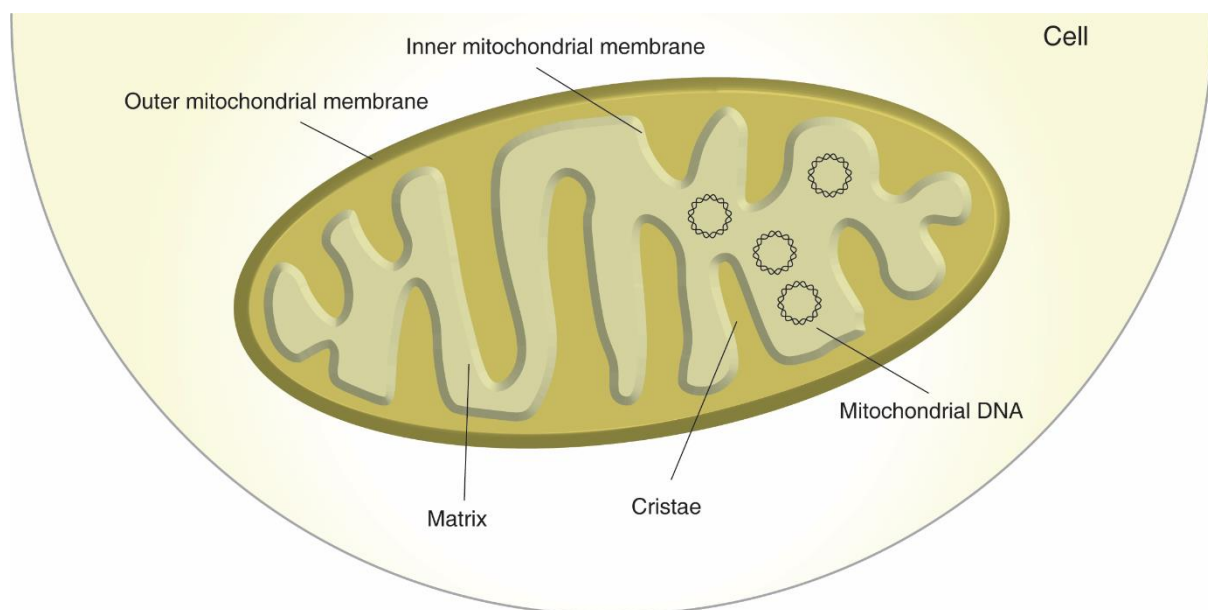
Figure 1.1. Mitochondrial structure.

Mitochondria are cytoplasmic organelles. They consist of two membranes, and inner and outer membrane. The inner mitochondrial forms cristae within a mitochondrion to maximise surface area for OXPHOS, which takes place alongside the inner membrane. A number of chemical reactions and metabolic processes take place in the matrix, and mitochondrial DNA is housed within.

Mitochondria contain their own genome (mtDNA), which has a number of key differences in comparison to nuclear DNA (nDNA). The ~16.5 kb dual-strand circular human mtDNA is responsible for encoding just 37 genes producing 13 proteins, all subunits involved in the ETC (Figure 1.2). Despite coding a relatively small number of protein subunits, a far greater proportion of mtDNA represents coding region (approximately 93%) when compared to nuclear DNA (nDNA, ~1.5%). Most genes are separated by only 1 or 2 non-coding base pairs and lack introns, although some overlap (*ATP8/ATP6* and *ND4L/ND4*); a common feature of bacteria and viruses. As well as these 13 proteins, mtDNA genes encode RNA molecules including 2 ribosomal subunits (rRNA) and 22 transfer RNAs (tRNAs) which facilitate mitochondrial protein translation (Chinnery and Hudson, 2013). The only significant non-coding region in mtDNA is the D-loop, which includes 2 hypervariable regions, an origin of replication, and a control region. This control region is the site of mtDNA interaction with nDNA encoded transcription and replication initiation factors. Proper maintenance and function of the mitochondria is reliant on proteins encoded by the nuclear genome, and so the mitochondria is under dual control of the two cellular genomes (St John, 2014).

Figure 1.2. The human mitochondrial genome.

The 16,539 bp double-stranded genome encodes 37 genes, including 13 polypeptides (complex I, green; complex III, pink; complex IV, red; complex V, orange), 22 tRNAs (white) and 2 rRNAs (yellow). Sites of the origin of heavy (O_H) and light (O_L) strand replication are highlighted in the heavy strand D-loop (grey) and downstream light strand.

Unlike nDNA, mtDNA is polyploid, existing in many copies within every cell; with copy number correlated to cellular energy demands similar to mitochondrial biomass. mtDNA is more susceptible to genetic mutation than nDNA, due to its lack of protective histones, less efficient repair mechanisms and its proximity to oxidative phosphorylation machinery which produces damaging free radicals (Taylor and Turnbull, 2005). The increased mutation rate means mtDNA often exists in a state of heteroplasmy where wildtype alleles exist alongside mutated alleles within cells and tissues (Figure 1.3). In a homoplasmic state 100% of mitochondrial genomes are identical. As in nDNA, variants within mtDNA can be pathogenic and give rise to mtDNA disease (Chinnery and Hudson, 2013).
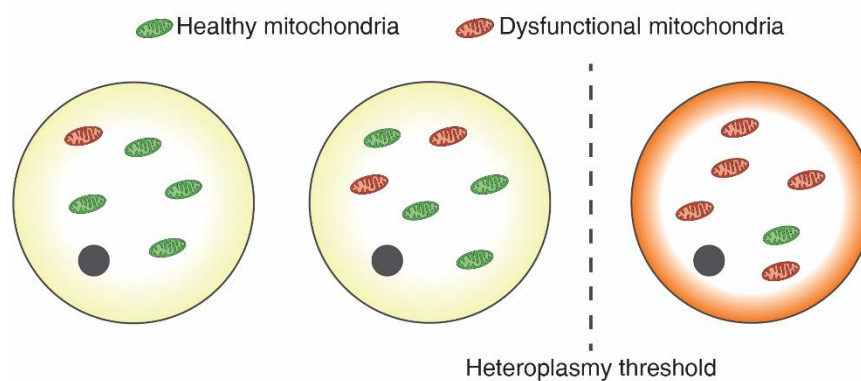
Figure 1.3. Cellular heteroplasmy of pathogenic mtDNA variants.

Wildtype (healthy, green) and mutated (dysfunctional, red) genomes coexist in the same cells. mtDNA diseases present when heteroplasmy of a pathogenic variant surpasses a threshold, which varies across known pathogenic mtDNA variants. In some examples of mtDNA disease the severity of a pathogenic phenotype thereafter correlates with levels of heteroplasmy, becoming more severe with a higher percent of mutated mtDNA genomes.

1.2. Mitochondrial disease

Mitochondrial diseases are a diverse array of debilitating or lethal genetic diseases which can present in any age group and are primarily characterised by impaired OXPHOS, meaning they often affect organs with high energy demands. Mitochondrial disease can also be caused by pathogenic variants in nDNA, when they disrupt the synthesis of proteins with a role in mitochondrial functions (Gorman et al., 2016).

For a mitochondrial disease arising from a variant in mtDNA to present a phenotype the mutation load must pass a heteroplasmic threshold, identified broadly as 18% (Hellebrekers et al., 2012), whereat it causes a sufficient biochemical defect to manifest disease (Gorman et al., 2016). Leber's hereditary optical neuropathy causing variants typically present a pathogenic phenotype only at homoplasmy, whereas other pathogenic variants across protein and RNA encoding regions induce disease at heteroplasmic levels (Taylor and Turnbull, 2005). Additionally, heteroplasmic mitochondrial disease generally leads to defects in multiple organs and the severity of disease within each organ correlates with the mutation load therein (Stewart and Chinnery, 2015).

A cohort study in the North East of England suggested an adult prevalence of 9.6 cases of mitochondrial disease caused by mtDNA variants per 100,000. The study also reported a prevalence of 2.9 cases of adult mitochondrial disease caused by nDNA variants per 100,000 (Gorman et al., 2015). In the wider UK population, the frequency of undetected mtDNA variants is thought to be higher. Around 1 in 200 healthy individuals have been suggested to carry pathogenic mtDNA variants at a low level of heteroplasmy, with potential for manifestation in later ages or future generations (Elliott et al., 2008).

1.3. The inheritance of mtDNA in humans

The human zygote contains a total of three genomes; a set of chromosomes (nDNA) inherited from each parent localised within two respective pronuclei (PN), and a mitochondrial genome inherited from the oocyte. The few mitochondria contained within a fertilising sperm are degraded at some point shortly after fertilisation (Friedman and Nunnari, 2014).

The inheritance of maternal mtDNA can include the inheritance of pathogenic mtDNA variants and so potentially mitochondrial disease. While shifts in heteroplasmy have been noted within an individual's lifespan, they are particularly notable across generations. Originally this was demonstrated in livestock models where non-pathogenic *de novo* variants in the D-loop were shown to be capable of expansion to homoplasmy across only two to three generations (Upholt and Dawid, 1977, Olivo et al., 1983). This was later demonstrated in human tissue in the context of mtDNA disease causing variants. Across three embryos of an asymptomatic woman carrying the pathogenic mtDNA variant m.8993T>G at 18% heteroplasmy in blood, one embryo showed a 100% mutation load in two blastomeres, while the other embryos

showed no detectable mutation load. The same woman also had children with 100% mutation load in blood and muscle (Steffann et al., 2006). In a study measuring heteroplasmy of m.3460G>A across four generations of a pedigree, heteroplasmy was recorded at an average mutation load of 11.3% in one generation, then 47.9% and 61.9% in the following two generations. Within this pedigree members carried variable levels of heteroplasmy; one mother gave birth to children with both higher and lower mutation loads than herself (Ghosh et al., 1996). Similarly abrupt changes in mutation load were also recorded across generations in several families carrying m.8344A>G (Larsson et al., 1992). In addition, the common and widely studied pathogenic mtDNA variant, m.3243A>G, was also demonstrated to show an erratic spread of heteroplasmy across embryos (Otten et al., 2018), and children (de Laat et al., 2013). This phenomenon can be partially explained by the existence of a mtDNA bottleneck whereby a small number of mitochondrial genomes are transmitted through cell divisions in early developmental tissues (Stewart et al., 2008a).

1.4. The mitochondrial bottleneck and purifying selection in model organisms

It has long been accepted that a mtDNA bottleneck occurs in the female germline, with female germ cells most often identified as facilitating the process. This acts alongside mechanisms of purifying selection against some pathogenic mtDNA variants (Figure 1.4). Within the developing fetus a small number of primordial germ cells (PGCs) develop, which later form the oocytes (Wear et al., 2016). However, investigation of mtDNA inheritance through germline development has faced technical challenges, and contradictory evidence exists in attempts to define the nature of this bottleneck. Initially it was reported in C57BL/6 mice that such a bottleneck occurs without any changes in the mtDNA copy number of PGCs between 7.5 days post-coitum (DPC) and 13.5 DPC. The authors suggested that the bottleneck may instead be due to uneven assembly of mtDNA molecules across a cell, with an accumulation of mitochondria around nucleoids which then act as a unit of segregation, or preferential replication of mitochondria in the perinuclear region (Cao et al., 2007).

Subsequent analysis of the same mouse model contradicted these findings (Cree et al., 2008). mtDNA copy number was shown to be stable in individual blastomeres up to the 16-cell stage embryo of preimplantation development. Post-implantation, PGCs at 7.5 DPC were shown to have fewer mtDNA copies than cells of the preimplantation embryo. This reduction in copy number continued at 8.5 DPC, but then increases by day 10.5 DPC. This suggests that the bottleneck does feature changes in mtDNA copy number, with lower numbers in PGCs 7.5

DPC relative to blastomeres preceding them, and a wave of biogenesis then elevating copy number. Using a mathematical model developed from their data the authors predict that this change in copy number is sufficient to generate dramatic shifts in heteroplasmy without any specific segregation unit. To explain the discrepancy between these two study's the authors point to the technical limitations of the approach employed by Cao *et al* (2007), suggesting inaccurate identification of PGCs (Cree et al., 2008). Later studies by Cao *et al* (2007) again reported no fluctuations in PGC copy number over the same developmental period, and in turn suggested technical limitations in the methods of PGC isolation used by Cree *et al* (2008) to explain discrepancies (Cao et al., 2009).
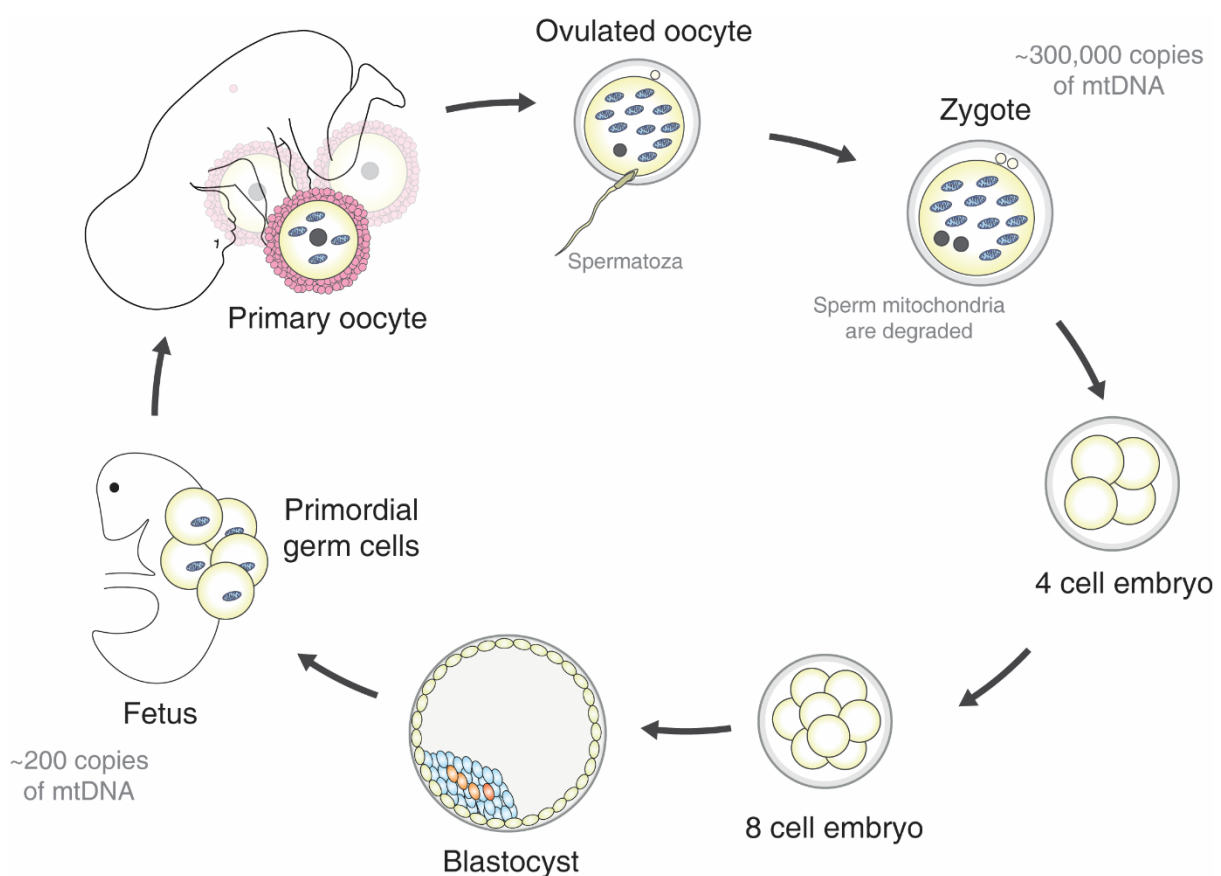
Figure 1.4. Genetic bottleneck of mtDNA in the female germline.

After fertilisation the small number of sperm mtDNA are degraded. The human zygote contains around 300,000 copies of mtDNA. Preimplantation development includes numerous cell divisions which dilute mtDNA copy number per cell, and a blastocyst is developed. The blastocyst implants in the uterine wall and a fetus develops, as do primordial germ cells (PGCs) which contain a smaller number of mtDNA copies relative to the oocyte. As a PGC develops into an oocyte, mtDNA copy number is restored through mitochondrial biogenesis, restoring the full cohort of copy number. Evidence has suggested these changes in copy number alone cannot entirely explain the unpredictable inheritance of mtDNA heteroplasmy.

Further work again reported an increase in mouse PGC mtDNA copy number between 8.5 DPC and 14.5 DPC (Wai et al., 2008). This study utilised a heteroplasmic mouse model generated by cytoplast transfer between two zygotes, each carrying different wildtype mtDNA genomes of different mouse strains, and incorporated measurements of heteroplasmy. Analysis suggested that this change in copy number is not accompanied by any changes in heteroplasmy. The study further reported an elevation in copy number of immature oocytes between the post-natal days 4 and 25. When oocytes containing under 10,000 mtDNA copies were compared to those with more than 10,000 (generally before and after day 8), shifts in mtDNA copy number were accompanied by shifts in heteroplasmy. This suggested that the bottleneck occurs over a more protracted period other studies suggest, in the maturation of ovarian follicles. The authors suggest that the initial drop in mitochondrial copy number in PGCs reflects a mechanism of selection against severe variants in mtDNA which were not present in the model (Wai et al., 2008).

Fluctuations in germ cell mtDNA copy number have recently been reported in the human female germ line (Floros et al., 2018). Human PGCs were shown to contain around 100-fold fewer mtDNA copies than oocytes. In addition, between Carnergie Stages (CS) 12 and 16/17 mtDNA copy number increased in female PGCs, before a drop between CS 16/17 and 23. Although the implications of a rise in PGC copy number before a subsequent reduction is unclear, the fluctuations in copy number are consistent with a bottleneck where sharp biogenesis would repopulate a mature oocyte from a small population of mitochondria (Floros et al., 2018), as suggested in mice (Cree et al., 2008, Wai et al., 2008). Furthermore, studies were expanded *in vitro* to include human embryonic stem cells (hESC) and human PGC-like stem cells, which model post-implantation development processes. Analysis suggested the mtDNA copy number of human blastocyst cells is higher than that of derived hESCs, while human PGC-like cells contained less than hESCs. This is again consistent with a bottleneck being generated by changes in copy number of the span of early development with reduced mtDNA copy number in PGCs. Moreover, analysis of the heteroplasmy of low-level mtDNA variants in PGCs at the same time points suggested purifying selection against non-synonymous mtDNA variants in protein encoding regions (Floros et al., 2018).

Given that measurements of heteroplasmy in individual late stage PGCs show a variable spread of variants, the authors suggested that a selection mechanism also acted to enforce segregation of genetic variants to high or low levels. Based on single cell ribo-nucleic acid sequencing (scRNA-seq) of PGCs, the authors explain this by a switch from glycolytic to

oxidative metabolism between CS12 to 21. As this occurs variants in protein-coding regions are more likely to manifest a biochemical defect in OXPHOS enabling selection against those mitochondria exhibiting a dysfunction. Likewise, the high rate of mitochondrial biogenesis necessitated by continued development may also act to highlight variants in tRNA and D-loop regions leading to selection against those organelles (Floros et al., 2018). The nature of shifting heteroplasmy and how this may manifest a bottleneck during human PGC development requires further characterisation, as do the mechanisms of any purifying selection within. Whether this selection occurs at the cellular or mitochondrial level remains unclear. However, the scarcity of human developmental tissues remains an issue.

Evidence of selection mechanism against mtDNA variants acting to skew the bottleneck were initially reported in a mouse model generated via cytoplast transfer (Fan et al., 2008). This mouse line carried pathogenic mtDNA variants in two protein-coding regions with different phenotypes; one severe (m.13885insC) and one mild (m.6589T>C). Measurements of the heteroplasmy of the severe variant in tail biopsies showed purifying selection against the variant in the germline, with the variant transitioning from full homoplasmy to being largely eradicated in four generations. However, a milder variant, was maintained despite a weak clinical manifestation.

The mtDNA mutator mouse is prone to mtDNA base repair errors due to an altered catalytic region in the mitochondrial DNA polymerase γ (*POLG*) gene, leading to a high frequency of *de novo* mtDNA variants across an array of organs (Trifunovic et al., 2004). Based on analysis of ear biopsies in mothers and pups across several generations variants affecting protein-coding regions were eliminated across generations, and at a higher rate than variants in other regions. In addition, the mtDNA mutator mouse displayed a higher degree of purification against variants in the first and second amino acid codon positions, which are more likely to force an amino acid substitution than that in the third position (Stewart et al., 2008b).

There is also evidence from mice that further events occur to modulate the inheritance of mtDNA after following oocyte maturation. In a model with a *tRNAmet* variant (m.3875delC) and a *tRNAcys* variant (m.5245T>C) derived from the mtDNA mutator mouse, heteroplasmy of m.3875delC remained consistent across an animal's lifespan, and in no postnatal samples surpasses 86% heteroplasmy. The m.5245T>C variant rapidly grew to homoplasmy. The difference in the inheritance of these variants suggests a selection mechanism preferentially

eliminates m.3875delC. PGCs at 13.5 DPC showed a wide variation of m.5245T>C heteroplasmy including up to 100%, and oocyte heteroplasmy was consistent with neutral drift. This suggests actions occur later to modulate mtDNA inheritance (Freyer et al., 2012).

The mtDNA bottleneck has been further characterised through zebrafish studies, where a reduction in mtDNA copy number was demonstrated in early development (Otten et al., 2016). Importantly, PGCs had a much lower mtDNA copy number than mature oocytes with a trend of further decreasing copy number as cells migrated across the fetus. Furthermore, the zebrafish model allows the harvest and analysis of oocytes from various stages of development. Across oocyte maturation, mtDNA copy number was shown to sharply increase, further supporting the canonical view of the mtDNA bottleneck. Interestingly, the reduction of mtDNA copy number in non-PGC cells of the fetus was sharper and more rapid than that of PGCs, suggesting the possibility of a further mechanism influencing the inheritance of mtDNA in the developing organism (Otten et al., 2016). Indeed, it was recently shown using the mtDNA mutator mouse that the number of mtDNA variants is consistent between the mother and derived blastocysts, but the number of variants present in a foetus was reduced, suggesting mechanisms act to purify the mitochondrial genome post-implantation (Ma et al., 2020a).

The broad events which modulate mtDNA require characterisation, and analysis of the inheritance of mtDNA variants must be interpreted in the context of each variant, as it has been shown that different pathogenic variants segregate differently (Brown et al., 2001, Otten et al., 2018). Preimplantation development remains an unexplored period of development in regard to mtDNA inheritance.

1.5. Preimplantation development

Preimplantation development describes the period between zygote fertilisation and implantation of the blastocyst into the uterine wall (Figure 1.5). Many studies of this period have utilised mouse models, where morphological progression matches that of human with differences being largely limited to changes in time frame and embryo size, although respective genetic profiles may limit some comparisons. The mammalian oocyte is housed with a zona pellucida (ZP), a glycoprotein layer which facilitates sperm penetration. In the

initial days after an oocyte is fertilised, the embryo undergoes several cell divisions and migrates. This period is understood to be transcriptionally silent until between the 4-8 cell stages (more precisely day 3) when a human embryo undergoes gradual embryonic gene activation (EGA) (Niakan et al., 2012). Paternal transcripts are detectable in the 4-cell embryo (Taylor et al., 1997), whereas maternal transcripts appear to be absent from the morula (Petropoulos et al., 2016), at which point transcriptional control has been handed to the developing embryo. As might be expected, a large number of mRNA show reduced abundance across the preceding days, and a number of more stable transcripts were shown to be relatively upregulated (Dobson et al., 2004). It is unclear what mechanisms mediate this transition of transcriptional control. However, coinciding with EGA, the cell cycle of blastomeres is extended allowing a longer time period for transcription of the zygote genome, including the expression of transcriptional activators. In addition, it is playable the titration of maternally-derived suppressors of transcription manifest a reducing effect as they are diluted across cell divisions (Schulz and Harrison, 2019).
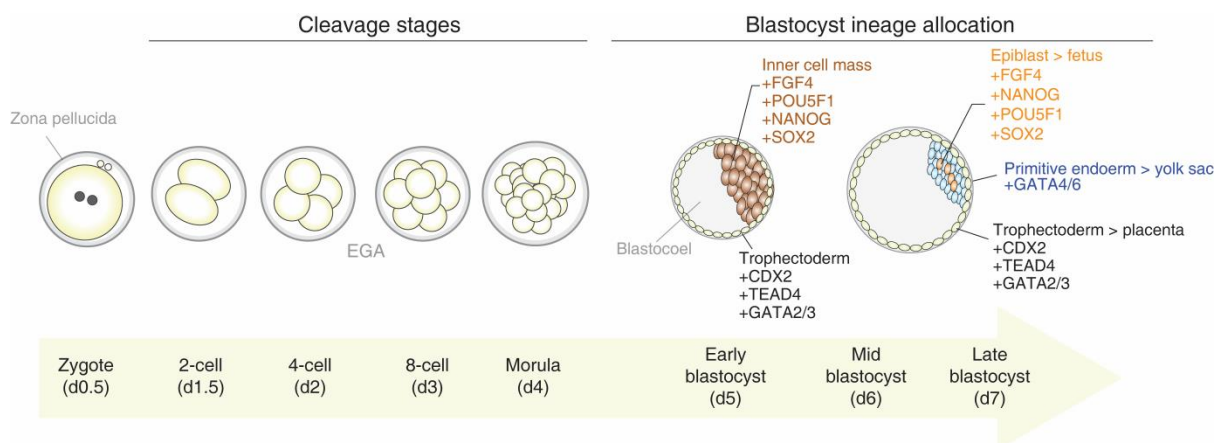
Figure 1.5. Human preimplantation development.

Beginning after fertilisation, the cleavage stages of preimplantation development feature a series of cell divisions lasting until day 4 (d4). Development is transcriptionally silent until between the 4 and 8-cell stages when embryonic genome activation (EGA) occurs. At day 3.5, the embryo will cavitate and form a morula, which develops to 32 cells before forming an early blastocyst. At this stage some cells will differentiate into a surrounding layer of trophectoderm (TE) cells, driven by expression of caudal type homebox 2 (*CDX2*), TEA domain transcription factor 4 (*TEAD4*) and GATA binding protein 2/3 (*GATA2/3*) amongst others. Expression of fibroblast growth factor 4 (*FGF4*), POU class 5 homeobox 1 (*POU5F1*), NANOG homeobox (*NANOG*) and SRY-Box transcription factor 2 (*SOX2*) (which maintain pluripotent status, and is maintained from cleavage stages) defines the inner cell mass (ICM) cells within. In the mid blastocyst the ICM cells will further differentiate into the epiblast (driven by expression of *FGF4, POU5F1, NANOG* and *SOX2*) and primitive endoderm (PE) (driven by *GATA 5/6*). The mid blastocyst continues to develop into a late blastocyst. After day 7 the embryo will hatch and implant into the uterine wall. At all times up until hatching, the embryo will be contained in a zona pellucida. Post-implantation the TE becomes the placenta, the PE the yolk sac, and the epiblast the fetus.

Following EGA the embryo undergoes compaction to form a 16-cell morula, and after further cell divisions to form a 32-cell late morula, forms a blastocyst which becomes morphologically distinct at day 5. The blastocyst consists of a blastocoeal, a fluid-filled central cavity, an external layer of cells called the trophectoderm (TE), and an internal bundle of pluripotent cells called the inner cell mass (ICM). By day 6 the blastocyst will grow in size and the ICM will diverge into two cell groups; the primitive endoderm (PE) and the still pluripotent epiblast. These cell groups continue to divide and the blastocyst continues to grow into day 7. During day 7 or 8 a blastocyst will hatch out of the ZP, enabling implantation (Niakan et al., 2012).

The three cell lineages of the blastocyst give rise to different tissues post-implantation. The TE becomes the placenta, the PE the yolk sac, while the epiblast cells give rise to fetus itself, thus is of primary interest in studying the inheritance of mtDNA. The establishment of cell lineages across days 5 (TE and ICM) and 6 (PE and epiblast) is in large part driven by changes in the expression of transcription factors (Rossant and Tam, 2009). Briefly TE specification is driven primarily by caudal type homeobox 2 (*CDX2*, Strumpf et al., 2005), acting alongside TEA domain transcription factor 4 (TEAD4, Yagi et al., 2007) and GATA binding protein 2/3 (*GATA2/3*, Krendl et al., 2017). Meanwhile fibroblast growth factor 4 (FGF4, Kang et al., 2013), POU class 5 homeobox (*POU5F1/OCT4*, Nichols et al., 1998), nanog homeobox (NANOG, Mitsui et al., 2003) and sex determining region y-box transcription factor 2 (SOX2, Avilion et al., 2003) expression maintains the ICM, before expression of *GATA4* and *6* (Rojas et al., 2010, Cai et al., 2008) drive PE specification, and maintained *FGF4*, *POU5F1*, *NANOG* and *SOX2* expression promote epiblast specification. While these changes were initially characterised in mice, changes in gene expression that drive lineage specification in the human blastocyst were shown to be largely conserved (Rossant and Tam, 2009, Blakeley et al., 2015).

These transcriptional changes were further characterised recently by means of a large scRNAseq dataset of human preimplantation embryos (Petropoulos et al., 2016). The open-source availability of this same dataset opens the possibility of further analysis, including of genes relating to mitochondrial functions. A dataset of this size is made even more valuable due to the lack of readily available human embryonic tissue and ethical constraints around the research of. The knowledge of which genes drive and maintain embryonic lineage differentiation also allow analysis to account for different cell lineages, and the ongoing process of their differentiation.

1.6. Segregation of heteroplasmy in preimplantation development

Previous work has suggested that blastocyst development may feature an increase in the intercellular variation of mtDNA heteroplasmy (Treff et al., 2012, Neupane et al., 2014) (Figure 1.6). However, previous work is complicated by the study of two fundamentally differing models; mtDNA heteroplasmy generated through the mixing of two mtDNA populations and mtDNA mutations in their natural nuclear background (the latter of which has thus far only examined in humans). It is unclear how the segregation of mtDNA might differ in embryos between these models. Analysis of the BALB/OlaHsd mouse model, generated via cytoplast transfer of two wildtype mitochondrial genomes of two mouse strains, has shown that intercellular variation undergoes a modest increase during this period, even when analysis of intercellular variation of the blastocyst is conducted at the level of a single TE biopsy compared to the remaining embryo (Dean et al., 2003, Neupane et al., 2014), which likely masks a large degree of variation. The BALB/OlaHsd mouse model does not feature any characterised pathogenic variant, and the two genotypes within differ by 101 mtDNA variants between the donated and recipient genomes, predicted to manifest 15 amino acid substitutions (Dean et al., 2003). It is unclear to what extent this model can replicate the transmission of a pathogenic mtDNA variant, or how this level of variation effects nuclear-mitochondrial DNA communication and the dynamics of inheritance.
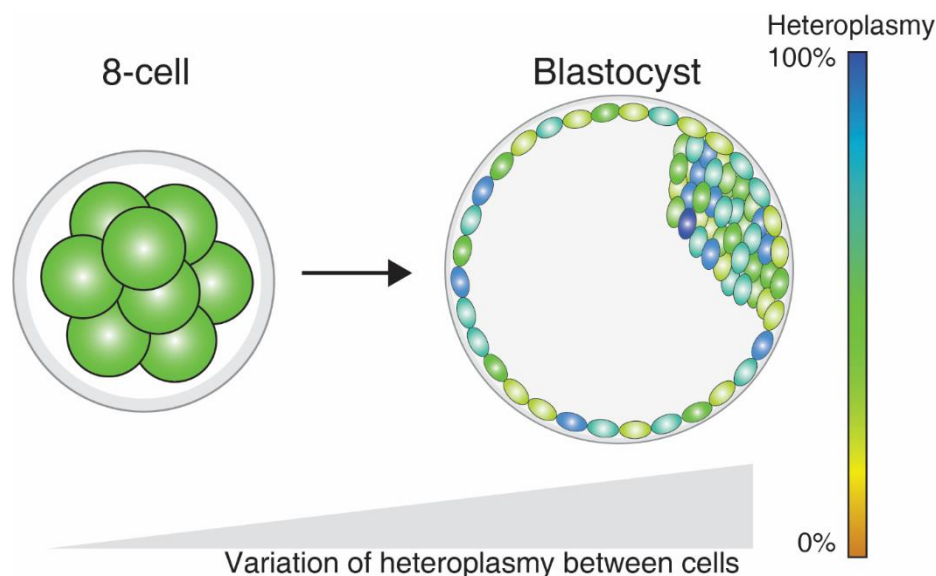
Figure 1.6. Model of intercellular variation of mtDNA heteroplasmy in late preimplantation development.

Evidence from murine and human embryos (Treff et al., 2012, Neupane et al., 2014) indicates a wider segregation of heteroplasmy in the blastocyst compared to the 8-cell embryo.

Human studies are limited by the availability of tissue. Initial work examined polymorphisms in the D-loop hypervariable regions, and reported a range of intercellular mtDNA heteroplasmy across cells of 4-8 cell embryos between 0 and 19 (Steffann et al., 2006). Analysis of the pathogenic m.3234A>G variant compared two single cell biopsies and showed a tighter range of intercellular heteroplasmy, ranging up to 6% in a small number of cases (Monnot et al., 2011). A later study again examining distribution of m.3234A>G reported a similarly tight range when a wider number of cells were measured (Treff et al., 2012). A study encompassing pathogenic variants m.3234A>G and m.8993T>G showed similar results but with a wider range across a minority of embryos (Sallevelt et al., 2013), as did a subsequent study encompassing a higher number of m.3234A>G carriers and embryos (Sallevelt et al., 2017a), the range of heteroplasmy across embryos often below 10%.

Work has also shown that that intercellular variation of the pathogenic m.3243A>G variant increases in the human blastocyst compared to the 8-cell (Treff et al., 2012). However, later analysis of post-natal samples collected from the child born during this study revealed elevated mutation load (Mitalipov et al., 2014), raising questions over the validity of the original heteroplasmy measurements during the PGD procedure. Later work on the m.3243A>G variant examined variation of heteroplasmy across numerous TE biopsies of blastocyst. Most embryos revealed variation of approximately 10% heteroplasmy, with one case extending to a range of 22% (Heindryckx et al., 2014). While no measurements of intercellular variation in the 8-cell embryo were reported, alongside available published data this would suggest an increase in intercellular variation in the blastocyst relative to the 8-cell embryo. Importantly, analysis of intercellular variation in the blastocyst has only been conducted at the level of TE and ICM cell clumps or a single TE biopsy compared to the remaining blastocyst, rather than following isolation of single cells. Therefore, the true extent of blastocyst intercellular variation relative to the 8-cell embryo remains unknown.

In a primate model generated via cytoplast transfer of two wildtype mtDNA genomes, larger ranges of intercellular heteroplasmy were apparent even in 2-cell embryos, and this pattern of segregation increased in 8-cell embryos. Although single cell measurements were not conducted at the blastocyst stage, TE and enriched ICM clumps were analysed and sharp segregation of heteroplasmy between the two portions was again apparent. When measurements within each stage were pooled the levels of heteroplasmy across the embryo was similar to the approximately 50% recorded in zygotes produced in the same study, suggesting no mechanism driving towards homoplasmy (Lee et al., 2012). This may further

suggest that preimplantation development can feature sharp shifts in cellular heteroplasmy, but embryos were analysed immediately after cytoplast transfer, as opposed to being bred across at least one generation, as were the BALB/OlaHsd mice of Neupane *et al* (2014). The extent to which two mitochondrial networks the karyoplast/cytoplast will fuse between transfer and blastocyst development is unclear, and this could influence the dynamics of mtDNA segregation. Therefore, it is unclear to what extent these data can be extrapolated to the inheritance of mtDNA diseases, and such models are worthy of further study.

While animal studies described above provide valuable insights into the segregation of mtDNA heteroplasmy, many study heteroplasmy in models produced through cytoplast transfer of wildtype mtDNA genomes. It is unclear to what extent this can replicate the inheritance of a single pathogenic mtDNA variant, and so the inheritance of human mtDNA diseases. Nor can they then take into account any mechanisms of selection against pathogenic mtDNA variants. The recently developed tRNA *alanine* (*tRNAala*) mouse, derived from the mtDNA mutator mouse, represents the first animal model to stably transmit a single pathogenic mtDNA variant (m.5024C>T). This opens a range of possibilities in the investigation of pathogenic mtDNA variant inheritance. The inheritance of m.5024C>T has already been demonstrated to be subject to a bottleneck, and purifying selection preventing the birth if offspring above 80% heteroplasmy. Although two variants are reported in the model, only one could be linked to a respiratory defect (Kauppila et al., 2016).

If intercellular heteroplasmy does increase in the blastocyst, it could have profound consequences for procedures aimed at the circumvention of the inheritance of pathogenic mtDNA mutations. Currently, procedures rely on a biopsy taken from a cleavage or blastocyst stage embryo to identify embryos carrying low heteroplasmy. Changes in the segregation of mtDNA could compromise the accuracy of a blastocyst biopsy. Furthermore, given the low cell number within the preimplantation embryo, and especially given the fact that a small number of epiblast cells within give rise to the fetus, preimplantation development represents an opportunity for the segregation of mtDNA heteroplasmy to have long-ranging implications.

This possibility has been made more intriguing by the recent discovery of mitophagy occurring in the preimplantation embryo of the mouse (Figure 1.7, Dr. Yuko Takeda, unpublished), and human. Confocal imaging of the mito-QC probe allows the identification of mitochondria undergoing degradation (Allen et al., 2013). This probe originally targeted the mitochondrial

outer membrane (OMM), but was modified in house to transolocate into the mitochondrial matrix (matrix-mito-QC) to guarantee accuracy of localisation. mito-QC carries mCherry and EGFP tags thus fluoresces both red and green. Mitochondria which are targeted for degradation via mitophagy are engulfed in mitolysosomes (Rodger et al., 2017), wherein acidic pH levels degrade a mitochondrion and EGFP tags within. The more stable mCherry can continue to be visualised, allowing red fluorescence to serve as a marker of mitophagy (Allen et al., 2013). Following microinjection of matrix-mito-QC into the zygote, red foci were visible beginning in the early blastocyst, and a growing mitophagy signal was detected across blastocyst development. Given the changes in intercellular heteroplasmy noted in this stage, and evidence that events occur to modulate the inheritance of pathogenic mtDNA variants outside of oogenesis, it is plausible that mitophagy influences cellular heteroplasmy in this period. The *tRNAala* mouse provides a model for further investigation.
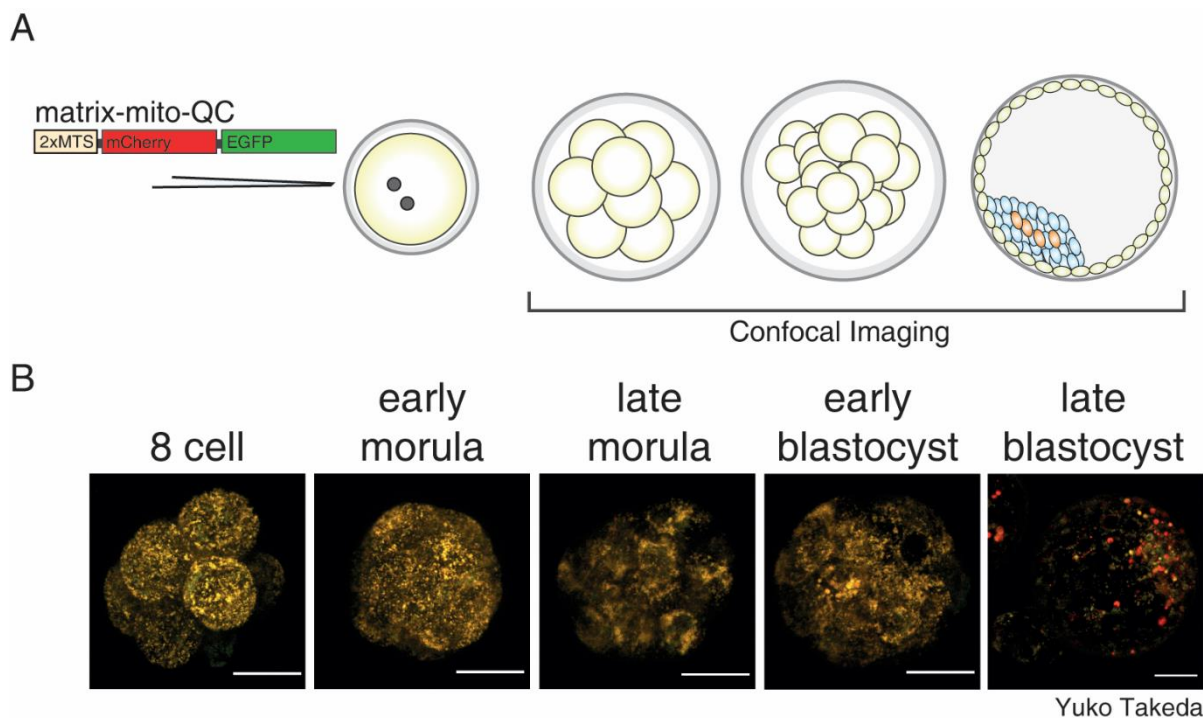
Figure 1.7. Mitophagy in the CD1 mouse preimplantation embryo.

(A) The matrix-mito-QC targets the mitochondrial matrix space. It carries a mCherry and EGFP tag, thus fluoresces red and green. In the process of mitochondrial degradation, the EGFP signal is quenched, leaving red foci as a marker of mitophagy. The matrix-mito-QC probe was microinjected into mouse zygotes and fluorescent signal tracked across preimplantation development using confocal imaging. (B) Red foci first appear in the early blastocyst, becoming more prevalent in the late blastocyst. Scale bars = 20 μm.

1.7. Prevention of mtDNA disease inheritance

Given the devastating effects mitochondrial disease can have on health, lack of curative treatments, and the difficulty in predicting inheritance, it is vital to pursue effective means of preventing transmission (Figure 1.8). For intending mothers at risk of transmitting a mtDNA encoded disease to offspring and carrying a moderate heteroplasmic mutation load, pre-implantation genetic diagnosis (PGD) is an option. In PGD an IVF pre-implantation embryo is biopsied with one or more cells being removed. In the context of mitochondrial disease, those embryos with an apparent low mutation load are transferred into the uterus of the intending mother. The procedure in any context has only been pioneered in the past 30 years and the continued good health of babies born via PGD is yet to be confirmed (Vermeesch et al., 2016). The earliest reported application for mtDNA disease occurred in 2006 with subsequent cases in the following years, so the safety of the procedure in relation to continued absence of mtDNA disease is not confirmed (Steffann et al., 2006, Thorburn et al., 2009, Treff et al., 2012, Sallevelt et al., 2013, Sallevelt et al., 2017b). Although Treff *et al* (2012) reported the birth of a child with mutation load ranging from 0% to 15% in buccal cells at 1 month (derived form an embryo reporting 12% mutation load), it has since been reported that the child has suffered a range of medical issues. At both 6 weeks and 18 months heteroplasmy ranging between 46% and 52% in blood and urine was measured (Mitalipov et al., 2014), suggesting that a more stringent minimum safety threshold for mutation load carryover must be established. In addition, due to the changing intercellular variation of heteroplasmy discussed above, it is still unclear which developmental stage and which cells of the embryo offers optimal prediction of mutation load in the vital epiblasts of the blastocyst, or of potential offspring, whilst offering a high rate of viability for implantation (Vanneste et al., 2009, Vermeesch et al., 2016). Continued monitoring of the health of patients will be vital in assessing the safety of PGD.

Whilst most evidence confirms PGD can be considered a safe risk-reduction strategy, it is not suitable for all patients. For instance, in women with a high or homoplasmic mutation load where embryos exhibiting a sufficiently low mutation load will be rare. Instead, these patients might undergo mitochondrial replacement therapy (MRT). MRT encompasses several techniques, but the only protocol with regulatory approval and licensed for application in the UK is pronuclear transfer (PNT). The PNT procedure was first established over thirty years ago in a mouse model with the production of healthy offspring following the procedure (McGrath and Solter, 1984), and was later utilised to reduce heteroplasmy in a mouse model expressing a rearrangement in mtDNA (Sato et al., 2005). Proof of concept of this procedure

in human zygotes was published in 2010 using abnormally fertilised eggs (Craven et al., 2010). Human PNT has underwent a period of optimisation primarily to increase embryo viability with earlier application of the procedure shown to be promising. In the procedure the maternal and paternal PN are enucleated from a patient IVF embryo at the early PN stage via an enucleation pipette, at which point they will be housed with a karyoplast. This karyoplast, consisting of patient cytoplasm and PN, is injected into an enucleated donor oocyte populated by healthy mitochondria wherein it fuses with the donor cytoplasm. This leaves a reconstituted fertilised zygote containing the nuclear DNA of a mtDNA variant carrying woman, but mtDNA of a healthy donor (Figure 1.8). In the latest report most PNT blastocysts carryover was reduced to <2% heteroplasmy. Some carryover of mutant mtDNA genome is inevitable because of the small amount of mitochondria in the karyoplast, but reported heteroplasmy at the blastocyst stage is well under known clinical thresholds for mitochondrial disease and far below the levels of heteroplasmy reported in PGD (Hyslop et al., 2016).
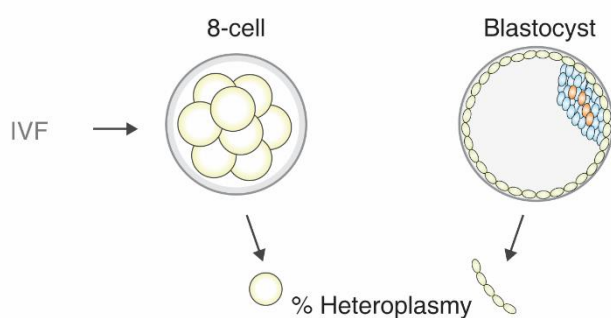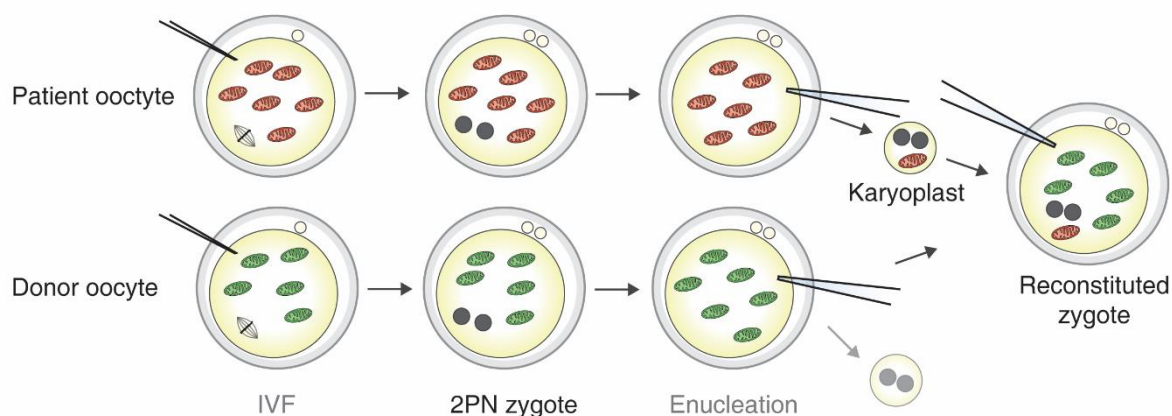
Figure 1.8. Strategies to prevent inheritance of pathogenic mtDNA variants.

In preimplantation genetic diagnosis, an *in vitro* fertilised (IVF) preimplantation embryo is biopsied at either the 8-cell or blastocyst stage. The biopsy undergoes measurement of mtDNA heteroplasmy, and an embryo with the most favourable chance of successful implantation and with low heterooplasmy of the pathogenic mtDNA variant is implanted. If all oocytes of an intending mother have a high heteroplasmy, the procedure cannot circumvent mtDNA variant inheritance. In pronuclear transfer, an intending mother's oocyte undergoes IVF and allowed to develop to a 2 pronuclei (2PN) stage zygote. At this point it is enucleated and a karyoplast withdrawn containing the nuclear DNA of both parents, and a small amount of mitochondria from the patient embryo. A donor oocyte is similarly enucleated and nuclear DNA discarded, and the patient karyoplast injected into the oocyte, where it fuses with surrounding cytoplasm. This reconstituted zygote is used for implantation.

Alongside technical challenges the clinical implication of PNT has faced regulatory hurdles owing to significant ethical issues surrounding the technique. In the UK research on human embryos is governed by Human Fertilisation and Embryology Act (HFEA). As of 2005 the HFEA research licence permitted the use of abnormally fertilised human eggs in experimentation. Following promising results and supportive campaigns, in 2015 regulations were loosened to allow clinical application of PNT in cases of severe mitochondrial disease, and in 2016 the HFEA allowed cautious use of PNT clinically in licenced clinics. In 2017 the HFEA granted a such a licence to the Newcastle Fertility Centre, and the first clinical

application of PNT was recently conducted. PNT is still tightly regulated; HFEA approval is currently required for each individual case and offered only to those for whom PGD is unlikely to be successful. Importantly, follow-up studies will be a requirement for any PNT conducted on National Health Service public funds (Herbert and Turnbull, 2018).

In the USA an alternative MRT procedure, maternal spindle transfer (MST), has gained greater prominence than PNT. MST is conducted in the metaphase II oocyte, from which the spindle-chromosomal complex is extracted within a karyoplast and transferred to an enucleated oocyte carrying heathy mitochondria (Tachibana et al., 2009). This procedure also underwent proof of principle studies in humans in 2016 (Kang et al., 2016). However, the birth of a healthy child has already been reported in Mexico, where a lack of regulations enabled rapid implementation of the procedure, allowing a female carrier of the Leigh Syndrome causing m.8993T>G variant to undergo IVF following MST (Zhang et al., 2017). A blastocyst carrying a reported mutation load of 5.70% in a TE biopsy was implanted, giving rise to a child with neonatal mutation load ranging from 2.36% to 9.23% in tissues tested. Whilst this mutation load appears well below the threshold of necessary for presentation of mtDNA disease, long-term monitoring of the child's health and mutation load will be important given the novelty of the procedure. Authors reported that annual health examinations up until 18 years of age are planned, and at last report the child was healthy at 7 months of age. However, no plan for monitoring mtDNA heteroplasmy and potential drift was in place (Zhang et al., 2017). Monitoring of heteroplasmy in children born from MRT will be fundamental to proving the safety of the procedures, especially given complications that have arisen from PGD (Mitalipov et al., 2014).

Despite the success of MRT experimentally and its clinical implementation, concerns remain regarding the post-natal mutation load of human offspring. Following MRT, when blastocyst ICM are explanted to generate hESC colonies and heteroplasmy measured across passages, a reversion towards the karyoplast mtDNA variants was documented in a minority of hESC lines (Hyslop et al., 2016, Kang et al., 2016), totalling 15% of hESC lines (Hudson et al., 2019). Clinical risk arising from the phenomenon is difficult to estimate, but mechanisms of mitochondrial segregation evidenced in primates with mechanically produced heteroplasmy suggest this reversion could continue in *in vivo* post-implantation development (Lee et al., 2012). Whilst mechanisms and causes of this reversion are unclear, this underlines the necessity to minimise carryover as much as possible to optimise MRT. One avenue is the induction of mitophagy to degrade dysfunctional mitochondria in the zygote of the karyoplast

donor. It is plausible the machinery responsible for mitophagy in the blastocyst can be harnessed to induce mitophagy at an earlier stage.

1.8. Mitophagy

Mitophagy refers to mechanisms of autophagy specifically targeting mitochondria which, coupled with mitochondrial biogenesis, conducts turnover of cellular populations of mitochondria maintaining their good health in most cells and tissues. Whilst fulfilling this housekeeping role, mitophagy activity level can be transiently increased to protect a cell from damaged mitochondria and the resulting defects. Numerous pathways of mitophagy are recognised with three somewhat distinct pathways better characterised than others (Figure 1.9). All of these pathways end with engulfment of the mitochondria in an autophagosome, which is attracted by a light chain 3 interacting region (LIR) motif on a mitochondrial surface protein/conjugate, and which enables interaction with proteins on the autophagosome surface. Most often these autopagosome surface partners are microtubule-associated protein 1A/1B-light chain 3 (*LC3*) and gamma-aminobutyric acid receptor-associated protein (*GABARAP*). Subsequently the autophagosome is trafficked to a lysosome, forming a mitolysosome, wherein its contents are degraded by an acidic pH level (Rodger et al., 2017).

One of these canonical mitophagy pathways is mediated by BCL2 Interacting Protein 3 (BNIP3) and BNIP3-Like Protein 3 XL (BNIP3L/NIX). These proteins bear the LIR themselves, being homologues to one another (Rodger et al., 2017). Both *BNIP3* and *BNIP3L* are primarily controlled transcriptionally by hypoxia-inducible factor 1-alpha (HIF1A), which is promoted under hypoxic conditions, but a thus far unidentified kinase also acts to enhance these proteins via phosphorylation of a residue close to or within the LIR (Chourasia et al., 2015, Rogov et al., 2017). Of the two, most studies have focused on BNIP3L, which evidence from mouse models and cell lines suggests is involved in cell specification and development. The role of BNIP3L in reticulocyte development in human cell cultures was first suggested by its higher level of expression in mature cells than immature counterparts (Aerbajinai et al., 2003). Later it's role was linked to mitophagy in mouse reticulocyte development, where its presence is necessary for the clearing of mitochondria during maturation. Additionally, this was shown to occur in the absence of a range of pro-apoptopic proteins, suggesting BNIP3L activity to be at least somewhat distinct from apoptosis. BNIP3L itself was not required for wider autophagy to occur, revealing its specificity. Ablation of *BNIP3L* leaves mitochondria incapable of signalling their own engulfment by autophagosomes, which proved to have severe consequences in the

mouse leading to anaemia, reticulocytosis and erythroid-myeloid hyperplasia (Schweers et al., 2007, Sandoval et al., 2008).
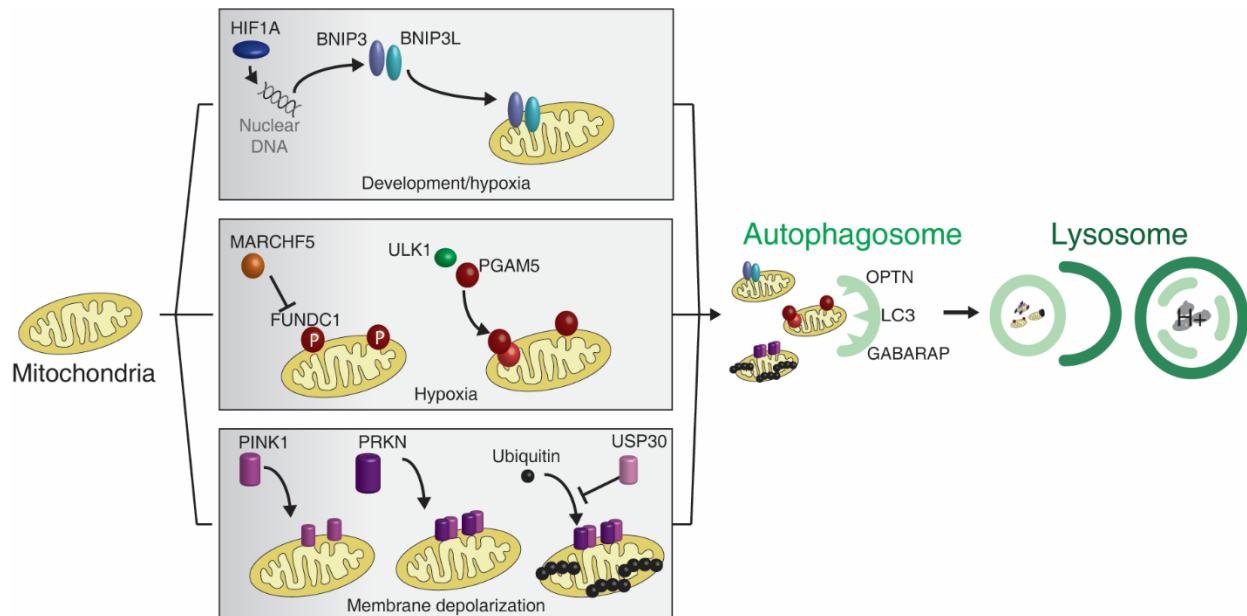
Figure 1.9. Main pathways of mitophagy.

The BCL2 interacting protein 3/like (BNIP3/BNIP3L) pathway (top) is promoted by the upregulation of the transcription factor hypoxia inducible factor 1 subunit alpha (HIF1A), itself upregulated in hypoxic conditions. BNIP3/3L translocate to the mitochondrial outer membrane where they communicate with the autophagosome network. The pathway has been linked to developmental processes. The FUN14 domain containing 1 (FUNDC1)/Phosphoglycerate mutase family member 5 (PGAM5) pathway (middle) is the least characterised of the three but has also been linked to hypoxic conditions. To inhibit this pathway, membrane associated ring-CH-type finger 5 (MARCHF5) can modify a residue of FUNDC1 and prevent its activation of FUNDC1. To activate the pathway, PGAM5 will dephosphorylate FUNDC1 to enable communication with the autophagosome network. Unc-51 like autophagy activating kinase 1 (ULK1), as well as enhancing wider autophagy, can enhance PGAM5 activity to promote this process. The phosphatase and tensin homolog induced kinase (PINK1)/parkin RBR E3 ubiquitin protein ligase (PRKN) pathway is best characterised, but unlike receptor-mediated mechanisms, is promoted by mitochondrial damage causing mitochondrial membrane depolarization. PINK1 is usually cleaved at the mitochondria but following mitochondrial damage this process is impaired. PINK1 accumulated on the mitochondrial membrane, then recruits and phosphorylates PRKN. PRKN catalyses the attachment of ubiquitin chains to the mitochondrial membrane proteins, facilitating communication with the autophagsome network. The pathway can be inhibited by ubiquitin specific peptidase 30 (USP30) mediated removal of ubiquitin chains. The autophagosome network communicates with the mitochondria via optineurin (OPTN), Microtubule-associated proteins 1A/1B light chain 3B (LC3) or Gamma-Aminobutyric Acid Receptor-Associated Protein (GABARAP) receptors, and engulfs mitochondria targeted for degradation, and is in turn engulfed by the lysosomal network. Acidic pH within degrades the mitochondria.

During mouse retinal ganglion cell differentiation local hypoxia induces *BNIP3L* expression thus triggering mitochondrial removal, and increased expression of glycolytic protein mRNA, suggesting a change in metabolic profile alongside mitophagy in cell differentiation. Underlining the importance of this mechanism; a model lacking *BNIP3L* retain these mitochondria and develop fewer retinal ganglion cells (Esteban-Martínez et al., 2017). In forced reprogramming of somatic cells into induced pluripotent stem cells, at least one method has been shown to rely on BNIP3L for clearance of mitochondria. Such stem cells rely on glycolytic metabolism so have little need for the levels of mitochondria in other cell lineages (Xiang et al., 2017). Perhaps contrary to the logical assumption, evidence indicates that BNIP3L mediated mitophagy can be activated to enhance OXPHOS when demand is high. In HeLa cells cultured in glucose-free media with glutamine to stimulate increased OXPHOS, the GTPase Ras homologue enriched in brain (*RHEB*) appears to be recruited to the OMM. There, it bound BNIP3L and facilitated recruitment of the autophagosome. This may then lead to accelerated biogenesis creating a healthy, unimpaired population of mitochondria, manifesting an overall increase in metabolic efficiency. Notably, knockdown of *BNIP3L* reduced this *RHEB* mediated mitophagy (Melser et al., 2013). Finally, both BNIP3 and BNIP3L have been implicated in the differentiation of cardiomysocytes in cell lines (Zhao et al., 2020). The data above and the importance of cell differentiation in the preimplantation blastocyst open the question as to whether mitophagy could have a role in differentiation during early development as well.

The second well-characterised pathway is mediated in large part by FUN14 Domain Containing 1 (*FUNDC1*), an OMM spanning protein being an LIR motif on its N-terminal, and PGAM Family Member 5 (*PGAM5*). Regulation of this pathway seems primarily controlled by the phosphorylation status of FUNDC1, which is monitored by a range of interacting partners. Whilst this mechanism applies to several residues, key among these FUNDC1 modifications is dephosphorylation at Serine 13 by PGAM5. PGAM5 is normally inhibited by B-cell lymphoma-extra large (BCL2), but this is degraded under conditions of hypoxia allowing activation of FUNDC1 and eventual formation of mitolysosomes (Chen et al., 2014, Wu et al., 2014a) This interaction can be further strengthened by Unc-51 Like Autophagy Activating Kinase 1 (ULK1) phosphorylation of FUNDC1 at serine 17 (Wu et al., 2014b). As well as its role specifically in FUNDC1 mediated mitophagy, ULK1 has a wider role in initiating non-specific autophagy (Russell et al., 2013). Meanwhile, Membrane Associated Ring-CH-Type Finger 5 (MARCHF5) can ubiquitylate FUNDC1 in early hypoxia, prior to FUNDC1 activation, to inhibit mitophagy and seemingly withhold excessive mitochondrial degradation (Chen et al.,

2017). No specific biological or developmental mechanisms have been identified for the FUNDC1/PGAM5 pathway.

The final of these three pathways is the best characterised and differs from others in that proteins signalling the autophagosome network are not expressed on the OMM. PTEN-induced putative kinase 1 (PINK1)/Parkin (PRKN) mitophagy pathway is currently the best characterised, owing to its key role in the pathology of Parkinson's Disease (Valente et al., 2004, Matsuda et al., 2010). Under basal conditions PINK1 is continuously cleaved at the mitochondria and targeted for degradation. However after mitochondrial membrane depolarisation, a consequence of damage to the organelle, this cleavage is inhibited leading of PINK1 accumulation of the OMM (Yamano and Youle, 2013). This allows PINK1 dimerisation and enhanced kinase activity leading to its auto-phosphorlyation at several residues, as well as recruitment and phosphorylation of PRKN (Okatsu et al., 2012). PINK1 additionally phosphorylates Ubiquitin to fully activate the pathway. Subsequently, PRKN catalyses the conjugation of Ubiquitin chains and their elongation on a range of OMM proteins (Koyano et al., 2014). Phospho-ubiquitin chains recruit a range of receptors bearing LIR motifs, with calcium-binding and coiled-coil domain-containing protein 2 (CCDC2) and optineuron (OPTN) being essential (Lazarou et al., 2015, Heo et al., 2015), allowing communication with the autophagosome network. Meanwhile, ubiquitin specific peptidase 30 (USP30) acts to inhibit this pathway by removing ubiquitin conjugates (Bingol et al., 2014). The PINK1/PRKN pathway is most often associated with mitophagy as a response to mitochondrial damage, but a report also indicates that it is active during cardiomyocyte development as fetal mitochondria are replaced with adult organelles optimised for postpartum metabolism (Gong et al., 2015).

Mitophagy in the preimplantation embryo is yet to be characterised. So far the importance of PINK1 to embryo mitochondria, specifically mitochondrial fission, has been demonstrated in porcine embryos. Even a modest knockdown of PINK1 in a porcine model has shown moderately impaired blastocyst formation, reduced mtDNA copy number, and mitochondrial swelling and elongation. These changes manifested impaired mitochondrial function, including elevated oxidative stress and reduced ATP, and increased autophagy and apoptosis. Dynamin 1 like (DNM1L) overexpression induced mitochondrial fission and rescued this effect. During this same period of porcine development PINK1 protein abundance gradually decreased, as did *PINK1* transcripts, suggesting its declining importance as preimplantation embryo progresses (Niu et al., 2019). The role of PINK1 and its signalling partners will need to be interpreted in light of one another, as will that of other mitophagy genes given evidence

of cross-talk exists between the three pathways described above (Zimmermann and Reichert, 2017). An unbiased analysis of the transcriptome via scRNAseq analysis will allow initial characterisation of mitophagy in the human embryo.

1.9. Mitochondrial maintenance and biogenesis

Whereas mitophagy is responsible strictly for the degradation of mitochondria, it operates alongside other quality control mechanisms exist to regulate mitochondrial shape. Mitochondria exist as a dynamic network which can be expanded or shrunk in accordance with a cell or tissues metabolic demands. This network can be made up of long, branching chains or more punctuate organelles (Friedman and Nunnari, 2014) (Figure 1.10).

The pathways by which the segments of the mitochondria network are separated (fission) or joined (fusion) are in constant balance to achieve the goal of meeting a cells energy demands (Figure 1.10). Both processes are performed by GTPases of the dynamin-related proteins family (Friedman and Nunnari, 2014). Mitochondrial fission requires recruitment of DNM1L by mitochondrial fission 1 protein (FIS1) and mitochondrial fission factor (MFF), amongst others. At the mitochondrial surface DNM1L multimerizes and encircles the site of fission before cleaving the mitochondria (Friedman and Nunnari, 2014). The importance of this process has been demonstrated in multiple models. Mice null for *DNM1L* show disrupted nervous system development (Ishihara et al., 2009, Wakabayashi et al., 2009), while *in vivo* and *in vitro* studies have shown that inhibition mitochondrial fission induced respiratory defects (Kageyama et al., 2012). Mitochondrial fission has also been implicated as an important regulator of mitophagy, as it may segregate less efficient or excess stretched of the mitochondrial network allowing their efficient degradation (Twig et al., 2008). Mitochondrial fusion requires merging of mitochondrial inner membrane (IMM) and OMM. Merging of the IMM is mediated by mitochondrial dynamin like GTPase (OPA1), whereas merging of the OMM in mediated by mitofusin 1 (MFN1) and MFN2. In both cases little is understood about the precise mechanisms which facilitate fusion (Friedman and Nunnari, 2014).
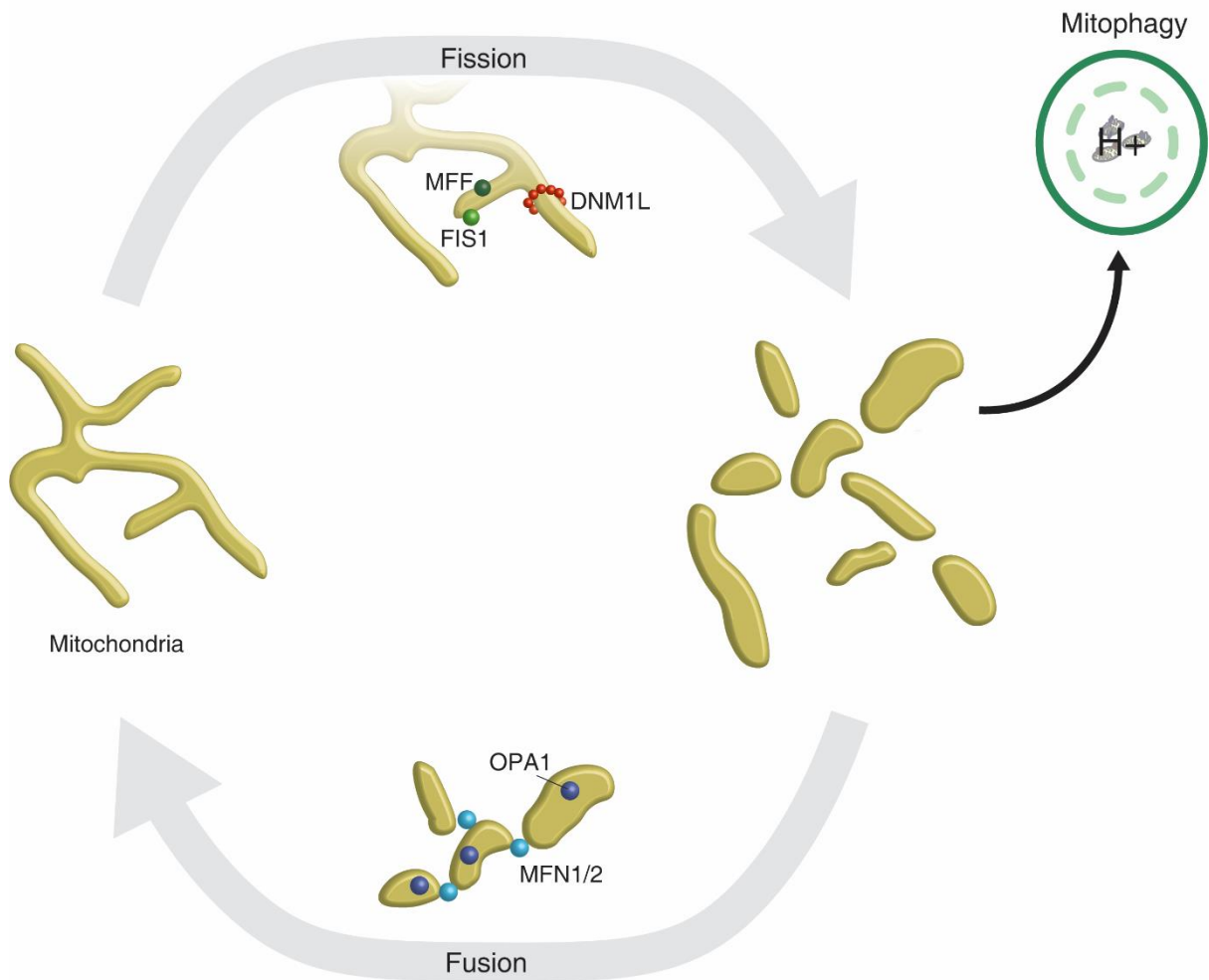
Figure 1.10. Mitochondrial fission and fusion.

In response to cellular energy demand, the processes of fission and fusion act to module the morphology of the mitochondrial network to increased OXPHOS capacity or reduce excess. The process of fission separates the mitochondrial network. Mitochondrial fission factor (MFF) and fission, mitochondrial 1 (FIS1) recruit dynamin-1-like (DNML1) to the mitochondrial surface, where it multimerises and surrounds the point of fission, then facilitates separation via its GTPase function. Fission of the mitochondrial network can facilitate mitophagy by separating regions of impaired or damaged mitochondria. Mitochondrial fusion can join mitochondria. Fusion is not as well characterised as fission but is mediated by mitofusin 1/2 (MFN1/2) and OPA1 mitochondrial dynamin like GTPase (OPA1).

Acting alongside mitophagy but towards opposite ends, mitochondrial biogenesis is the process by which mitochondrial biomass and mtDNA copy number is increased (Figure 1.11). The central regulator of mitochondrial biogenesis is peroxisome proliferator-activated receptor gamma coactivator 1-alpha (PPARGC1A). *PPARGC1A* is subject to regulation at both transcriptional and post-translational levels, and regulates the expression of a wide array of

genes itself. Increased expression of *PPARGC1A* in turn elevates expression of nuclear respiratory factor 1 (*NRF1*) and *NRF2*, and peroxisome proliferator activated proteins (*PPARs*). NRFs mediate expression of a number of nDNA encoded OXPHOS proteins, including mitochondrial transcription factor A (*TFAM*), a transcriptional activator which is integral to biogenesis and intimately linked to mtDNA copy number. A fundamental part mitochondrial biogenesis is the replication of mtDNA, performed by POLG, alongside subunit POLG2 and Twinkle (TWNK). Transcription of mtDNA is performed by mitochondrial DNA-directed RNA polymerase (POLRMT) (Friedman and Nunnari, 2014, Gureev et al., 2019).

As with mitophagy, other mechanisms of mitochondrial homeostasis are poorly characterised in the preimplantation embryo. Aside from the work of Niu *et al* (2019) showing an elongated mitochondrial network in porcine embryos following PINK1 inhibition, followed by rescue via DMN1L overexpression (Niu et al., 2019), no reports exist on mitochondrial fission or fusion in this period. Knockout of both of these processes, fission via *DNM1L* KO and fusion via *MFN1* or *MFN2* KO, were embryonically lethal post-implantation (Chen et al., 2003, Wakabayashi et al., 2009, Ishihara et al., 2009). Similarly, a study on Peroxisome proliferator-activated receptor gamma coactivator-related protein 1 (*PPRC1*) KO mouse embryos found embryonic lethality after implantation only. PPRC1, alongside PPARGC1A and PPARGC1B make up the PGC-1 family of biogenesis regulators. *PPRC1* showed decreasing mRNA abundance between the 4-cell embryo and blastocyst, suggesting no mitochondrial biogenesis occurs in this period (He et al., 2012). Mitochondrial biogenesis is a highly complex process and analysis of a wider range of genes is required to elucidate any activity in the embryo. Although the above suggests that mechanism of mitochondrial homeostasis are not fundamental to preimplantation development, it does rule out that they are entirely inactive in the period.
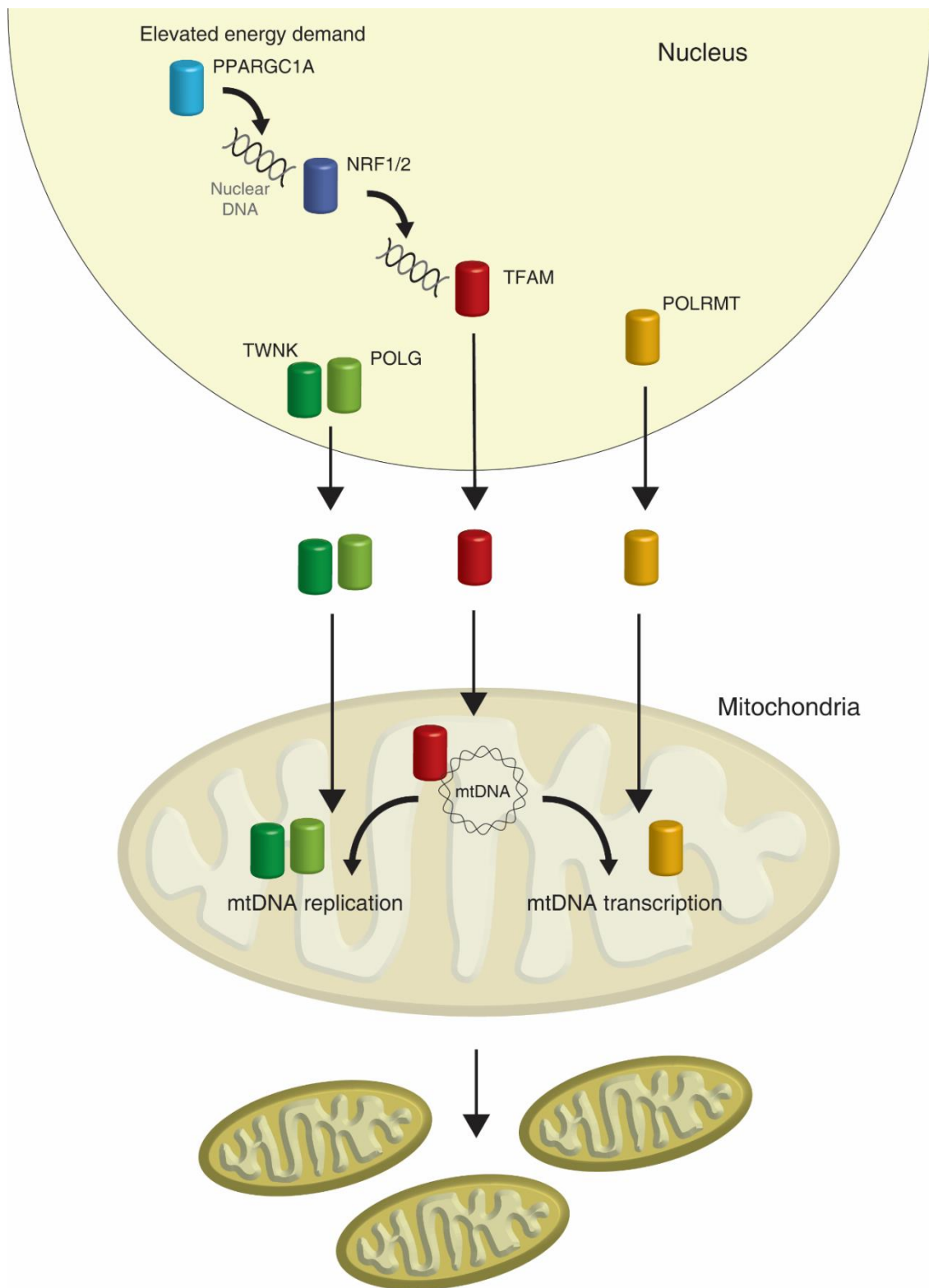
Figure 1.11. Mitochondrial biogenesis.

In response to elevated energy demand mitochondrial biomass and mtDNA copy number can be increased, coordinated by nuclear-mitochondrial DNA interaction. Mitochondrial biogenesis begins with upregulation of peroxisome proliferator-activated receptor gamma coactivator 1-alpha (*PPARGC1A*), the master regulator of the process. *PPARGC1A* promotes expression of nuclear respiratory factor 1/1 (*NRF1/2*), which in turn upregulate the expression of nuclear-encoded mitochondrial proteins, including transcription factor A, mitochondrial (*TFAM*). *TFAM* translocates to the mitochondria and binds mtDNA, promoting both its transcription and regulation. mtDNA replication relies of DNA Polymerase Gamma (*POLG*) and twinkle (*TWNK*), whereas transcription is performed by polymerase, mitochondrial (*POLMRT*).

Energy demand and mitochondrial network maintenance are linked, and so the onset of mitophagy or action of other mitochondrial maintenance mechanisms may be linked to changes in the metabolic demands and processes of embryos. Cellular metabolism can be divided into two branches: anabolism, the biosynthesis of new biomolecules, and catabolism, the breakdown of molecules to generate energy. The primary function of mitochondria is the supply of energy to the cell, which is primarily achieved via OXPHOS. OXPHOS can occur only under aerobic conditions. Following its transport into the cell via glucose transporters (GLUT), glucose is processed via a series of reactions to form pyruvate, also producing nicotinamide adenine dinucleotide + hydrogen (NADH), an electron carrier. In aerobic conditions, pyruvate is transported into the mitochondria and converted into NADH and acetyl coenzyme A (CoA) by pyruvate dehydrogenase (*PDH*). Acetyl CoA feeds the tricarboxylic acid cycle, where NADH is reduced and flavin adenine dinucleotide + H_2 ($FADH_2$) generated. NADH and $FADH_2$ then feed the ETC of OXPHOS (Figure 1.12) (Benard et al., 2010, Chaban et al., 2014).

OXPHOS is carried out along the mitochondrial inner membrane by a series of protein complexes. In brief, the electron carriers NADH and $FADH_2$ donate electrons to complexes I and II, which are transported across the ETC. This allows protons to be pumped across the mitochondrial intermembrane space forming an electrochemical gradient, which is harnessed enzymatically to generate ATP form ADP. Although all mtDNA encoded proteins are incorporated into OXPHOS, the vast majority of subunit components are encoded in nDNA (Benard et al., 2010, Chaban et al., 2014).

Glucose
Cell membrane
GLUT
Glucose

Glycolysis

Glucose
ATP
ADP
HK1

Glucose 6-phosphate

Hexose biosynthetic pathway

Oxidative pentose phosphate pathway

Glucosamine
ATP
ADP
GNK

Glutamine
GFAT
GPI

G6PD
NADP⁺
NADPH

Glucosamine-6-phosphate

Fructose 6-phosphate

6-phosphoclucono-nolactone

H_2O
H^+
6PGL

Acetly-CoA
CoA-SH
GNPNAT1

ADP
ATP
PKFM

6-phosphoglucco-nate

NADP⁺
NADPH
6PGD

N-acetylglucosamine-6-phosphate

Fructose 1,6-biphosphate

ALDOA

Ribulose-5-phosphate

PGM3

Glyceraldehyde 3-phosphate

Non-oxidative pentose phosphate pathway

N-acetylglucosamine-1-phosphate

NAD
NADH
GAPDH

RPE
RPI

UTP
PPi
UAP1

1,3-biphospho-glycerate

ADP
ATP
PGK1

Xylulose-5-phosphate

Ribose-5-phosphate

Nucleotides, coenzymes, DNA, RNA

Uridine diphosphate-N-acetylglucosamine

3-phospho-glycerate

TKT

PGAM

Xylulose-5-phosphate

Ribose-5-phosphate

Glyceraldehyde 3-phosphate

S7P

N-linked glycolysation (via MGAT)
O-linked glycolysation (via MGAT)
O-GlcNAc modification (via OGT)

2-phospho-glycerate

Xylulose-5-phosphate

E4P

Glyceraldehyde 3-phosphate

Fructose 6-phosphate

H_2O
ENO1

TALDO1

Phosphoenol-pyruvate

Glyceraldehyde 3-phosphate

S7P

E4P

Fructose 6-phosphate

ADP
ATP
PK

Mitochondria

Anaerobic glycolysis =x2ATP

Pyruvate

TCA cycle
OXPHOS
=32xATP

Aerobic glycolysis:
Cancer cells,
Blastocyst?

Figure 1.12. Cellular metabolism of glucose.

Glucose is imported by glucose transporters (*GLUTs*) and is converted into a series of metabolic intermediates (boxes), generating pyruvate. Aerobically, pyruvate is transported into mitochondria to feed the tricarboxylic acid cycle (TCA) cycle and oxidative phosphorylation (*OXPHOS*). Anaerobically pyruvate is converted to lactate by lactate dehydrogenase (*LDH*), producing reduced levels of ATP but more quickly. Glucose derivatives can be used to facilitate growth. The pentose phosphate pathway (red/orange) utilises glucose-6-phosphate to produce ribose-5-phosphate to enable nucleotide synthesis; with the oxidative branch producing ribulose-5-phosphate and the non-oxidative branch converting ribulose-5-phosphate to xylulose-5-phosphate and ribose-5-phosphate. Additionally, the non-oxidative branch, facilitated by transketolase (*TKT*) and transaldolase (*TALDO1*), can convert intermediates back into intermediates of glycolysis (Boxed). The hexose biosynthetic pathway (blue) derives from fructose-6-phosphate and glutamine, or from glucosamine, to produce uridine diphosphate-N-acetylglucosamine for protein modification. *6PGD*; 6-phosphogluconate dehydrogenase, *6PGL*; 6-phosphogluconolactonase, *ALDOA*; aldolase A, *E4P*; erythrose 4-phosphate, *ENO1*; enolase 1, *GAPDH*; Glyceraldehyde-3-Phosphate Dehydrogenase, *GNK*; N-Acetylglucosamine kinase, *GNPNAT1*; Glucosamine-Phosphate N-Acetyltransferase 1, *GPI*; Glucose-6-phosphate isomerase, *HK1*; Hexokinase 1, *PGK1*; Phosphoglycerate Kinase 1, *PGAM*; Phosphoglycerate mutase, *PGM3*; Phosphoglucomutase 3, *PKFM*; 6-phosphofructokinase, *RPE*; Ribulose-5-Phosphate-3-Epimerase, *RPIA*; Ribose 5-Phosphate Isomerase A, sedoheptulose-7-phosphate , *S7P*; *UAP1*; uridine diphosphate-N-Acetylglucosamine Pyrophosphorylase 1.

The process of anaerobic glycolysis can also provide energy without the need for oxygen, but does so with far less efficiency than OXPHOS. The reaction sees pyruvate converted into lactate via lactate dehydrogenase (LDH), generating only 2 ATP molecules, albeit far faster that OXPHOS can generate its output of 32 ATP molecules. Therefore, each having their own advantages, these two processes are active at different levels depending on different physiological demands and environmental conditions (Benard et al., 2010). Cancer cells have been noted to undergo the process of pyruvate conversion into lactate even in aerobic conditions, a phenomenon labelled aerobic glycolysis or the Warburg effect. The benefits of this are still unclear, but it has been suggested that these metabolic changes fuel cell growth (Lunt and Vander Heiden, 2011).

Studies on metabolism and how energy is generated or glucose processed in the preimplantation embryo have largely focused on the mouse. Evidence from the mouse and bovine models suggests the cleavage stage embryo is relatively metabolically inactive in comparison to the blastocyst; oxygen consumption, glucose uptake, ATP production and lactate production increased in the blastocyst stage (Thompson et al., 1996, Houghton et al., 1996, Sturmey and Leese, 2003). This would appear logical given the sudden increase pace of cellular division and necessity of ion pumps to maintain the blastocoel (Gardner and Harvey, 2015). A limited study on human embryos suggested that glucose uptake is higher on day 5 of development compared to day 4 (Gardner et al., 2011).

Glucose has been shown to be fundamental to the successful *in vitro* culture of mouse embryos beyond compaction of the morula (Brown and Whittingham, 1991). However, evidence from the mouse indicates that elevated glucose uptake is part an artefact of *in vitro* culture. Glycolysis occurred at a higher rate in mouse blastocysts after 24 h in culture compared to those developed *in vivo* (harvested directly from the reproductive tract and assayed immediately), as measured by resulting lactate in the media (Gardner and Leese, 1990). In culture with glucose as the sole energy substrate, mouse blastocysts showed a dramatic increase in their rate of glycolysis after only three hours in culture, demonstrating remarkable metabolic flexibility (Lane and Gardner, 1998). These lines of evidence illustrating the effect different culture conditions can have on embryo metabolism, and the disparity in metabolism between *in vivo* and i*n vitro* developing embryos.

Other evidence has suggested that embryos exhibiting a high level of glucose metabolism are less-viable for fetal development post-IVF, further supporting evidence that elevated glycolysis is an effect of *in vitro* culture (Lane and Gardner, 1996). It has been theorised that increased metabolic activity in the context of *in vitro* development is in fact a hallmark of embryos in a poorer state of health leading to reduced viability post clinical procedures, though the cause of this is unclear (Leese, 2002, Leese et al., 2007). Evidence in support of this includes reports that human embryos giving rise to a successful pregnancy following IVF showed a lower level of pyruvate consumption (Conaghan et al., 1993, Turner et al., 1994). Inhibiting OXPHOS via 2,4-*Dinitrophenol* or sodium azide enhanced development of bovine and porcine embryos to the blastocyst stage (Krisher et al., 1999). Other markers besides energy metabolism favour this hypothesis; human cleavage stage embryos with a lower level of amino acid turnover later successfully developed to blastocysts at a higher rate (Stokes et al., 2007). This hypothesis warrants further exploration, either in mouse or human embryos, to further define metabolic changes in embryos which subsequently fail to develop, and identify the precise causes of those metabolic changes.

Anaerobic and aerobic glycolysis is an inefficient means of energy production relative to OXPHOS, and oxygen consumption is also increased in the blastocyst. Thus it would be unlikely that glycolysis can make a significant contribution to ATP stores of the blastocyst. Indeed, it has been demonstrated that glycolysis in the mouse embryo is independent of oxygen levels, thus is not fluid in response to reducing OXPHOS activity (Lane and Gardner, 2005). This metabolic profile, and the fact that the blastocyst proliferates rapidly, have led to embryo metabolism being likened to the Warburg effect reported in tumour cells (Smith and Sturmey, 2013). This concept theorizes that when ATP is not limited, aerobic glycolytic activity may be elevated to supply intermediates to biosynthetic pathways such as the pentose phosphate pathway/shunt (PPP) and hexosamine biosynthetic pathway (HBP). When glucose was radioactively labelled in mouse embryo culture media, the same label was not present in lactate following culture. Although glucose supply is fundamental to *in vitro* blastocyst development, obstruction of glycolysis did not impair blastocyst development, suggesting glucose and its derivatives are more important as an intermediate other processes in the blastocyst (Vander Heiden et al., 2009, Chi et al., 2020).

The PPP branches from the first step of glycolysis, consuming glucose-6-phopshate (G6P) to form fructose 6-phosphate and glyceraldehyde 3-phosphate. Through a series of enzymatic reactions, NADPH and ribose 5-phosphate (R5P) are produced, and carbons fed back to

glycolysis. No ATP is produced via the PPP. However, *R5P* is a metabolite in nucleic acid synthesis, and NADPH is a reducing agent in the synthesis of nucleotides and amino acids. As such, both NADPH and *R5P* are fundamental to cell survival and proliferation. The PPP entails an oxidative and non-oxidative branch, both occurring in the cytosol. In the oxidative branch, glucose 6-phosphate dehydrogenase (G6PD) catalyses G6P conversion into 6-phosphogluconolactone (6PGN), with NADPH as a by-product. 6PGN is converted into 6-phosphogluconate (6PG) via 6-phosphogluconolactonase (6GPL). 6PG itself is converted into to ribulose 5-phosphate (Ru5P) by 6-phosphogluconate dehydrogenase (6PGD), producing another NADPH molecule (Kowalik et al., 2017, Ge et al., 2020).

The non-oxidative branch of the PPP consists of reversible reactions. Building on the chain of reactions in the oxidative branch, ribose 5-phosphate isomerase (RPI) can convert Ru5p to R5P, which is utilised in biosynthesis. Meanwhile, ribulose 5-phosphate epimerase (RPE) can catalyse xylulose 5-phosphate (Xu5P) conversion to R5P. Xu5P itself is generated via transketolase (TKT), which alongside transaldolase 1 (TALDO) is responsible for several reversible conversions of metabolic intermediates, allowing it regulate carbon flux between the PPP or glycolysis in accordance to cellular needs (Kowalik et al., 2017, Ge et al., 2020).

The HBP begins with F6P, and produces UDP-GlcNAc, a key component in protein modification. First, glutamine fructose-6-phosphate amidotransferase (GFAT) converts F6P and glutamine into glucosamine-6-phosphate and glutamate. Glucosamine-6-phosphate is also generated from glucosamine taken into by a cell by GlcNAc kinase (GBK), feeding the HBP. Glucosamine-6-phosphate and Acetyl-CoA are then converted into N-acetylglucosamine-6-phosphate (GlcNAc-6P) and CoA by glucosamine-phosphate N-acetyltransferase (GNPNAT). Subsequently, GlcNAc-6P is isomerised to form GlcNAc-1-phosphate (GlcNAc-1-P) by GlcNAc phosphomutase (PGM3/AGM1). Finally, UDP-GlcNAc is produced via UTP and the pyrophosphorylase (UAP1/AGX1) enzyme, also producing residual pyrophosphate for nucleotide metabolism. UDP-GlcNAc is required for O-GlcNAc modification of proteins, catalysed by O-GlcNAc transferase (OGT), as well as O- and N-linked glycosylation of proteins, the latter of which is catalysed by N-acetylglucosaminyltransferases (MGAT) (Akella et al., 2019).

The extent to which biosynthetic pathways are active has only been examined in the mouse, where metabolites of these pathways were abundant and derived from labelled glucose in

culture media (Chi et al., 2020). Analysis of gene expression relating to these pathways will begin to elucidate to what extent respective forms of metabolism are active in the human embryo.

1.11. Apoptosis in the preimplantation embryo

As mitophagy and other mechanisms may act to protect a cells mitochondrial network and ensure inheritance of healthy and functional mtDNA at a molecular, so too may mechanisms act to protect the embryo at the cellular level. The highest level of embryonic quality control would be whole embryo survival; embryos exhibiting too much dysfunction will fail to undergo the cell divisions and form blastocysts. At this scale, the process of apoptosis is likely to be important.

The process of apoptosis ensures the health of wider tissues via the removal of unnecessary or damaged cells without significant widespread damage and is implicated in the healthy development of a range of tissues. Briefly, apoptosis can be initiated by external or internal factors, referred to as the intrinsic or extrinsic pathway respectively. Both pathways ultimately lead to the activation of caspase proteins, of which caspase 3 (CASP3) and 7 dismantle the cell (Figure 1.13) (Singh et al., 2019).

Intrinsic apoptosis, mediated in large part by mitochondria and the physiologically dominant pathway, is primarily regulated by the B-cell lymphoma *2* (BCL-2) proteins. Modulation and interaction of pro- and anti-apoptotic proteins within family group determine a cells fate. Pro-apoptotic members of the group are promoted by stress and/or damage to a cell, and act either to induce formation of a mitochondrial permeabilisation pore (MOMP) or inhibit the inhibitors of apoptosis. The apoptosis inhibitors themselves act to sequester activator proteins which induce the MOMP. The result of a shift towards pro-apoptotic protein activity is the opening of the MOMP pore on the mitochondrial surface via BCL2 antagonist/killer 1 (BAK1) or BCL2 associated x, apoptosis regulator (BAX) proteins. This allows the release of further pro-apoptotic factors to the cytosol. These factors, key among them cytochrome c (CYTC), enable the activation of caspases (Singh et al., 2019).

The extrinsic pathway of apoptosis makes a lesser but still significant contribution to physiological apoptosis, especially in light of crosstalk between the two pathways. This pathway is activated by extracellular ligands (FasL, TRAIL, TNFα) which specifically activate associated transmembrane receptors of the tumour necrosis factor family (FGFRs, TNFRSF10A/B, TNFRSF1A). Once activated, these death receptors form a signalling complex incorporating FADD or TRADD and recruit caspases. In some cells the recruited caspases are sufficient to induce apoptosis. In others, CASP8 must activate BH3 Interacting Domain Death Agonist (tBID), which subsequently activates BAK or BAK1 to increase mitochondrial permeability (Singh et al., 2019).

Apoptosis in the healthy human preimplantation embryo was first evidenced by the incidence of fragmented nuclei of both the ICM and TE, and increased at day 7 of development compared to days 5 and 6. Importantly, no apoptosis was reported prior to blastocyst formation (Hardy et al., 1989, Hardy and Handyside, 1996). Later, using a combination of terminal transferase-mediated DNA end labelling (TUNEL) and electron microscopy, the absence of apoptosis in healthy cleavage stage human embryos was reported again, alongside evidence of apoptosis in morphologically unhealthy embryos identified by fragmentation of cellular components (Jurisicova et al., 1996).

Broader attempts to observe apoptosis in embryos have only been conducted in animal models. In the mouse, no apoptosis was detected via TUNEL staining in the 8-cell or morula, but was apparent in the blastocyst, similarly to human embryos (Brison and Schultz, 1997, Kamjoo et al., 2002). Both these studies also evaluated the effects of *in vitro* culture on blastocyst apoptosis. Although apoptosis did occur in *in vivo* developed blastocysts, a higher rate of apoptosis compared to *in vitro* developed blastocysts, suggesting apoptosis to be an artefact of *in vitro* development.
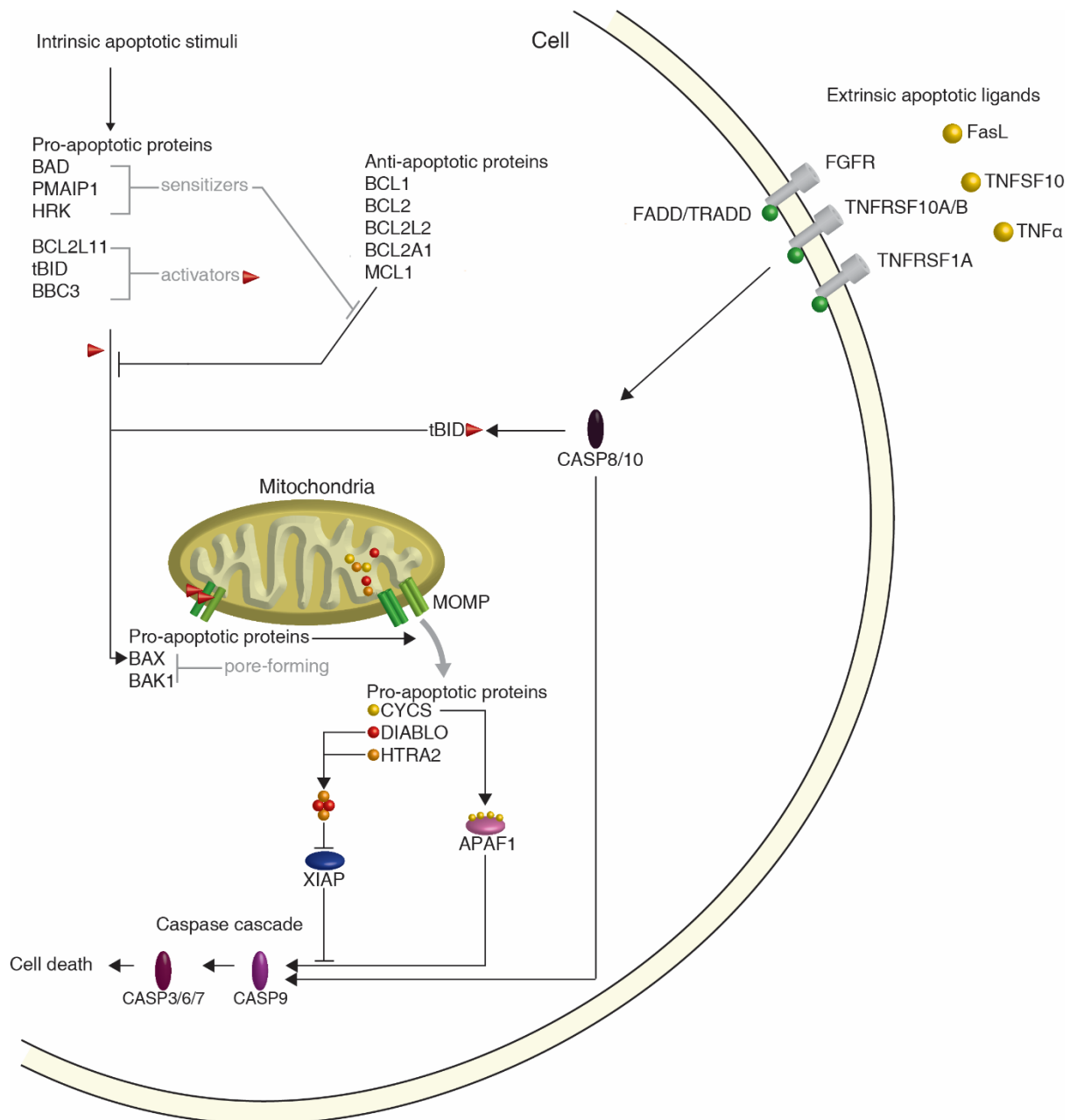
Figure 1.13. Intrinsic and extrinsic apoptosis.

Intrinsic apoptosis is initiated by cellular stress or damage signalling, and is a fundamental to development and tissue homeostasis. BCL2-like-11 (BCL2L11) and BCL2 binding component 3 (BBC3/PUMA) are upregulated, whereas BH3 interacting domain death agonist (BID) is truncated to form activated tBID. Negative regulator proteins act to bind and sequester peptides and are inhibited by pro-apoptotic sensitizer proteins. If negative regulators are saturated or insufficient, promoters of apoptosis activate BCL2 associated X, apoptosis regulator (BAX) and BCL2 antagonist/killer 1 (BAK1) to form mitochondrial outer membrane permeabilization (MOMP) pores. This allows release of the mitochondria-derived activator of caspase (DIABLO), HtrA serine peptidase 2 (HTRA2) and cytochrome c (CYCS). DIABLO and HTRA2 inhibit x-linked inhibitor of apoptosis (XIAP), which otherwise prevents caspase (CASP) activation. CYCS binds apoptotic peptidase activating factor 1 (APAF1), forming an apoptosome which activates CASP9, triggering the caspase cascade. Extrinsic apoptosis is triggered by extracellular signalling. Cell death ligands (FasL, tumor necrosis factor ligand superfamily member 10 (TNFSF10), tumour necrosis factor alpha (TNFα)) bind their associated receptors (fibroblast growth factor receptor (FGFR), tumor necrosis factor receptor superfamily member 10A/B (TNFRSF10A/B), tumor necrosis factor receptor superfamily member 1A (TNFRSF1A)), which recruit adapter proteins (fas associated via death domain/ TNFRSF1A associated via death domain (FADD/TRADD)). This complex activates caspases (CASP8/10) and in some cells activates the caspase cascade. In other cells, crosstalk between the two pathways is necessary to induce cell death, and relies upon activation of tBID. BAD; BCL2 associated agonist of cell death, BCL1; B cell lymphoma-1, BCL2L1; BCL2 like 1, BCL2L2; BCL2 like 2, BCL2A1; BCL2 related protein A1, HRK; harakiri, MCL1; induced myeloid leukemia cell differentiation protein, PMAIP1; phorbol-12-myristate-13-acetate-induced protein 1.

Further evidence for a lack of apoptosis in the cleavage stages has come from mice; when staurosporine was used to induce apoptosis in embryo cultures, a far higher dosage is required to induce apoptosis in 1 to 4-cell embryos compared to blastocysts and a variety of organ explants (Weil et al., 1996). The authors argue that mammalian cells all express constitutive apoptotic machinery and onset of programmed cell death await the expression of particular mRNA and proteins. Therefore, despite the presence of such machinery, cleavage stage mouse embryos would not undergo any form of apoptosis due to inappropriate gene expression.

In addition, measurements of apoptosis in the human preimplantation embryo have consistently reported an association with cellular lineage, with a higher degree of apoptosis occurring in the ICM (Hardy et al., 1989, Hardy and Handyside, 1996). The underlying causes of apoptosis specifically in the mouse epiblast was recently characterised. Epiblast cells failing to adequately express TEAD proteins, and thus associated pluripotency factors, were preferentially eliminated (Hashimoto and Sasaki, 2019). A range of studies have attempted to identify particular genes involved in the promotion and suppression of embryonic apoptosis, but no conclusive answers have been forthcoming. Utilising the scRNAseq dataset of Petropoulos *et al* (2017) will allow an unbiased analysis of apoptosis related gene expression in the human preimplantation embryo.

1.12. Age-related mtDNA variants and the oocyte

Ageing has a profound impact on the success of mammalian reproduction. In humans, as well as a decrease in general fertility, an increase in miscarriages and neonatal chromosomal abnormalities is widely reported, and a modest reduction in the capacity of zygotes to form blastocysts. This occurs in large part due to the effect of age on the oocyte, including changes to mitochondrial activity (Cimadomo et al., 2018). Oocyte mitochondrial regulation of Ca^{2+} signalling, ROS and efficient energy metabolism is vital for several key processes of the oocyte; germinal vesicle breakdown, and microtubule assembly and disassembly (Cimadomo et al., 2018). In the ageing human oocyte, changes to mitochondrial morphology have been reported (Müller-Höcker et al., 1996) and membrane potential is reported to change progressively (Wilding et al., 2001), consistent with impaired mitochondrial function. Similarly, in mice, oocytes of aged mice have been shown to be deficient in energy metabolism, have a lower membrane potential, develop to blastocyst at a lower rate compared to controls (Thouas et al.,

2005). Furthermore, a reduction in stored Ca^{2+}, a dysregulation of Ca^{2+} signalling and the oscillation of intracellular Ca^{2+} fluctuations has been reported (Haverfield et al., 2016, Szpila et al., 2019), which could in part be explained by dysfunctional mitochondria. These factors may give rise to impairments in energy metabolism and key processes of fertilisation, the cell cycle, development and implantation. In part, the impairments may present due to an accumulation of mtDNA variants.

Deficiencies in OXPHOS are generally accumulated with age in the healthy population in a variety of somatic tissues. At least in part, these defects are caused by the acquisition of mtDNA variants, including variants which are associated with mtDNA disease, and which have the potential to clonally expand over time. Most evidence suggests these arise due to deficiencies in the mtDNA proof-reading enzyme *POLG* (Larsson, 2010). It is unclear if the acquisition of mtDNA variants occurs in the oocyte. However, given the oocytes long quiescent period, lasting from early development until puberty, the oocyte becomes one of the oldest cells in the adult body (Figure 1.14) (Pan and Li, 2019), proving a long period wherein variants could accumulate. It has been shown mothers of more advanced age give birth to offspring carrying more *de novo* variants (Rebolledo-Jaramillo et al., 2014), and similar phenomenon is reported in the oocytes of aged women albeit at low levels of heteroplasmy (Yang et al., 2020). Analysis of human oocytes has derived from a clinical IVF setting, therefore limiting the extent to which analysis can be extrapolated to women without reproductive challenges. Earlier studies are further limited by the fact they report on a singular variant and an outdated technical approach. A 4977 bp deletion commonly associated with mtDNA has been demonstrated to both not accumulate in aged oocytes compared to young (Keefe et al., 1995), and accumulate (Chan et al., 2005). A single point variant m.414T>G was shown to be more frequent in oocytes of older women (Barritt et al., 2000). However, these studies make no measurement of relative frequency to wildtype. In a more unbiased study, human oocytes did not acquire variants above 2% heteroplasmy in comparison to younger oocytes, but the technical limitations of this approach mean low level heteroplasmies could be excluded. Furthermore, the aged of oocyte was determined biochemically, which may have less impact on the acquisition of variants than chronological time (Boucret et al., 2017).
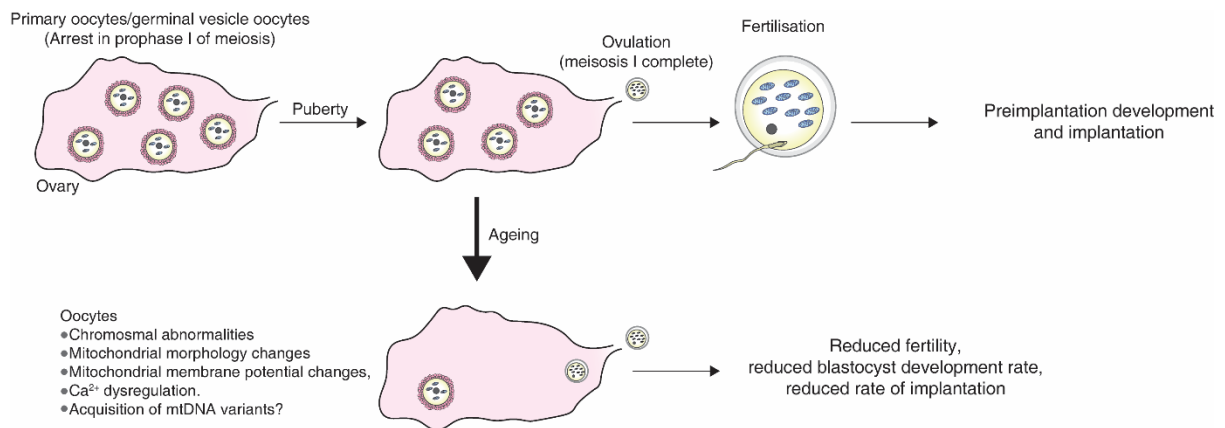
Figure 1.14. Oocyte arrest and ageing.

Primary oocytes are arrested in prophase I of meiosis I from early development until the onset of puberty. During ovulation, an oocyte completes meiosis 1 and is released from the oocyte, enabling fertilisation. In ageing, as well as diminished ovarian reserve, oocytes lose potential for fertility with reduced rates of blastocyst development and successful implantation. In large part this can be attributed to increased rates of chromosomal abnormalities, However, impairment of mitochondrial morphology and functions are reported, which could be explained by the acquisition of *de novo* mtDNA variants during the prolonged prophase I arrest.

Conflicting evidence exists in attempt to identify whether the acquisition of ageing-related mtDNA variants in human somatic cells is conserved in mice, with an accumulation shown to be present (Pikó et al., 1988, Tanhauser and Laipis, 1995), and absent (Ma et al., 2018). Nonetheless, a recent study in mice using more stringent sequencing methods revealed an accumulation of mtDNA variants in the oocytes mice aged 10 months, albeit at low heteroplasmy (Arbeithuber et al., 2020).

The effect of an accumulation of mtDNA variants could be made more complex by the presence of an inherited pathogenic variant, as both may contribute to declining oocyte health. It has been demonstrated that a mouse with a pathogenic 4696bp mtDNA deletion introduced through cytoplast transfer had lower heteroplasmy across oocytes harvested in advanced age, suggesting this variant contributed to premature oocyte death of those with a high mutation load (Sato et al., 2007). A similar effect manifested in mice with two wildtype mtDNA genomes generated via cytoplast transfer where numerous mtDNA bases differed between alleles (Latorre-Pellicer et al., 2019). The *tRNAala* mouse presents the opportunity to explore this phenomenon further through next-generation sequencing (NGS).

2. Aims and hypotheses

Using a combined experimental and bioinformatics approach, I aim to explore mitochondrial biology in early development. In particular, I will focus on mitophagy, the mechanisms underlying its onset, and its wider role or impact.

1) Utilise a large scRNAseq dataset from across human preimplantation development to analyse gene expression relating to mitophagy and mitochondrial functions, with a focus on cellular health and mitochondrial quality control. I hypothesise this will allow identification of key genes in preimplantation embryo mitophagy, allowing establishment of a method of manipulating mitophagy. Furthermore, potential roles for mitophagy in the blastocyst will be identified.

2) Explore the segregation of heteroplasmy in the preimplantation embryo of the *tRNAala* mouse, specifically in the period of mitophagy uncovered by the lab, and the effect of mitophagy on intercellular variation of heteroplasmy. I hypothesise intercellular variation of heteroplasmy will be elevated in the blastocyst relative to the 8-cell embryo, and manipulation of mitophagy will alter this segregation of mtDNA.

3) Explore the effect of ageing on the accumulation of mtDNA variants in the *tRNAala* mouse oocyte, and the effect of both germline pathogenic and acquired variants on oocyte survival. I hypothesise that oocytes carrying high levels of a pre-existing pathogenic mtDNA mutation will be absent from aged mice, suggesting a selection mechanism acts against those oocytes.

3. Methods

3.1. Mouse management and tissue harvesting

Mice were housed at the Functional Genomics Unit, Newcastle University and all procedures were approved by a local Ethical Review Committee and licenced by the Home Office under the Animal (Scientific Procedures) Act 1986. Progenitor *tRNAalanine* (*tRNAala)* mice were kindly provided by Dr James Stewart, Max Planck Institute for Biology of Ageing, Cologne, Germany. Ear tissue was collected from *tRNAala* mice at approximately 3 weeks of age for genotyping. Only mice showing heteroplasmy of 70% or higher were bred for colony maintenance.

Germinal vesicle (GV)-stage oocytes were harvested by puncturing ovaries with 29G needles in M2 media (Sigma) supplemented with 200 µM 3-isobutyl-1-methylxanthine (IBMX, Sigma). Cumulus cells were removed by repeatedly aspirating and expelling oocytes using a 75 µm denudation pipette (Cooper Surgical).

For embyro harvest, female mice were super ovulated by intraperitoneal injection of 5 IU of pregnant mare's serum gonadotropin (PMSG, Intervet) followed by intraperitoneal injection of 5 IU of human chorionic gonadotrophin (hCG, Intervet) 44–48 hours later. Female mice were then caged with male mice overnight. The following morning female mice were inspected for a vaginal plug to indicate the mice have mated.

If a plug was present, female mice were sacrificed by cervical dislocation and the ovaries, oviduct and uterus removed and placed into M2 media (Sigma-Aldrich - M7167).under an inverted microscope, the oviduct was gently split using an insulin needle to release embryos at zygote stage. Embryos were moved into a 50 µl M2 10% hyase (Vitrolife Ltd -10017) drop to remove cumulus cells.

Embryos were cultured in KSOM-AA media (Sigma-Aldrich - MR-101) drops overlaid with mineral oil (Sigma-Aldrich - M5310), in a 35mm petri dish in a humidified incubator at 37°C with 5% CO_2. Culture drop size was 2 µL media per embryo. All KSOM media was equilibrated in the same incubator overnight before embryo harvest. For embryo cultures containing a

pharmacological agent embryos were staged, and once morula embryo was identified the agent was added. Images for tracking embryo development were captured via OCTAX eyeuSB2 camera.

3.2. Microinjection of zygotes

Microinjection pipettes were prepared by pulling 780um inner diameter capillary tubes (Harvard Apparatus) via micropipette puller (Sutter P-97) to form two straight microinjection pipettes. A 30⁰ bend was then formed below the pipette tip via microforge (Narishige MF-900). Microinjections were performed with zygotes in M2 media on Nikon TE2000U with micromanipulators for both a holding pipette and microinjection pipette (Narishige), using a Narishige IM-300 to produce specific microinjections of around 3-4% size of the zygote.

Microinjections utilised piezo-impact unit (PM150FU, Prime-tech) to facilitate piercing of the zygote. Microinjection pipettes were back-filled with 20 µl of Fluorinert FC-770 (Sigma), before being front-filled with the microinjection mRNA. Once microinjection pipette invaginated a zygote, a piezo pulse was applied followed by injection pressure. Following microinjection zygotes were immediately returned to KSOM-AA.

3.3. Imaging matrix-mito-QC probe

A matrix-mito-QC probe was adapted from mito-QC (Allen et al., 2013), modified to translocate to the mitochondrial matrix (Dr. Magomet Aushev). Imaging was performed via Zeiss LSM 880 with Airyscan (a serial array of 32 GaAsP detectors), with the chamber maintained at 37°C and 5% CO_2. Images were captured using the Plan-Apochromat 40x/1.3 oil DIC UV-IR M27 (Zeiss). Fluorescence was captured using multibandpass filters: Filter Set 38 HE (Zeiss) for 488nm and Filter Set 43 HE (Zeiss) for 561 nm. Lasers used were as follows: 25-mW 458/488/514nm Argon Laser (Zeiss) and 561 DPSS 561-10 Laser (Zeiss). Emission was collected using the Airyscan detector. Wherever possible imaging was performed with consistent laser power, gain and zoom. Z-stack imaging was captured at intervals of 0.5 um. Image processing was performed via Zen Black 2.3 using the "Airyscan Processing" function to improve spatial resolution by applying a Wiener filter and pixel re-allocation, then Fiji. Image quantification utilised the mito-QC Counter tool (Montava-Garriga et al., 2020), with default Fiji

thresholding on the red channel. Only the lower half of a Z-stack was quantified as samples were large. As a result, the upper half of embryos could not be imaged with adequate focus inside the working distance of the objective lens.

3.4. Embryo micromanipulation

Embryo disaggregation was performed under an Olympus IX73 microscope (Research Instruments) in a 60 mm petri dish with media overlayed with mineral oil. 8-cell and morulae embryos were incubated in pronase (Sigma) for 5mins, then placed in drops of G-PGD supplemented with 5% HSA-solution (Vitrolife). 8-cell embryos were repeatedly drawn into a 35 µm inner diameter blastomere biopsy pipette (Origio) to dissociate single cells. Morula were repeatedly drawn into 30 µm and 25 µm inner diameter biopsy pipettes (Origio). Single cells were washed through PBS (ThermoFisher) and isolated in 0.5ml tubes using a 128 µm inner diameter denudation pipette (Vitrolife), then flash frozen in dry ice.

For 8-cell embryo single cell biopsy, 8-cell embryos were placed in drops of G-PGD (Vitrolife) supplemented with 5% HSA-solution (Vitrolife), and biopsy mode of a Saturn 5 laser (Research instruments) used to create an opening in the zona pellucida. A 30 µm inner diameter bevelled blastomere biopsy pipette was inserted and a single blastomere drawn out. Single cells were washed through PBS (ThermoFisher) and isolated in 0.5ml tubes using a 128 µm inner diameter denudation pipette (Vitrolife), then flash frozen in dry ice. Remaining 8-cell embryos were washed through KSOM and returned to culture.

Blastocysts were placed in drops of G-PGD (Vitrolife) supplemented with 5% HSA-solution (Vitrolife) and secured in place using a holding pipette and 20 µm inner diameter blastomere biopsy pipette (Origio). Biopsy mode of a Saturn 5 laser was used to separate the inner cell mass (ICM) from the polar trophectoderm (TE). ICM and TE portions were incubated in TrypLE (ThermoFisher) for 5-10 mins. Portions were washed through PBS and transferred to G-PGD (Vitrolife) supplemented with 5% HSA-solution (Vitrolife), then drawn repeatedly into 20 µm inner diameter blastomere biopsy pipette and 16 µm inner diameter polar body biopsy pipette. Single cells and clumps of cells were washed through PBS (ThermoFisher) and isolated in 0.5 ml tubes using a 128 µm inner diameter denudation pipette (Vitrolife), then flash frozen in dry ice.

3.5. Molecular Cloning

Molecular cloning was used to generate DNA constructs of matrix-mito-QC and 34/35 phosphorylated isoform of BNIP3L (pBNIPL, designed by Dr. Yuko Takeda). Plasmids were streaked via sterile loop across LB agar plates with 100 µg/ml ampicillin and cultures for 16-18 hours at 37ºC. Single colonies were used to inoculate 2ml of antibiotic-supplemented LB broth and cultured for 16-18 hours. Bacterial cultures were centrifuged for 5 mins at 10,000 RPM before DNA was isolated via Wizard SV Mini-prep kit (Promega) according to manufacturer's instructions. PCR fragments, either matrix-mito-QC or pBNIP3L DNA, were amplified using Q5 PCR Kit (NEB) according to manufacturer's instructions. PCR product was cleaned via Macherey -Nagel™ NucleoSpin™ Gel and PCR Clean-up Lit (Macherey-Nagel) as per manufacturer's instructions, and concentration measured via NanoDrop™ (ThermoFisher). The amplified DNA of genes of interest were ligated into the pGEM®-T Easy Vector system (Promega) via In-Fusion® HD Cloning kit (Takara) as per manufacturer's instructions. Post ligation, 2.5 µl of each reaction was used to transform Stellar Competent Cells (ThermoFisher) according to manufacturer's instructions, and then plated on LB agar plates with 100 µg/ml ampicillin and cultured for 16-18 hours at 37ºC. Colony screening was performed using the OneTaq polymerase (NEB) according to manufacturer's instructions. Positive clones were used to inoculate 2ml of antibiotic-supplemented LB broth and cultured for 16-18 hours. Bacterial cultures were centrifuged for 5 mins at 10,000 RPM before DNA was isolated via the Wizard SV Mini-prep kit (Promega) according to manufacturer's instructions. Glycerol stocks were prepared for all constructs, consisting of 1330 µl miniprep culture and 570 µl 50% glycerol (Sigma) in cryogenic vials (ThermoFisher). The mixture was vortexed and stored at -80ºC.

3.6. *In Vitro* Transcription

For the generation of mRNA from constructs, 2 µg of plasmid DNA was first linearised using either PacI or AscI according to manufacturer's instructions. 2 µl of 10mg/ml proteinase K and 5 µl of 10% SDS were added and reaction incubated at 50ºC for 30 mins. The reaction was madeup to 150 µl with DEPC-treated water, then 150 µl phenol:chloroform:isoamyl alcohol added. The reaction was mixed thoroughly to form an emulsion, then centrifuged at 15,000 RPM for 1 mins. The top phase of this reaction was collected and chloroform was added at a 1:1 ratio. The reaction was thoroughly mixed and centrifuged at max speed for 1 mins. Theupper phase was again collected, and mixed with 1 µl 20 mg/ml glycogen, 15 µl 3M sodium

acetate (pH 5.2) and 300 µl 100% ice-cold ethanol. The reaction was placed at -80ºC overnight, then centrifuged for 15 mins at room temperature. The supernatant was discarded. The pellet was briefly spun and residual ethanol discarded, then the pellet was allowed to dry for approximately 5 mins. The pellet was then re-suspended in 6 µl of nuclease-free H_2O.

Working under RNAase free conditions, *in vitro* transcription was performed with the mMessage mMachine T7 kit (Ambion) according to manufacturer's instructions, followed by 15 mins Turbo DNase treatment. mRNAs were poly-A tailed via Poly A Tailing Kit (Ambion) according to manufacturer's instructions. The mRNA was made up to 100 µl with DEPC-treated water and purified via RNeasy micro kit (Qiagen) according to manufacturer's instructions. RNA was quantified using a nanodrop (ThermoFisher) and diluted to 2000 ng/µl in DEPC water, then stored at -80ºC.

3.7. Tissue homogenisation

Ear tissue of mice was lysed in 250 µl lysis buffer (10mM pH 8.5 Tris-HCl, 1% SDS, NaCl, 5 mM EDTA and 0.1 mg/ml proteinase K) overnight at 55°C. The reaction was then heated to 95°C to inactivate proteinase K. 250 µl phenol:chloroform:isoamyl alcohol was added. The reaction was mixed thoroughly to form an emulsion, then centrifuged at 15,000 RPM for 5min. The top phase of this reaction was removed, and isopropanol was added at a 1:1 ratio, and 2 µl 20 mg/ml glycogen was added. Samples were mixed thoroughly and centrifuged at max speed at 4ºC. Supernatant was discarded and 500 µl of 70% Ethanol added. Reaction was centrifuged for 5 mins at max speed at room temperature. Supernatant was discarded and pellet allowed to dry for approximately 5 mins. The pellet was then re-suspended in 20 µl of nuclease-free H_2O.

3.8. Cell Lysis

Single cells and clumps of cells were lysed overnight in 10 ul lysis buffer (50mM pH 8.5 Tris-HCl, 1% Tween-20 and 0.2 mg/ml proteinase K) at 55°C in a Veriti™ 96-Well Thermal Cycler (Veriti). The reaction was then heated to 95°C to inactivate proteinase K.

3.9. Amplification of mouse mtDNA

Amplification of mtDNA was performed before sequencing protocols. For pyrosequencing, a ~200bp region of mtDNA containing m.5024C>T was amplified. For NGS, either the whole mtDNA genome, or a ~3000bp region of mtDNA containing m.5024C>T was amplified. PCR primers were designed to amplify portions of the C57BL/6NJ genome (CM004277.1) (Table 3.1). Primers for pyrosequencing amplification were supplied by Prof. Robert Taylor. Primers for two fragment amplification of oocyte whole mtDNA were sourced from literature (Ma et al., 2018). Other primers were designed in house. Pyrosequencing amplification used GoTaq® G2 Hot Start Taq Polymerase (Promega) as per manufacturer's instructions. Ear lysates used 1 µl, while embryonic clumps and single cells used 10 µl template. Amplification for NGS used PrimeSTAR GXL DNA polymerase (Takara) as per manufacturer's instructions. Amplification of oocyte mtDNA used two overlapping fragments with 4.5 µl template each. Amplification of blastocyst single cell mtDNA used five overlapping fragments, with 1.8 µl template each. Successful amplification of PCR products was verified via separation on a 1% (w/v) agarose gel made with 1g agarose powder (Bioline) and 100ml 1x Tis-acetate-EDTA buffer (Formedium), prestained using SYBR Safe DNA Gel Stain (Thermo Scientific). Orange G loading dye (Promega) was added to PCR products before loading, and Sci 1kb plus ladder (ThermoFisher) loaded. Gels were visualised using ChemiDocä XRS+ Imaging Systems (BioRad) with Image Lab software (BioRad).

Fragment	Forward Primer	Reverse Primer	Annealing T°C	Region
Pyrosequencing				
Amplification	ATACTAGTCCGCGAGCCTTCAAAG	[BIO]GAGGGTTCCGATATCTTTGTGATT		4963-5381
Conditions: Initial activation 95°C for 2 mins; denaturation 95°C for 30 s, annealing 62°C for 30 s, extension 72°C for 30 s, 35 cycles (ear tissue) or 40 cycles (embryonic tissue/cells); final extension 72°C for 10 mins.				
NGS				
Two fragments: A	GGATCCTACTCTCTACAAAC	TAGTTTGCCGCGTTGGGTGG		3222-11423
Two fragments: B	CTACCCCCTTCAATCAATCT	CCGGTTTGTTTCTGCTAGGG		11271-3335
Conditions: Initial activation 94°C for 5 mins; denaturation 94°C for 30 s, annealing 56°C 20 s, extension 68°C 7 mins with 40 cycles; final extension 68°C for 5 mins.				
Five fragments: A	CTCTTCACACAAACATAACCAC	GCTGAATTAGCAAGAGATGG	55	13609-676
Five fragments: B	AGAGAACTACTAGCCATAGC	TGGTGCTGGATATTGTGATTAC	65	556-3840
Five fragments: C	TTATCCACGCTTCCGTTACG	TCGTAGCTTCAGTATCATTGG	61	3578-7338
Five fragments: D	TCCAACTTGGTCTACAAGAC	GTAGGTTGAGATTTTGGACG	55	7026-10162
Five fragments: E	ACCATCTTAGTTTTCGCAGC	ATGATGTTGGAGTTATGTTGG	55	10060-13685
Conditions: Initial activation 94°C for 5 mins; denaturation 94°C for 30 s, annealing 20 s, extension 68°C 4.5 mins with 40 cycles; final extension 68°C for 3 mins.				

Table 3.1. Primers and conditions for amplification.

Primers in a five overlapping fragment format used differing annealing temperatures.

3.10. Pyrosequencing

Pyrosequencing was performed on the PyroMark Q24 system according to the manufacturer's instructions. Quantification of the heteroplasmy level was achieved using PyroMark Q24 v2.0.8 to directly compare the relevant peak heights of both the wild-type (C) and polymorphic (T) nucleotides at the 5024 position. For ear tissue 10 µl PCR product was sequenced, for single cell PCR products 15 µl was sequenced. Pyrosequencing primer was AAGTTTAACTTCTGATAAGG.

3.11. NGS and variant analysis

Amplicons were purified via AMPure XP beads (Beckman Coulter Life Sciences) as per manufacturer's instructions, and quantified via Qubit 2.0 fluorimeter (Life Technologies). The Broad Range Assay kit was used to quantify samples with a concentration above 2 ng/µl, and High Sensitivity Assay kit for samples below this concentration. In the case of a two or five fragment protocol, amplicons of a cell were pooled at equal concentrations. NGS libraries were prepared using the Illumina Nextera XT DNA Library Preparation Kit with Nextera XT Index Kit v2 Set A (Illumina) as per manufacturer's instructions by Dr Angela Pyle (NUTCRI, Newcastle University). Pooled amplicons were 'tagmented', amplified, cleaned, normalized and pooled in equimolar concentrations for library preparation. The size of the libraries was verified using an Agilent 2200 Tape Station and software, with Agilent High Sensitivity D5000 Screen Tape. The range for optimal library was set to 200 bp up to 1.5 kb. Concentration of the library preps were measured using the Qubit dsDNA Broad Range Assay kit. Sequencing of the libraries was performed by Rafiqul Hussain (Genomics Core Facility, NUBI, Newcastle University). Pooled libraries were sequenced using MiSeq Reagent Kit v3.0 (Illumina) and the MiSeq sequencing platform (Illumina) in paired-end, 250 bp reads.

Post-run FASTQ files passing QScore thresholds were analysed using an in-house-developed bioinformatic pipeline by Dr. Gavin Hudson and Dr. Fiona Robertson (NUBI, Newcastle University, Figure 3.1). Duplicates were removed via Picard v2.2.4 (http://broadinstitute.github.io/picard/) and reads aligned to the mouse mtDNA reference genome (NC_005089.1) using BWA v0.7.15 invoking –mem36 for long read alignment. Aligned reads were sorted and indexed using Samtools v1.3.1. Variant calling was performed

in tandem using VarScan v2.4.3 (minimum depth=1,500, supporting reads=10, base-quality=>30, mapping quality=>20 and variant threshold=1.0%), then compressed and indexed via BCFtools (http://samtools.github.io/bcftools/bcftools.html). Variants were annotated using Ensembl VEP (Variant Effect Predictor, Ensembl). Heteroplasmic variants are defined as >1% minor allele frequency. Our previous work using this method showed that variants present at >1% heteroplasmy were highly likely to have been present in the original DNA sample, and unlikely to be artefacts. In-house Perl scripts were used to extract base/read quality data and coverage data. Mutation rate in oocytes was calculated via number of heteroplasmic positions divided by base pairs sequenced. Mutation rate was calculated for two thresholds; heteroplasmies between 1% and 98% and between 2% and 98%. Heteroplasmies underneath primer binding sites were disregarded.
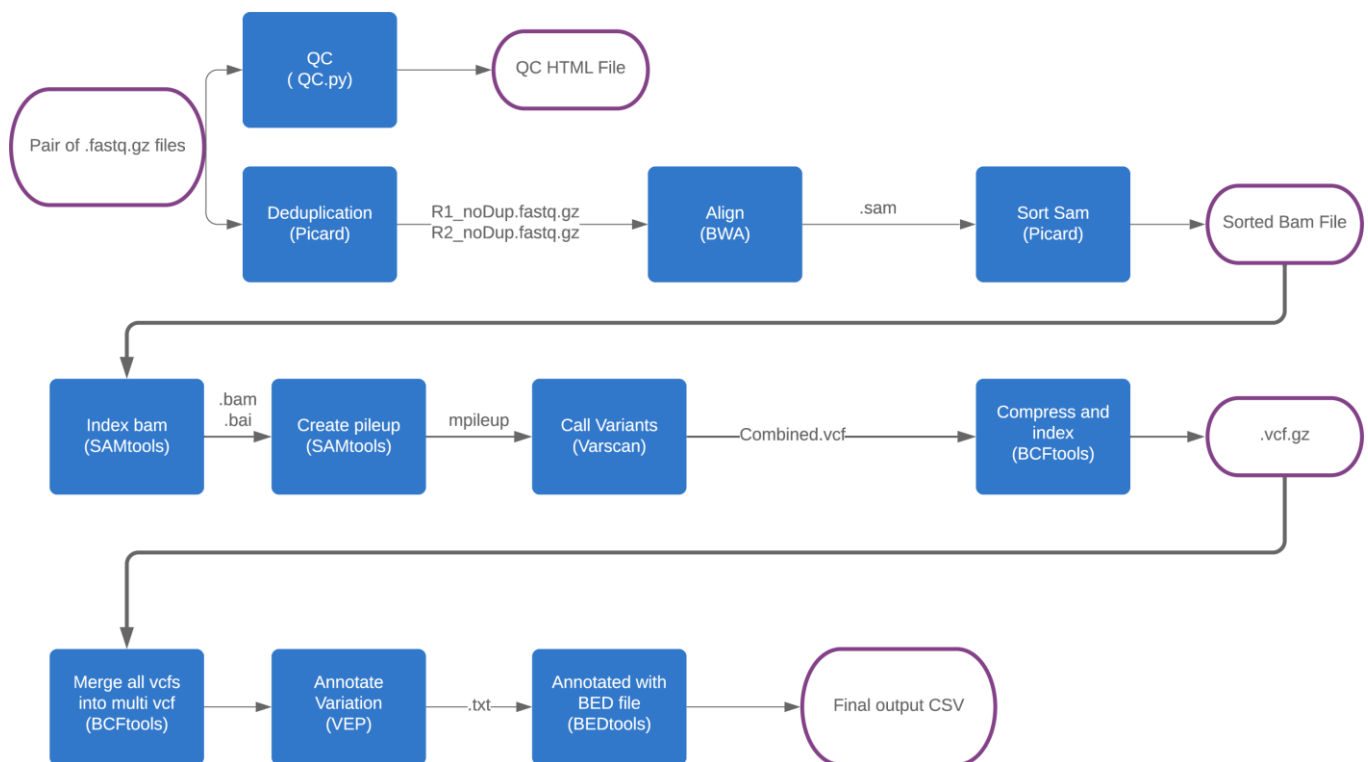
Figure 3.1. Mitochondrial genome sequence analysis pipeline.

Flow diagram depicts the steps of analysis, including file conversions and software used. Schematic supplied by Angela Pyle/Gavin Hudson.

A Ka/Ks ratio for mtDNA variants was calculated by calculating the ratio of the number of variants causing amino acid replacements per possible sites (Ka) to the number of silent variants per possible sites (Ks), adding a numerical constant (1) to Ks to avoid dividing by 0 (Mishmar et al., 2003). A Ts/Tv ratio was calculated by calculating the ratio of transition variants to transversion variants.

3.12. RNAseq data processing and gene expression analysis

Raw single cell RNA sequencing (scRNAseq) FASTQ files (Petropoulos et al., 2016), post cell-quality filtering, were downloaded from the EBI ArrayExpress data repository (n=1529) (Accession - E-MTAB-3929). Two quality control pipelines, Celloline and Cellity (Ilicic et al., 2016), were used to further identify and remove abnormal cells. Data was re-mapped to the human reference genome GRCh38using salmon (https://combine-lab.github.io/salmon/). Data was filtered to remove genes with high occurrence of 0 values. Data was normalised via Limma (https://academic.oup.com/nar/article/43/7/e47/2414268) using a model accounting for cell lineage, embryo of origin, sex, and day of development.

Biological process gene ontologies as defined by ensembl were selected based on their relevance to mitochondrial biology. For analysis, expression of the genes constituting an ontology were averaged for each cell. For gene expression data relating to both pathways and specific genes, ANCOVA was performed with respect to day of development and cellular lineage, accounting for sex, embryo of origin and day/lineage, via R. For significantly variable measurements Tukey HSD analysis was performed via R base functions. Differentially expressed (DE) genes were identified between day and lineage groups utilising a model accounting for the same parameters as above using Limma. An absolute logFC threshold of 1.5 and FDR corrected statistical significance of 0.05 were used in identifying significant DE genes. Correlations were analysed using the R corrplot package.

3.13. RNAseq variant analysis

Raw PNT blastocyst scRNAseq FASTQ files were sourced via an open source archive of genomic data (Hyslop et al., 2016). Files were processed in accordance with GATK best practice guidelines for variant calling with RNAseq (Van der Auwera et al., 2013). FASTQ files

were mapped to the human reference genome GRCh38 using STAR (Dobin et al., 2012) with a two-pass method. The resulting SAM files were grouped via Picard (http://broadinstitute.github.io/picard/), and converted to BAM files. Pileup files were generated via Samtools and annotated.

3.14. Statistical analysis

Base R v.4.0.5 functions where used to conduct statistical analysis using RStudio.

4. *In silico* characterisation of mitophagy and mitochondrial metabolism in the preimplantation embryo

4.1. Introduction

Recent work has uncovered the occurrence of mitophagy in the preimplantation embryo of the mouse and human (Chapter 1), but the precise mechanisms underlying this mitophagy and its role in the embryo requires characterisation. Mitophagy is the process by which mitochondria which are damaged, dysfunctional or excess to cellular demands are degraded. Mitophagy is typically described in the terms of several semi-distinct pathways, which are active under different conditions. The PTEN-induced putative kinase 1 (*PINK1*)/Parkin (*PRKN*) pathway is most often associated with the removal of damaged mitochondria. The two other best characterised pathways, the BCL2 Interacting Protein 3 (*BNIP3*)/*BNIP3*-Like Protein 3 XL (*BNIP3L*) and the FUN14 Domain Containing 1 (*FUNDC1*)/PGAM Family Member 5 (*PGAM5*) pathways, are most frequently associated with hypoxia and developmental process (Rodger et al., 2017). Access to a large open source dataset of single cell RNA sequencing (scRNAseq) derived from human preimplantation embryos presents the opportunity to begin elucidating blastocyst mitophagy through analysis of the human transcriptome (Petropoulos et al., 2016).

RNA sequencing (RNAseq) has significant advantages over preceding methods in transcriptomics; RNAseq can be conducted in a high-throughput workflow whilst measuring expression of the whole transcriptome across a much larger dynamic range, and reports less background noise (Wang et al., 2009). Arising from bulk RNAseq methods, single cell RNAseq (scRNAseq) was first reported in 2009 (Tang et al., 2009). This technology was more recently applied in a large number single cells of the human preimplantation embryo to explore the timing and nature of cellular lineage allocation (Petropoulos et al., 2016).

Analysing changes in gene expression during the period when mitophagy begins will allow identification of candidates for manipulation, and guide further work in characterisation of embryo mitophagy. Furthermore, upregulation of the same candidate may prove useful in the process of optimising pronuclear transfer (PNT), where mitophagy could be upregulated in early developmental tissues to reduce carryover of mutated mitochondria to a donor zygote (Hyslop et al., 2016).

Intriguingly, the onset of mitophagy coincides with other changes in the blastocyst which may offer clues as to the impact of mitophagy. In human embryos, apoptosis is reported to begin in the blastocyst, and is elevated in the inner cell mass (ICM) (Hardy et al., 1989, Hardy and Handyside, 1996). Relationships between mitophagy and the promotion and inhibition of apoptosis have been reported (Kubli and Gustafsson, 2012, Wanderoy et al., 2021), raising the question of whether the two are related in the blastocyst. Similarly, embryo metabolism and the demands of cells of the blastocyst undergo dramatic changes in comparison to the preceding cleavage stage embryos (Thompson et al., 1996, Houghton et al., 1996, Trimarchi et al., 2000, Sturmey and Leese, 2003). The regulation of the mitochondrial network is linked to these same demand (Montava-Garriga and Ganley, 2020), opening the possibility that mitophagy is a response to this. Analysis of the genes involved in the processes and their relationship with mitophagy genes may offer clues as to the impact of mitophagy.

The process of blastocyst cell lineage establishment begins in this period, driven by expression of specific transcription factors, forming cells of the trophectoderm (TE), primitive endoderm (PE) and epiblast (Niakan et al., 2012). Differentiation of the TE is promoted during day 5 by expression of genes such as by caudal type homeobox 2 (CDX2, Strumpf et al., 2005) and GATA Binding Protein 2/3 (GATA2/3, Krendl et al., 2017). At day 6, differentiation of the PE is driven by *GATA 4/6* (Rojas et al., 2010, Cai et al., 2008), while the pluripotent epiblast is maintained by genes such as nanog homeobox (NANOG, Mitsui et al., 2003), POU class 5 homeobox (POU5F1/OCT4, Nichols et al., 1998), fibroblast growth factor 4 (FGF4, Kang et al., 2013), and sex determining region y-box transcription factor 2 (SOX2, Avilion et al., 2003). Mitophagy has previously been linked to cell differentiation (Cairns et al., 2020), but not in the blastocyst, and it is plausible the two are linked. Analysis of these lineage specific genes will allow allocation of cellular lineage to samples of the dataset, allowing analysis of genes of interest in the context of cellular lineage.

Alongside mitophagy, analysis of the expression of genes relating to wide maintenance of the mitochondrial network, encompassing mitochondrial biogenesis, fission and fusion, will allow further elucidation of regulation of mitochondrial morphology in the preimplantation embryo. Mitochondrial homeostaisis has been little studied in the preimplantation embryo. Thus far the importance of mitochondrial fission has been demonstrated in porcine preimplantation embryos, where *PINK1* inhibition resulted in elongate mitochondria and modest metabolic dysfunctions (Niu et al., 2019).

To better understand how each of these processes are regulated in the human preimplantation embryo I analysed the aforementioned human scRNAseq data set, encompassing 1,529 cells from across preimplantation development.

4.2. Aims and hypotheses

The overall goal of this chapter is to analyse a large scRNAseq dataset to identify genes responsible for the onset of mitophagy in the preimplantation embryo, and guide future work in related areas. Exploration of links between the expression of key mitochondria-related processes and mitophagy genes across preimplantation development will identify the implications of this mitophagy.

A1. To analyse the expression of genes relating to mitophagy. I hypothesise genes involved in mitophagy will be differentially expressed at different stages of development. Exploring these expression patterns will allow identification of mechanisms that underlie the mitophagy we have revealed through live-cell imaging. Furthermore, it allow the identification of genes which could be artificially upregulated to induce mitophagy in the PNT procedure, potentially reducing carryover of karyoplast mtDNA.

A2. To analyse the expression of apoptotic genes to better understand apoptosis in the human preimplantation embryo. I hypothesise genes regulating apoptosis will be differentially expressed across developmental stages, particularly at the time of blastocyst development. Confirming evidence of apoptosis in the blastocyst is reflected in gene expression, and identifying genes which may regulate this apoptosis, will allow analysis of links between apoptosis and mitophagy at the level of the human blastocyst transcriptome.

A3. To analyse the expression of metabolic genes to better understand metabolic changes in the human preimplantation embryo. I hypothesis expression of these genes will reflect an increase in metabolic demands at the time of blastocyst frromation. Confirming mechanisms characterised in animal models are conserved in the human, and reflected in the transcriptome, will allow the exploration of links between mitophagy and the fluid metabolic demands of an embryo.

A4. To explore correlations between mitophagy gene expression and the differentiation of cell lineages in the blastocyst. I hypothesis correlations will suggest a role for mitophagy relating to the establishment of cell lineage in the blastocyst. Analysis of correlations between the

expression of lineage specific genes at the time of cell specification and mitophagy genes will explore possible links between the two.

A5. To analyse the expression of genes relating to mitochondrial maintenance, to expand our understanding of how embryonic mitochondria are regulated beyond mitophagy. I hypothesis expression of these genes will suggest a lack of mitochondrial biogenesis accompanying or following mitophagy.

4.3 Methods

Raw single cell RNA sequencing (scRNAseq) FASTQ files (Petropoulos et al., 2016), post cell-quality filtering, were downloaded from the EBI ArrayExpress data repository (n=1529) (Accession - E-MTAB-3929). Data was mapped to the human reference genome GRCh38using salmon (Patro et al., 2017). Data was filtered to remove genes with high occurrence of 0 values. Data was normalised via Limma (Ritchie et al., 2015), using a model accounting for cell lineage, embryo of origin, sex, and day of development.

Biological process gene ontologies (GOs) as defined by ensembl were selected based on their relevance to mitochondrial biology (Appendix 1). For analysis, expression of the genes constituting an ontology were averaged for each cell. For gene expression data relating to both pathways and specific genes, ANCOVA was performed using R. Analysis was conducted with respect to day of development and cellular lineage, accounting for sex, embryo of origin and day/lineage. For significantly variable measurements Tukey HSD analysis was performed via R. Differentially expressed (DE) genes were identified between day and lineage groups utilising a model accounting for the same parameters as above using Limma. An absolute logFC threshold of 1.5 and FDR corrected statistical significance of 0.05 were used in identifying significant DE genes. Correlations were analysed using the corrplot package.

4.3. Results

4.4.1. Data processing, quality control and confirmation of cellular lineage

Although researchers who generated the scRNAseq applied some appropriate quality control metrics, some common quality control parameters were not included, such as the proportion of total counts which can be mapped to mtDNA. Given my interest specifically in mitochondrial processes, I applied a published quality control pipeline to raw FASTQ files (Ilicic et al., 2016), designed to ensure RNAseq datasets exclude all but cells which were living and undamaged at time of cell processing (Figure 4.1). This pipeline identifies irregular cells based on percentage of reads successfully mapped, and percentage of genes associated with the cytoplasm GO (high in good quality samples), and percentage of genes mapped to mtDNA and percentage of mitochondrial genes downregulated (low in good quality samples).
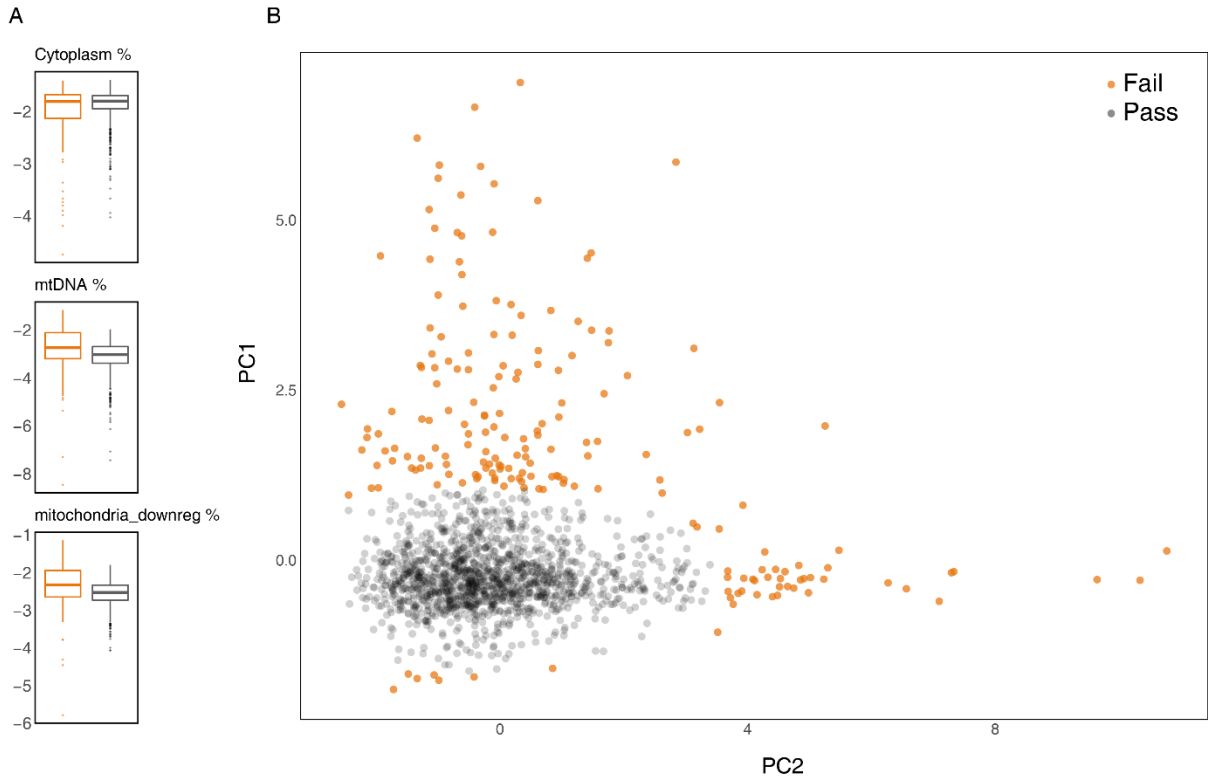
Figure 4.1. Quality control metrics applied to scRNAseq data.

Output adapted from quality control tool (Ilicic et al., 2016). (A) Relevant metrics; percent of reads mapped to the cytoplasm GO, percent reads mapped to mtDNA, and percentage of mtDNA genes downregulated. (B) PCA of all cells based on quality control metrics. Orange dots (cells failing quality control, n=196) were removed from analysis.
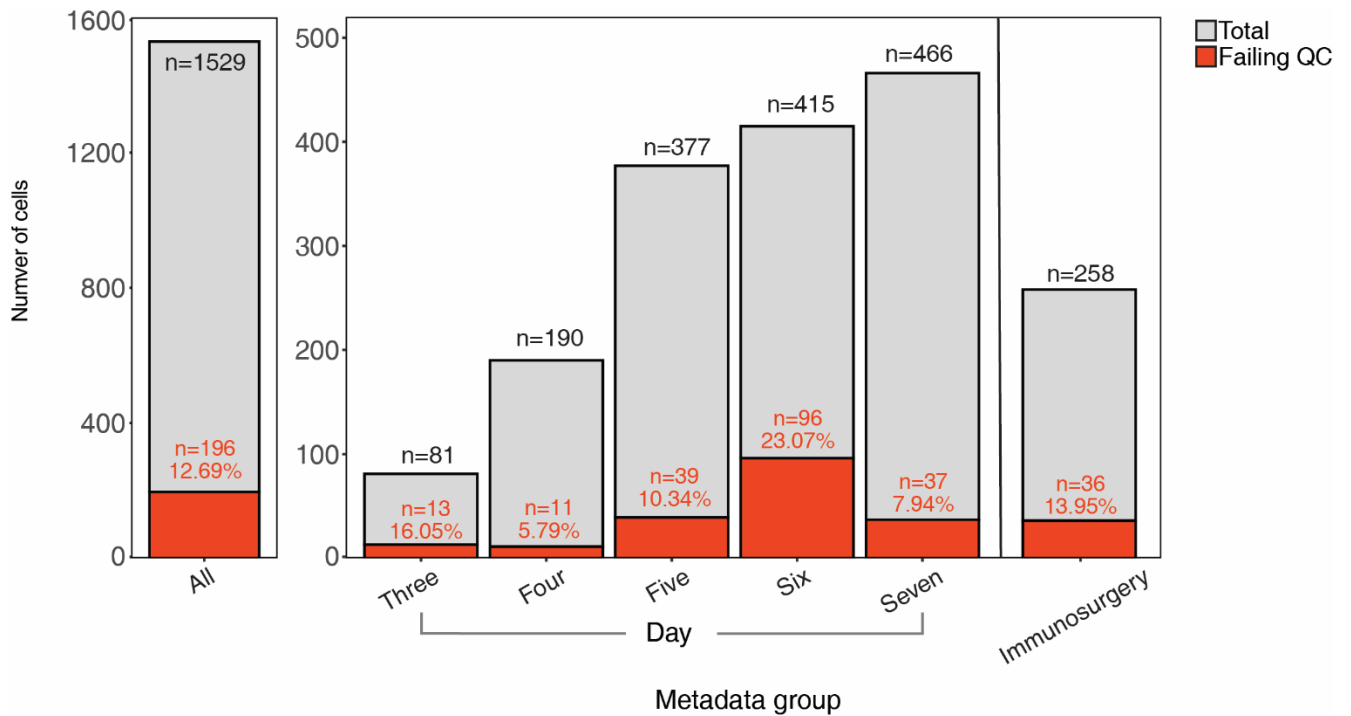
Figure 4.2. Demographics of cells failing quality control tool across available metadata categories.

Failing cells were largely balanced across days with enrichment at day 6. Immunosurgery cells were counted distinct from cell lineage. No bias was detected relating to method of single cell isolation.

From the 1529 scRNAseq cells, removal of those failing quality control left 1333 cells (Figure 4.2). Cells failing QC showed enrichment at day 6. This may suggest the metrics of the QC tool may have some overlap with the features of day 6 blastocyst cells. It may also reflect an elevated level of apoptosis at this stage of development (Hardy et al., 1989, Hardy and Handyside, 1996), or the more rigorous methods of single cell isolation that may be applied to a blastocyst compared to a cleavage stage embryo. Quantification and normalisation were repeated for cells passing quality control and using preferred tools (see Methods), and carried forward to subsequent analysis. The authors who presented the scRNAseq identified the lineage of analysed cells based on gene expression (Petropoulos et al., 2016). However, 294 cells within the dataset were isolated via immunosurgery, of which 147 were later identified as TE. Immunosurgery is a process in which TE cells are killed via application of antibodies and complement factors, leaving only the ICM cells to be harvested. Although a small number of TE cells could survive the process, it is surprising to see that half of the cells harvested were labelled as TE.

To ensure confidence in the allocation of cellular lineage, and due to the inconsistincies described above, I re-confirmed the lineage of all post-QC blastocyst cells in the dataset (n=1086). Clustering analysis displayed in a t-SNE plot a subset of day five cells cluster with pre-lineage day 4 cells (Figure 4.3A), as suggested by Petropoulos *et el* (2016). I labelled these as pre-lineage day 5 cells. Next, remaining blastocyst cells underwent unsupervised hierarchal clustering day by day based on a more recent published list of 12 canonical genes (Stirparo et al., 2018), 4 applicable to each of the 3 cell lineages of the mature blastocyst (Figure 4.3B/C). In the remaining day 5 cells, an indistinct cluster emerged between cells of the TE and ICM, and as such were deemed of unclear lineage and grouped with the pre-lineage cells. In the remaining day 5 cells and cells of days 6 and 7, three clusters within each could be distinguished. Based on gene expression of canonical genes lineage of each group was identified (Figure 4.4). In cells of day 5, cells of the PE and epiblast overlap in a t-SNE plot, likely representing only weak divergence in gene expression between the two. This is likely due to the early stage of their differentiation, which occurs primarily in day 6 (Figure 4.3).

A large proportion of cells isolated via immunosurgery remained TE cells. This would suggest an unexpectedly large number of cells survived the cell isolation protocol. However, this provided me with more confidence in lineage identity and re-allocated lineages were taken forward for analysis.
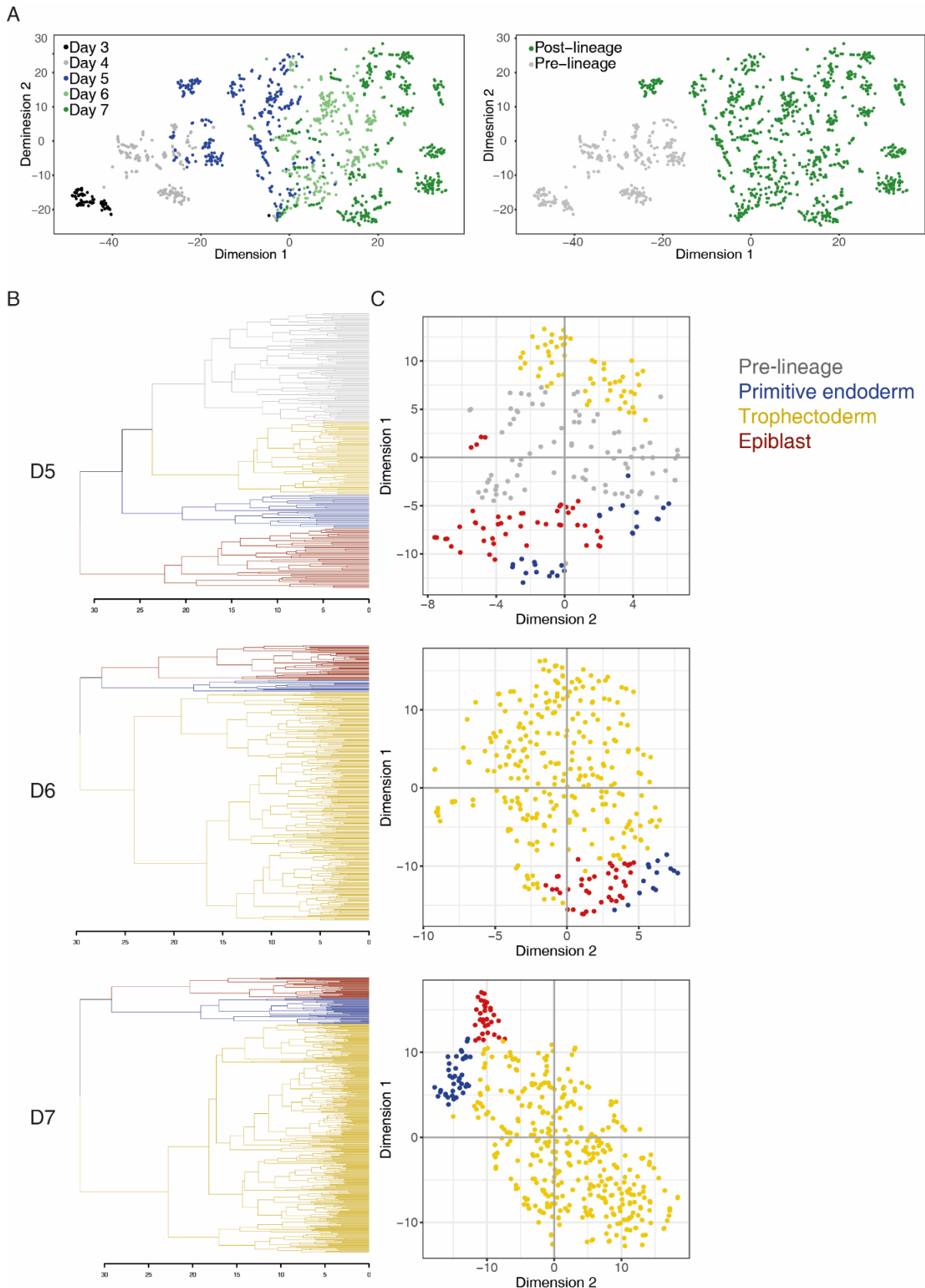
Figure 4.9. Allocation of lineage to blastocyst scRNAseq.

Pre-lineage cells of day 5 were identified by clustering of day 5 cells with day 4 (A). On the basis of expression of 12 canonical genes, cells were clustered and lineage identified. (B/C) Clustering trees and t-SNE plots demonstrating the variation in 12 canonical genes day by day. A mixing of PE and epiblast cells is evident at day 5, which may be due establishment of lineage being ongoing.

Primitive endoderm = blue, trophectoderm = yellow; epiblast = red; pre-lineage = grey.

60
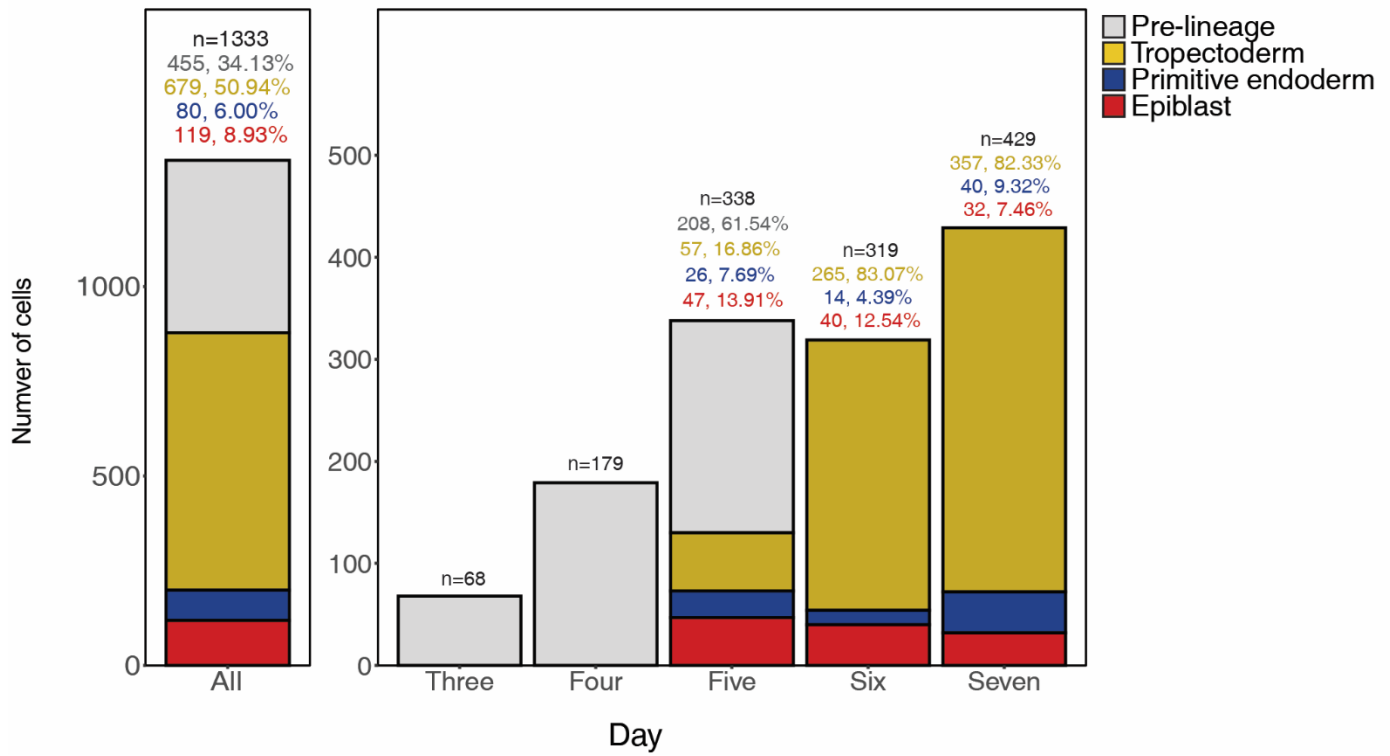
Figure 4.4. Cell lineage demographics stratified by day.

Lineage of blastocyst cells (days five, six and seven) was re-identified on a day by day basis after QC filtering. Pre-lineage = grey, trophectoderm = gold, primitive endoderm = blue, epiblast = red.

4.4.2. Expression of mitophagy genes in the human preimplantation embryo

I first analysed the expression of mitophagy genes to identify which key genes and pathways might be responsible for mitophagy in the preimplantation embryo (Chapter 1). Analysing the expression of gene ontologies (GOs), and the genes contained within collectively through calculation of their mean expression level, allows me to explore the broad activity of pathways (Barchiesi and Vascotto, 2019). The dataset encompasses day 3 (8-cell embryos), day 4 (morula) and days 5 to 7 (early, mid and late blastocysts).

To elucidate expression of mitochondrial genes, the GOs 'mitophagy', 'negative regulation of mitophagy', and 'positive regulation of mitophagy' were analysed across day of development. All GOs were significantly variable in expression across developmental day in ANOVA analysis accounting for cellular lineage, embryo of origin and sex (ANCOVA, P<0.001, Figure 4.5), allowing Tukey analysis. According to Tukey analysis, genes of the 'mitophagy' GO rose significantly from day 3 to 4 (P<0.001), but surprisingly declined significantly day to day between days 4 to 6 (P<0.001), being at their lowest level in the mature blastocyst. Genes of 'negative regulation of mitophagy' also showed a significant rise from day 3 to 4 (P<0.001), with levels of expression then maintained until the late blastocyst of day 7. Genes of 'positive regulation of mitophagy' showed a significant rise in expression between days 3 and 4 (P<0.001), followed by day to day reductions between days 5 to 7 (P<0.001). This expression profile is surprising given the evidence of mitophagy occurring in the blastocyst (Chapter 1).

As the expression of GOs did not reflect our previous work, I curated a list of key mitochondrial genes curated from literature (n=23, Appendix 2) in order to identify candidate genes for manipulation. I examined the DE of these genes across developmental day and lineage using limma (Table 4.1). Of 23 curated genes, 11 were DE in at least one comparison between days. Amongst mitophagy genes, 5 were significantly downregulated between days 3 and 4; positive regulators *BNIP3L* and *VPS13D* (Montava-Garriga and Ganley, 2020) (P<0.05), negative regulator *CITED2* (Bakker et al., 2007) (P<0.05), and autophagosome network signalling partners *GABARAP* and *SQSTM1* (Nishimura and Tooze, 2020, Sánchez-Martín and Komatsu, 2018) (P<0.001). Both *GABARAP* and *CITED2* were elevated at day 5 (P<0.05 and P<0.001), whilst *UBB* was downregulated (P<0.001). Across days 6 and/or 7, all DE mitophagy genes were downregulated (P<0.05), excluding *UBB* and *CITED2* which remained static, and *GABARAP* which was again upregulated (P<0.001).

A

B

Pre-lineage
Trophectoderm
Epiblast
Primitive endoderm

mitophagy (n=25)

negative regulation of mitophagy (n=7)

positive regulation of mitophagy (n=10)
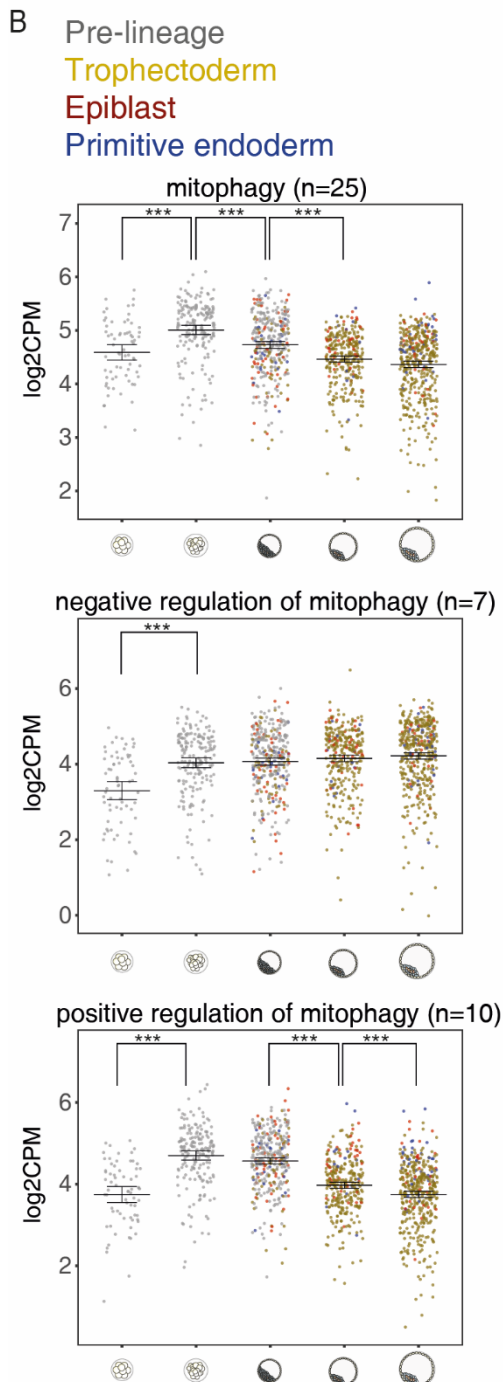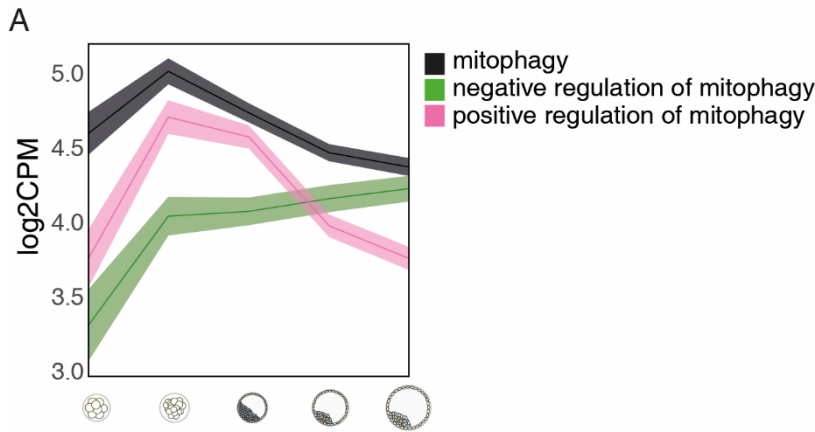
Figure 4.5. Expression of mitophagy related GOs across developmental day/stage.

(A) Overview of expression of chosen GO terms by day. Shading represents 95% confidence interval. (B) Expression of GO terms between days 3 to 7, then across cellular lineages in days 5 to 7. n indicates number of genes analysed within a GO term. Expression of mitophagy genes and promoters of mitophagy increased in the morula, but decreased in the blastocyst when mitophagy occurs. Negative regulators of mitophagy were increased in the same time period. X-axis represents developmental day. Colour of point represents cell lineage. Gray = pre-lineage, yellow = trophectoderm, red = epiblast, blue = primitive endoderm. Error bars indicate 92% confidence intervals. Significance bars indicate outcome of Tukey analysis. ***=P$\leq$0.001.

63

Gene		D3 → D4	D4 → D5	D5 → D6	D6 → D7
ATG9A	LogFC	0.69	-2.00	-3.66	2.11
	P	6.63E-01	1.12E-01	6.87E-04	1.00E-01
BNIP3L	LogFC	-3.45	1.37	-2.86	1.27
	P	6.69E-03	3.64E-01	4.20E-03	2.19E-01
CITED2	LogFC	-3.08	6.63	-1.62	-0.54
	P	1.99E-02	2.13E-11	7.12E-02	5.91E-01
FUNDC1	LogFC	-1.05	0.39	-2.14	0.79
	P	3.04E-01	7.50E-01	7.66E-04	3.73E-01
GABARAP	LogFC	-5.14	1.93	2.20	0.60
	P	2.72E-10	4.05E-02	9.04E-04	3.29E-01
OPTN	LogFC	0.21	0.12	-2.29	-0.67
	P	9.26E-01	9.57E-01	2.65E-02	5.88E-01
PINK1	LogFC	2.87	0.81	-2.90	-1.82
	P	6.29E-02	5.59E-01	8.51E-05	1.00E-01
PRKN	LogFC	-0.44	-1.27	-1.22	-2.05
	P	8.10E-01	3.58E-01	2.04E-01	2.66E-02
SQSTM1	LogFC	-4.20	1.03	0.41	-1.60
	P	4.96E-11	2.27E-01	5.75E-01	1.15E-02
UBB	LogFC	1.03	-1.58	0.74	0.76
	P	1.02E-02	2.92E-09	9.06E-03	1.36E-02
VPS13D	LogFC	-3.49	0.84	1.13	-2.40
	P	2.36E-02	6.83E-01	3.72E-01	4.14E-02

Table 4.1. Differential expression of key mitophagy genes between developmental days.

Red log fold change (logFC) denote an increased in expression moving forwards through development, blue a reduction. Genes that were not significantly (P>0.05) differentially expressed were excluded from the table. P; P value.

Across the period when live-cell imaging experiments report mitophagy, becoming prevalent in the day 5 blastocyst, only *GABARAP* and *CITED2* where upregulated. The family of *GABARAP* proteins and *SQSTM1* are have a broad role in the regulation of autophagy (Schaaf et al., 2016, Sánchez-Martín and Komatsu, 2018), which is reported to be important to blastocyst development (Wang et al., 2019). Thus its upregulation in the blastocyst cannot be directly linked to mitophagy. *CITED2* is an inhibitor of *HIF1A* (Bakker et al., 2007), which promotes *BNIP3/BNIP3L* mediated mitophagy (Montava-Garriga and Ganley, 2020). The transcription factor *HIF1A* was not differentially expressed in any comparison. This does not preclude the possibility of *BNIP3/BNIP3L* being involved in the mitophagy we have identified, as *CITED2* may play a role in negative feedback, itself induced by *HIF1A* (Bhattacharya et al., 1999), to constrain the mitophagy. It has been shown in cell lines that an upregulation of *CITED2* can prevent apoptosis following hypoxia and *HIF1A* upregulation, including by downregulation of *BNIP3L* (Bakker et al., 2007). Although the occurrence of mitophagy was not examined by Bakker *et al* (2007), *CITED2* expression may fine tune mitophagy to prevent excessive degradation and the onset of apoptosis. Finally, *UBB*, which encodes ubiquitin which is utilised in *PINK1/PRKN* mitophagy (Montava-Garriga and Ganley, 2020), was downregulated suggesting no role for this pathway in blastocyst mitophagy. Thus no explanations of blastocyst mitophagy were apparent in DE gene analysis.

As no explanations for blastocyst mitophagy appeared in DE analysis, nor any candidates which may be upregulated to induce mitophagy, I examined trends in log2CPM expression of the best characterised mitophagy genes in literature. I sought to identify expression patterns which coincide with mitophagy, and thus may explain live cell imaging experiments and guide further experiments (Figure 4.6). Mitophagy can be divided into three somewhat interlinked pathways (Rodger et al., 2017). It is evident that genes of *PINK1/PRKN* mitophagy, which promotes degradation of damaged mitochondria (Montava-Garriga and Ganley, 2020), are downregulated in the mature blastocyst. In addition to mitophagy, *PINK1* has an important role in mitochondrial fission when mitochondrial membranes are not depolarised, including in the blastocyst (Yang et al., 2008, Niu et al., 2019), which may explain its elevation in the morula. Whilst I cannot comment on the polarity of mitochondrial membranes based on this analysis, the reduction of both key genes of this pathway suggests it is inactive. An inhibitor of the pathway, *USP30* (Bingol et al., 2014), also showed downregulation in the blastocyst. *PGAM5*, an activator of mitophagy was upregulated during mitophagy, but signalling partner *FUNDC1* was not, and the inhibitor of the pathway, *MARCHF5* (Montava-Garriga and Ganley, 2020), was upregulated. Genes of the *BNIP3/BNIP3L* pathway were generally upregulated over the period of mitophagy, and have been implicated in mitophagy during other post-implantation developmental processes (Montava-Garriga and Ganley, 2020). Therefore, these genes presented candidates whose manipulation may allow upregulation of mitophagy in the blastocyst.

As such we upregulated *BNIP3L* gene expression and examined mitophagy in a separate cohort of mouse preimplantation embryos. The level of mitophagy occurring was analysed using a modified mito-QC probe (Allen et al., 2013). This probe, matrix-mito-QC consists of an EGFP-mCherry fusion protein targeted to the mitochondrial matrix. Mitochondria undergoing mitophagy are engulfed in mitolysosomes wherein acidic pH degrades the mitochondria (Rodger et al., 2017). At the same time the signal of EGFP is quenched, leaving the more stable mCherry intact and appearing indefinitely as red foci, providing a marker of mitophagy. When mRNA of a serine 34/35 phosphorylated isoform of *BNIP3L* (pBNIP3L) was injected alongside mRNA of matrix-mito-QC, a large degree of mitophagy was accelerated into the morula stage, and in subsequent stages of the blastocyst red foci were detectable at a higher level.
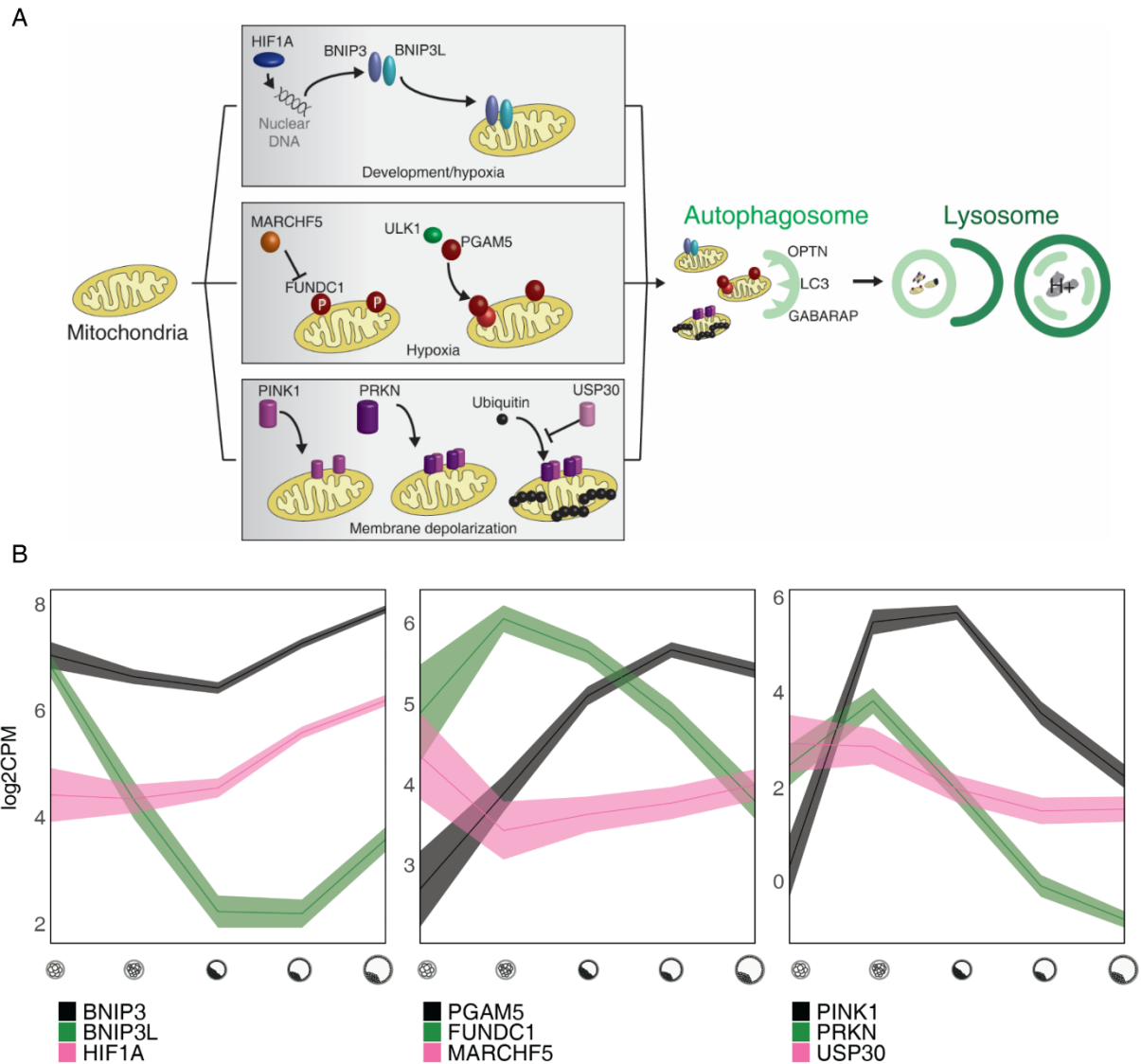
Figure 4.6. Analysis of trends in log2CPM of mitophagy genes.

(A) Schematic of the best characterised mitophagy pathways; BCL2 interacting protein 3/like (BNIP3/BNIP3L), FUN14 domain containing 1 (FUNDC1)/Phosphoglycerate mutase family member 5 (PGAM5) and phosphatase and tensin homolog induced kinase (PINK1)/parkin RBR E3 ubiquitin protein ligase (PRKN) pathways (B) Expression of key genes separated by pathways. X-axis represents developmental day. Mitophagy was first detected in live-cell imaging at day 5, the early blastocyst. Pathway inhibitors: MARCHF5; membrane associated ring-CH-type finger 5, USP30; ubiquitin specific peptidase 30.
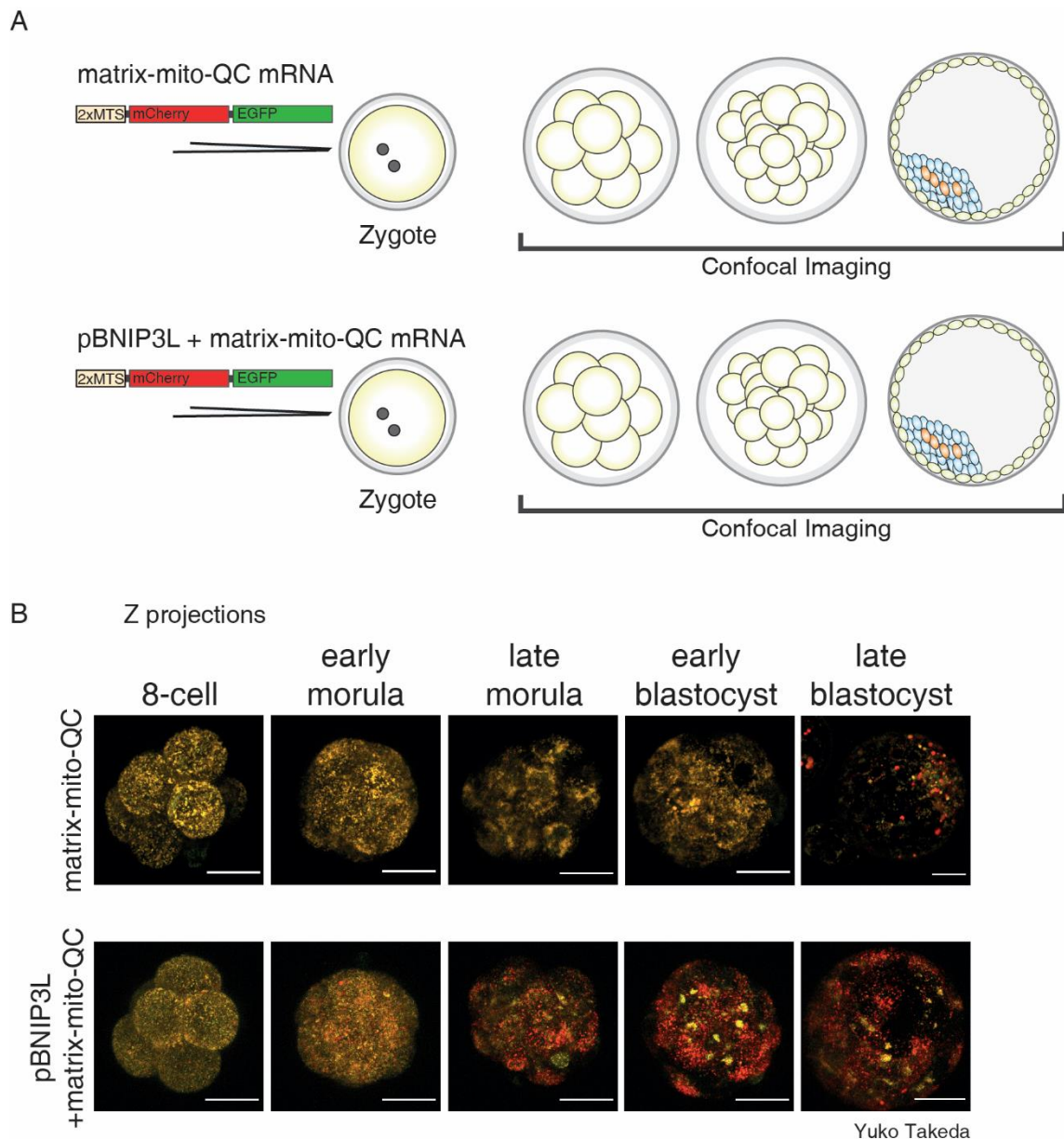
Figure 4.7. Overexpression of pBNIP3L induced mitophagy in CD1 mouse embryos.

(A) Schematic of experiment. pBNIP3L was overexpressed in the CD1 mouse zygote, and red foci tracked to measure mitophagy. (B) Z-projections of CD1 mouse embryos. Red foci appear earlier and at higher levels thereafter relative to controls.

The above suggests that the mitophagy we report in the preimplantation embryo is orchestrated by proteins of the *BNIP3/BNIP3L* pathway. This is not surprising given examples of both *BNIP3* and *BNIP3L* being involved in developmental processes (Aerbajinai et al., 2003, Schweers et al., 2007, Sandoval et al., 2008, Xiang et al., 2017, Esteban-Martínez et al., 2017, Lampert et al., 2019, Zhao et al., 2020), and suggests mitophagy of the preimplantation embryo is not a consequence of damaged mitochondria in the embryo. Instead, it may be linked to ongoing developmental processes. Importantly, this also provides a platform for the lab to explore the upregulation of mitophagy to prevent mtDNA carryover in the karyoplast during PNT.

To better characterise mitophagy in the blastocyst, I examined the expression of aforementioned mitophagy GOs and genes across cellular lineages of the blastocyst (Figure 4.8, Table 4.2). ANOVA analysis performed for cellular lineages across days of development individually, accounting for embryo of origin and sex was sufficiently variable to allow Tukey analysis in most instances (ANCOVA, $P<0.05$).

Across cellular lineage, at day 5 genes of the 'mitophagy' GO were significantly elevated in pre-lineage cells compared to the TE ($P<0.001$), which reflects its elevated expression in the morula. By day 6 they were significantly upregulated in the epiblast compared to the TE ($P<0.001$), and at day 7 in both populations of the ICM compared to the TE ($P<0.001$ to PE, $P<0.01$ to epiblast). The 'positive regulation of mitophagy' GO was significantly upregulated in the cells of the ICM compared to the TE at day 6 ($P<0.01$ to PE, $P<0.001$ to epiblast) and 7 ($P<0.001$). Furthermore, across cellular lineage several differences in expression of curated mitophagy genes emerge. The TE showed elevated expression of *CITED2* at day 5, suggesting mitophagy might be more tightly constrained in those cells. An elevation of autophagy genes *ATG5/9* in the ICM suggests an increased importance of autophagy in cells of the ICM (Nishimura and Tooze, 2020), but offer few clues regarding the activity of mitophagy given their broad roles. Some mitophagy proteins also show an elevation in both lineages of the ICM; *BNIP3L* was upregulated in the day 5 PE. More convincingly, *PINK1* and *PRKN* showed upregulation in the ICM across several comparisons, most prevalently in the epiblast. The above analysis may suggest a greater occurrence of and importance of mitophagy in the ICM.

mitophagy (n=25)

negative regulation of mitophagy (n=7)

positive regulation of mitophagy (n=10)
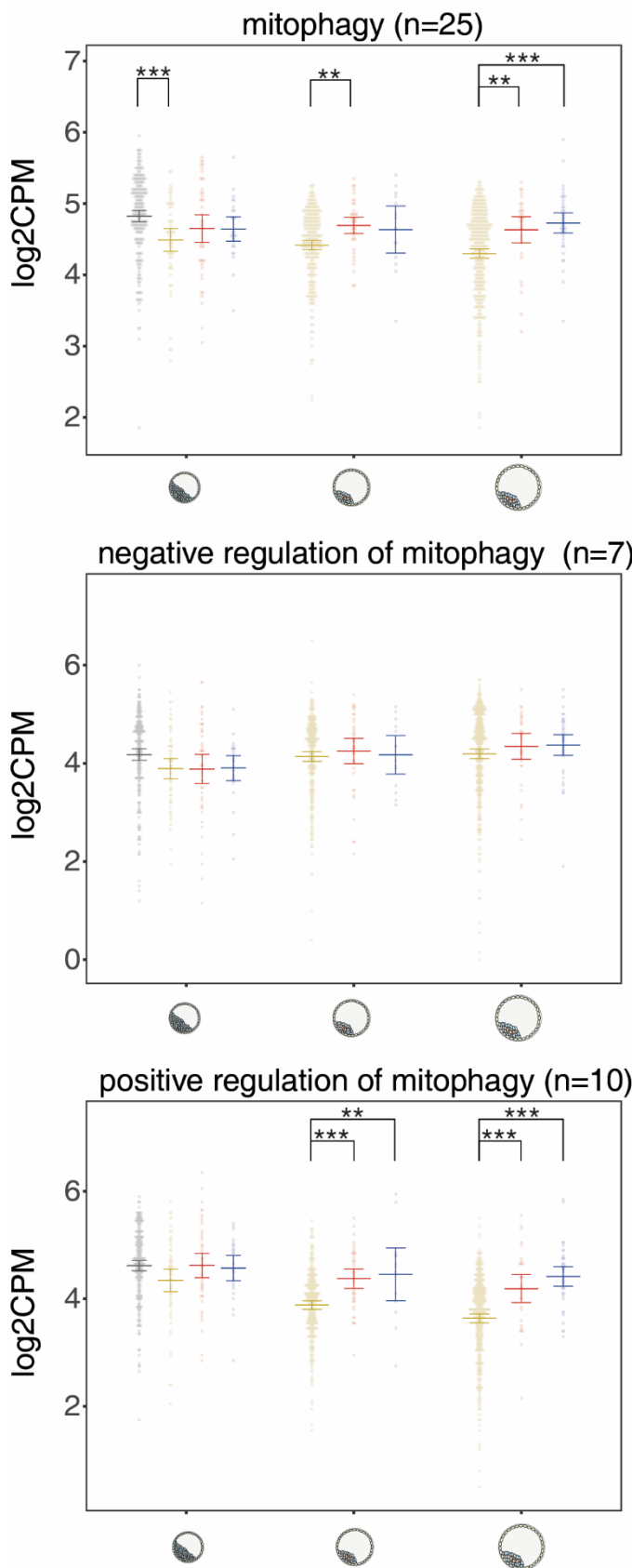
Gene	Comparison	logFC	P
ATG5	Day 5 Epi → TE	-1.60	9.80E-21
ATG9A	Day 5 Epi → TE	-1.72	2.20E-04
ATG9A	Day 5 PE → TE	-1.58	1.71E-02
ATG9A	Day 5 Pre → TE	-1.74	3.22E-04
BNIP3L	Day 5 PE → TE	-1.89	6.00E-03
CITED2	Day 5 Epi → TE	2.12	1.80E-06
CITED2	Day 5 PE → TE	2.15	2.73E-04
PINK1	Day 6 Epi → TE	-1.83	2.52E-04
PINK1	Day 7 Epi → TE	-2.27	5.14E-06
PRKN	Day 6 Epi → TE	-1.57	4.06E-04
PRKN	Day 7 PE → TE	-1.67	2.48E-05

Table 4.2. Differential expression of key mitophagy genes between cellular lineages of the blastocyst.

Notably, PINK1/PRKN were often elevated in the inner cell mass. Developmental days were analysed individually. Red log fold change (logFC) denote an increased in expression in the trophectoderm (TE), blue a reduction. Genes that were not significantly (P>0.05) differentially expressed were excluded from the table. PE, primitive endoderm; Epi, epiblast. P; P value.

Figure 4.8. Expression of mitophagy related GOs across cellular lineage of the blastocyst.

Expression of mitophagy genes and promoters of mitophagy was frequently elevated in the primitive endoderm or epiblast. X-axis represents developmental day. n indicates number of genes analysed within a GO term. Colour of point represents cell lineage. Gray = pre-lineage, yellow = trophectoderm, red = epiblast, blue = primitive endoderm. Error bars indicate 95% confidence intervals. Significance bars indicate outcome of Tukey analysis. **=P<0.01 ,***=P<0.001.

Whilst the above analysis identified a gene, BNIP3L, which can be manipulated in further work, and suggests specific mechanisms underlying embryo mitophagy, it does not explore the causes or implications of mitophagy in the preimplantation embryo.

4.4.4. Apoptosis gene expression in the preimplantation embryo

Apoptosis is an important part of blastocyst development (Hashimoto and Sasaki, 2019), and as such is it plausible mitophagy represents a part of a cell degrading its contents in anticipation of cell death. Before exploring possible links between mitophagy and apoptosis, I first characterised the gene expression of apoptotic genes in the preimplantation embryo, which thus far has been constrained by the lack of unbiased transcriptome measurements, instead relying on targeted RT-PCR and whole embryo measurements (Jurisicova et al., 2003, Haouzi et al., 2018).

First, across both developmental day then cellular lineage, I analysed the expression of a curated selection of GOs relating to apoptosis; 'apoptotic process', 'execution phase of apoptosis', 'negative regulation of execution phase of apoptosis' and 'positive regulation of execution phase of apoptosis'. All GOs were significantly variable across day of development according to ANOVA accounting for lineage, sex and embryo of origin (ANCOVA, $P<0.001$, Figure 4.9). Gene involved in the 'execution phase of apoptosis' showed increased expression from day 3 to 4 ($P<0.05$) and again at day 5 ($P<0.001$), then remained elevated until day 7. Genes of 'negative regulation of execution phase of apoptosis' showed reduction from day 5 to 6 ($P<0.001$), before rising again at day 7 ($P<0.001$). Genes of 'positive regulation of execution phase of apoptosis' showed significant rises day by day from day 3 to 6 ($P<0.01$ 3v4, $P<0.001$ others).
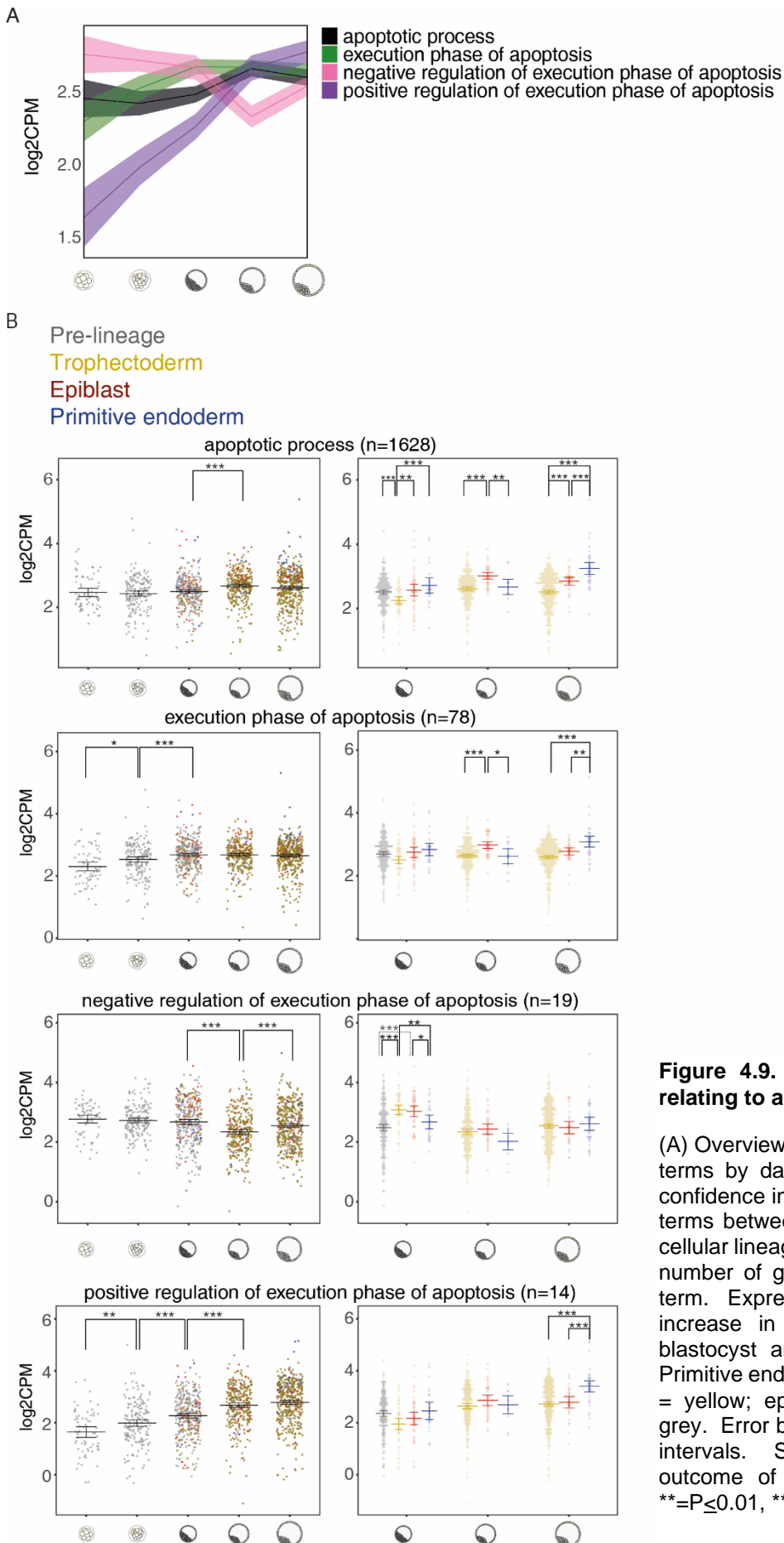
Figure 4.9. Expression of GO terms relating to apoptosis.

(A) Overview of expression of chosen GO terms by day. Shading represents 95% confidence interval. (B) Expression of GO terms between days 3 to 7, then across cellular lineages in days 5 to 7. n indicates number of genes analysed within a GO term. Expression profile suggests an increase in apoptosis is likely in the blastocyst and in the inner cell mass. Primitive endoderm = blue, trophectoderm = yellow; epiblast = red; pre-lineage = grey. Error bars indicate 95% confidence intervals. Significance bars indicate outcome of Tukey analysis. *=P$\leq$0.05, **=P$\leq$0.01, ***=P$\leq$0.001.

ANOVA analysis performed for cellular lineages across days of development individually accounting for embryo of origin and sex was sufficiently variable to allow Tukey analysis in most instances (ANCOVA, $P<0.05$, Figure 4.9). At day 5, expression of genes relating to the 'apoptotic process' GO was significantly lower in expression in the TE compared to all other groups ($P<0.01$ to epiblast, $P<0.001$ to others). Genes relating to 'negative regulation of execution phase of apoptosis' were significantly more highly expressed in the TE and epiblast compared to the PE and pre-lineage cells ($P<0.01$ Epi v PE, $P<0.001$ TE v PE, $P<0.001$ others).

On day 6, expression of genes involved in the 'apoptotic process' and 'execution phase of apoptosis' GOs were significantly upregulated in epiblast cells relative to others ($P<0.01$). At day 7, 'apoptotic process' genes were more highly expressed in the PE than other groups ($P<0.001$), and more highly expressed in the epiblast than TE ($p<0.001$). Genes of 'execution phase of apoptosis' were more highly expressed in the PE compared to the TE ($P<0.001$) and epiblast ($P<0.01$), as were those of 'positive regulation of execution phase of apoptosis' ($P<0.001$).

This profile of GO expression across developmental day and cellular lineage (Figure 4.9), with the higher broad GOs and positive GOs elevated in the blastocyst and in the ICM, is largely in agreement with the occurrence of apoptosis evidenced in terminal deoxynucleotidyl transferase dUTP nick end labeling (TUNEL) staining in the human and mouse blastocyst (Hardy et al., 1989, Hardy and Handyside, 1996). These imaging studies have suggested the onset of apoptosis in the blastocyst and elevated apoptosis in the ICM (Hardy et al., 1989, Hardy and Handyside, 1996). This confirms that these events are reflected in the human transcriptome. Unlike previous studies, analysis at the single cell level allows me to differentiate the PE and epiblast cells, and explore differences in apoptosis gene expression between them. During day 6, the epiblast shows significantly higher expression of genes of 'apoptotic process' and 'execution phase of apoptosis', suggesting apoptosis may be more common in the epiblast, but by day 7 this is reversed and apoptosis favours the PE. This suggests that excess or out-competed epiblast cells are removed prior to corresponding PE cells. This question has not previously been explored, but it has been demonstrated that epiblast cells failing to appropriately differentiate undergo cell death (Hashimoto and Sasaki, 2019).

Furthermore, expression of GOs in the pre-lineage cells is often similar to that of the ICM or higher than the TE. This supports the hypothesis that apoptosis in the blastocyst is a means to remove cells with an undesirable specification status, removing the cells which have failed to attain a specific lineage or cells in the ICM environment which maintain potential to become TE cells (Pampfer and Donnay, 1999, Hashimoto and Sasaki, 2019). It cannot be ruled out that cells are undergoing apoptosis due to stress or dysfunction, which could be exacerbated by *in vitro* culture (Brison and Schultz, 1997, Kamjoo et al., 2002), or due to the chromosomal abnormalities reported following IVF (Vanneste et al., 2009).

I next sought to explore the DE of specific apoptosis genes and their potential role in embryo apoptosis. I curated a list of the best characterised apoptosis genes according to literature (n=28, Appendix 3, Figure 4.10), and examined their DE across developmental day (Table 4.3). Notably, apoptosis inhibitors *BCL2* and *BCL2A1* were not detectable in the dataset, and some positive and negative regulators were not differentially expressed in any comparison (*MCL1, BMP4, CYCS, BAD, APAF1, DIABLO, CASP3*).
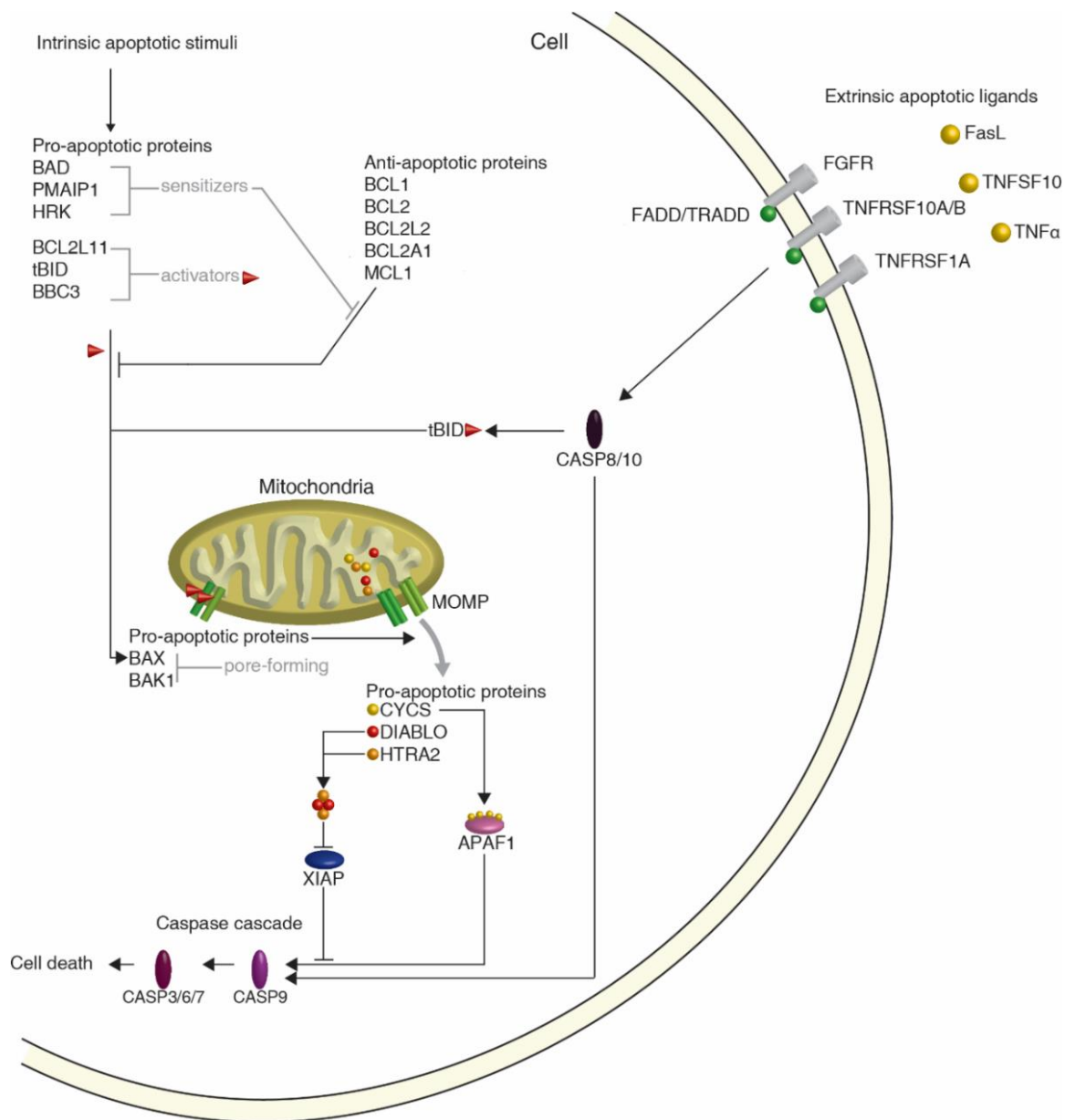
Figure 4.10. Intrinsic and extrinsic apoptosis.

Intrinsic apoptosis is initiated by cellular stress or damage signalling, and is a fundamental to development and tissue homeostasis. BCL2-like-11 (BCL2L11) and BCL2 binding component 3 (BBC3/PUMA) are upregulated, whereas BH3 interacting domain death agonist (BID) is truncated to form activated tBID. Negative regulator proteins act to bind and sequester peptides and are inhibited by pro-apoptotic sensitizer proteins. If negative regulators are saturated or insufficient, promoters of apoptosis activate BCL2 associated X, apoptosis regulator (BAX) and BCL2 antagonist/killer 1 (BAK1) to form mitochondrial outer membrane permeabilization (MOMP) pores. This allows release of the mitochondria-derived activator of caspase (DIABLO), HtrA serine peptidase 2 (HTRA2) and cytochrome c (CYCS). DIABLO and HTRA2 inhibit x-linked inhibitor of apoptosis (XIAP), which otherwise prevents caspase (CASP) activation. CYCS binds apoptotic peptidase activating factor 1 (APAF1), forming an apoptosome which activates CASP9, triggering the caspase cascade. Extrinsic apoptosis is triggered by extracellular signalling. Cell death ligands (FasL, tumor necrosis factor ligand superfamily member 10 (TNFSF10), tumour necrosis factor alpha (TNFα)) bind their associated receptors (fibroblast growth factor receptor (FGFR), tumor necrosis factor receptor superfamily member 10A/B (TNFRSF10A/B), tumor necrosis factor receptor superfamily member 1A (TNFRSF1A)), which recruit adapter proteins (fas associated via death domain/ TNFRSF1A associated via death domain (FADD/TRADD)). This complex activates caspases (CASP8/10) and in some cells activates the caspase cascade. In other cells, crosstalk between the two pathways is necessary to induce cell death, and relies upon activation of tBID. BAD; BCL2 associated agonist of cell death, BCL1; B cell lymphoma-1, BCL2L1; BCL2 like 1, BCL2L2; BCL2 like 2, BCL2A1; BCL2 related protein A1, HRK; harakiri, MCL1; induced myeloid leukemia cell differentiation protein, PMAIP1; phorbol-12-myristate-13-acetate-induced protein 1.

Analysis by day of development revealed no obvious pattern of expression in apoptosis regulators (Table 4.3). Focusing on inhibitors of apoptosis, few changes in expression were apparent; *BCL2L1* was reduced at day 6 compared to day 5 ($P<0.05$). Meanwhile *SIRT1* expression fell between day 3 to 4 ($P<0.001$), then rose to at a plateau at days 5 and 6 ($P<0.05$), before dropping at day 7 ($P<0.01$). An inhibitor of caspases, *XIAP*, was elevated at day 5 compared to day 4 ($P<0.05$). Promoters of apoptosis showed a wider array of DE genes. Key genes BAX and *BAK1* both increased in expression after between day 3 and 4 ($P<0.001$), then fell at day 6 ($P<0.001$). Meanwhile *BCL2l11* and *PMAIP1* dropped in expression between days 3 and 4 ($P<0.001$ and $P<0.01$) then rose at day 5 ($P<0.001$ and $P<0.01$), before dropping after day 6 ($P<0.00$ and $P<0.05$). Similarly, *BBC3* showed an elevation between days 4 and 5 ($P<0.05$), before dropping at day 6 ($P<0.01$), and *TP53* increased in expression from day 3 to 4 ($P<0.05$) where it was sustained before dropping between day 6 and 7 ($P<0.05$). Although largely stable, *BID* and *HRK* were lower at day 7 compared to day 6 ($P<0.01$). Broadly, the expression patterns are perhaps unsurprising given evidence of apoptosis in the blastocyst, as a number of positive regulators of apoptosis are elevated in the blastocyst at day 5. The downregulation of genes in the same category at day 7 suggests apoptosis subsides around the time of implantation. The expression of genes in this curated list is highly variable, suggesting dynamic and rapidly evolving regulation of apoptosis in the embryo. Further genetic studies of embryo apoptosis should account for a larger number of genes and distinguish stages of blastocyst development.

Effectors of apoptosis were more stable (Table 4.3). *CASP2* showed an elevation from day 4 to 5 ($P<0.05$), before elevating ay day 6 ($P<0.001$). Expression of *CASP8* and *CASP10* increased from days 4 to 5 ($P<0.05$ and $P<0.01$), then decreased at day 7 compared to 6 ($P<0.05$ and $P<0.01$). Expression of *CASP6* and *CASP*9 each increased in expression between days 3 and 4, then decreased at day 5. Caspases are largely regulated by cleavage of their mature peptides (Riedl and Shi, 2004), and as such the conclusions that can be drawn from their transcript abundance is limited. Their mRNA levels may simply reflect an mRNA pool. The activators of the caspase cascade (*CYCS, DIABLO* and *APAF1*) showed no differential expression in any comparison, suggesting the important stages of apoptosis regulation involve other genes.

Gene		D3 → D4	D4 → D5	D5 → D6	D6 → D7
BCL2L1	LogFC	-0.98	1.30	-1.94	1.10
	P	5.30E-01	2.94E-01	2.33E-02	2.77E-01
XIAP	LogFC	-1.05	1.69	-0.07	-1.35
	P	9.42E-01	1.28E-02	9.11E-01	2.05E-02
SIRT1	LogFC	-6.07	2.64	0.29	-2.81
	P	2.42E-08	3.47E-02	8.06E-01	3.63E-03
BAK1	LogFC	5.26	-1.53	-4.18	2.00
	P	1.22E-04	1.35E-01	3.85E-08	7.61E-02
BAX	LogFC	2.84	1.62	-2.78	0.38
	P	7.98E-03	5.62E-02	4.32E-07	6.52E-01
BAG1	LogFC	-1.26	3.91	-0.86	-2.01
	P	3.61E-01	1.41E-06	2.11E-01	6.96E-03
BBC3	LogFC	1.94	3.43	-2.92	-2.09
	P	3.13E-01	1.98E-02	5.09E-03	7.41E-02
BCL2L11	LogFC	-5.71	4.29	0.14	-3.07
	P	9.85E-06	4.28E-04	9.12E-01	2.70E-03
BID	LogFC	0.55	-0.54	1.68	-2.38
	P	7.78E-01	7.71E-01	8.91E-02	1.67E-02
PMAIP1	LogFC	-5.59	4.99	-2.11	-2.98
	P	1.04E-03	1.43E-03	6.03E-02	3.34E-02
HRK	LogFC	-0.34	1.96	-0.28	-2.25
	P	8.24E-01	5.36E-02	7.63E-01	3.39E-03
TP53	LogFC	2.73	1.57	0.45	-2.24
	P	4.27E-02	1.79E-01	6.17E-01	1.39E-02
CASP2	LogFC	0.25	-2.22	5.07	-0.67
	P	8.91E-01	4.44E-02	1.29E-11	3.65E-01
CASP6	LogFC	5.58	-2.89	-1.33	1.44
	P	3.47E-06	2.58E-04	9.41E-02	9.12E-02
CASP8	LogFC	-0.82	2.25	-1.00	-1.54
	P	5.66E-01	1.52E-02	1.58E-01	4.57E-02
CASP9	LogFC	5.37	-3.82	-0.29	0.92
	P	3.16E-03	2.21E-02	8.63E-01	5.16E-01
CASP10	LogFC	0.04	2.61	-1.48	-2.05
	P	9.83E-01	2.92E-03	2.72E-02	5.97E-03

Gene	Comparison	logFC	adj.P.Val
BCL2L2	Day 7 Epi → PE	1.71	4.73E-02
BAK1	Day 5 Epi → TE	-1.88	6.19E-13
BAK1	Day 5 PE → TE	-2.14	3.55E-11
BAK1	Day 7 Epi → TE	-1.60	9.63E-04
BAK1	Day 7 PE → TE	-2.11	6.97E-07
BBC3	Day 6 Epi → TE	-2.55	1.42E-06
BBC3	Day 7 Epi → TE	-1.64	5.27E-03
PMAIP1	Day 5 Epi → TE	-2.63	3.04E-07
PMAIP1	Day 5 PE → TE	-3.15	2.92E-06
PMAIP1	Day 5 Pre → TE	-1.90	6.26E-04
PMAIP1	Day 6 Epi → TE	-3.36	1.14E-08
PMAIP1	Day 7 Epi → TE	-4.31	9.74E-14
PMAIP1	Day 7 PE → TE	-3.71	6.39E-11
CASP7	Day 7 PE → TE	-2.59	4.62E-07
CASP8	Day 5 Epi → TE	-2.18	4.81E-12
CASP8	Day 5 PE → TE	-1.86	9.34E-06
CASP8	Day 6 Epi → TE	-1.88	3.24E-08
CASP8	Day 7 Epi → TE	-2.25	3.24E-12
CASP8	Day 7 PE → TE	-1.85	3.62E-09
CASP9	Day 5 Epi → TE	-1.52	4.55E-02
CASP9	Day 7 PE → TE	-1.58	8.33E-03
CASP10	Day 5 Epi → TE	-1.75	8.29E-08
CASP10	Day 5 PE → TE	-2.33	1.84E-08
CASP10	Day 7 Epi → TE	-1.77	4.88E-08
HRK	Day 7 Epi → TE	-1.94	4.18E-09

Table 4.4. Differential expression of key apoptosis genes between cellular lineages of the blastocyst.

A trend emerges of elevated apoptosis gene expression in the inner cell mass. Developmental days were analysed individually. Red log fold change (logFC) denote an increased in expression in the trophectoderm (TE), blue a reduction. Genes that were not significantly (P>0.05) differentially expressed were excluded from the table. PE, primitive endoderm; Epi, epiblast. P; P value.

Table 4.3. Differential expression of key apoptosis genes between developmental days.

Red log fold change (logFC) denote an increased in expression moving forwards through development, blue a reduction. Genes that were not significantly (P>0.05) differentially expressed were excluded from the table. P; P value.

I next analysed DE of the same gene list across blastocyst cell lineages (Table 4.4). At days 5 and 7, BAK1 was expressed more highly in the ICM calls than the TE (P<0.001). At days 6 and 7 BBC3 was more highly expressed in the epiblast compared to TE (P<0.001 and P<0.01). The day 7 epiblast showed a higher level of expression of HRK than the TE (P<0.001). A number of comparisons were statistically significant for PMAIP1 with expression lower in the TE compared to other cell groups in all but one comparison (P<0.001). Amongst executor genes, CASP8 was more highly expressed in the ICM in most relevant comparisons (P<0.001), whereas CASP7 was more highly expressed in the PE compared to the TE at day 7 (P<0.001). CASP9 was more highly expressed in the epiblast than the TE at day 5 and in the PE of day 7 compared to the TE of day 7 (P<0.05 and P<0.01), and CASP10 was more highly expressed in the ICM compared to the TE at day 5, and in the Epiblast at day 7 compared to the TE (P<0.001). Only one negative regulator of apoptosis showed variation in its expression; *BCL2L2* was more highly expressed in the PE than the epiblast at day 7 (P<0.05).

Unsurprisingly a number of pro-apoptotic genes were elevated in their expression in the cells of the ICM compared to the TE (Table 4.4), offering further explanation for the reported elevated apoptosis in the ICM (Hardy and Handyside, 1996). This is particularly convincing in the case of *PMAIP1*, a weaker promoter of apoptosis, which was elevated in the ICM at all stages of development. Only one gene was significantly differently between the PE and epiblast; *BCL2L2* was elevated in the day 7 PE. The limited differences in expression of key apoptotic genes between the two cell groups suggests mechanisms of apoptosis act similarly between the two,

I next performed a more unbiased analysis of the DE of genes within the 'apoptotic process' GO. Of the genes extracted from a literature search (Appendix 3), all except BMP4 are included in this GO. Within this GO, 1017 genes of 1628 detected were significantly differentially expressed in at least one comparison between days (a total of 4 comparisons) (Table 4.5). This list was dominated by members of the (*PRAME*) protein family. This likely reflects the role of retinoic acid signalling in development (Rhinn and Dollé, 2012), as PRAME inhibits F acid signalling (Epping et al., 2005). Downregulation of *PRAME*s may unleash new mechanisms of differentiation as an embryo develops. Although *PRAME* has been linked to apoptosis all evidence arises from studies of tumour cells and tissue (Wadelin et al., 2010). While I cannot rule out a role for *PRAME* genes in apoptosis, this also represents a note of caution in GO analysis. Evidence for the inclusion of genes in a GO may need to surpass a low threshold and can be context-dependant, hampering interpretation of analysis.

Gene		D3 → D4	D4 → D5	D5 → D6	D6 → D7
PRAMEF13	LogFC	-10.90	0.26	1.44	-3.58
	P	4.26E-42	8.64E-01	7.22E-02	7.25E-07
PRAMEF9	LogFC	-9.82	-3.26	1.08	-6.70
	P	7.11E-39	1.08E-03	2.98E-01	8.27E-19
PRAMEF11	LogFC	-11.04	-0.84	1.83	-4.80
	P	2.06E-37	5.52E-01	3.02E-02	4.42E-10
HINT1	LogFC	-6.22	0.68	4.45	-0.20
	P	1.41E-36	4.06E-01	2.92E-23	5.19E-01
RYR2	LogFC	-6.15	0.20	1.83	6.22
	P	4.66E-15	8.76E-01	5.51E-03	2.14E-33
AKR1C3	LogFC	-9.67	-0.09	2.15	-1.95
	P	2.24E-30	9.56E-01	7.05E-03	9.42E-03
PRAMEF2	LogFC	-8.79	-1.37	1.72	-3.06
	P	1.09E-27	1.95E-01	2.15E-02	1.67E-05
RTKN	LogFC	-1.61	8.95	-0.56	-1.13
	P	2.95E-01	1.85E-27	4.56E-01	1.53E-01
PRAMEF5	LogFC	-8.86	0.32	-3.83	-4.90
	P	3.02E-27	8.60E-01	8.76E-05	1.44E-08
MAG	LogFC	2.98	6.34	-8.04	-1.51
	P	7.28E-02	4.73E-08	8.52E-27	1.69E-01
RFPL1	LogFC	-9.59	-0.18	2.54	-3.43
	P	1.68E-26	9.13E-01	9.16E-04	1.24E-05
HIPK2	LogFC	-6.68	1.30	0.50	4.93
	P	1.12E-25	1.06E-01	4.78E-01	6.97E-26
PRAMEF27	LogFC	-7.95	-4.69	1.67	-5.87
	P	7.09E-26	1.90E-07	6.72E-02	6.52E-15
PRAMEF27	LogFC	-7.95	-4.69	1.67	-5.87
	P	7.09E-26	1.90E-07	6.72E-02	6.52E-15
PTN	LogFC	-5.91	-0.58	8.97	0.89
	P	9.83E-06	7.52E-01	3.42E-24	2.39E-01
CD24	LogFC	-1.74	2.10	7.92	-0.70
	P	2.68E-01	8.48E-02	1.51E-23	1.48E-01
ANXA6	LogFC	3.23	-3.29	8.49	-0.78
	P	4.99E-02	1.21E-02	6.29E-22	2.38E-01
CRIP1	LogFC	2.76	7.18	0.92	-0.79
	P	3.61E-02	7.35E-21	2.00E-02	1.46E-01
ASNS	LogFC	-0.79	-0.04	7.20	-2.20
	P	6.87E-01	9.83E-01	3.33E-18	7.03E-03
EPCAM	LogFC	-4.60	6.12	2.41	0.29
	P	6.23E-05	1.60E-16	6.50E-09	5.06E-01

Table 4.5. Differential expression of genes within the apoptotic process gene ontology.

Genes were ranked by P value (P). Red log fold change (logFC) denote an increased in expression moving forwards through development, blue a reduction.

As with curated apoptosis genes, many top DE genes show variability during progression towards implantation, suggesting experiments should also be designed to account for changing gene expression as blastocyst development progresses. The variable expression of a number of genes between days 3 and 4 may be surprising given the lack of apoptosis

reported in this period. Instead this may reflect zygotic genome activation, and expression of regulatory transcripts to establish a balance of regulatory elements as final maternal transcripts are degraded (Petropoulos et al., 2016).

Although intrinsic apoptosis is they most predominant branch of homeostatic programmed cell death (Singh et al., 2019), genes involved in the extrinsic pathway appeared in the unbiased DE list, such as *TNFRSF1A* and *FADD*. This necessitates exploration of whether wider apoptosis mechanisms could be active in the embryo. Although the function of extrinsic apoptosis is predominantly related to immune functions, it cannot be ruled that that specific mechanisms have a role in developmental stages and/or stress (Flusberg and Sorger, 2015). Therefore, a selection of genes from the pathway were analysed in greater detail (n=8, Appendix 4, Table 4.6). Two genes, *TNF* and *FASLG*, where not detected in the dataset.

Gene		D3 → D4	D4 → D5	D5 → D6	D6 → D7
FADD	LogFC	7.22	-2.46	-2.37	1.92
	P	3.38E-07	5.59E-02	1.52E-02	9.09E-02
TNFRSF1A	LogFC	1.28	-0.42	3.06	0.96
	P	4.95E-01	8.42E-01	3.37E-03	4.05E-01
TNFRSF25	LogFC	2.21	0.94	-1.79	0.33
	P	8.67E-02	5.08E-01	3.52E-02	7.35E-01
TNFRSF10B	LogFC	-4.12	4.94	-3.16	-0.27
	P	1.59E-02	1.54E-04	1.61E-03	8.37E-01
TNFSF10	LogFC	-2.17	1.40	1.35	-1.60
	P	3.54E-02	1.50E-01	5.27E-02	2.31E-02
TRADD	LogFC	2.14	3.00	-2.18	-1.28
	P	3.15E-01	9.59E-02	1.00E-01	3.54E-01

Table 4.6. Key extrinsic apoptosis genes differentially expressed in at least one lineage comparison based on a literature search.

Red log fold change (logFC) denote an increased in expression moving forwards through development, blue a reduction. Genes that were not significantly (P>0.05) differentially expressed were excluded from the table. P; P value.

Amongst genes involved in the extrinsic pathway of apoptosis, *FADD* showed a strong elevation from day 3 to 4, before dropping at day 5 (P<0.001), and elevating again at day 7 (P<0.05). While *TNFRSF1A* was elevated after day 5 (P<0.01), its ligand could not be detected.

Although *TNFRSF25* was reduced at day 6 compared to day 5 (P<0.05), its key ligand, *TNFSF25*, showed no changes in expression. *TNFSF10B* was reduced in day 4 compared to day 3 (P<0.05), then elevated again at day 5 (P<0.001), before decreasing again (P<0.01). Its ligand, *TNFSF10*, also fell at day 4 (P<0.05), but showed only a gentle rise before dropping significantly between days 6 and 7 (P<0.05). Across cellular lineage only one gene was differentially expressed; *TNFRSF1A* was reduced in the TE in every comparison (P<0.01).

A key effector of extrinsic apoptosis, *FADD*, was downregulated in the blastocyst, suggesting activity would be minimal. Ligands involved in extrinsic apoptosis (*TNF* and *FASLG*) were not detectable in this analysis, while a key receptor, *TRADD*, showed no changes in expression level, broadly suggesting key pathways of extrinsic apoptosis are inactive. One such ligand-receptor pair, *TNFS10* and *TNFS10B*, were detected, as is the broad signalling modulator *TRADD*. Both receptor and ligand showed reduced expression from day 3 to 4, and although the receptor then elevated, the ligand remained low, suggesting the pathway remains inactive.

Relationships between mitophagy, specifically *BNIP3* protein family members, and the promotion and inhibition of apoptosis have been reported (Kubli and Gustafsson, 2012, Wanderoy et al., 2021). It is plausible the mitophagy reported in live cell imaging experiments (Chapter 1) is part of the reported apoptosis in the blastocyst. If mitophagy were linked to the process of apoptosis, it would suggest upregulation of mitophagy during PNT may compromise the health of human embryos. With a better understanding of apoptotic gene expression established, I explored links between apoptosis and mitophagy in the blastocyst. As live-cell imaging experiments suggested the *BNIP3*/*BNIP3L* machinery is important to blastocyst mitophagy, I examined correlation between the expression of the *BNIP3*/*BNIP3L* pathway genes with apoptosis GOs and positive regulator of apoptosis. I focused this analysis on day 6 and 7 blastocyst cells when live-cell imaging suggests mitophagy is abundant, and gene expression is most suggestive of these pathways being active (Figure 4.11). No meaningful correlations (r>0.3 and p<0.05) emerged between any apoptotic genes or mitophagy genes. One significant correlation emerged between *HRK* and *HIF1A* (Pearson correlation, P<0.05), but with a Pearson coefficient of only -0.12. Therefore, no links between mitophagy and apoptosis are apparent in the transcriptome of the human blastocyst.
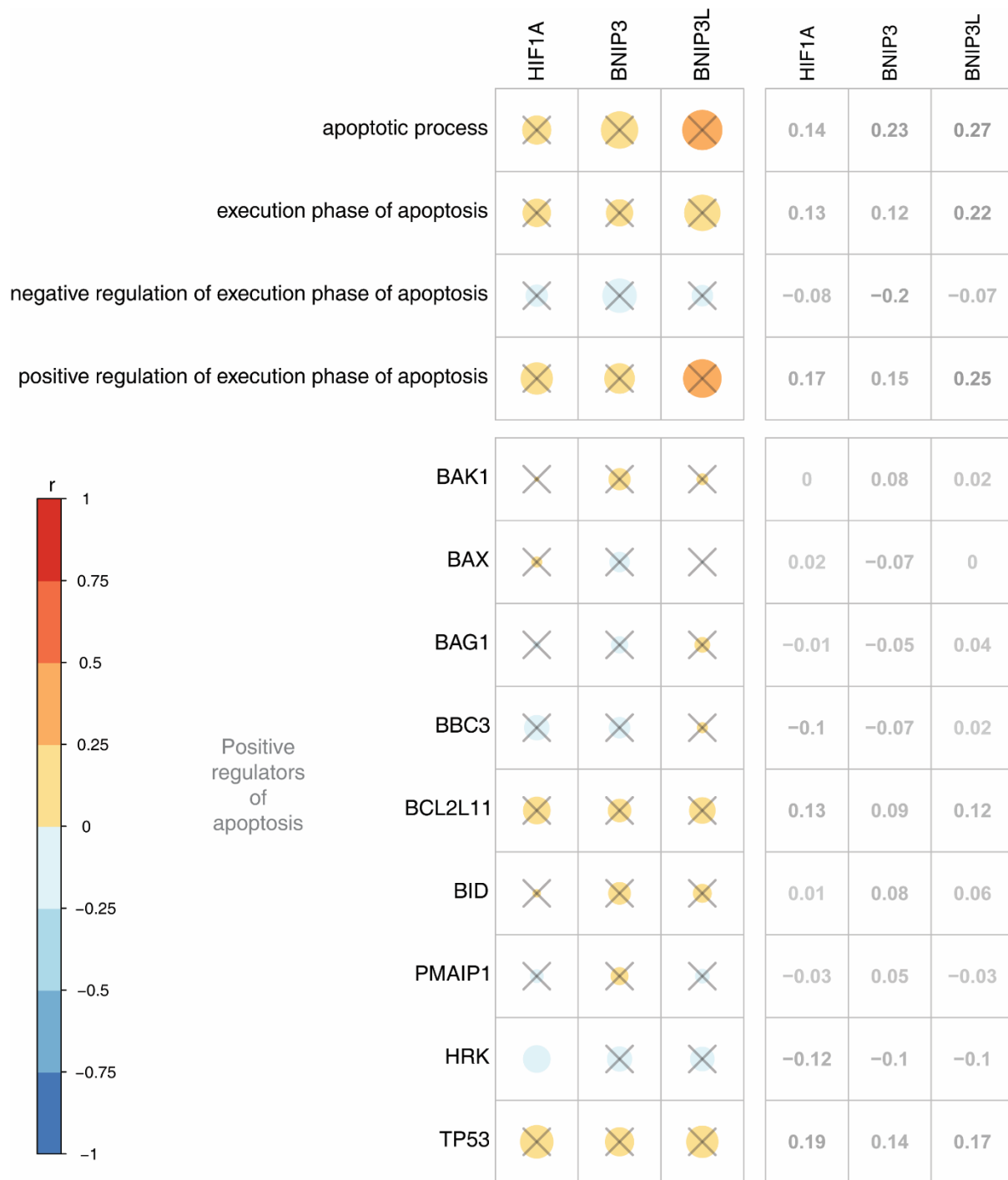
Figure 4.11. Pearson correlations between mitophagy and apoptosis genes in cells of day 6 and 7 blastocysts.

No meaningful correlations (r>0.3 and p<0.05) emerged between mitophagy genes and apoptosis gene ontologies or positive regulators of apoptosis. Crosses represent correlations with P>0.05. Left: red shades represent positive correlations, blue negative. Right: r values.

4.4.5. Expression of metabolic genes in the preimplantation embryo

Changes to cellular metabolism are reported in the blastocyst relative to cleavage embryos, encompassing both increased oxidative phosphorylation (OXPHOS) and glycolysis (Thompson et al., 1996, Houghton et al., 1996, Trimarchi et al., 2000, Sturmey and Leese, 2003). Changes to cellular metabolism may be reflected in remodelling the mitochondrial network, which may encompass mitophagy (Montava-Garriga and Ganley, 2020). Before exploring any relationships between these processes, I characterised the wider expression of metabolic genes in the preimplantation embryo.

Several GOs were selected to broadly analyse the metabolic profile of human preimplantation embryos; 'oxidative phosphorylation' ('OXPHOS'), 'negative regulation of oxidative phosphorylation', 'positive regulation of oxidative phosphorylation', and 'glycolytic process'. ANOVA of GO expression revealed significant changes in expression patterns of all GOs across developmental day, accounting for cellular lineage, embryo of origin and sex (ANCOVA, $P<0.001$, Figure 4.12).

Genes relating to 'OXPHOS' showed repeated significant increases in expression from developmental days 3 to 5 ($P<0.001$), then dropped significantly between days 6 and 7 ($P<0.001$). Genes of 'negative regulation of OXPHOS' were static until day 6 before dropping significantly ($P<0.001$). Genes relating to 'positive regulation of OXPHOS' increased form day 3 to 4 ($P<0.001$), and successive drops at day 5 ($P<0.05$) and 6 ($P<0.001$). Genes involved in the 'glycolytic process' show a significant increase in expression between days 3 to 4 then remained static before reducing from day 6 to 7 ($p<0.001$). The expression patterns of OXPHOS and 'glycolytic process' ontologies suggest that metabolic processes are broadly upregulated in the blastocyst relative to the cleavage embryo, and reflects reports from mouse and bovine models that metabolic pathways increase in activity during this (Thompson et al., 1996, Houghton et al., 1996, Trimarchi et al., 2000, Sturmey and Leese, 2003). The stable expression of 'negative regulation of OXPHOS' in this period suggests an increase in OXPHOS could be attributed to an upregulation of positive and effector genes instead of reduced expression in negatively regulating genes.
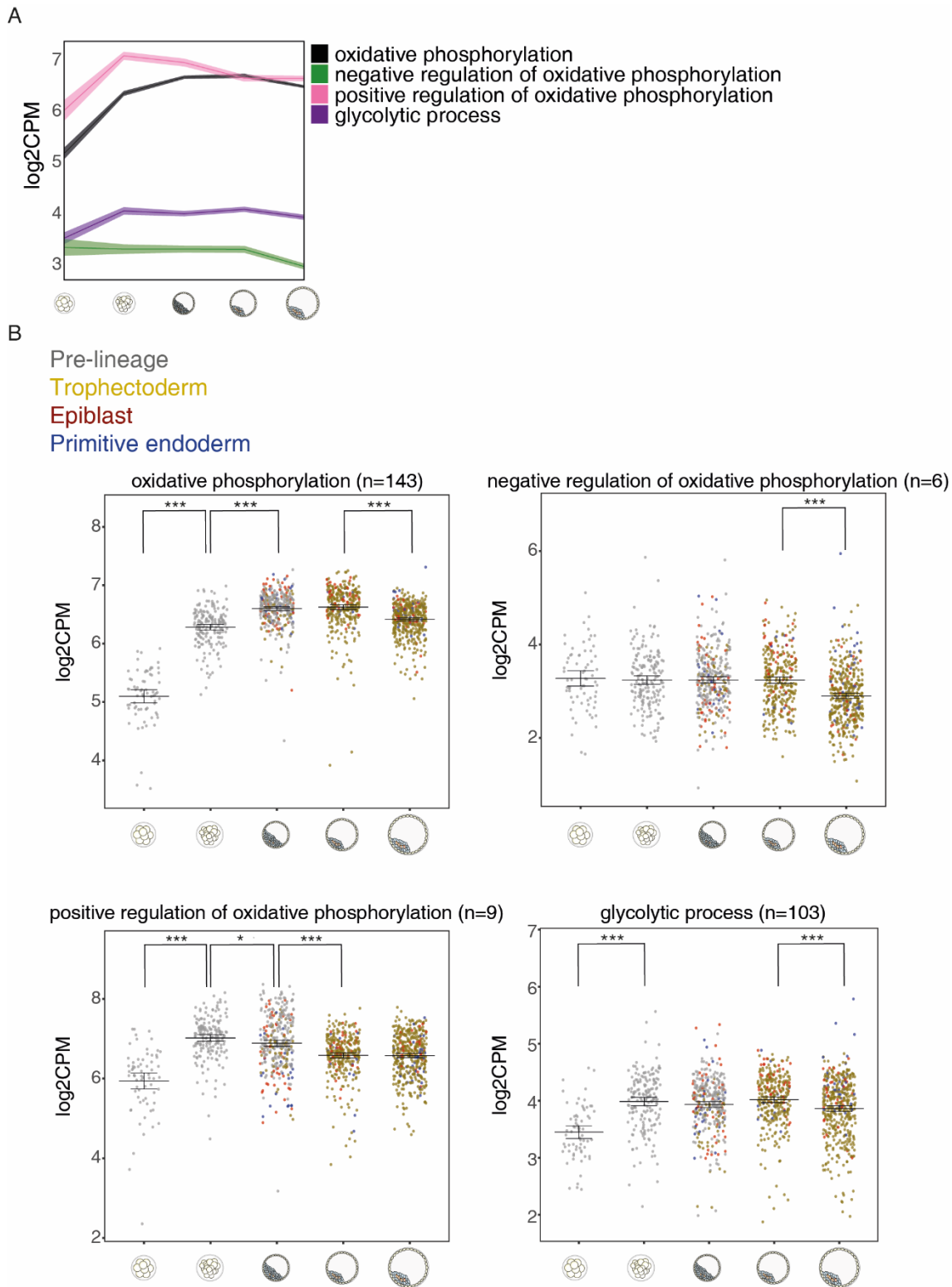
Figure 4.12. Expression of energy metabolism related GOs across developmental day/stage.

(A) Overview of expression of chosen GO terms by day. Shading represents 95% confidence interval. (B) Expression of GO terms between days 3 to 7, then across cellular lineages in days 5 to 7. n indicates number of genes analysed within a GO term. Expression of metabolic genes was increased in the blastocyst. Negative regulators of mitophagy were increased in the same time period. X-axis represents developmental day. Colour of point represents cell lineage. Gray = pre-lineage, yellow = trophectoderm, red = epiblast, blue = primitive endoderm. Error bars indicate 95% confidence intervals. Significance bars indicate outcome of Tukey analysis. *=P≤0.05, ***=P<0.001.

Glycolysis is an inefficient means of energy production, and reports have demonstrated that only 44% of glucose taken up is metabolised in such a way that lactose is produced, i.e. is used for means of energy production (Gardner and Leese, 1990). Furthermore, oxygen consumption is also increased in the blastocyst. This may suggest aerobic glycolysis makes a less significant contribution to ATP stores that might be otherwise assumed. This metabolic profile, and the fact that the blastocyst proliferates rapidly, have led to embryo metabolism being likened to the Warburg effect reported in tumour cells (Smith and Sturmey, 2013). This concept theorizes that when ATP is not limited, aerobic glycolytic activity may supply intermediates to biosynthetic pathways such as the pentose phosphate pathway/shunt (PPP) and Hexosamine biosynthetic pathway/UDP-N acetylglucosamine metabolic process (HBP) (Vander Heiden et al., 2009, Chi et al., 2020). The PPP is responsible for producing producing metabolites used for synthesis of nucleic acids, nucleotides amino acids (Ge et al., 2020), and the HBP produces metabolite necessary for protein modifications (Akella et al., 2019) (Figure 4.13). Derivates of glucose metabolism feed into both pathways before conversion to pyruvate. Therefore, I analysed the expression of GOs relating to these two biosynthetic pathways (Figure 4.14).

Genes relating to the 'PPP' ('pentose-phosphate shunt' GO) showed significant rises from day 3 to 4 and 4 to 5 ($P<0.001$), with a reduction shown from day 6 to 7 ($P<0.001$). Genes relating to the 'HBP' ('UDP-N-acetylglucosamine biosynthetic process' GO) showed a significant increase from day 4 to 5 ($P<0.001$) and 5 to 6 ($P<0.01$). Genes of both the 'PPP' and 'HBP' were elevated in the blastocyst, suggesting a portion of glucose taken up but cells of the blastocyst direct its derivatives proliferation and suggesting mechanisms evidenced in the mouse are conserved in human embryos. This model of metabolism would support the existence of the Warburg effect in the blastocyst.
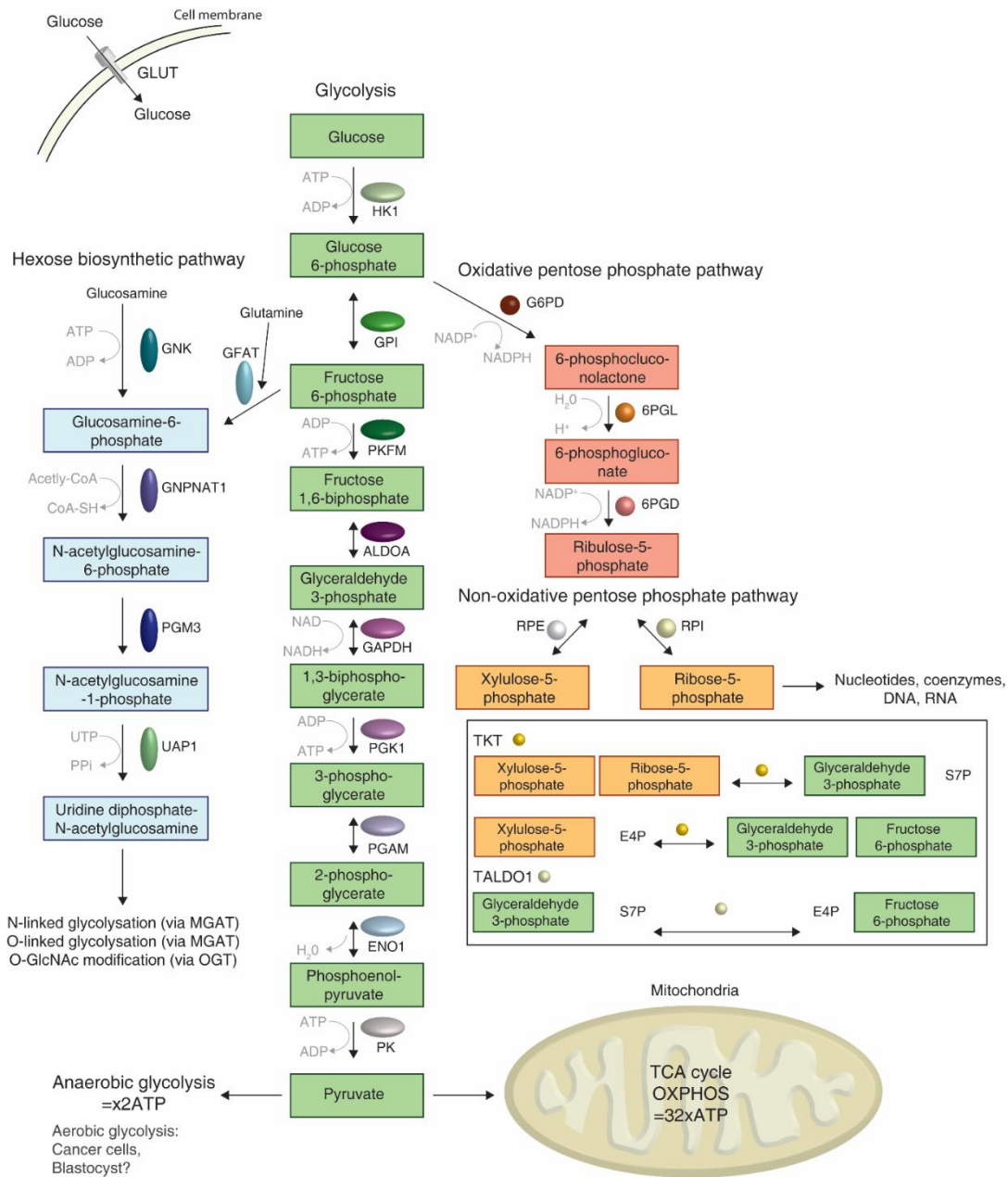
Figure 4.13. Cellular metabolism of glucose.

Glucose is imported by glucose transporters (*GLUTs*) and is converted into a series of metabolic intermediates (boxes), generating pyruvate. Aerobically, pyruvate is transported into mitochondria to feed the tricarboxylic acid cycle (TCA) cycle and oxidative phosphorylation (*OXPHOS*). Anaerobically pyruvate is converted to lactate by lactate dehydrogenase (*LDH*), producing reduced levels of ATP but more quickly. Glucose derivatives can be used to facilitate growth. The pentose phosphate pathway (red/orange) utilises glucose-6-phosphate to produce ribose-5-phosphate to enable nucleotide synthesis; with the oxidative branch producing ribulose-5-phosphate and the non-oxidative branch converting ribulose-5-phosphate to xylulose-5-phosphate and ribose-5-phosphate. Additionally, the non-oxidative branch, facilitated by transketolase (*TKT*) and transaldolase (*TALDO1*), can convert intermediates back into intermediates of glycolysis (Boxed). The hexose biosynthetic pathway (blue) derives from fructose-6-phosphate and glutamine, or from glucosamine, to produce uridine diphosphate-N-acetylglucosamine for protein modification. *6PGD*; 6-phosphogluconate dehydrogenase, *6PGL*; 6-phosphogluconolactonase, *ALDOA*; aldolase A, *E4P*; erythrose 4-phosphate, *ENO1*; enolase 1, *GAPDH*; Glyceraldehyde-3-Phosphate Dehydrogenase, *GNK*; N-Acetylglucosamine kinase, *GNPNAT1*; Glucosamine-Phosphate N-Acetyltransferase 1, *GPI*; Glucose-6-phosphate isomerase, *HK1*; Hexokinase 1, *PGK1*; Phosphoglycerate Kinase 1, *PGAM*; Phosphoglycerate mutase, *PGM3*; Phosphoglucomutase 3, *PKFM*; 6-phosphofructokinase, *RPE*; Ribulose-5-Phosphate-3-Epimerase, *RPIA*; Ribose 5-Phosphate Isomerase A, sedoheptulose-7-phosphate , *S7P*; *UAP1*; uridine diphosphate-N-Acetylglucosamine Pyrophosphorylase

A

B

Pre-lineage
Trophectoderm
Epiblast
Primitive endoderm

pentose−phosphate shunt (n=15)

UDP−N acetylglucosamine metabolic process (n=16)

Figure 4.14. Expression of biosythentic pathway related related GOs across developmental day/stage.

(A) Overview of expression of chosen GO terms by day. Shading represents 95% confidence interval. (B) Expression of GO terms between days 3 to 7, then across cellular lineages in days 5 to 7. n indicates number of genes analysed within a GO term. Expression of relevant genes was increased in the blastocyst. Negative regulators of mitophagy were increased in the same time period. X-axis represents developmental day. Colour of point represents cell lineage. Gray = pre-lineage, yellow = trophectoderm, red = epiblast, blue = primitive endoderm. Error bars indicate 95% confidence intervals. Significance bars indicate outcome of Tukey analysis. **=P<0.01, ***=P<0.001.

Previous studies of embryo metabolism have been unable to distinguish cellular lineage. To better characterise embryo metabolism, I also measured differences in expression of the 6 aforementioned GOs across lineage of the blastocyst (Figure 4.15). In day 5 blastocysts, 'positive regulation of OXPHOS' was significantly higher in pre-lineage cells compared to all other groups, while the PE was significantly lower than other groups ($P<0.001$). Genes of the 'glycolytic process' where significantly lower in the TE compared to all groups ($P<0.05$ to PE, $P<0.001$ to others), and the same was true of the 'PPP' ($P<0.001$). At day 6 genes of 'negative regulation of OXPHOS' were lower in the TE compared to the epiblast. ($P<0.001$). Genes of the 'glycolytic process' also showed higher expression in the epiblast but compared to both groups ($P<0.001$ v TE, $P<0.01$ v PE). Genes of the 'PPP' were again lower in the TE compared to the epiblast ($P<0.001$). By day 7, genes relating to OXPHOS where lower in the TE compared to the PE ($P<0.001$), as were those of 'negative regulation of OXPHOS '. Genes of 'negative regulation of OXPHOS' were additionally lower in the epiblast compared to PE ($P<0.01$). Genes of the 'glycolytic process' were significantly higher in the PE compared to both other groups ($P<0.01$).

The profile of OXPHOS GOs is generally flat across cellular lineages of the blastocyst (Figure 4.15). Genes relating to 'positive regulation of OXPHOS' were elevated in pre-lineage cells, which may be a reflection of an 'earlier' status given that the morula showed slightly higher expression of than the day 5 blastocyst. Although the same GO was slightly reduced in expression in the PE this may not manifest any functional changes, given the stable expression of wider OXPHOS genes, and the same is likely true of the slight changes apparent in other OXPHOS GOs at days 6 and 7. Genes of the 'glycolytic process' show a consistent elevation in the ICM throughout the blastocyst. This would suggest that the glucose favoured for energy production is accounted for primarily by the ICM. This may not be surprising given their position within the blastocoel where a supply of 0_2 is not directly available, and an increased burden on anaerobic metabolism may be required. Biosynthetic pathways examined are broadly elevated in the ICM and downregulated in the TE, and a higher level of biosynthesis may also explain why glycolysis genes are elevated. It is surprising that biosynthetic pathways are not elevated in the TE given the greater cell number in that population, and thus the higher rate of cell division and biosynthesis required.

.
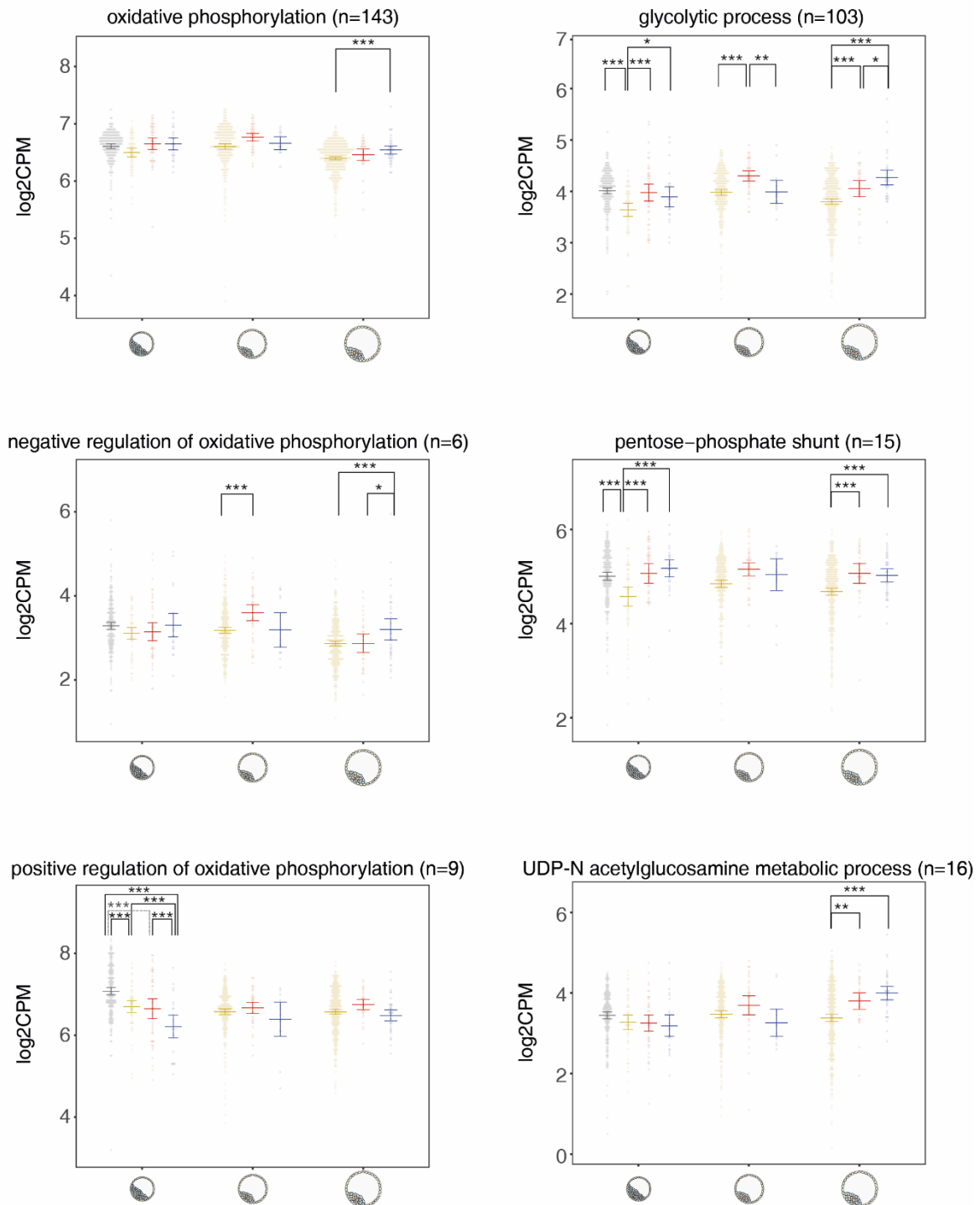
Figure 4.15. Expression of metabolism related GOs across cellular lineage of the blastocyst.

Several categories were upregulated in the inner cell mass. X-axis represents developmental day. n indicates number of genes analysed within a GO term. Colour of point represents cell lineage. Gray = pre-lineage, yellow = trophectoderm, red = epiblast, blue = primitive endoderm. Error bars indicate 95% confidence intervals. Significance bars indicate outcome of Tukey analysis. *=P<0.05, **=P<0.01, ***=P<0.001.

Given comparisons between the preimplantation embryo metabolism and the Warburg effect (Krisher and Prather, 2012), I examined trends in the temporal expression of key genes (n=8, Appendix 5) in the process of lactate formation and transport (Figure 4.16, Table 4.7). Three showed an elevation between days 3 and 4 in DE gene analysis; *LDHA* (P<0.001), *LDHB* (P<0.001) and *PKM* (P<0.01) which was sustained in the blastocyst, whereas *SLC16A3* showed an insignificant trend towards elevation.

PKM catalyses the final stage of pyruvate generation (Israelsen and Vander Heiden, 2015), and its expression pattern further suggests an increase in energy metabolism in the blastocyst relative to the cleavage embryo. *LDHA/LDHB* catalyse conversion of pyruvate into lactate at the end of aerobic glycolysis (Klein et al., 2020), and the elevation of these genes suggests a greater proportion of pyruvate is being process through aerobic glycolysis than in the cleavage stage embryo. *SLC16A3* catalyses the cellular internalisation of nutrients such as pyruvate and lactate (Jansen et al., 2008), and a slight increase in its expression in the blastocyst reinforces other suggestions of other trends expression.

Pre-lineage
Trophectoderm
Epiblast
Primitive endoderm

LDHA

LDHB

SLC16A3

PKM
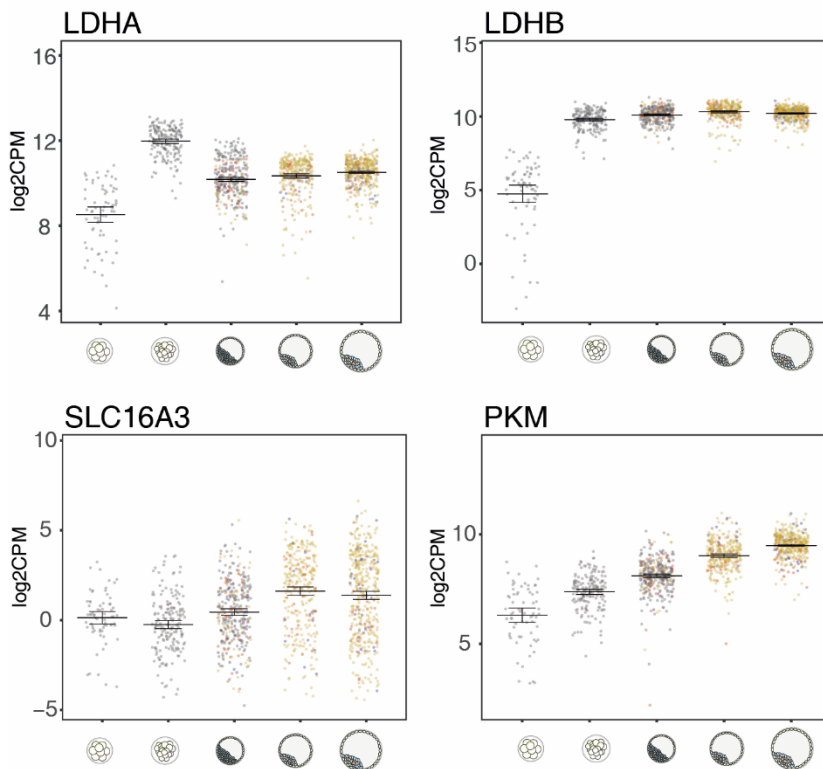
Figure 4.16. Significantly differentially expressed glycolysis genes from day 3 to 7.

Genes expression elevated in the blastocyst. X-axis represents developmental day. Colour of point represents cell lineage. Gray = pre-lineage, yellow = trophectoderm, red = epiblast, blue = primitive endoderm. Error bars indicate 95% confidence intervals.

Gene		D3 → D4	D4 → D5	D5 → D6	D6 → D7
LDHA	LogFC	3.48	-0.96	-0.81	0.39
	P	3.54E-03	7.32E-02	6.07E-02	4.99E-01
LDHB	LogFC	3.27	0.20	0.77	0.10
	P	3.55E-04	6.11E-01	5.25E-04	7.19E-01
PKM	LogFC	1.86	0.99	0.26	0.30
	P	1.79E-02	1.37E-02	3.91E-01	3.62E-01

Table 4.7. Key glycolysis genes differentially expressed in at least one lineage comparison based on a literature search.

Red log fold change (logFC) denote an increased in expression moving forwards through development, blue a reduction. Genes that were not significantly (P>0.05) differentially expressed were excluded from the table. PE, primitive endoderm; Epi, epiblast. P; P value.

A recent report demonstrated the importance of the PPP and HBP to the transcriptional control of blastocyst maturation and differentiation of the TE in mouse embryos, particularly incorporating four genes; *CDX2, TEAD4, TFAP2C*, and *YAP1* (Chi et al., 2020). It was shown that in the TE the HBP induced *YAP1* activation leading to its nuclear localisation, whereas the PPP induced *TFAP2C* translation. These proteins then form a complex with *TEAD4* and induce *CDX2* expression to promote TE differentiation. Although a great deal of this mechanism is regulated at the post-transcriptional level in the mouse, I examined the human transcriptome to explore whether I could identify the signature of this mechanism in human embryos (Figure 4.17, Table 4.8, Table 4.9).

As expected, at day 5 some of these genes were each more highly expressed in the TE compared to the ICM. Only some of these comparisons were significant in DE gene analysis; but *TFAP2C* was significantly upregulated in the TE compared to the ICM cells at day 5 ($P<0.001$). *YAP1* showed an upregulation at day 6 compared to day 5 ($P<0.001$) Both *YAP1* and *TFAP2C* are regulated post transcriptionally (Pocaterra et al., 2020, Chi et al., 2020), and so their largely flat expression over development is difficult to interpret. However, an elevation in the expression of *TFAP2C* in the TE at day 5 suggests that this mechanism of TE differentiation occurs similarly in mouse and human. *TEAD4* was also upregulated at day 4 relative to day 3 ($P<0.001$). *CDX2* was upregulated in the day 5 blastocyst compared to day 4 ($P<0.01$), and elevated again in the day 6 blastocyst ($P<0.001$). Furthermore, *TEAD4* was elevated in the TE at day 5 relative to the epiblast ($P<0.001$). As a canonical TE specification factor *CDX2* this would be expected (Strumpf et al., 2005).Downregulation of *TFAP2C* and *CDX2* in the day 5 ICM may be reflection of the onset of ICM differentiation (Rossant and Tam, 2009). Similarly, *CDX2* is strongly downregulated in the epiblast of day 7 blastocysts when TE cells should be firmly established. However, GOs of the associated biosynthetic pathway were not elevated in the TE. Nonetheless, the expression of these specific genes suggests this mechanism is conserved in the human blastocyst.
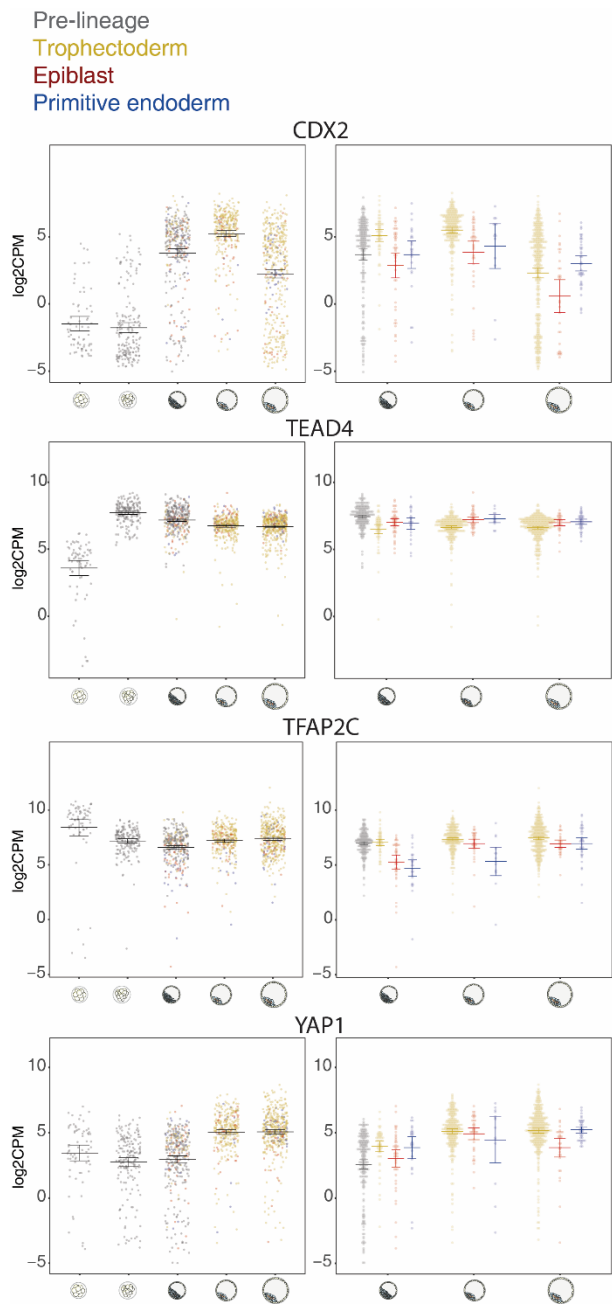
Figure 4.12. Significantly differentially expressed biosynthetic pathway mediated differentiation genes from day 3 to 7 and cellular lineage.

X-axis represents developmental day. Colour of point represents cell lineage. Gray = pre-lineage, yellow = trophectoderm, red = epiblast, blue = primitive endoderm. Error bars indicate 95% confidence intervals.

Gene		D3 → D4	D4 → D5	D5 → D6	D6 → D7
CDX2	LogFC	-3.91	3.81	5.61	-1.38
	P	2.97E-02	8.39E-03	3.43E-07	1.49E-01
TEAD4	LogFC	2.90	0.11	-1.31	-0.03
	P	7.05E-05	8.85E-01	1.39E-04	9.59E-01
TFAP2C	LogFC	-0.77	0.51	0.13	-2.08
	P	3.61E-01	5.30E-01	8.33E-01	5.47E-04
YAP1	LogFC	-2.72	0.43	3.13	-1.63
	P	4.11E-02	8.05E-01	4.51E-04	4.62E-02

Table 4.8. Biosynthetic pathway mediated differentiation genes differentially expressed in at least one developmental day comparison.

Red log fold change (logFC) denote an increased in expression moving forwards through development, blue a reduction. Genes that were not significantly (P>0.05) differentially expressed were excluded from the table. P; P value

Gene	Comparison	logFC	P
CDX2	Day 5 Epi → TE	2.32	4.96E-04
TFAP2C	Day 5 Epi → TE	1.67	3.71E-14
	Day 5 PE → TE	2.12	1.24E-08

Table 4.9. Biosynthetic pathway mediated differentiation genes differentially expressed in at least one lineage comparison.

Red log fold change (logFC) denote an increased in expression moving forwards through development, blue a reduction. Genes that were not significantly (P>0.05) differentially expressed were excluded from the table. PE, primitive endoderm; Epi, epiblast. P; P value.

It is plausible that as the energy metabolism of the embryo changes in the blastocyst relative to the cleavage stage embryo, the mitophagy apparent in live-cell imaging experiments (Chapter 1) is involved in remodelling the mitochondria network to meet cellular needs. Mitophagy would act to constrain the mitochondrial network likely to increase glucose metabolites directed to OXPHOS alternatives. To explore this possibility, I examined correlations between *BNIP3*/*BNIP3L* pathway proteins and previously examined metabolic GOs and with several key genes involved in aerobic glycolysis. Again, I focused on the day 6 and 7 blastocyst when these pathways are both active (Figure 4.18). However, no meaningful correlations (r>0.3 and p<0.05) between mitophagy and cellular metabolism emerged. Therefore, it appears that changes to mitochondrial metabolism are mediated without any remodelling of the mitochondrial network via mitophagy.
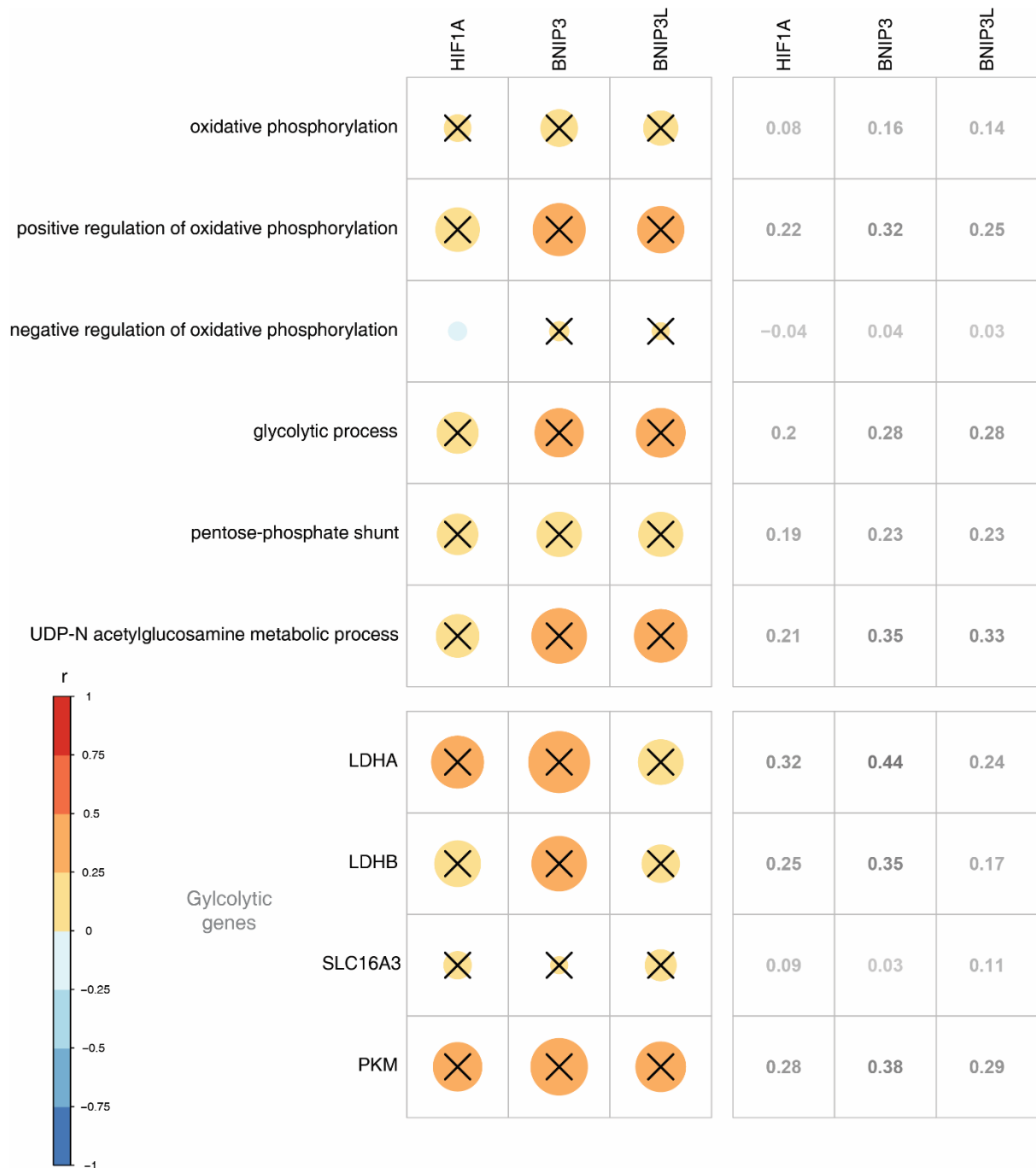
Figure 4.18. Pearson correlations between mitophagy and metabolism genes in cells of day 6 and 7 blastocysts.

No meaningful correlations (r>0.3 and p<0.05) emerged between mitophagy genes and apoptosis gene ontologies or positive regulators of apoptosis. Crosses represent correlations with P>0.05. Left: red shades represent positive correlations, blue negative. Right: r values.

4.4.6. Mitophagy and segregation of blastocyst cell lineage

Mitophagy has been implicated in cell specification in a variety of development contexts (Naik et al., 2019, Cairns et al., 2020), although to date not in the preimplantation embryo. To explore whether mitophagy could be linked to the ongoing process of cell differentiation in the day 5 (TE) and 6 blastocyst (PE and the pluripotent epiblast), I analysed correlations in gene expression of *BNIP3*/*BNIP3L* pathway genes and to expression of transcription factors (Figure 4.19) which drive differentiation of blastocyst cell lineages (Rossant and Tam, 2009, Blakeley et al., 2015).

In day 5 TE cells, which will be freshly differentiated or undergoing differentiation, negative correlations were apparent between mitophagy mediators and *GATA2/3*, most strongly between *BNIP3* and *GATA3* (r=-0.54, Pearson correlation, p<0.001), which promote differentiation of the TE (Krendl et al., 2017). Thus during day 5 of developmental a reduced level of mitophagy can be associated with TE differentiation. In cells of the day 6 ICM, significant negative correlations appeared between mediators of mitophagy and genes associated with pluripotency; *FGF4, NANOG, POU5F1/OCT4* and *SOX2* (Nichols et al., 1998, Mitsui et al., 2003, Kang et al., 2013). This occurred most prevalently between *BNIP3* and *NANOG* and *POU5F1* in the PE (r=-0.52, Pearson correlation, p<0.001), and *HIF1A* and POU5F1 in the epiblast (r=-0.52, Pearson correlation, p<0.001). Additionally, in the PE, significant positive associations appeared between mediators of mitophagy and drivers of PE differentiation *GATA 4/6* (Chazaud et al., 2006, Morris et al., 2010), most strongly between *BNIP3* and *GATA4* (r=0.64, Pearson correlation, p<0.001). Therefore, a low level of mitophagy could be associated with higher levels of NANOG and POU5F1 and thus the differentiation of the pluripotent epiblast. Meanwhile during day 6, elevated mitophagy gene expression appears to be associated with *GATA4/6* and thus PE specification. Additionally, glycolysis has been associated with cell specification with mitophagy often linked to this glycotic switch (Krendl et al., 2017, Cairns et al., 2020). Interestingly the correlations of the 'glycolytic process' GO and differentiation factors largely mirrors that of the mitophagy mediators and differentiation factors. (Figure 4.18).

Functional studies would be required to confirm and characterise these associations, especially as an association is apparent between reduced mitophagy and differentiation at day 5 but between increased mitophagy and the maintenance of pluripotency at day 6. Although

correlations are relatively weak they are consistent mediators of mitophagy and drivers of specification, and thus this represents the first suggestion of a role for mitophagy in differentiation of blastocyst cellular lineages.
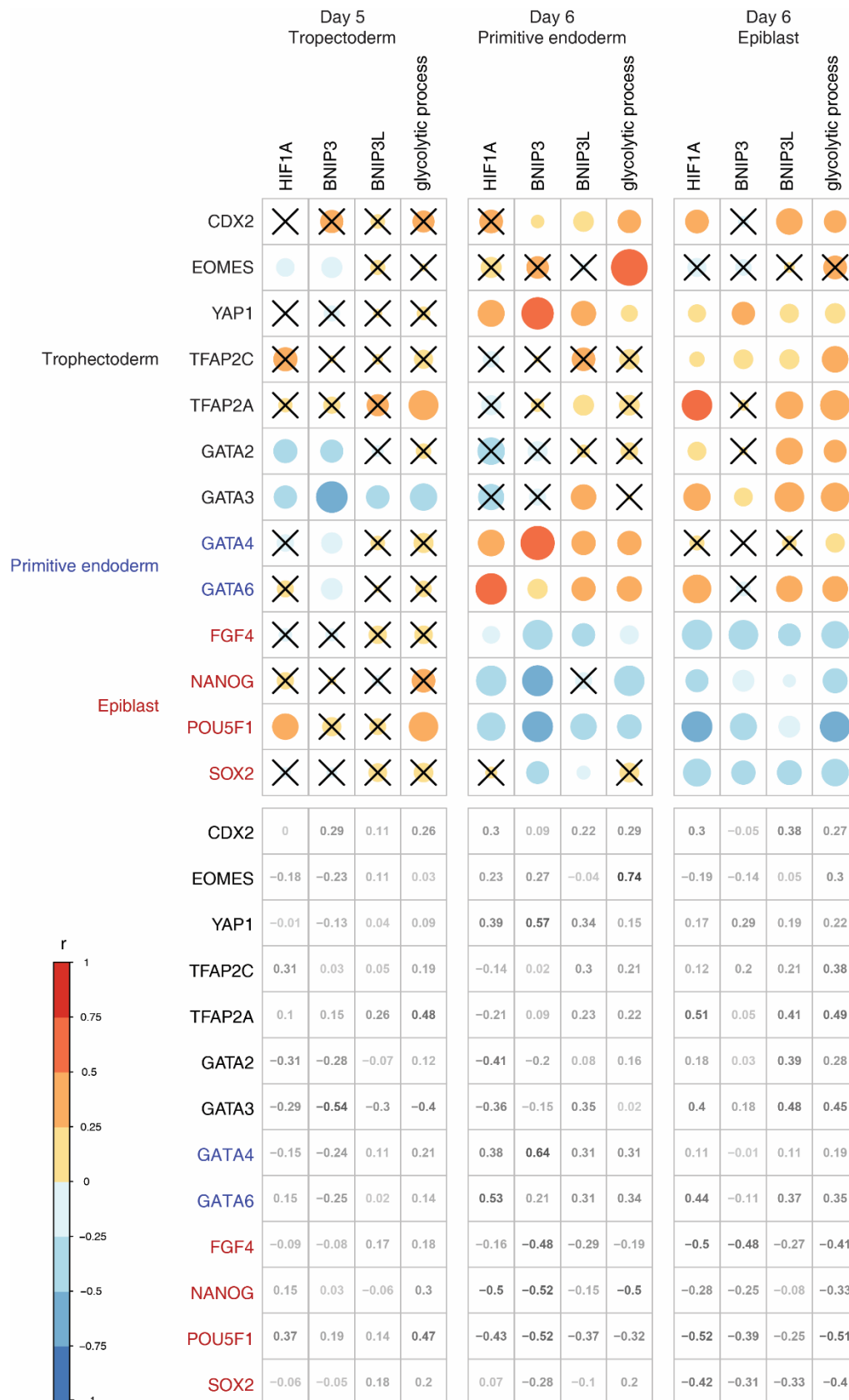
Figure 4.19. Pearson correlations between mitophagy and differentiation genes in cells of day 5 and 6 blastocysts.

Significant correlations were apparent between mitophagy genes and lineage specific genes are different time points. These correlations were mirrored in the glycolytic process gene ontology. Crosses represent correlations with P>0.05. Top: red shades represent positive correlations, blue negative. Bottom: r values.

4.4.7. Expression of genes involved in wider mitochondrial network maintenance

Selective removal of mitochondrial biomass by mitophagy is an important quality control mechanism for the maintenance of a viable mitochondrial network (Twig and Shirihai, 2011). Therefore, the implications of mitophagy and its effect on the morphology of mitochondria in the embryo must be assessed alongside other methods of mitochondrial homeostasis, but little is known about mitochondrial dynamics in the preimplantation embryo. The most pertinent question would be whether mitophagy is accompanied by mitochondrial biogenesis to replenish lost mitochondrial biomass. No precise GOs currently exist to define the complex process of mitochondrial biogenesis, instead I examined the GOs of 'mitochondrial DNA replication', 'mitochondrial transcription' and 'mitochondrial translation' across developmental day and cellular lineage (Figure 4.20).

Across day of development, the expression of genes relating to 'mitochondrial DNA replication' show a significant rise from day 3 to 4 (P<0.001), followed by a fall at day 5 (P<0.001), and subsequent rise at day 6 (P<0.001). Genes of 'mitochondrial transcription' were elevated at day 4 compared to day 3 (P<0.001), before falling in the day 5 blastocyst (P<0.001), and falling slightly again at day 7 (P<0.05). Genes of 'mitochondrial translation' elevated sharply at day 4 compared to day 3 (P<0.001) before remaining stable.

Genes of the 'mitochondrial DNA replication' GO are generally lowly expressed and are highly variable across developmental day (Figure 4.20). Their expression was similar in the blastocyst to that at the morula stage, while the genes of mitochondrial transcription are lower in the blastocyst compared to the morula. Despite a strong increase in expression of genes involved in mitochondrial translation suggesting of an increase in mtDNA encoded protein levels, this suggests a lack of broad mitochondrial biogenesis in this period of development. An elevation in mitochondrial translation in the morula may be linked with an increase in OXPHOS. Indeed, it has been demonstrated that translation of *MT-ND5* is repressed via N^1-methyladenosine methylation until the morula stage (Safra et al., 2017), and same may be true of other MT-RNAs.

Across cellular lineage the' mitochondrial transcription' GO was variable across lineage in day 5 (Figure 4.20), where pre-lineage cells showed a higher expression than the TE and PE

(P<0.01), perhaps reflecting higher expression in the morula. Expression of the mitochondrial translation GO was also elevated in the day 5 pre-linage cells compared to other groups (P<0.05). The OXPHOS GO was also elevated in pre-lineage cells. Together this may reflect an elevated energy demand in cells which are approaching differentiation. Alternatively, these pre-lineage cells may be destined for apoptosis, which has been linked with a higher level of ATP in the cytosol (Zamaraeva et al., 2005), and this may be reflected in expression of relevant GOs. As such no evidence of mitochondrial biogenesis in the preimplantation embryo emerges.
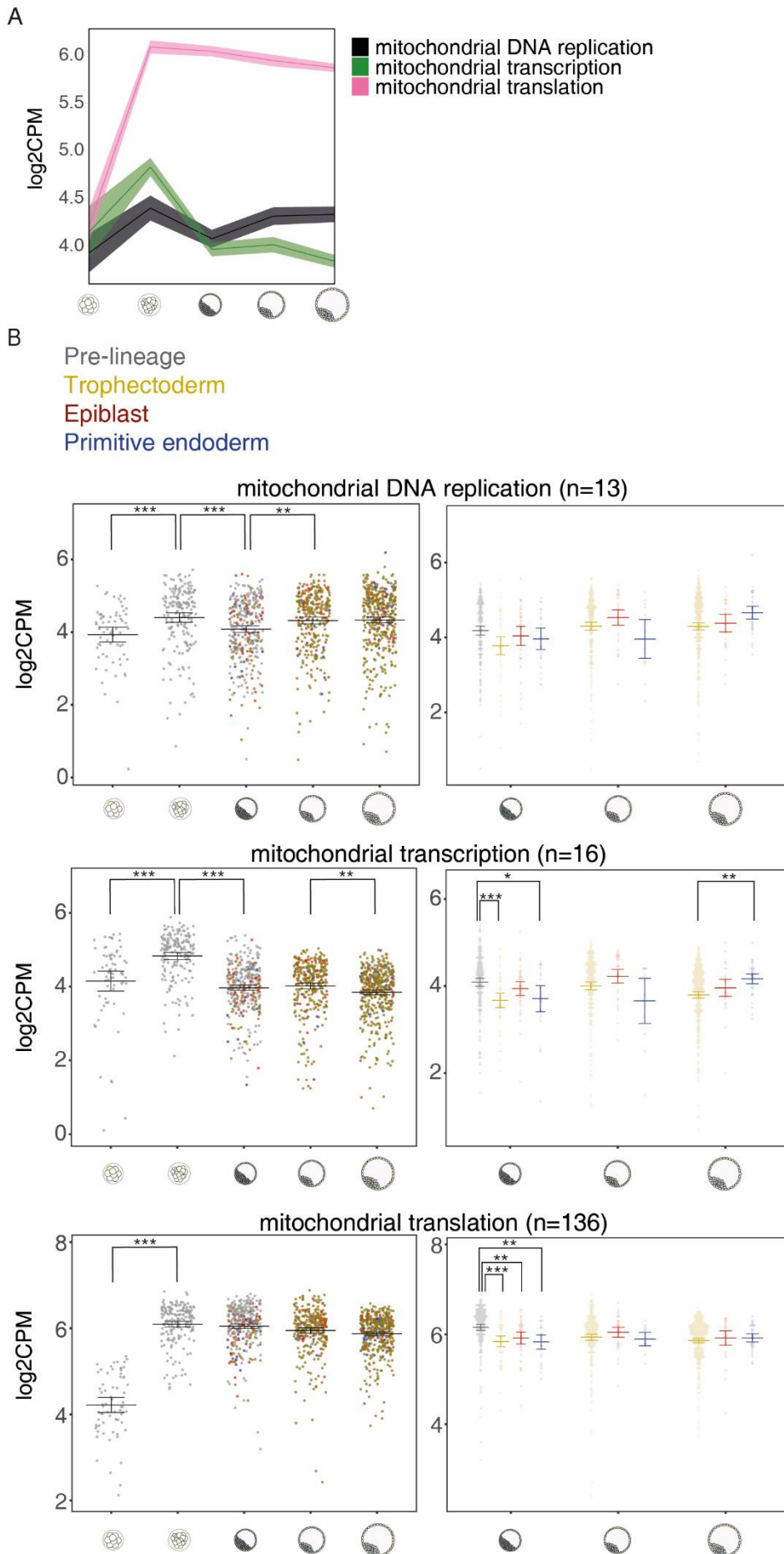
Figure 4.20. Expression of GO terms relating to maintenance of the mitochondrial network.

(A) Overview of expression of chosen GO terms by day. Shading represents 95% confidence interval. (B) Expression of GO terms between days 3 to 7, then across cellular lineages in days 5 to 7. n indicates number of genes analysed within a GO term. Primitive endoderm = blue, trophectoderm = yellow; epiblast = red; pre-lineage = grey. Error bars indicate 95% confidence intervals. Significance bars indicate outcome of Tukey analysis. *=P<0.05, **=P<0.01, ***=P<0.001.

To further characterise wider mitochondrial dynamics I curated a list of genes which mediate mitochondrial fission and fusion and mtDNA replication/translation (n=34, Appendix 6, Figure 4.21, Figure 4.22), and analysed their DE (Table 4.10). All key mitochondrial fission genes, *DNM1L, FIS1* and *MFF* were downregulated at day 4 compared to day 3 (P<0.05), while both *DNM1L* and *MFF* elevated in expression again at day 5 (P<0.001). Of the *MFN* genes, key regulators of mitochondrial fission, *MFN2* was elevated between days 3 and 4 (P<0.05), whereas both *MFN1* and *MFN2* were downregulated at day 6 (P<0.001). Meanwhile *OPA1* was reduced at day 4 (P<0.001) compared to day 3 then elevated again at day 5 (P<0.05). This expression profile is variable and suggests no widespread changes occur to mitochondrial morphology despite changing energy demands. However, conclusions cannot be drawn on how important the maintenance of mitochondrial morphology is to the embryo.

A number of genes which mediate mtDNA replication/translation where not DE in any comparison across day (eg *TWNK, TFAM, PPRC1, TOP2B* and *POLG2*) whereas the important regulator of mitochondrial replication, *PPARGC1A*, was not detectable. Several genes (Table 4.10) increased from day 3 to 4; *SSBP1, RAD51* and *TOP1MT* (P<0.05), and *NFE2L2* increased between days 4 and 5 (P<0.001), prior to the onset of mitophagy. Across days 6 and/or 7, 5 genes were downregulated; *MGME1, POLG, POLRMT, RAD51* and *TOP1MT* (P<0.05). In the same period the only upregulated gene was DNA2 at day 6 (P<0.05). Given that important genes like *TWNK* and *TFAM* were not DE, this again suggests a lack of mitochondrial biogenesis in the preimplantation embryo. None of the curated genes were DE across cellular lineage (data not shown). Therefore, at the level of DE analysis no evidence emerges to suggest mitochondrial biogenesis occurs in the preimplantation embryo.

Figure 4.13. Mitochondrial biogenesis.

In response to elevated energy demand mitochondrial biomass and mtDNA copy number can be increased, coordinated by nuclear-mitochondrial DNA interaction. Mitochondrial biogenesis begins with upregulation of peroxisome proliferator-activated receptor gamma coactivator 1-alpha (PPARGC1A), the master regulator of the process. PPARGC1A promotes expression of nuclear respiratory factor 1/1 (NRF1/2), which in turn upregulate the expression of nuclear-encoded mitochondrial proteins, including transcription factor A, mitochondrial (TFAM). TFAM translocates to the mitochondria and binds mtDNA, promoting both its transcription and regulation. mtDNA replication relies of DNA Polymerase Gamma (POLG) and twinkle (TWNK), whereas transcription is performed by polymerase, mitochondrial (POLMRT).

Figure 4.22. Mitochondrial fission and fusion.

In response to cellular energy demand, the processes of fission and fusion act to module the morphology of the mitochondrial network to increased OXPHOS capacity or reduce excess. The process of fission separates the mitochondrial network. Mitochondrial fission factor (*MFF*) and fission, mitochondrial 1 (*FIS1*) recruit dynamin-1-like (*DNML1*) to the mitochondrial surface, where it multimerises and surrounds the point of fission, then facilitates separation via its GTPase function. Fission of the mitochondrial network can facilitate mitophagy by separating regions of impaired or damaged mitochondria. Mitochondrial fusion can join mitochondria. Fusion is not as well characterised as fission but is mediated by mitofusin 1/2 (*MFN1/2*) and mitochondrial dynamin like GTPase (*OPA1*).

101
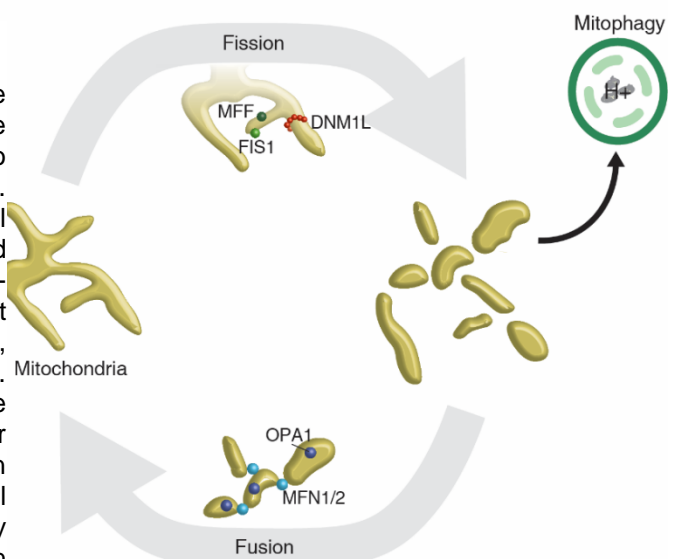
Gene		D3 → D4	D4 → D5	D5 → D6	D6 → D7
Fission					
DNM1L	LogFC	-2.14	3.69	0.50	0.10
	P	3.70E-02	3.15E-08	3.48E-01	8.71E-01
FIS1	LogFC	-2.29	-0.16	0.23	-0.26
	P	2.55E-03	8.95E-01	7.82E-01	7.37E-01
MFF	LogFC	-5.06	5.48	0.34	-0.47
	P	9.13E-05	2.62E-08	7.32E-01	6.13E-01
Fusion					
MFN1	LogFC	0.71	-0.68	-3.41	-0.61
	P	3.38E-01	3.08E-01	4.30E-10	4.11E-01
MFN2	LogFC	1.64	0.51	-2.10	-0.22
	P	3.55E-02	4.33E-01	1.52E-06	7.42E-01
OPA1	LogFC	-4.31	2.32	0.14	-0.29
	P	1.22E-05	2.53E-02	8.96E-01	7.44E-01
mtDNA replication					
DNA2	LogFC	-2.21	-0.81	2.28	-0.08
	P	1.33E-01	6.52E-01	2.63E-02	9.45E-01
MGME1	LogFC	1.55	0.25	-2.57	1.24
	P	2.81E-01	8.65E-01	6.59E-04	1.77E-01
POLG	LogFC	-2.26	1.03	1.04	-2.61
	P	1.19E-01	5.06E-01	3.17E-01	7.55E-03
POLRMT	LogFC	-1.37	0.97	-2.30	-1.75
	P	2.25E-01	3.52E-01	2.33E-03	5.56E-02
RAD51	LogFC	2.25	0.60	-2.12	0.23
	P	1.51E-02	4.18E-01	3.40E-05	7.61E-01
SSBP1	LogFC	3.32	-0.53	0.51	0.04
	P	1.94E-10	9.87E-02	2.22E-02	9.05E-01
TOP1MT	LogFC	3.16	-1.54	-1.93	1.47
	P	2.34E-02	1.30E-01	2.29E-02	1.39E-01

Table 4.10. Differential expression of key mitochondrial network maintenance genes.

Red log fold change (logFC) denote an increased in expression moving forwards through development, blue a reduction. Genes that were not significantly (P>0.05) differentially expressed were excluded from the table. P; P value.

4.4. Discussion

Live-cell imaging in the mouse and human embryo revealed the occurrence of mitophagy in the preimplantation embryo, sparsely detectable in the morula and growing across blastocyst maturation (Chapter 1). However, the specific mechanisms of this mitophagy and its implications require characterisation. Analysis of a large scRNAseq database derived from human embryos ranging from the 8-cell to late blastocyst stage (days 3 to 7) presented an opportunity to investigate these processes during development.

Analysis of the expression of mitophagy genes guided identification of a method of upregulating mitophagy via overexpression of pBNIP3L. Expression of mitophagy genes related to the *BNIP3L* mitophagy pathway were significantly correlated with the expression of genes relating to establishment of cellular lineages in the blastocyst at different developmental days. Furthermore, processes previously explored in animal models were explored at the level of the human transcriptome. Expression of apoptosis genes was highly variable and suggested dynamic regulation in the blastocyst. No links between apoptosis and mitophagy were detected. The metabolic profile of preimplantation embryos, previously explored in mouse and bovine models (Thompson et al., 1996, Houghton et al., 1996, Trimarchi et al., 2000, Sturmey and Leese, 2003), appears similar to that of human embryos based on analysis of the human transcriptome. No links between changing metabolic demands of the blastocyst and mitophagy genes were detected.

Mitophagy in the preimplantation embryo

Expression of GOs relating to mitophagy revealed an unexpected pattern given the occurrence of mitophagy suggested by live-cell imaging experiments (Chapter 1). Similarly, analysis of DE gene lists revealed no candidate genes of which expression could fully explain mitophagy in the blastocyst. My analysis suggests that the *BNIP3*/*BNIP3L* genes and associated cellular machinery could be important, as expression of *HIF1A* and both *BNIP3* genes was elevated coinciding with mitophagy. Overexpression of pBNIP3L succeeded in upregulating mitophagy further suggesting a role for the machinery of this pathway. This establishes overexpression of pBNIP3L as a tool to upregulate mitophagy and allow further characterisation of its role,

and a candidate for inducing degradation of mitochondria in the zygote to prevent carryover in PNT.

In my analysis genes of the *PINK1/PRKN* pathway were downregulated at different stages of blastocyst development. A role for *PINK1* has been previously evidenced in porcine embryos in relation to mitochondrial fission (Niu et al., 2019). *PINK1* mRNA abundance in the porcine embryo was higher at the 8-cell stage relative to the porcine blastocyst, as was protein levels, and so the results of my analysis is not unexpected. Whilst downregulation at the time of mitophagy suggests *PINK1* is not involved in mitophagy, it is plausible it maintains a role in background maintenance globular mitochondria in the human preimplantation embryo via its role in regulating mitochondrial fission (Yang et al., 2008). Although changes in *PINK1/PRKN* expression across day of development did not suggest a role in mitophagy revealed by live-cell imaging, as expression dropped beginning in the day 5 blastocyst. Their expression in the epiblast may represent an upregulation of quality control mechanisms to ensure robustness of mitochondrial in tissues which give rise to the fetus, or differences in how the mitochondrial network is maintained.

Evidence of the *BNIP3/BNIP3L* pathway machinery being active in the blastocyst suggests the removal of mitochondria is targeted to excess or unneeded mitochondrial biomass, as opposed to defective mitochondria. I therefore analysed correlations between expression of *BNIP3/BNIP3L* pathway genes and other mechanisms to attempt to identify the cause or role of this mitophagy. When cells of the day 6 and 7 blastocyst were analysed collectively across day and lineage, expression of mitophagy genes (*BNIP3*, *BNIP3L* and *HIF1A*) could not be associated with apoptosis or metabolic pathways. Instead, significant and broad, but relatively weak, correlations emerged between the expression of genes which promote differentiation of blastocyst cell lineages. In day 5 TE cells reduced expression of mitophagy genes was associated with elevated expression of genes which promote TE differentiation, while in Day 6 ICM cells reduced mitophagy genes was associated with elevated pluripotency factors which are a hallmark of the epiblast lineage. Further positive correlations with promoters of PE differentiation were apparent in the day 6 PE.

Mitophagy has been implicated in both the differentiation of stem cells and their maintenance (Cairns et al., 2020). Activity of the *BNIP3/BNIP3L* pathway specfically has been implicated in the differentiation of retinal ganglion cells in the mouse embryo (Esteban-Martínez et al., 2017),

differentiation of mouse cardiac progenitor cells *in vitro* (Lampert et al., 2019), and differentiation of a human cell line into cardiomyoblasts (Zhao et al., 2020). Although my analysis is conducted only at the level of the transcriptome, this represents the first suggestion that mitophagy has a role in cell differentiation in the human blastocyst. Mitophagy in the context of cell differentiation has been linked with a switch to glycolytic metabolism in preference to OXPHOS (Shyh-Chang and Ng, 2017), and interestingly, correlations of mitophagy genes were matched in correlations between the lineage-associated transcription factors and expression of the 'glycolytic process' GO.

Apoptosis in the preimplantation embryo

Broad GO expression profile showed genes of 'apoptotic process', 'execution phase of apoptosis' and positive regulation of 'apoptotic process' elevating at day 5 or 6 and peaking in the blastocyst, with expression of 'negative regulation of execution phase of apoptosis' dropping in the day 6 blastocyst. Evidence for the onset of apoptosis in day 5 is also provided in the differential expression of canonical apoptosis genes, where most positive regulators are upregulated. During this period of heightened apoptotic gene expression, GOs are also frequently higher in at least one ICM population compared to the TE. Together, this reflects the elevated apoptosis evidenced in the human blastocyst compared to the cleavage stage embryo, and in the ICM compared to the TE, demonstrated using imaging methods such as TUNEL staining (Hardy et al., 1989, Hardy and Handyside, 1996, Jurisicova et al., 1996).

Changes in the expression of specific apoptosis regulators can offer insights into the mechanisms of apoptosis in the blastocyst. Previous studies have attempted to identify genes acting in blastocyst apoptosis by means of RT-PCR. These studies are difficult to correlate with my own analysis as they regard all blastocyst stages singularly, often focus on earlier stages of development, lack analysis at the single cell level so do not account for cell lineage, and in some cases lack statistical analysis. Amongst these, the most convincing focused on embryos with a slight morphological abnormality of fragmented cells (Jurisicova et al., 2003). Most reported changes in mRNA levels correlate with my own analysis; in both reports *BAG1, BAX*, and *CASP2* were elevated in the blastocyst, whereas *MCL1* and *CASP3* where not differentially expressed. Discrepancies arise in *BCL2L1*, which is stable in my analysis but shows decreased expression in the blastocysts of Jurisicova *et al* (2003), and *HRK*, which is stable in my expression but elevated in the morula of Jurisicova *et al* (2003). This may be for

aforementioned reasons, or because Jurisicova *et al* (2003), focused on embryos with fragmentation as a model of cell death. To what extent this represents a model of broad programmed cell death is unclear (Martinez et al., 2002).

A more recent study utilised imaging techniques to demonstrate that *BMP4* and *TP53* proteins can induce apoptosis in human preimplantation blastocysts, whereas *SIRT1* was inhibitive (De Paepe et al., 2019). In my analysis these genes were consistently expressed across all lineages. However, *SIRT1* showed reduced expression from day 3 to 4 before elevating. The expression of *TP53* could be modulated by range of factors given its diverse roles (Hafner et al., 2019), so likely provides a weak indicator of this mechanism, and *BMP4* remained stable. As *BMP4* expression is consistent, and as *SIRT1* is elevated during the period when apoptosis has been reported, it appears the mechanism suggested by De Paepe *et al* is not detectable in my analysis. This may be because apoptosis was artificially induced by DE Paepe *et al* (2019). However, interpreting changes in the expression of *SIRT1* is complicated by its role in regulating cellular metabolism (Rahman and Islam, 2011), which could be occurring in the human preimplantation embryo.

PMAIP1 shows strikingly consistent differences in expression across cellular lineage, being consistently more highly expressed in the ICM than the TE. The onset of apoptosis depends on the fine balance between positive and negative regulators and although *PMAIP1* is not characterised as a potent activator of apoptosis (Singh et al., 2019), its activity may represent the key regulatory protein that causes the higher incidence of ICM apoptosis that has been reported (Hardy et al., 1989). It has previously been suggested that *PMAIP1* is important in apoptosis in embryogenesis based on elevated expression in the embryo compared to the oocyte, but the effect of lineage was not analysed (Boumela et al., 2014).

A *Pmaip1* knockout mice survives until at least one year of age with no unexpected morbidity (Shibue et al., 2003). This is not surprising as a triple knockout model of *Bax/Box/Bak*, heavily resistant to apoptosis, show developmental abnormalities but survives preimplantation development (Ke et al., 2018), suggesting that the apoptosis within the preimplantation embryo is not fundamental, with abnormalities only presenting in perinatal development. In the wildtype mouse, no apoptosis was detected via TUNEL staining in the 8-cell or morula, in contrast to the blastocyst, mirroring human embryos and suggesting it represents a faithful model (Brison and Schultz, 1997, Kamjoo et al., 2002). However the structure of mouse

Pmaip1 is considerably different to that of the human *PMAIP1* with one additional exon in its transcript and it is not entirely clear how well their functions correlate (Ploner et al., 2008), which may allow an increased importance to human development.

The target of *PMAIP1* regulation, the anti-apoptotic *MCL1*, did not show any changes in its expression at the mRNA level across lineage. The importance of *Mcl1* has been demonstrated in the mouse embryo where *Mcl1* -/- blastocysts die following implantation, with an earlier modest impairment suggested by a reduced number of mature -/- blastocysts (Rinkenberger et al., 2000). However, TUNEL staining revealed no increase in apoptosis in the explanted ICM of -/-mice, suggesting a TE deficiency originating from the loss of another Mcl1 function as opposed to unrestrained apoptosis. A 24 hour window prior to implantation was not available for analysis by the authors, and it cannot be ruled out that the onset of apoptosis occurs rapidly during this time period in the absence of *Mcl1*.

It must be considered that the minority of cells of a blastocyst cell undergo apoptosis (Hardy et al., 1989), and the changes in gene expression occurring as a result of programmed cell death will be difficult to identify. Cells that have undergone programmed cell death are unavailable, and it is plausible quality control processing of RNAseq data may result in exclusion of transcriptome data from cells that have undergone, or are in the process, of apoptosis. A high level of mtDNA transcripts can be an indicator of cells which have undergone apoptosis, but owing to the impact of this on wider transcriptome analysis, cells with elevated levels of mtDNA transcripts are generally removed form analysis (Osorio and Cai, 2020). Thus It is likely I can only identify a genetic environment where cells are more liable to be directed to cell death or are primed for cell death, rather than explore genetic changes occurring as a result of imminent cell death. This may be reflected in that fact that a direct activator of caspases, *APAF1*, was not DE in any comparison.

Cellular metabolism in the preimplantation embryo

The majority of metabolic studies of the preimplantation embryo have been conducted in mouse and bovine models (Thompson et al., 1996, Houghton et al., 1996, Trimarchi et al., 2000, Sturmey and Leese, 2003), and as such my analysis represents the first step in

confirming mechanisms in human embryos. Genes of 'OXPHOS' and 'positive regulation of OXPHOS' each increase in expression in the blastocyst relative to the 8-cell embryo, and for the former to the morula, suggesting a higher level of OXPHOS activity in the blastocyst. The stable expression of genes associated with 'negative regulation of OXPHOS' in this period suggests an increase in OXPHOS could be attributed to an upregulation of positive and effector genes instead of reduced expression in negatively regulating genes. Similarly, genes of the 'glycolytic process' are elevated in this same period suggesting higher glycolytic activity, beginning in at the morula stage. In both these processes a reduction in gene expression is apparent at day 7 compared to day 6, suggesting some small scale changes in metabolism as the blastocyst progresses towards implantation.

Combined, this supports evidence from mouse and bovine models suggesting elevated cellular metabolism in the blastocyst relative to the cleavage embryo. Evidence has indicated that oxygen consumption, glucose uptake, ATP production and lactate production all increase in the blastocyst stage (Thompson et al., 1996, Houghton et al., 1996, Trimarchi et al., 2000, Sturmey and Leese, 2003). Glucose has been shown to be integral to culture of mouse embryos beyond compaction of the morula (Brown and Whittingham, 1991). Early reports from the mouse blastocyst suggested that roughly half of glucose taken up by a mouse blastocyst is accounted for by lactate production (Gardner and Leese, 1990), a marker of anaerobic glycolysis. However, more recent work has suggested glucose intermediates are directed to other pathways (Chi et al., 2020). Metabolic analysis of human embryos has scarcely been conducted, but limited studies on human embryos suggested that glucose uptake and lactose production is higher in the blastocyst (Gott et al., 1990, Gardner et al., 2011), similar to the mouse.

That glucose is integral to blastocyst development confirms the importance of the metabolite (Brown and Whittingham, 1991). However, evidence from the mouse indicates that elevated glucose uptake measurements are at least in part an artefact of *in vitro* culture. Lactate production occurred at a higher rate in mouse blastocysts after 24h in culture compared to those developed *in vivo* (harvested directly from the reproductive tract and assayed immediately) as measured by resulting lactate in the media (Lane and Gardner, 1998). Other evidence has suggested that embryos exhibiting a high level of glucose metabolism are less-viable for fetal development post-IVF, reinforcing the idea that elevated glycolysis is an aberrant side effect of *in vivo* culture (Lane and Gardner, 1996). A similar phenomenon may exaggerate the expression of relevant genes here, but it must be noted different media

compositions have been used between studies. None the less it is likely this upregulation of glycolytic genes reflects a change in metabolism with the embryo.

The gene expression profile I report above at the level of GOs, further suggests the activity of aerobic glycolysis in the blastocyst despite ongoing OXPHOS. Similar patterns emerged for several specific *LDH* genes linked to the Warburg effect and lactate production (the final step in anaerobic glycolysis and a hallmark of the Warburg effect). Although insignificant, a trend of upregulation in *SLC16A3* is apparent. The *SLC16A3* protein, MCT4, is a cell membrane protein responsible for export of lactate in highly glycolytic cells (Dimmer et al., 2000), amongst other transport roles (Javaeed and Ghauri, 2019). An increase in lactate production would serve to increase production of intermediates for biosynthetic pathways (Vander Heiden et al., 2009), but lactate excretion mediated by *SLC16A3* may aid implantation (Ma et al., 2020b). Furthermore, *PKM* was elevated in the blastocyst. The PKM protein performs a late step of glycolysis, forming ATP and pyruvate. The embryonic form of PKM is evidenced to be the PKM2 isoform (Redel et al., 2012), although I could not resolve *PKM* to individual transcripts from the data available. Based on analysis performed in tumour tissue exhibiting the Warburg effect, the PKM2 isoform has been reported less active than other isoforms in formation of pyruvate; instead an accumulation of an earlier intermediate leads to conversion into pyruvate via other protein interactions in a more efficient manner (Vander Heiden et al., 2010). Based on the gene expression profile of PKM2, this may represent another mechanism shared between the blastocyst and tumour tissue. Thus the gene expression profile described here supports the evidence that the human preimplantation exhibits a metabolic profile similar to the Warburg effect, with glycolytic activity and lactate production rising despite ongoing OXPHOS activity.

The Warburg effect is suggested to aid proliferation by allowing increased supply of intermediates to biosynthetic pathways. Analysis of gene expression relating to alternative anabolic metabolism allows me to hypothesis on the fate of glucose metabolised, and its derived intermediates, in the preimplantation embryo. In contrast to older studies which suggested glucose derivatives were directed towards ATP production based on the release of lactate (Thompson et al., 1996, Houghton et al., 1996, Trimarchi et al., 2000, Sturmey and Leese, 2003), more recent work has suggested that when glucose is labelled in media only 0.5% of pyruvate is derived from glucose and even less lactate (Chi et al., 2020). Differences to early studies in glucose metabolism are likely explained by different culture media composition, culture conditions used and methodology of analysis. Glucose carbons where

instead identified within PPP and HBP derivatives, suggesting glucose drawn from culture media is primarily directed to biosynthetic pathways. Furthermore, specific inhibition of glycolysis did not prevent full development to the blastocyst stage, whereas inhibition of either the PPP or HBP prevented development (Chi et al., 2020). My gene expression analysis strongly supports evidence that biosynthetic pathways are highly active in the blastocyst, with both the 'PPP' and 'HBP' GOs elevated in the blastocyst relative to preceding stages. Whilst I cannot directly analyse the fate of metabolised glucose, it seems likely that an upregulation occurs in metabolism of glucose encompassing all three of the branches examined in the human preimplantation embryo. Transcriptome analysis cannot substitute for metabolomics measurements suggesting a low level of lactate production in the mouse embryo, especially given that transcriptome studies cannot account for multiple levels of RNA and protein regulation. None the less, the importance of the PPP and HBP to mouse blastocyst development is clear, and my analysis suggests it is similarly important in the human.

Mitochondrial network maintenance in the preimplantation embryo

Under normal conditions mitophagy acts in balance with other processes which modulate the mitochondrial network in response to a cells metabolomic demands (Killackey et al., 2020). I therefore examine the expression of genes involved in associated mechanisms (mtDNA replication/translation and mitochondrial fission and fusion), to elucidate wider changes to the mitochondrial network in the preimplantation embryo.

Mitochondrial fission can play a key role in mitophagy by partitioning components of mitochondria for easier degradation (Killackey et al., 2020). In my analysis the key fission gene *DN1ML* is upregulated at the time when the onset of mitophagy is observed by live cell imaging, as is *MFF*, an essential factor required for *DNM1L* recruitment, suggesting mitochondrial fission may help to facilitate preimplantation embryo mitophagy. However, the mitochondria of an embryo exist in a more punctuate state compared with many other cell types (Van Blerkom, 2008). Therefore, it would be surprising for fission to play an important role in isolating mitochondria for degradation. It is plausible that instead the upregulation of these genes plays a role in preventing the formation of mitochondrial networks. Notably, mitochondrial fusion genes *MFN2* and *OPA1* are upregulated at the morula stage, suggesting that alongside

mitophagy other aspects of mitochondrial maintenance are upregulated without wholesale changes in morphology. A subsequent downregulation of fusion genes may play some part in maintaining individual mitochondria to facilitate mitophagy.

A role for mitochondrial fission in the preimplantation embryo has been demonstrated only in a porcine model. Even a modest knockdown of *PINK1* led to elongated mitochondria with impaired function, leading to impairments in blastocyst development and an increase in apoptosis (Niu et al., 2019). Upregulation of *DNM1L* prevented this phenotype by the upregulation of mitochondrial fission. The mRNA profile of *PINK1* transcripts differed from the human, with high expression seen in the 8-cell stage of the pig, though differences between these models are possible. Similarly, knockdown of *MFN2* in the mouse embryo also lead to higher levels of apoptosis and impaired mitochondrial functions (Zhao et al., 2015). My RNAseq analysis suggests that the machinery required for fission and fusion is expressed in the human preimplantation embryo and shows fluid expression, and so may be similarly important in the human blastocyst. Additionally, *PINK1* may play a key role in its regulation. Given that *PINK1* generally promotes mitophagy in response to mitochondria damage and depolarisation (Yang et al., 2008), it is not necessarily involved in mitophagy in the blastocyst despite its expression, and will require further investigation.

The lack of DE amongst key mtDNA replication or translation genes suggests a lack of change in the activity mitochondrial biogenesis, and so suggests no compensatory response to mitophagy. Although the GO of 'mitochondrial DNA replication' shows significant rises and falls, they are modest and inconsistent, and expression of key canonical genes likely represents a better measure. Those genes that were DE are not major regulators in the replication of mtDNA. Despite some elevating in the morula, where the presence of maternal transcripts might still skew changes relative to the 8-cell, the majority were downregulated in the blastocyst. As such it appears biogenesis does not occur in the human blastocyst before blastocyst implantation. This is similar to reports from the mouse, where embryos of a *PPRC1* knockout mouse showed embryonic lethality after implantation only (He et al., 2012). It also largely corroborates measurements of copy number, which suggest mitochondrial biogenesis occurs only in very late preimplantation development in a porcine model (Spikings et al., 2007). The lack of transcriptional changes in my analysis may reflect changes between model organisms, or a lack of transcriptional regulation.

Concordance of the transcriptome to protein abundance and function

While the above represents the beginning of characterisation of mitochondrial dynamics in the human preimplantation embryo and the confirmation of suggestions from animal studies, there is a clear need for lab-based study to validate changes in the transcriptome at the protein level. This will allow assessment of the functional implications of changes in gene expression. Although RNAseq offers significant advantages over previous transcriptomic methods, it remains unclear to what extent gene expression correlates with protein levels. When the proteome and transcriptome of the mouse preimplantation embryo was compared at the level of whole embryos differences in the two measurements where clear, but improved dramatically at the morula stage. Despite this, Pearson correlation between the two peaked at only 0.29 in the blastocyst for a subset of genes. However, it must be noted that analysis was conducted using pools of ~600 embryos for protein abundance, and around ~200 embryos for transcriptome analysis, likely contributing to differences in the analyses (Israel et al., 2019). Given the ZGA onsets at a later stage in human, in the 8-cell/morula as opposed to the 2-cell embryo (Schultz, 1993, Niakan et al., 2012), it is also possible the relationship may be different in the samples I analysed. Poor concordance between proteome and transcriptome is reported in the eggs of *Xenopus laevis* (Smits et al., 2014), and human cell lines (Schwanhäusser et al., 2011, Edfors et al., 2016).

It must also be considered that a large degree of post-transcriptional and post-translational modification is unaccounted for by transcriptomic analysis. For example in the regulation of mitophagy, *PINK1* cleavage forms a key part of its regulation by preventing the recruitment of *PRKN* and thus mitophagy (Narendra et al., 2010). It has been shown that *BNIP3* inhibits this cleavage and promote mitophagy (Zhang et al., 2016b). Further work in mouse embryos will allow functional analysis of protein activity, and further characterise proteins involved in preimplantation embryo mitophagy.

Conclusion

Analysis of the expression of mitophagy genes in scRNAseq of the human preimplantation embryo suggests a key role for *BNIP3*/*BNIP3L* in the mitophagy revealed by live-cell imaging.

Upregulation of pBNIP3L successfully upregulated mitophagy in the mouse embryo, providing a candidate for artificial upregulation of mitophagy to reduce carry over in PNT, and for experimental characterisation of preimplantation embryo mitophagy. Expression of mitophagy genes correlated with the expression of specific regulators of cell differentiation in the blastocyst, suggesting a role for this mitophagy. Expression of apoptosis genes was as predicted by previous studies suggesting elevated apoptosis in the blastocyst and ICM, and suggested a complex regulatory network in the blastocyst which requires further study. Expression of metabolic genes was largely as expected based on studies of mouse blastocysts, and my analysis begins the process of confirmation of the conservation of these mechanisms in humans. No correlation between expression of mitophagy genes and apoptotic or metabolic gene expression was apparent. Although mitochondrial fission and fusion genes were variably expressed, there was no evidence to suggest mitochondrial biogenesis occurs in the preimplantation embryo,

4.5. Future work

Further work would need to be conducted in mouse embryos due to limited access to human embryos. Deeper characterisation of mitophagy and its role in the blastocyst will require the establishment methods of inhibiting mitophagy (Chapter 4). If mitophagy can be inhibited, the relationship between mitophagy and cell specification could be further explores. Visualisation of lineage specific proteins through immunofluorescence protocols would allow cell counts of each cell lineage at different stages of mouse embryo development, and the impact of increased or decreased mitophagy on these counts could be examined. The drug 2-Deoxy-d-glucose could be used to block glycolysis and explore its effect on the same processes.

Further work could also be conducted in zebrafish models, which offers the advantages of easier collection of early developmental tissues and a faster reproductive cycle. Application of the mitoQC probe to this model could allow exploration of the role of mitophagy in reducing copy number during early development (Otten et al., 2016), and explore the possibility of mitophagy being active during oocyte development.

The utility of upregulating mitophagy to reduce carryover in PNT requires proof of principle. pBNIP3L will be upregulated in the mouse zygote, and PNT conducted thereafter before culturing embryos to the blastocyst stage. mtDNA heteroplasmy will then be measured to analyse levels of 'patient' mtDNA carried over in resulting blastocysts.

The extent to which transciptome abundance correlates with protein abundance is questionable, and study of proteins in the blastocyst will provide further clues as to the activity of the processes and pathways studied above. Measurement of the abundance of specific proteins presents a challenge in the preimplantation embryo owing to generally low abundance of proteins, making quantitative methods such as western blots unsuitable. High throughput proteomics allows quantification, but suffers from a lack of sensitivity thus detects a limited number of proteins, and must be conducted at the level of whole several hundred pooled embryos (Israel et al., 2019). Analysis of an open source proteomics dataset would provide a cheaper and faster analysis of protein levels.

Whilst measurement of protein abundance would prove challenging, analysis of protein localisation remains a possibility to confirm some indications from transcriptome analysis. Transcriptome analysis suggested a higher level of *PINK1/PRKN* expression in cells of the ICM. Utilising antibodies to these proteins in conjunction with antibodies to lineage specific markers, will allow analysis of protein levels across cells of blastocyst lineages. Interesting trends in the expression of apoptosis genes, such as that of *PMAIP1*, could be explored similarly. Furthermore, TUNEL staining could be used to identify cells undergoing apoptosis. In conjunction with antibodies to proteins of interest (such as PMAIP1), analysing the localisation or accumulation of proteins in these cells undergoing apoptosis would suggest a key role for those proteins in apoptosis. In addition, manipulation of expression of the same proteins and its effect on the prevalence of apoptosis could be explored.

The metabolic profile of preimplantation embryos requires characterisation to clarify contradictory evidence previously reported. This institute has access to an Agilent Seahorse metabolic analysis platform, which will allow measurements of embryo metabolism with more modern methods than previously utilised. However, adapting this technology to the mouse blastocyst would require work. Thereafter, inhibitors of metabolism could be verified, and their application used to explore links between metabolism and mitophagy, and vice versa.

Analysis of apoptosis and its relationship to other features of the transcriptome were held back by an inability to identify cells in the process of apoptosis. A recent study on the epiblast tissues post implantation suggested that mouse epiblast cells accumulating mtDNA variants were eliminated preferentially (Lima et al., 2021). Application of a variant calling pipeline to examine mtDNA variants in the dataset I analysed may provide additional measures which can be used in combination with gene expression to identify cells likely undergoing apoptosis. Subsequently, the relationship of apoptosis genes and mitophagy or other processes could be explored in greater detail. The study of Lime *et al* (2021) also used caspase inhibitors to prevent apoptosis of cells being out-competed, allowing identification of the transcriptomic signature of cells in the terminal stages of apoptosis. Similar protocols could be used in earlier developmental stages, but availability of human embryos remains a challenge.

5. Intercellular variation of heteroplasmy and the role of mitophagy in preimplantation development

5.1. Introduction

Changes in the intercellular segregation of heteroplasmy has been reported during preimplantation development in both the mouse (Neupane et al., 2014), and human (Treff et al., 2012). Work on mice using the BALB/OlaHsd mouse model, generated via cytoplast transfer of two wildtype mtDNA genomes, suggested that intercellular variation in the 8-cell is low, generally within a range of 6%, with a slight increase in intercellular variation at the blastocyst stage, even when a single trophectoderm (TE) biopsy was compared to a remaining whole embryo (Dean et al., 2003, Neupane et al., 2014). Specific analysis of blastocyst intercellular variation at the level of a biopsy, rather than isolation of single cells, likely masks a degree of intercellular variation. Work on a primate model generated by similar means reported a more expansive segregation of mitochondrial DNA (mtDNA) genomes, increasing as preimplantation development proceeded (Lee et al., 2012). Reports from murine and primate models have relied on embryos generated via cytoplast transfer and the mixing of two wild type genotypes, with analysis either immediately following the procedure in primates (Lee et al., 2012), or after breeding of progeny in mice (Dean et al., 2003, Neupane et al., 2014). Thus, these models do not carry a singular pathogenic mtDNA variant, and the extent to which they resemble a naturally arising pathogenic mtDNA variant is unclear. Furthermore, this BALB/OlaHsd mouse model (Dean et al., 2003, Neupane et al., 2014), harbours 101 mtDNA variants between the donated and recipient genomes at significant levels of heteroplasmy, predicted to manifest 15 amino acid substitutions (Dean et al., 2003). This level of variation could conceivably have an effect on nuclear-mitochondrial interactions and on segregation during the early embryonic cell divisions. Therefore, further characterisation is needed to explore the impact and consequences of this mtDNA segregation in more animal models that better reflect human mtDNA heteroplasmy.

The recently produced *tRNAalanine* (*tRNAala)* mouse reportedly carries a single pathogenic mtDNA variant, m.5024C>T in the *tRNAala* gene (alongside one non-pathogenic variant), and its genotype was generated biologically through a deficient DNA proof-reading enzyme (Kauppila et al., 2016). Thus, compared to previous work this represents a model which more closely mimics pathogenic variants in the human population and is more easily interpretable,

making it a more appropriate model for examination of the segregation of a heteroplasmic pathogenic mtDNA variant in preimplantation embryos. In human embryos carrying an inherited pathogenic variant, reports suggest that the range of intercellular variation is modest in the 8-cell (generally under 3%) (Monnot et al., 2011, Sallevelt et al., 2013), while evidence from analysis of blastocysts indicates a higher level of variation between samples of cells even when analysed at the level of cell clumps (Treff et al., 2012).

The segregation of heteroplasmy in the blastocyst has implications for clinical interventions designed to prevent the inheritance of mtDNA disease such as preimplantation genetic diagnosis (PGD) and pronuclear transfer (PNT). Successful PGD relies on the identification of embryos carrying low mutation load, below a threshold variable across pathogenic mutations but generally around 15% (Sallevelt et al., 2013), based on biopsy of a single or small number of cells (Vermeesch et al., 2016). Whether the 8-cell or blastocyst embryo is the optimal stage for collection of this biopsy remains unclear (Vermeesch et al., 2016, Cimadomo et al., 2016), and changes to heteroplasmy over the course of blastocyst formation may influence this decision. Following mitochondrial replacement therapy, 15% of all hESC lines derived from PNT blastocysts revert to donor mtDNA genotype showing increasing heteroplasmy across passages (Hudson et al., 2019). Whilst the reasons for this are unclear, each hESC line is derived from a small number of epiblast cell within the inner cell mass (ICM). If there is significant intercellular variation, it is possible that stem cell lines are gradually dominated by epiblast derived cells with higher heteroplasmy.

Segregation of mtDNA heteroplasmy in the blastocyst may also have implications for the inheritance of mtDNA. The inheritance of mtDNA is subject to a genetic bottleneck in maternal inheritance, and in the case of some pathogenic mtDNA variants, purifying selection against these pathogenic variants. This is predominantly believed to occur in maternal primordial germ cells (PGCs) as they mature into oocytes (Cree et al., 2008, Wallace and Chalkia, 2013), but this does not preclude modulating events at other stages influencing their inheritance. There is some evidence to suggest that events occur following oocyte maturation to modify mtDNA inheritance (Freyer et al., 2012). Moreover, recent work in our lab indicates that the onset of differentiation during preimplantation development is characterised by a wave of mitophagy (Chapter 1), raising the question of whether this mitophagy wave can affect mtDNA inheritance, either modulating random segregation between cells or selecting against pathogenic variants.

It remains unclear to what extent findings from an embryo harbouring heteroplasmy generated by cytoplast transfer in the zygote, such those utilised by Lee *et al* (2016), can be extrapolated to a naturally inherited occurring heteroplasmies. Studies on heteroplasmy generated by cytoplast transfer or karyoplast transfer (transfer of mtDNA surrounding the nucleus) in the mouse indicated that the level of heteroplasmy variation between cells in mice is greater following cytoplast transfer compared with karyoplast transfer (Meirelles and Smith, 1998). Analysis of our previously published single cell RNA sequencing (scRNAseq) data from PNT blastocysts (Hyslop et al, 2016) provides an opportunity to explore segregation of mtDNA during preimplantation development following karyoplast transfer. PNT blastocysts contain a mix of two mitochondrial genomes, albeit at low levels of heteroplasmy (<13%, Hyslop et al., 2016), which can be distinguished using haplogroup specific variants. Variant calling of mtDNA in RNAseq data has recently been demonstrated to reliably detect variants, but with lower statistical power than traditional methods (Ludwig et al., 2019).

Investigation of the impact of preimplantation embryo mitophagy on heteroplasmy will require the application of methods capable of artificially modulating mitophagy. We have established a method of upregulating mitophagy in preimplantation embryos (Chapter 4). The simplest method of downregulating mitophagy may be using pharmaceutical agents. Two pharmaceutical agents have been reported to inhibit mitophagy and appear promising for application in preimplantation development; Cyclosporine A (CsA) (Rodriguez-Enriquez et al., 2009), and MRT68921 (Petherick et al., 2015).

To determine whether the extent of segregation of mtDNA heteroplasmy blastocyst development, I performed biopsies and/or disaggregation of 8-cell embryos and blastocysts of the *tRNAala* mouse, and subsequently measured heteroplasmy in these cells and tissues. Next, to determine whether intercellular variation of heteroplasmy is modulated by mitophagy, I upregulated mitophagy through over-expression of a phosphomimetic BNIP3L isoform (Chapter 3), and repeated analysis of heteroplasmy. Furthermore, a scRNAseq dataset of PNT blastocysts produced within the lab (Hyslop et al., 2016) was analysed to measure intercellular variation of heteroplasmy in human embryos with mtDNA heteroplasmy generated via karyoplast transfer during PNT, and compared to pyrosequencing data from the same embryos to test the accuracy of a variant calling pipeline.

5.2. Aims and hypotheses

The aims of this chapter are designed to investigate the inheritance and prevention of mtDNA disease.

A1. Investigate the implications of the mitophagy we observe during the morula/blastocyst stage (Chapter 1) for inheritance of mtDNA variants by testing the following hypotheses using mice carrying the m.5024C>T pathogenic mtDNA variant:

1) If heteroplasmy levels are modulated by mitophagy, the level of intercellular variation of heteroplasmy will increase between the 8 cell and the blastocyst stage.
2) Upregulation and downregulation of mitophagy will respectively increase and decrease the level of variation between cells of the preimplantation embryo.

A2. In addition to elucidating the effect of mitophagy on heteroplasmy, data generated in A1 will be also analysed to determine whether biopsy of blastomeres at the 8-cell stage provides a more accurate measure of the wider mtDNA heteroplasmy levels of an embryo, compared with trophectoderm cells biopsied at the blastocyst stage. This will address an important clinical question relevant to use of PGD for reducing the transmission of pathogenic mtDNA variants.

A3: Determine whether heteroplasmy levels can be accurately measured in scRNAseq data from human PNT blastocysts. This would shed light on the extent of intercellular variation in heteroplasmy levels following karyoplast transfer during PNT in human embryos using existing data.

5.3. Methods

Experimental procedures are detailed in the methods section. Briefly, raw PNT blastocyst scRNAseq FASTQ files were sourced from an open source archive of genomic data (Hyslop et al., 2016). Files were processed in accordance with GATK best practice guidelines for variant calling with RNAseq (Van der Auwera et al., 2013). FASTQ files were mapped to the human reference genome (UCSC GRCh37/hg19GRCh38) using STAR (Dobin et al., 2012) with a two-pass method. The resulting SAM files were grouped via Picard (http://broadinstitute.github.io/picard/), and converted to BAM files. Pileup files were generated via Samtools and annotated.

5.3. Results

5.4.1. Establishment of *tRNAala* mouse model colony

To address the aims of this chapter, I established a colony of *tRNAala* mice. To guide breeding of the colony ear biopsies were collected from mice at ~3 weeks of age, and heteroplasmy of the m.5024C>T mutation measured by pyrosequencing. Mice with a m.5024C>T mutation load over 70% were used in breeding to maintain stability of mtDNA heteroplasmy, and those <70% were used in experimentation. As expected, m.5024C>T showed variability in heteroplasmy between mothers and offspring in each generation (Figure 5.1.A). Notably, while both increases and decreases of heteroplasmy between mothers and pups were apparent, most pups had lower heteroplasmy than their mother (65.57% of 61 pups). There was no significant correlation between mother and pup (r=0.20), further confirming the presence of modulating factors in m.5024C>T inheritance (Figure 5.1.B). This data are supportive of the suggestion that m.5024C>T, due to causing only a mild dysfunctional phenotpye, is under only weak selection pressure <80% heteroplasmy, and is not removed by purifying selection (Kauppila et al., 2016).

A
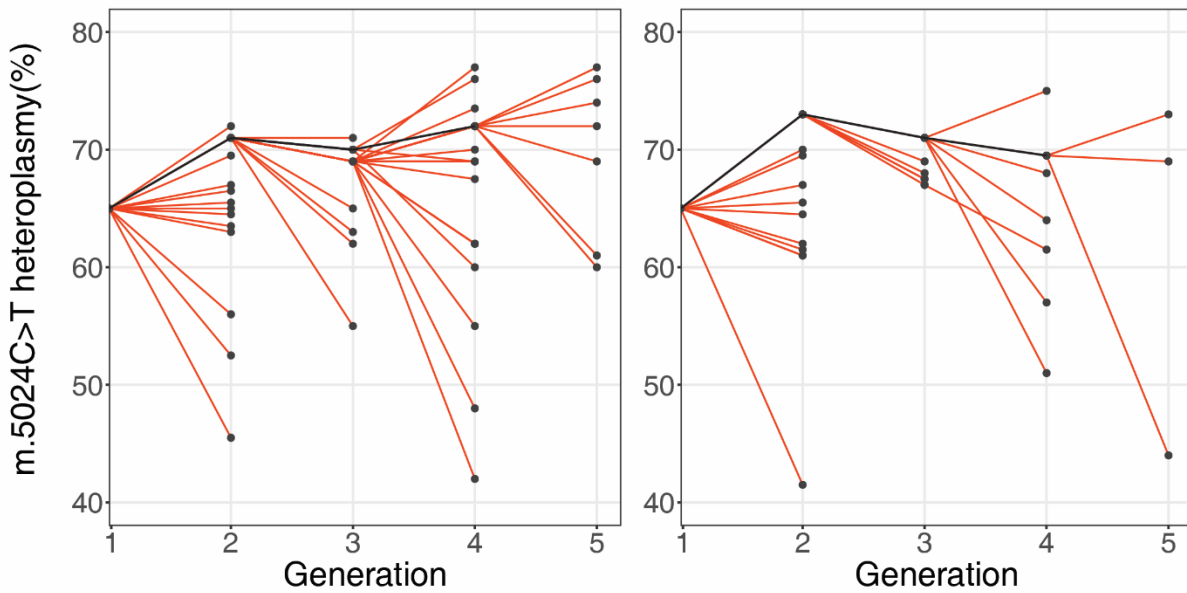
B
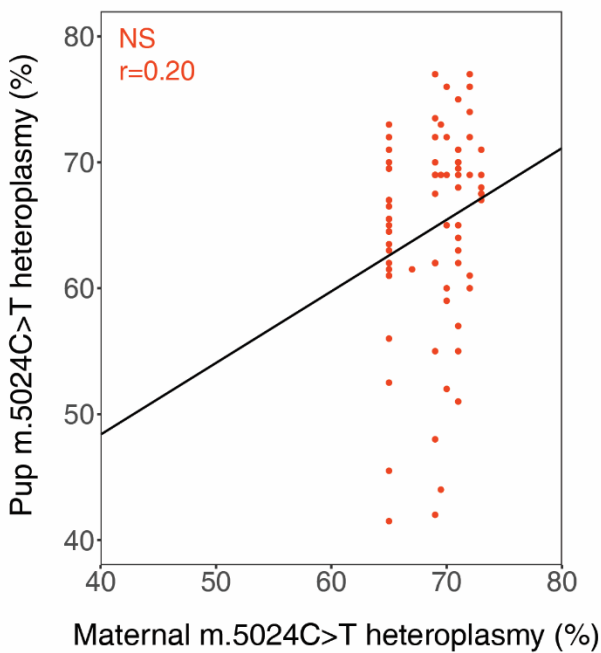
Figure 5.1. The inheritance of the m.5024C>T mutation measured via pyrosequencing of ear biopsy.

(A) Inheritance in two representative lineages of female mice over 5 generations. Graphs show the variation in m.5024C>T heteroplasmy levels in 3-12 litter mates per generation, typically ranging from ~45-75%. The black line shows the female breeders used in successive generations. A bottleneck effect and weak purifying selection is apparent in m.5024C>T inheritance. (B) Correlation between maternal m.5024C>T heteroplasmy and pup m.5024C>T heteroplasmy. No correlation was detected. NS, non-significant.

5.4.2. Reliability of biopsy in preimplantation development in predicting embryo mutation load.

The clinical viability of PGD is reliant on accurate prediction of heteroplasmy of cells of the blastocyst epiblast through collection and analysis of a biopsy. Currently, PGD uses biopsy of the 8-cell (single cell biopsy) or blastocyst stage embryo (TE clump biopsy), but it is not clear at what stage a biopsy more accurately reflects heteroplasmy of the epiblast.

Although in the context of PGD clinics analysis of the epiblast is not possible to verify PGD success, post-natal analysis of a child is routine and likely correlates with the earlier epiblast. After implantation of an embryo assessed via 8-cell biopsy to carry <18% heteroplasmy, a child carrying m.14487T>C mutation load <5% in cord blood was born (Sallevelt et al., 2017b). When an embryo was asses via the same means to carry 0% m8993T>G mutation load was implanted, a child free of the mutation was born (Sallevelt et al., 2013). Similarly, following TE biopsy to identify an embryo with 0% mutation load of m.3423A>G, the new born child was wild type in the same position (Heindryckx et al., 2014). However following a further instance of TE biopsy and embryo implantation (Treff et al., 2012), dramatic increases in mutation load were reported in the new born child (Mitalipov et al., 2014). Biopsy of the TE is associated with health benefits to the embryo (Vermeesch et al., 2016, Cimadomo et al., 2016), and as such validation of the accuracy of respective biopsies is paramount to safe implementation and optimisation of PGD.

Purifying selection is seen in the inheritance of a subset of human pathogenic mtDNA variants. For example, high levels of heteroplasmy of the m.3243A>G variant was consistently absent in early developmental tissues (Otten et al., 2018). Furthermore, it has been shown that a range of low-level non-synonomous mutations were not inherited in children (Rebolledo-Jaramillo et al., 2014), and are selectedS against in PGC development (Floros et al., 2018). However, a number of pathogenic mtDNA mutations escape this selection, and the characteristics which allow this remain unclear. The periods of development which facilitate an mtDNA bottleneck or purifying selection against pathogenic mtDNA variants are not entirely characterised (Burr et al., 2018). The observation of mitophagy in early development (Chapter 1), raises the question that this is an opportunity for mtDNA selection to take place through the selective degradation of dysfunctional mitochondria, which are likely to contain higher levels of pathogenic mtDNA variation. Evidence that mitophagy can remove mtDNA mutations is sparse, but in heteroplasmic cybrid lines overexpression of mitophagy genes can eliminate a deletion in the *COX1* gene of mtDNA (Suen et al., 2010), with a similar mechanism demonstrated in *Drosphila* carrying a large scale deletion (Kandul et al., 2016). Given the relatively few number of cells within the blastocyst, and even fewer epiblast cells, the preimplantation embryo presents the opportunity for events which modulate heteroplasmy to have abroad impact on the developing organism (Burr et al., 2018). Furthermore, this would compromise the use of an 8-cell biopsy in PGD.

To examine this possibility, I performed single-cell biopsy from 8-cell *tRNAala* mouse embryos, before culturing the embryo to blastocyst stage and collecting the whole embryo, then comparing heteroplasmy between the two (Figure 5.2.A). Analysis of a whole embryo avoids the loss of cells during embryo disaggregation, thus allowing measurement of an embryos true average heteroplasmy. Heteroplasmy between these two stages of development remained virtually the same within each embryo (Figure 5.2.B), with an average absolute shift of only 0.88% heteroplasmy. 3 embryos showed a trend towards increasing heteroplasmy (>1%), 1 a trend towards decreasing (>-1%), and 3 remained the same (i.e. a change of <1%). This suggests blastocyst mitophagy does not represent purifying selection.
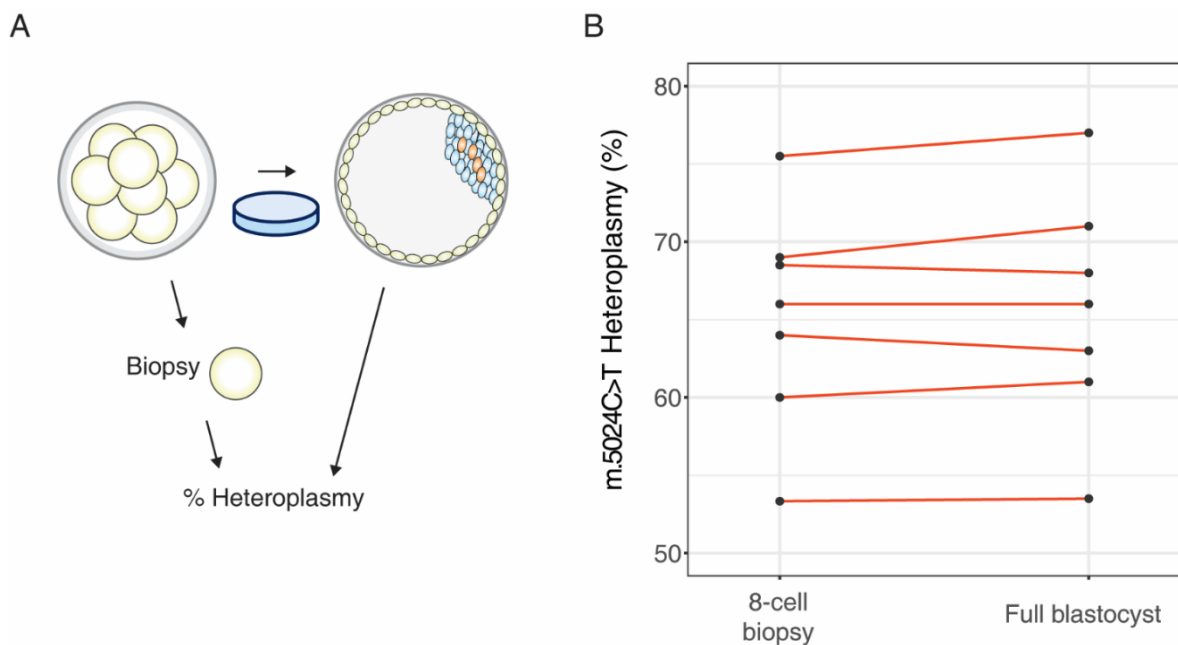
Figure 5.2. Absence of purifying selection during blastocyst formation in the *tRNAala* mouse.

(A) Schematic depicting the isolation of a single cell biopsy from an 8-cell embryo, and subsequent culture to blastocyst stage. Corresponding blastocysts were sequenced whole. (B) m.5024C>T heteroplasmy detected in each single cell biopsy and corresponding blastocyst from 7 embryos. Analysis was conducted in triplicate. Average embryo heteroplasmy levels remain stable during blastocyst development.

Previous work has suggested changing variation between cells of human embryos in different stages of development (Treff et al., 2012). This phenomenon requires further characterisation to understand the consequences for PGD, but human embryos are scarcely available for

124

research. As such, characterising this segregation of mtDNA heteroplasmy in mice could facilitate optimisation of PGD protocols. Establishing the dynamics of intercellular heteroplasmy in this period will also allow further study of the impact of mitophagy, which may influence the segregation of mtDNA in the blastocyst. To gain further insight into changes in intercellular heteroplasmy between stages of preimplantation development, I disaggregated 8-cell embryos (n=10) into single cells and blastocyst stage embryos into single cells (n=4) or clumps of cells (n=4, Figure 5.3.A), and measured heteroplasmy within individual cells or cell clumps using pyrosequencing (Figure 5.3.B-D). Embryo disaggregation using the protocols employed allows separation of ICM-enriched clumps and cells from the blastocyst, but a portion of blastocyst TE is lost due to application of a laser.

Intercellular variation was higher between cells of the blastocyst compared to the 8-cell (average coefficient of variation (CoV) across 8-cell embryo cells 1.08$\pm$0.18% compared to 11.94$\pm$1.73% across blastocyst single cells, two-tailed t-test, P<0.05, Table 5.1, Figure 5.3). Variation between clumps of cells of the blastocyst was also higher than across cells of the 8-cell (average CoV across 8-cell embryo cells 1.08$\pm$0.18% compared to 17.39$\pm$5.00% across blastocyst cell clumps), but the difference in CoV did not reach statistical significance, likely because few samples were analysed.

Between cells of 8-cell embryos the average range was 3.07% heteroplasmy, with maximum deviation between average embryo heteroplasmy and a single cell of 2.08%. Across blastocyst cell clumps, average range was 7.71% between cell clumps of the blastocyst, and maximum deviation between average blastocyst heteroplasmy and a TE clump/biopsy was 5.66%. Across single cells of the blastocyst, average range was 10.08%. This suggests a biopsy of the cleavage embryo provide a more reliable indication of wider embryo heteroplasmy in PGD. It also confirms an increase in intercellular variation in mouse blastocysts harbouring a single pathogenic mtDNA variant relative to the 8-cell embryo.

Cells/tissue	Coefficient of variation (%)	Standard deviation (%)	Range (%)
8-cell single cells	1.08 (0.37)	0.98	3.07 (0.53)
Blastocyst clumps	17.39 (11.20)	2.93	7.71 (1.43)
Blastocyst single cells	11.94 (3.46)	2.95	10.08 (1.46)
Trophectoderm single cells	4.8 (3.76)	2.05	6.25 (2.60)
Inner cell mass single cells	5.7 (3.33)	1.86	5.08 (1.93)

Table 5.1. Summary of intercellular variation analysis in *tRNAala* mouse embryos.

Data are expressed as mean with standard deviation.
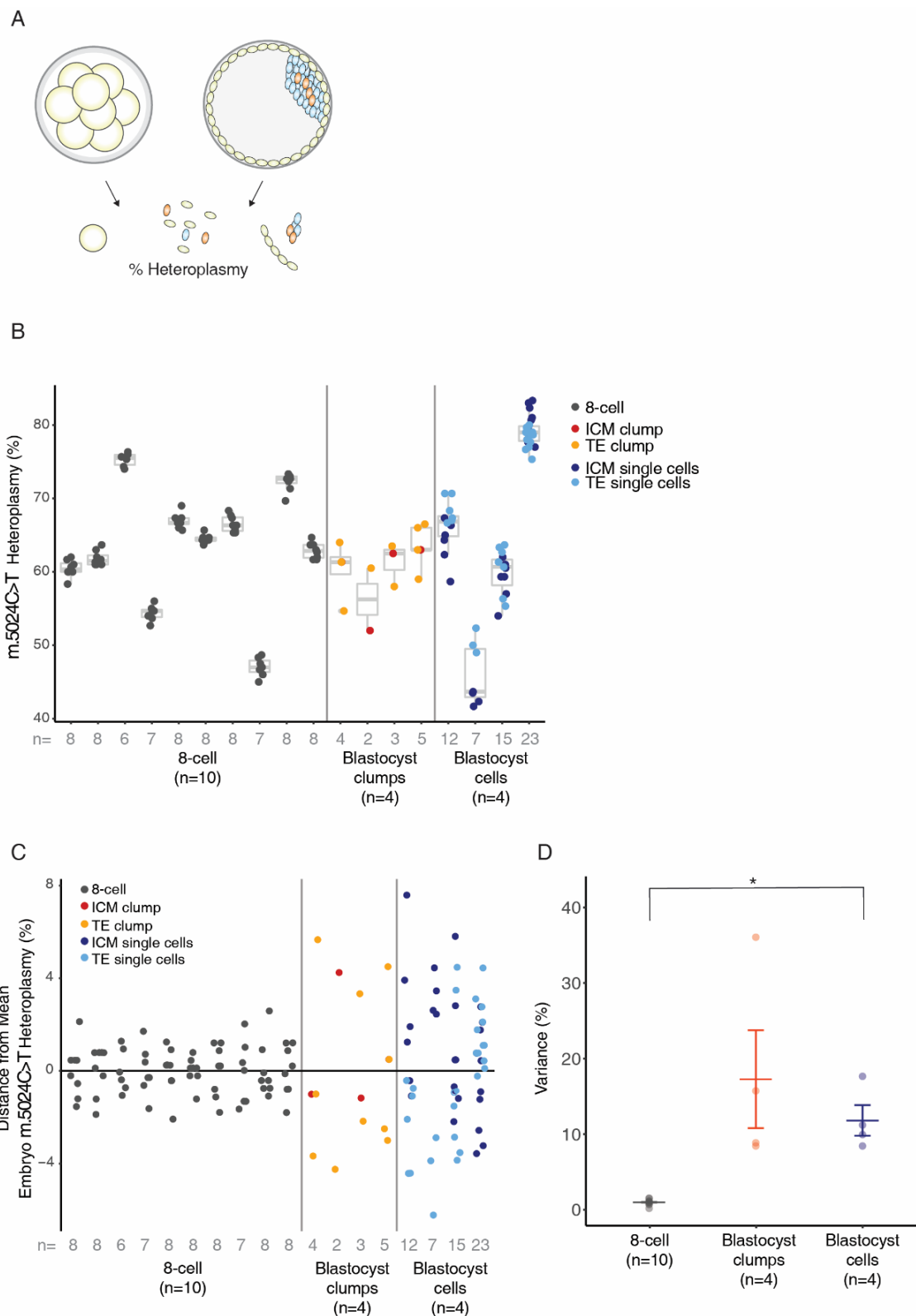
Figure 5.3. Intercellular variation of heteroplasmy in the 8-cell and blastocysts of the *tRNAala* mouse.

(A) 8-cell embryos were disaggregated into single cells, blastocyst into clumps or single cells, and heteroplasmy measured via pyrosequencing. (B) Boxplots of all embryos that underwent pyrosequencing. Grey dots represent 8-cell embryo cells. Red dots represent inner cell mass (ICM) clumps, orange tropechtoderm (TE) clumps. Dark blue dots represent ICM single cells, light blue TE single cells. (C) As in (B) but expressed as deviation from the mean heteroplasmy of an embryo. (D) Coefficient of variation/variance in all groups. Analysis was conducted in triplicate. Central bar represents mean, outer bar standard error. Statistical significance was measure via two-tailed t-test. *=P$\leq$0.05.

Given that the epiblast of the ICM gives rise to the fetus itself, it is also important to analyse whether changes in heteroplasmy levels are apparent between cells of the ICM and TE. Previously, in the BALB/OlaHsd mouse model, it was shown that an isolated TE biopsy carried a different level of heteroplasmy compared to the remaining blastocyst by on average 4% (Neupane et al., 2014). In my analysis of the m.5024C>t variant, between cell clumps, heteroplasmy of an ICM-enriched clump was comparable to TE clumps in 3 of 4 instances (Figure 5.4A/B). An increased number of samples allows statistical testing of this relationship in blastocysts disaggregated to single cells, where 3 of 4 embryos showed a significant difference between the TE portion and ICM-enriched portion (two-tailed t-test. $P < 0.05$ or $P < 0.01$). This trend moved in either direction, with average ICM heteroplasmy both higher and lower than the TE, suggesting this segregation proceeds randomly.
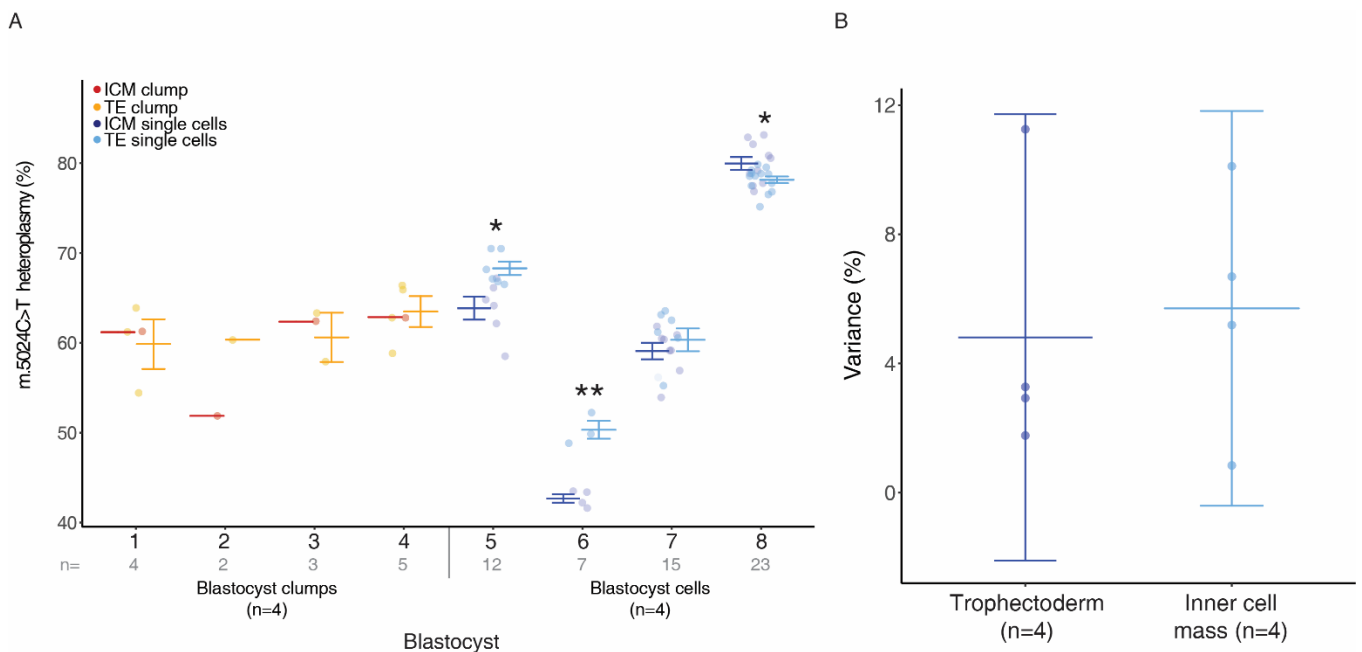
Figure 5.4. Heteroplasmy of inner cell mass and trohpectoderm in blastocysts of the *tRNAala* mouse.

(A) Heteroplasmy of inner cell mass (ICM) enriched and trophectoderm (TE) portions of embryos disaggregated into clumps (red/orange) or single cells (blue/light blue). (B) Coefficient of variation/variance in ICM-enriched and TE single cells. Central bar represents mean, outer bar standard error. t-test, *=$P \leq 0.05$, **=$P \leq 0.01$.

With the caveat that large numbers of each blastocysts cells were not featured in this analysis owing to loss in both collection and amplification, I also averaged the heteroplasmy of all samples of a blastocyst to mimic the collection of an 8-cell embryo. Based on above data, this allowed me to examine whether an 8-cell biopsy reflects the ICM heteroplasmy more than a TE biopsy. I compared this whole-average to the average heteroplasmy of the ICM of each

blastocyst. Encompassing both analysed cell clumps and single cells, the highest divergence between '8-cell biopsy' heteroplasmy and average ICM heteroplasmy was on average 1.75%, with a maximum of 4.24% (Table 5.2). I also compared average heteroplasmy across all TE samples to average heteroplasmy across all ICM samples of each embryo, and found average deviation was 3.42% with maximal deviation of 8.50% (Table 5.3). Focusing on the analysis of ICM and TE cell clumps individually, the highest divergence between a TE biopsy and a corresponding ICM clump was 9.33%. It must be remembered that methods of disaggregation provide an ICM-enriched cell clump or cohort of cells, which are inevitably contaminated by a small number of TE cells, which may mask some differences between the two groups.

	Blastocyst	Average all samples (%)	Average ICM (%)	Deviation (%)
	1	60.33	61.33	1.00
Clumps	2	56.25	52.00	4.25
	3	61.33	62.50	1.17
	4	63.50	63.00	0.50
Average				1.73
	5	66.22	64.00	2.22
Single cells	6	46.07	42.79	3.28
	7	59.81	59.23	0.58
	8	79.10	80.13	1.03
Average				1.78
Combined Average				1.75

Table 5.2. Summary of relationship between average heteroplasmy of a blastocyst and heteroplasmy of the inner cell mass.

Average blastocyst heteroplasmy was used as a model of an 8-cell biopsy. TE, trophectoderm; ICM, inner cell mass.

	Blastocyst	Average TE (%)	Average ICM (%)	Deviation (%)
	1	60.00	61.33	1.33
Clumps	2	60.50	52.00	8.50
	3	60.75	62.50	1.75
	4	63.63	63.00	0.63
Average				3.05
	5	68.45	64.00	4.45
Single cells	6	50.44	42.79	7.65
	7	60.48	59.23	1.25
	8	78.31	80.13	1.82
Average				3.79
Combined Average				3.42

Table 5.3. Summary of relationship between average heteroplasmy of trophectoderm clumps and heteroplasmy of the inner cell mass.

Trophectoderm (TE) clump heteroplasmy was averaged to estimate ability of a TE biopsy to predict inner cell mass (ICM) heteroplasmy.

Nonetheless, together the above data suggest the 8-cell embryo biopsy is the more reliable biopsy in predicting an embryos wider mutation load. Based on using a blastocysts average heteroplasmy as a model of an 8-cell biopsy, the 8-cell biopsy is likely also a better predictor of heteroplasmy in the epiblast cells. The risk of a misestimating the heteroplasmy of an embryo by ~3% suggests that despite reduced accuracy the additional risk of a TE biopsy is negligible, even with rare instances of divergence of over 7%, but will be important for clinicians to be aware of. This remains true even at higher mutation loads where inheritance of the m.5024C>T mutation cannot be explained by neutral drift (Kauppila et al., 2016). However, it must be noted that the m.5024C>T variant relatively is phenotypically weak, and

other, more severe, mtDNA variants may behave differently (Otten et al., 2018). The increase in intercellular variation of heteroplasmy in the blastocyst is also in keeping with the possibility the mitophagy acts to influence the segregation of mtDNA.

5.4.3. Design of a sequencing format for whole mtDNA of single blastomeres

In subsequent analysis m.5024C>T heteroplasmy was assessed by targeted NGS to take advantage of its ability to sequence the entire mtDNA genome and its high throughput format (Figure 5.5.A). It is plausible that other regions of variation could be missed by targeting the m.5024C>T variant specifically. To establish a *tRNAala* mouse mtDNA baseline for further analysis, I sequenced the entire mtDNA extracted from an ear tissue biopsy in a selected cohort of 7 *tRNAala* mice (Kauppila et al., 2016), amplified as two overlapping PCR amplicons. Surprisingly, a total of 5 additional variants were detected (Figure 5.5.B).

These additional variants showed reciprocal heteroplasmy levels to m.5024C>T and m.13715C>T, indicating that they exist on distinct mtDNA molecules. Of these additional variants, m.3009G>T and m.13614C>T are located in protein-coding regions (MT-ND1 and MT-ND6 respectively) and produce a missense mutation (Val to Phe and Ile respectively) thus have increased likelihood to induce a pathogenic phenotype compared to other additional variants in RNR2 (m.1781C>T and m.1866A>G) and *tRNAglutamine* (m.3823T>C).

Reports indicate that the phenotype observed in the *tRNAala* mouse correlates with m.5024C>T heteroplasmy (Kauppila et al., 2016). However, only two mtDNA variants were originally reported. It is possible that there were no additional mtDNA variants in the original mouse experiments, suggesting that *tRNAala* mice are still accumulating mtDNA variation or that these variants were at undetectable levels in previous animals. It remains unclear whether they can exert a phenotype or affect the dynamics of mitochondrial inheritance.

The mtDNA of single-cells of the 8-cell embryo could be amplified via a two-amplicon strategy (data not shown). To assess heteroplasmy in single cells of the mouse blastocyst, which contain relatively fewer copies of mtDNA, I needed to alter the mtDNA amplification strategy

as a two-amplicon and three-amplicon format both failed to amplify sufficient yield for analysis. After experimentation, a 5-amplicon design was determined to be the optimal (Figure 5.5.C).
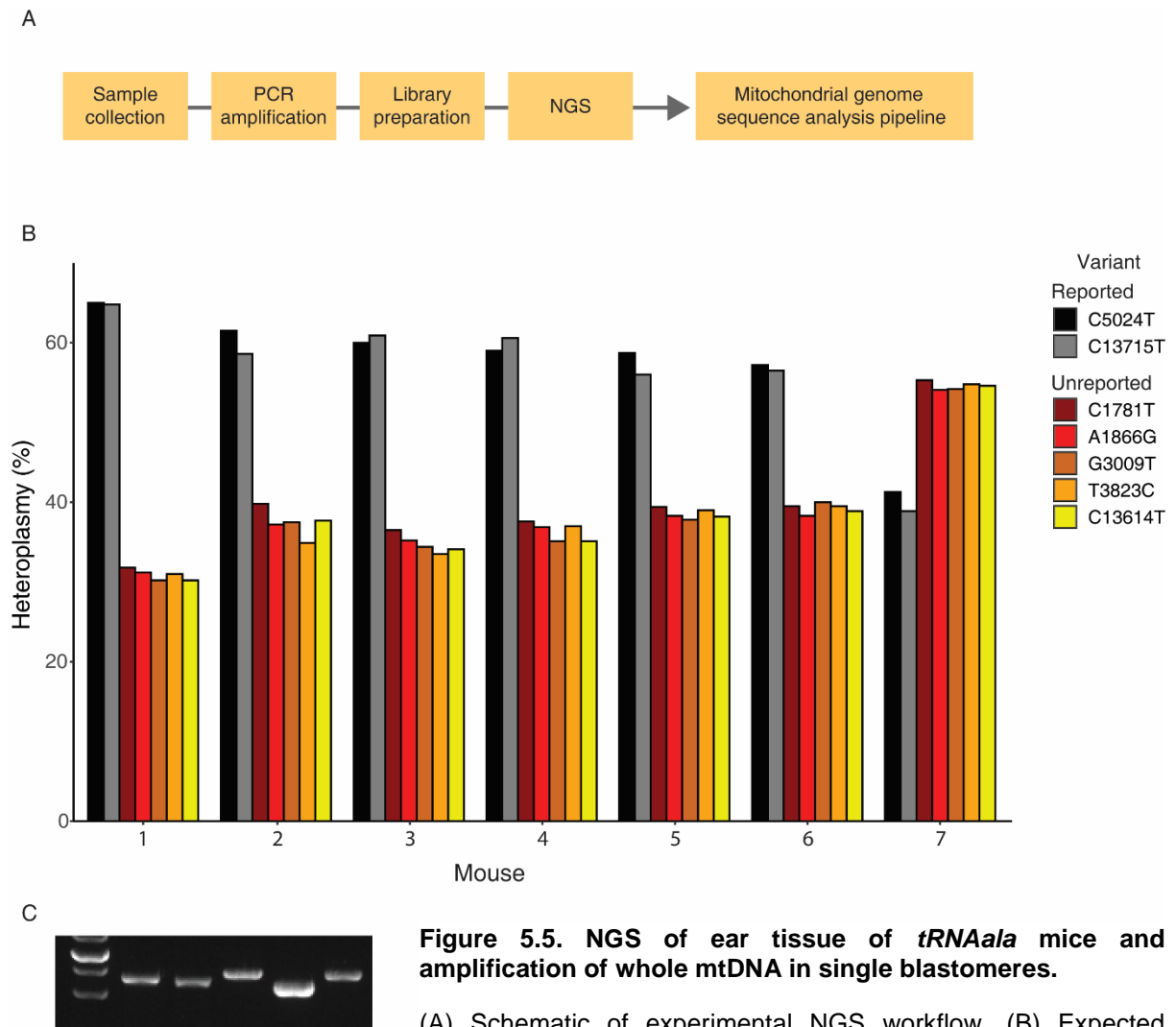
Figure 5.5. NGS of ear tissue of *tRNAala* mice and amplification of whole mtDNA in single blastomeres.

(A) Schematic of experimental NGS workflow. (B) Expected variants (greyscale) and additional unreported variants (coloured bars) were detected in the ear tissue of 8 *tRNAala* mice. The 5 unreported variants are located on separate mtDNA molecules to the reported m.5024C>T and C13715T variants, so move in opposition. (C) Agarose gel of the final amplification format of mtDNA in single cells of the blastocyst with 5 overlapping fragments of ~3000 bp.

5.4.4. Effect of mitophagy on segregation of mtDNA in the preimplantation embryo

With established methods of measuring mtDNA heteroplasmy of single cells of the embryo, I next explored the impact of mitophagy in intercellular variation of heteroplasmy in the preimplantation embryo. To this end, a phoshomimetic isoform of BNIP3L was injected into zygotes of the *tRNAala* mouse to upregulate mitophagy (Chapter 3). Analysis of the level of mitophagy in the preimplantation embryo can be performed using a modified mito-QC probe (Allen et al., 2013), and confocal live-cell imaging. This probe, matrix-mito-QC consists of an eGFP-mCherry fusion protein targeted to the mitochondrial matrix. Mitochondria undergoing mitophagy are engulfed autophagosomes which subsequently fuse with lysosomes, forming mitolysosomes wherein acidic pH degrades the mitochondria (Montava-Garriga and Ganley, 2020). At the same time the signal of EGFP is quenched, leaving the more stable mCherry intact red foci as a marker of mitophagy (Allen et al., 2013). Image quantification was conducted using an ImageJ plug in designed by the creators of mito-QC (Montava-Garriga et al., 2020), with some adjustments made in initial processing to adapt for embryo sample Z-stacks. Only the lower half of a Z-stack was quantified as samples were large. As a result, the upper half of embryos could not be imaged with adequate focus inside the working distance of the objective lens. Upregulation of pBNIP3L successfully upregulated mitophagy in late morula stage embryos of the *tRNAala* mouse (0.52 ± 0.074 v 2.92 ± 0.49 mitolysosomes per μm^2, two-tailed t-test, P<0.01, Figure 5.6.C). As mitophagy was accelerated into the morula by pBNIP3L upregulation, I disaggregated embryos at the late morula stage. This allows analysis of the effect of mitophagy without the complications of accelerating cellular division and specification of cellular lineages, which may influence mitophagy and/or segregation of mtDNA. Furthermore, control samples would exhibit little to no mitophagy in live-cell imaging, presenting a model that is evidently free of mitophagy.

After validation of mitophagy upregulation, embryos were subsequently disaggregated into single cells for analysis of heteroplasmy. The mtDNA amplification strategy employed allows sequencing of both the m.5024C>T pathogenic variant and the previously unreported m.3823T>C variant, which exist at opposite ends of the spectrum of heteroplasmy, in each cell.
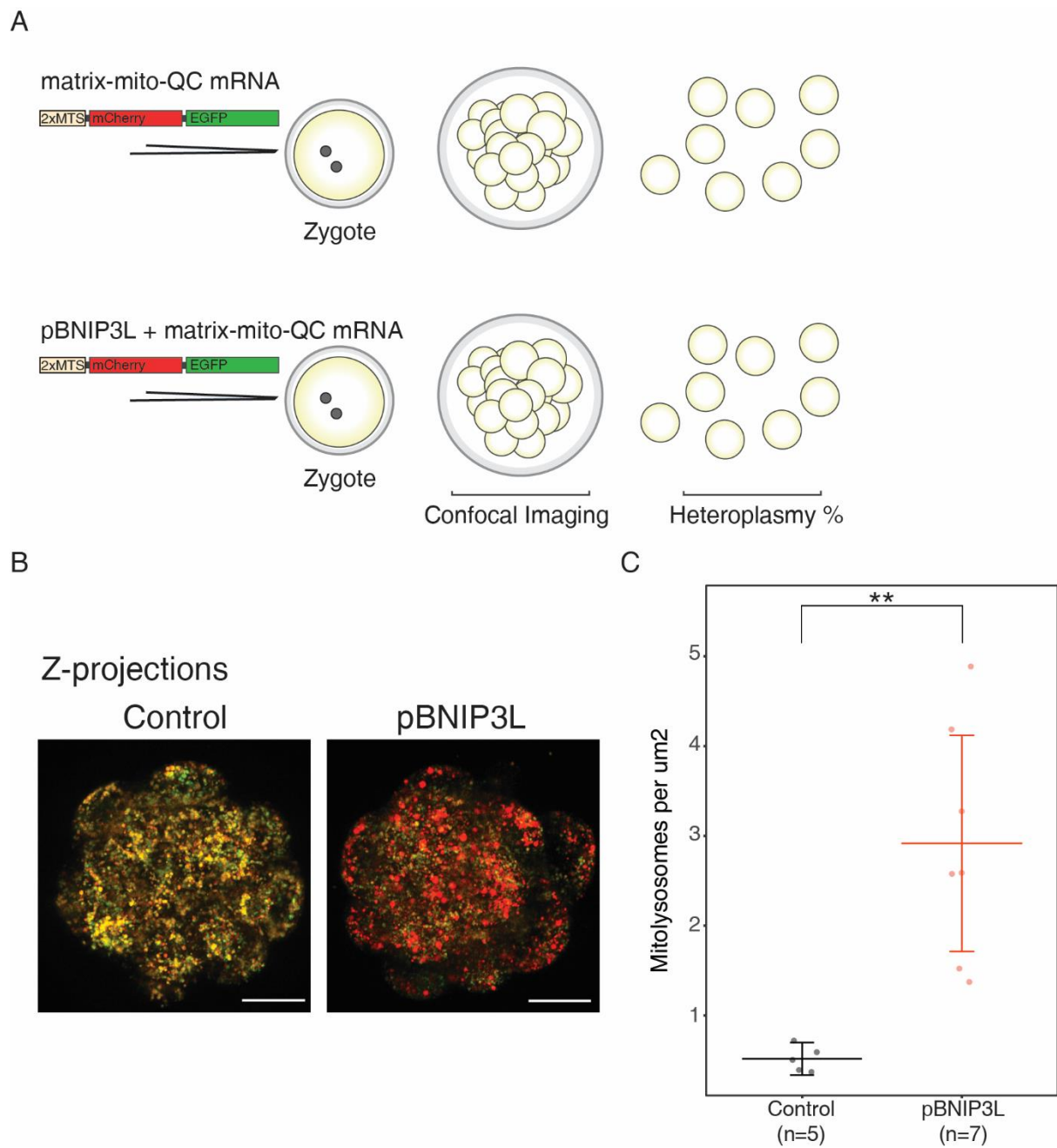
Figure 5.6. Upregulation of mitophagy in the *tRNAala* mouse late morula.

(A) Schematic of experiment design. (B) Representative z-projections of late morula stage embryos following injection of matrix-mito-QC mRNA with or without injection of mRNA encoding pBNIP3L at the zygote stage. 40x zoom. Scale bars = 20μM. (C Quantification of mitophagy via quantification of matrix-mito-QC signal at late morula. Central bar represents mean, outer bars 95% confidence intervals. Statistical significance was measure via two-tailed t-test. ** = P$\leq$0.01.

Upregulation of mitophagy did not have a significant effect on the segregation of mtDNA or intercellular variation of heteroplasmy between cells in the late morula (Figure 5.7.A-B, Table 5.4). CoV was similar between control and pBNIP3L groups (Figure 5.7.C), with differences driven by one outlier. This remained true when each variant was analysed separately or in combination. Sample size remains small and thus a wider analysis is required. Given that microinjection of pBNIP3L mRNA is variable in injection load, and thus likely the level of mitophagy promoted, it is plausible that the outlying embryo was subject to a higher level of mitophagy. Therefore, pBNIP3L may increase intercellular variation with sufficient levels of mitophagy induced. A more stringent method of quantifying the level of mitophagy may allow better resolution of this. Alternatively, one late morula may show elevated variation because analysis was conducted on roughly one third of the total cells of a given embryo, and the cells sampled in this instance stochastically represent the outer limits of this embryo. It is also possible culturing embryos to the blastocyst stage, thus allowing a greater degree of mitophagy to occur, will change this. Indeed, it is unclear how rapidly mtDNA can be degraded in the lysosome, potentially allowing mtDNA to be sequenced despite mitophagy. Changes in variation may have been more detectable had embryos analysed carried a level of heteroplasmy in the region of 40-60% more frequently, which may facilitate sharper segregation of mitophagy. These caveats mean further study is required. Nonetheless, these data suggest mitophagy in the preimplantation embryo has no influence on the inheritance of weakly pathogenic mtDNA mutations, and uneven inheritance of mitochondria as across cell division events likely causes changes in intercellular variation of the blastocyst.

Interestingly, intercellular variation in the late morula was similar to that of the blastocyst and substantially higher than that of the 8-cell of the same model (10.67% in control late morula compared to 1.08% in the 8-cell embryo). This suggests a rapid segregation of mtDNA even with a modest number of cellular division events in the period when an 8-cell embryo divides into a roughly 32 cell late morula.
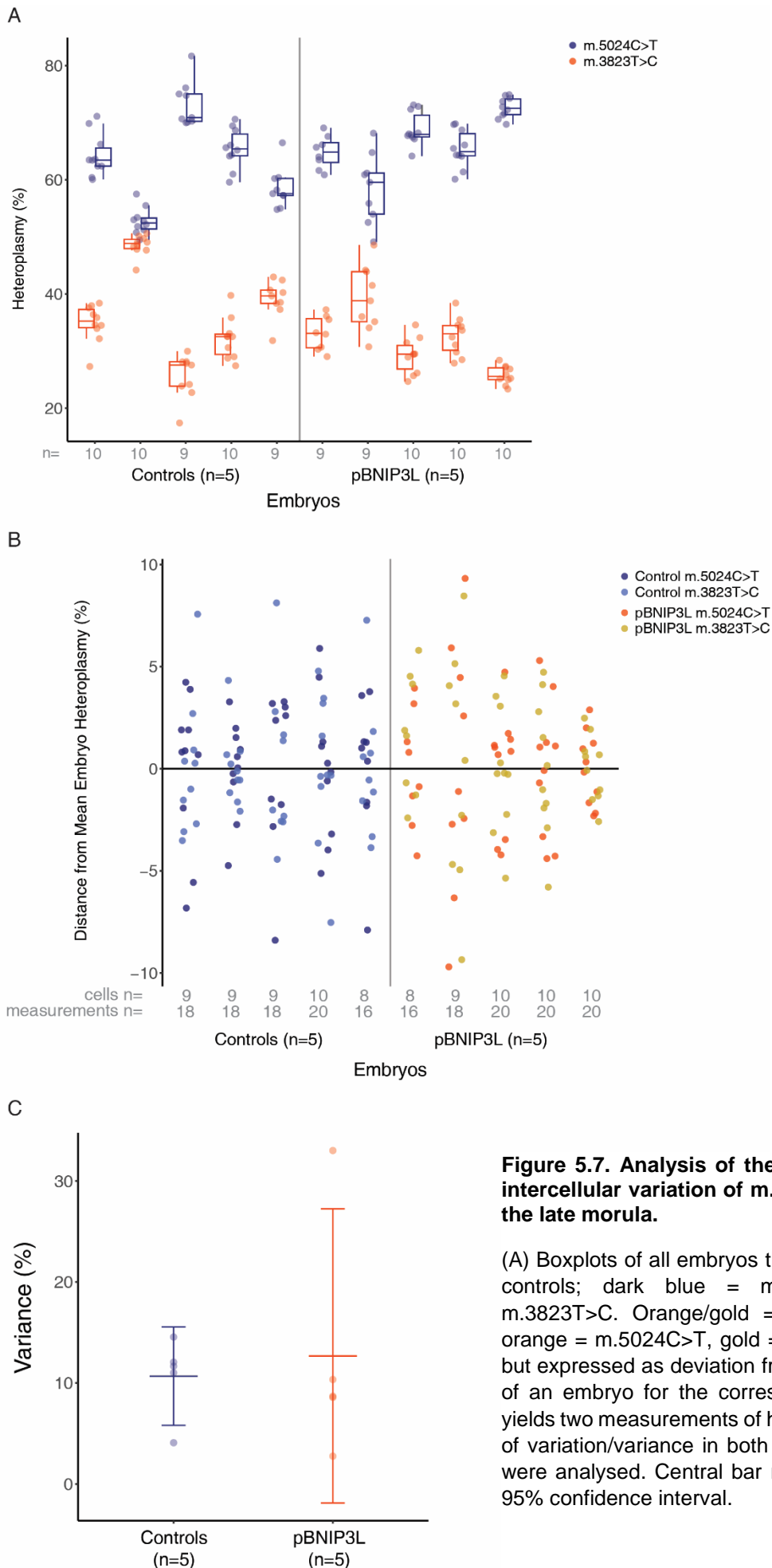
Figure 5.7. Analysis of the impact of mitophagy on intercellular variation of m.5024C>T heteroplasmy in the late morula.

(A) Boxplots of all embryos that underwent NGS. Blue = controls; dark blue = m.5024C>T, light blue = m.3823T>C. Orange/gold = pBNIP3L overexpressed; orange = m.5024C>T, gold = m.3823T>C. (B) As in (A) but expressed as deviation from the mean heteroplasmy of an embryo for the corresponding variant. Each cell yields two measurements of heteroplasmy (C) Coefficient of variation/variance in both groups when both variants were analysed. Central bar represents mean, outer bar 95% confidence interval.

Group/variant	Coefficient of variation (%)	Standard deviation (%)	Range (%)
Control	10.67 (3.92)	3.21	13.71 (2.83)
m.5024C>T	11.93 (3.91)	3.41	10.69 (1.53)
m.3823T>C	10.67 (4.52)	3.18	10.70 (2.49)
pBNIP3L	12.67 (11.72)	3.30	11.14 (4.91)
m.5024C>T	13.55 (13.48)	3.39	10.21 (5.21)
m.3823T>C	13.01 (11.62)	3.35	10.30 (4.70)

Table 5.4. Summary of the effect of mitophagy on intercellular variation of mtDNA heteroplasmy in *tRNAala* mouse embryos.

Data are expressed as mean with standard deviation.

5.4.5. Downregulation of preimplantation embryo mitophagy

With upregulation of mitophagy having no detectable effect on the segregation of mtDNA in the preimplantation embryo, I next sought to determine downregulation os mitophagy would prevent the shift in heteroplasmy observed between the 8-cell and blastocyst stage. To identify a method of inhibiting mitophagy in CD1 mice embryos, I tested two pharmaceutical agents, Cyclosporine A (Rodriguez-Enriquez et al., 2009), and MRT68921 (Petherick et al., 2015) which have been reported to inhibit mitophagy. Before analysis of mitophagy, the effect of these agents on the development of embryos needed to be determined to identify a maximal concentration that can be used in analysis.

Cyclosporine A

CsA is a specific inhibitor of mitochondrial outer membrane permeability transition (MOMP), preventing mitochondrial depolarization and thus mitophagy by interfering with the opening of MOMP pores (Broekemeier et al., 1989, Osman et al., 2011). Exposure to CsA had a strong impact on the development of CD1 mouse embryos at 250 µM when added to embryo cultures at the early morula stage, reducing the number of fully grown and hatching blastocysts relative to DMSO controls at day 5 (75.00% v 16.67%), with development either slowed or arrested (Figure 5.8.B-C). When mitophagy was tracked as described previously in CD1 mouse embryos exposed to CsA at the early morula stage, no change in red foci was detected (Figure 5.9.C), and presentation of red foci was similar to previous experiments (Chapter 1) Levels of

mitolysosomes per μm^2 were similar between controls and CsA-exposed groups at all stages analysed.

As CsA is understood to inhibit mitophagy by preventing mitochondrial membrane depolarisation (Osman et al., 2011), is it likely that it acts to prevent PINK1/PRKN mediated mitophagy, which is triggered by mitochondrial membrane depolarisation, more so than receptor-mediated mitophagy pathways. This supported the hypothesis the blastocyst mitophagy is regulated independently of membrane potential and mediated by BNIP3L pathway proteins. However, evidence for CsA an inhibitor of mitophagy arises from cell culture, and in most cases when mitophagy has been induced experimentally (Rodriguez-Enriquez et al., 2009, Wei et al., 2015, Liu et al., 2020).

Figure 5.8. Effect of CsA on CD1 mouse embryo development.

(A) CsA was added to embryo cultures at the early morula stage. Effect on development was measured as rate of embryos developing to fully grown blastocysts with hatching by day 5 of culture. (B) Embryos cultured (grey) and number of embryos developed (blue = controls, orange = CsA-exposed) at each measured concentration of CsA exposure. (C) Percent of fully grown blastocysts with hatching at day 5 at each concentration of CsA examined developed (blue = controls, orange = CsA-exposed). (D) Representative images of embryos in each group at day 5. Control embryos were largely fully grown and hatching at example time point, whereas CsA-exposed embryos largely failed to hatch at 250μM. 20x zoom. Scale bars = 20μm. Blastocysts growing to full size with hatching were considered successfully developed.

Figure 5.9. Effect of CsA on mitophagy in the preimplantation embryo of CD1 mice.

(A) Zygotes were injected with matrix-mito-QC mRNA and cultured with cyclosporine A (CsA) from the early morula stage, and the effect on mitophagy measured via confocal imaging. (B) Representative matrix-mito-QC z-projections of control and 250µM CsA exposed groups at analysed stages of embryo development. 40x zoom. Scale bars = 20µM. (C) Quantification of mitophagy via quantification of matrix-mito-QC signal at relevant stages of embryonic development. In all experiments the control grouped was exposed to DMSO only. Central bar represents mean, outer bar confidence limits. (D) Schematic of the mechanism of CsA mediated inhibition of mitophagy. CsA prevents depolarisation of the mitochondrial membrane, possibly inhibiting PINK1/PRKN mediated mitophagy specifically.

138

MRT68921

MRT68921 is an inhibitor of Unc-51 Like Autophagy Activating Kinase 1 (ULK1), which acts upstream of phosphatidylinositol 3-kinase (PIK3C3) to regulate the formation of autophagophores, the precursors of autophagosomes (Lee et al., 2010). As ULK1 is a regulator of general autophagy, MRT68921 acts to inhibit autophagy of a range of cellular components, as well as mitochondria. Exposure to MRT68921 as the early morula stage had a strong impact on the development of CD1 mouse embryos at 0.5 μM, with fewer embryos developing to fully grown, hatching blastocysts (90.91% compared to 9.10%) at day 5 (Figure 5.10.B-C). Many embryos failed to develop to the blastocyst stage at all. However, exposure to MRT68921 at the early morula stage had no impact on the appearance of red foci or number of mitolysosomes per μm^2 (Figure 5.11.D). Presentation of red foci was again similar to previous experiments (Chapter 1). Evidence for MRT68921 as an inhibitor of autophagy arises only from stem cell cultures where autophagy was induced in via Earle's balanced salts solution (Petherick et al., 2015), potentially explaining why physiological mitophagy was not inhibited in the blastocyst.

Blastocyst mitophagy could not be inhibited through the use of pharmacological agents. Most likely this is because their inhibitive action towards mitophagy is demonstrated in cell lines. It remains to be established whether CsA or MRT68921 can inhibit physiological mitophagy or autophagy. Instead, avenues such as gene editing technology will likely be required to inhibit mitophagy, through specific knock down of gene expression of gene knockout of key mitophagy genes.
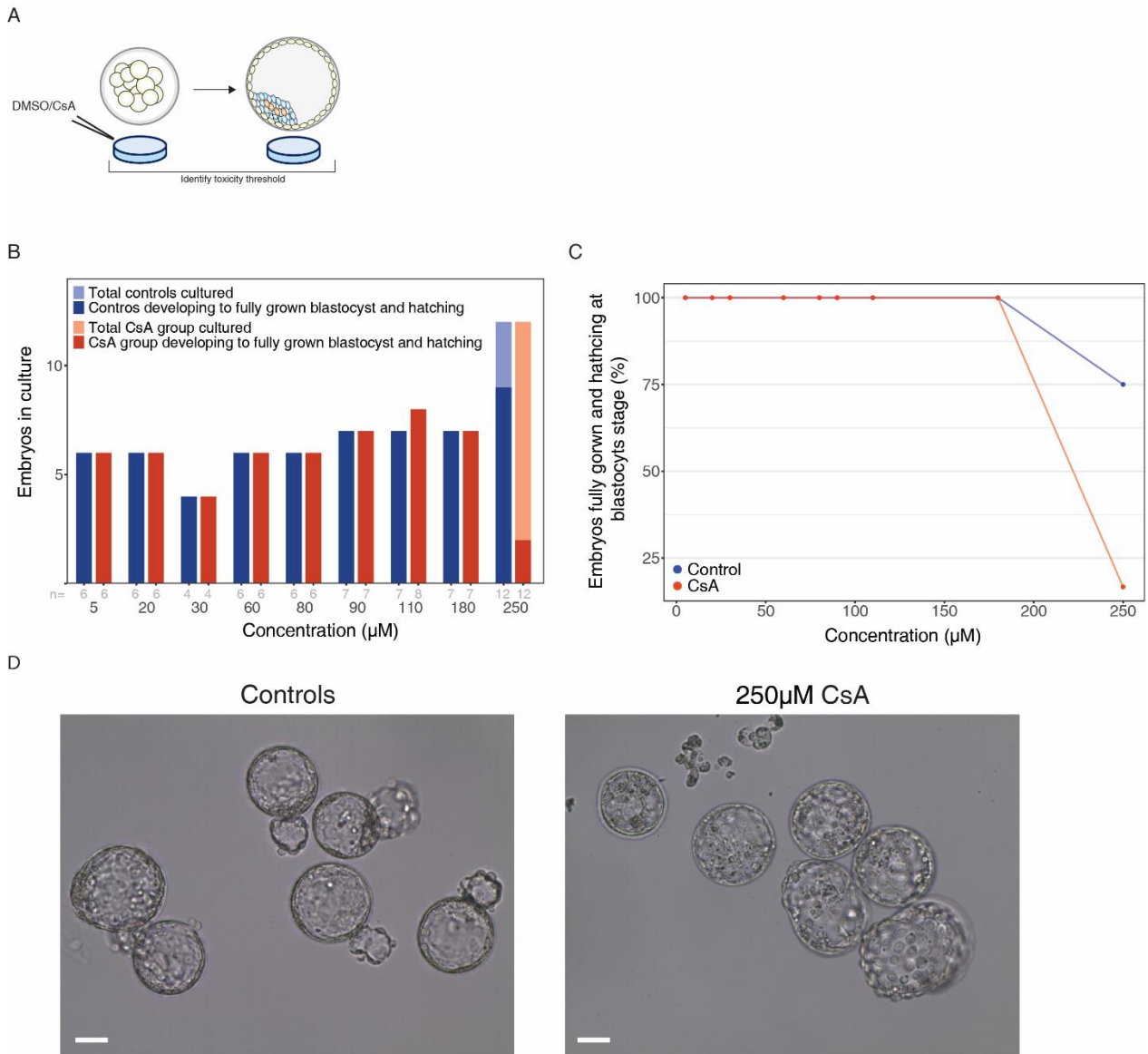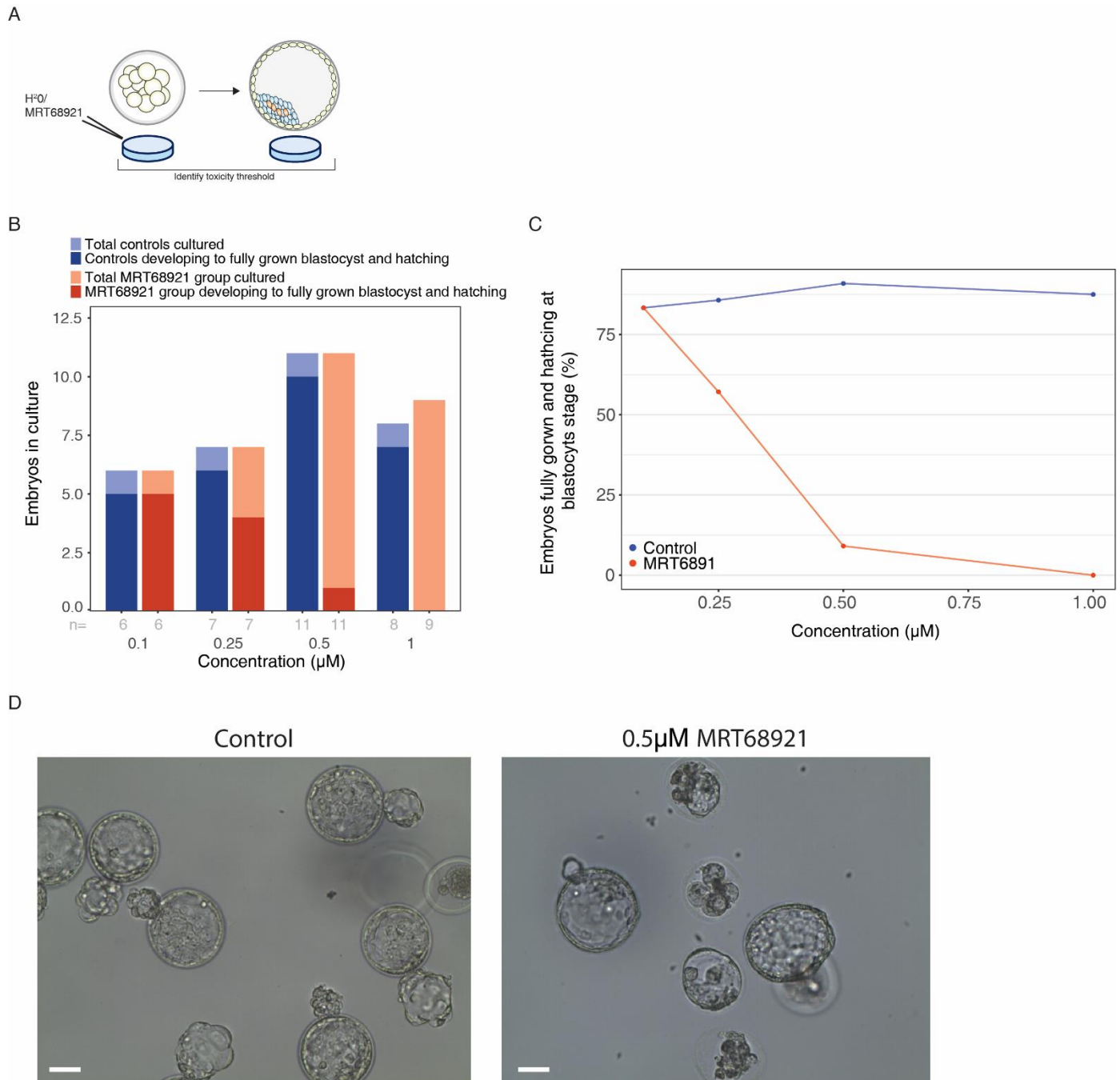
Figure 5.10. Effect of MRT68921 on CD1 mouse embryo development.

MRT68921 was added to embryo cultures at the early morula stage. Effect on development was measured as rate of embryos developing to fully grown and hatching blastocysts by day 5 of culture. (B) Embryos cultured (grey) and number of embryos developing (blue = controls, orange = MRT68921-exposed) at each measured concentration of MRT68921 exposure. (C) Percent of embryos fully grown and hatching at day 5 at each concentration of MRT68921 examined (blue = controls, orange = MRT68921-exposed). (D) Representative images of embryos in each group at day 5. Control embryos were fully grown and hatching at example time point, whereas MRT68921-exposed embryos largely failed to develop at 0.5μM. 20x zoom. Scale bars = 20μm. Blastocysts growing to full size with hatching were considered successfully developed.
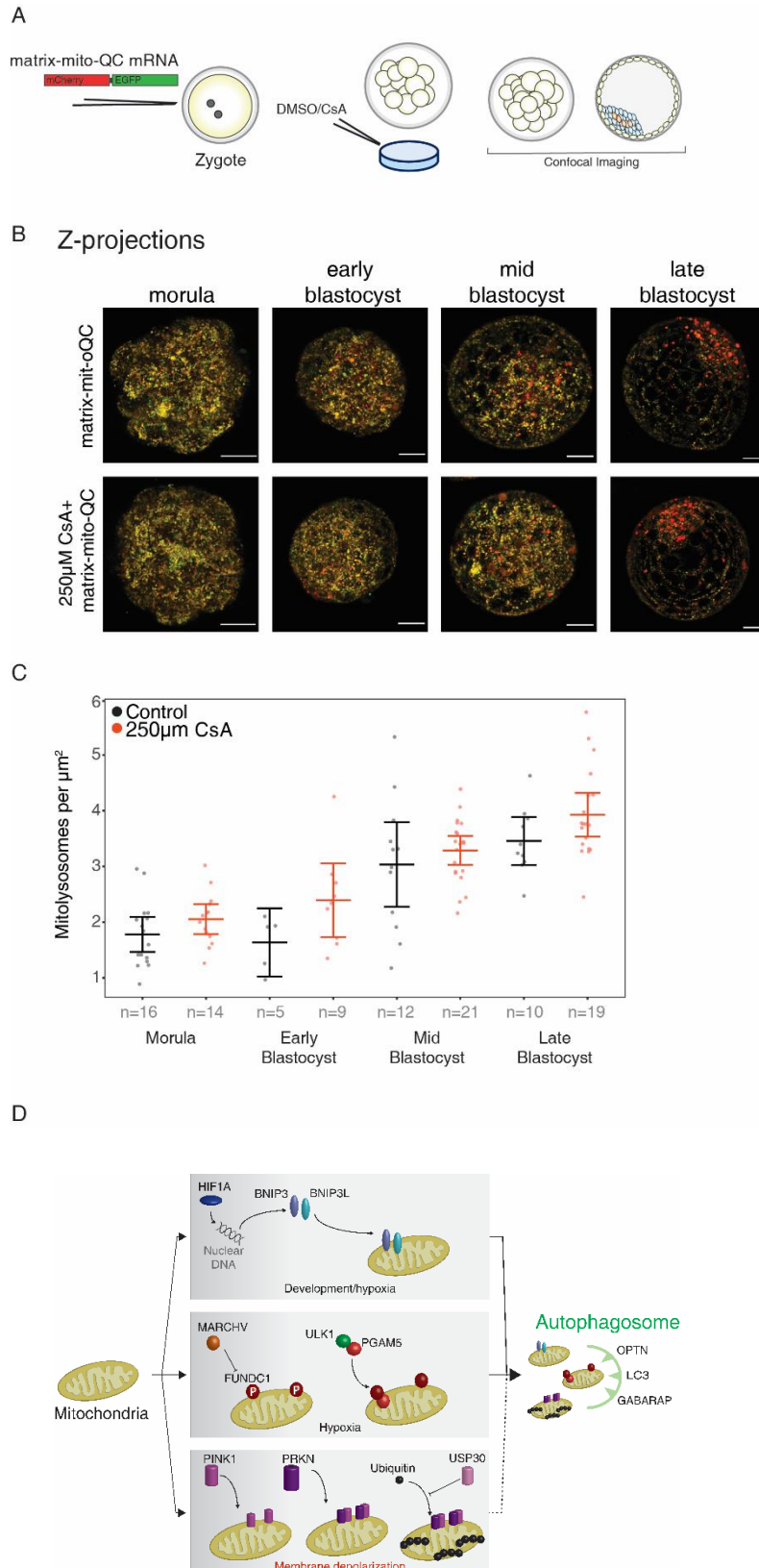
140
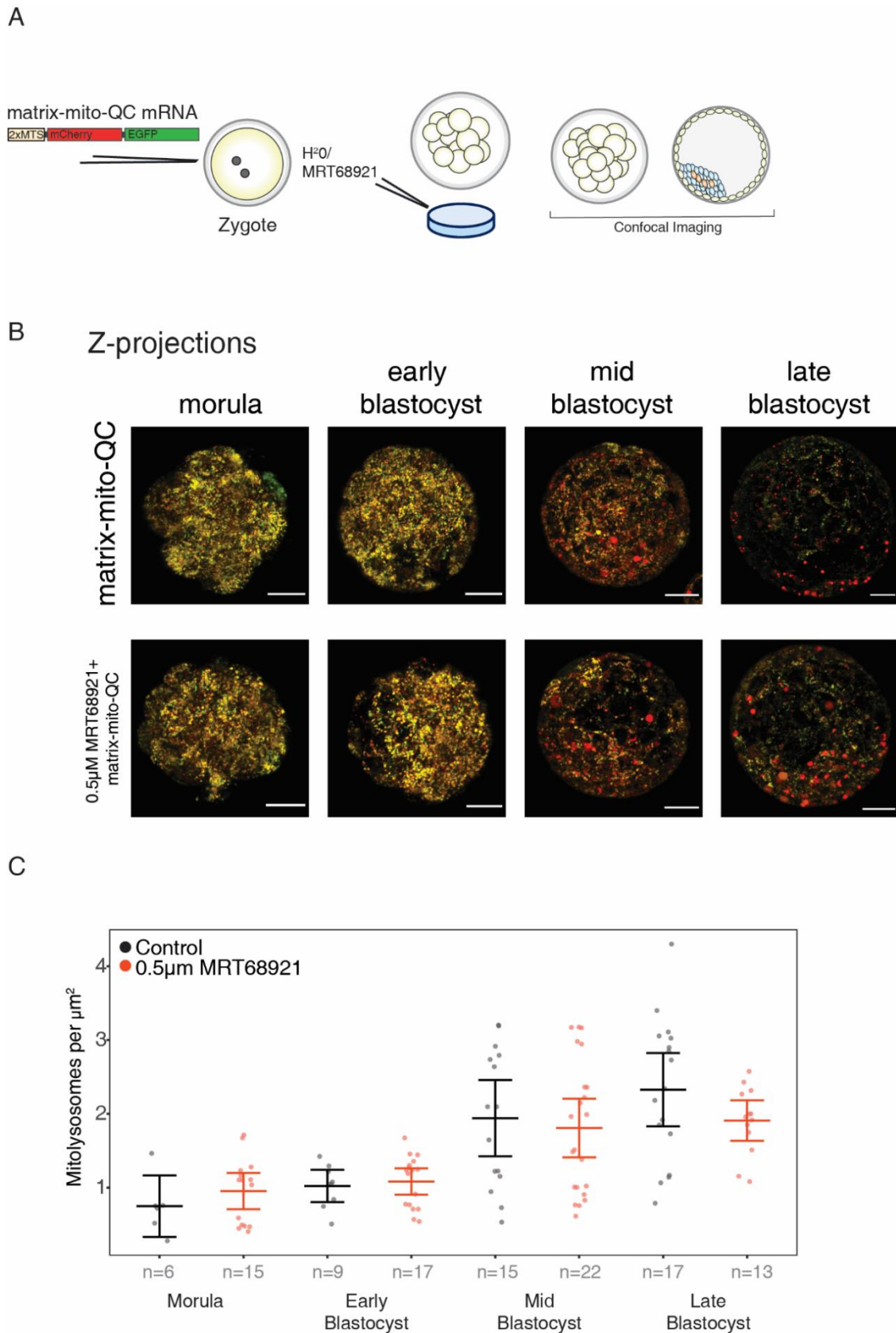
Figure 5.11. Effect of MRT68921 on mitophagy in the preimplantation embryo of CD1 mice.

(A) Zygotes were injected with RNA encoding matrix-mito-QC mRNA and cultured with MRT68921 from the early morula stage, and the effect on mitophagy measured via confocal imaging. (B) Representative mito-QC images of the control and $0.5\mu m$ MRT68921 exposed groups at analysed stages of embryo development. 40x zoom. Scale bars = 20µm. (C) Quantification of mitophagy via quantification of matrix-mito-QC signal at relevant staged of embryonic development. In all experiments the control grouped was exposed to H_2O only. Central bar represents mean, outer bar confidence limits

5.4.6. Accuracy of mtDNA variant calling in scRNAseq and intercellular variation between single cells of the human PNT blastocyst

Previous work examining the intercellular segregation of mtDNA heteroplasmy during preimplantation development has utilised models of heteroplasmy generated by means of cytoplasmic transfer between oocytes (Lee et al., 2012). Measurement of mtDNA heteroplasmy using scRNAseq has recently been demonstrated in human cells (Ludwig et al., 2019). scRNAseq data previously gathered from PNT blastocysts (Hyslop et al., 2016), provided a unique and rare opportunity to investigate intercellular mtDNA variation in a human model similarly generated by transfer of cytoplasm (Figure.5.12), and compare this to variation of a pathogenic mtDNA variant occurring in the *tRNAala* mouse.

This human PNT scRNAseq dataset comprises 54 PNT blastocyst cells, obtained from 9 PNT blastocysts, produced from the donated oocytes of women of diverse mtDNA haplogroups. RNA was sequenced as described previously (Hyslop et al., 2016). After processing of fastq files and normalisation, analysis of the expression of mtDNA encoded genes showed that, similar to others (Zhang et al., 2019), *tRNA* and *rRNA* gene expression was largely undetectable, whereas other protein coding regions showed sufficient expression for the analsyis of mtDNA variants (Figure.5.12.A). Analysis of read depth and sequencing coverage of mtDNA confirmed tRNA genes were only detectable at low depth (Figure 5.12.B). This loss of mtDNA genome coverage has been observed before (Zhang et al., 2019), particularly across the *tRNA* genes, and is likely due to poly-A selection in library preparation which enriches only a subset of mtRNAs, or differential stability of mtRNAs (Borowski et al., 2010). The role of polyadenylation in mtRNA processing is not fully understood, with polyadenylation promoting the degradation of some gene transcripts (*COI/II/III, ATP6/8*) and the stabilisation of others (*ND1/2/3/4/4L/5*). *ND6* was shown to lack a poly-A tail (Barchiesi and Vascotto, 2019). This is not reflected in the expression profile of these transcripts I detect, suggesting the mechanism of mRNA polyadenylation require further characterisation.

None the less mtDNA haplogroup (confidence > 0.8) was identified in all samples using Haplogrep (Weissensteiner et al., 2016). In conjunction, PhyloTree (van Oven, 2015) was used to identify a number of potential positions relating to the majority haplogroup (the mitochondrial donor). This allowed the identification of all possible 'expected' heteroplasmies that would be generated when mixing 2 mtDNA haplogroups. In light of the lack of data yielded

on *tRNA* genes, data were filtered at read depth of >2000x to ensure accuracy of variant calling (1% heteroplasmy would be resolved using 20 reads). Due to a lack of field depth in a number of samples, only 27 (50.00%) cells yielded sufficient data for analysis (Figure 5.13.B), and a number of specific variants within these cells failed to pass the 2000x threshold. Final analysis included 8 variants, observed across 27 cells from 4 embryos. All heteroplasmic variants observed within a given cell were averaged, as they form part of the same phylogeny, to give cells a final mean heteroplasmy value.
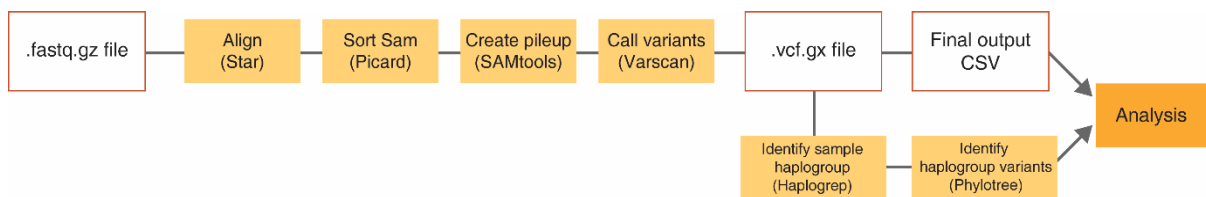
Figure 5.12. Schematic of PNT blastocyst scRNAseq data processing.

FASTQC files were aligned to the human genome (UCSC GRCh37/hg19GRCh38) via Star, and processed to variant call format (VCF). VCF files were uploaded to Haplogrep to identify haplogroup, and Phylotree used to expand a catalogue of associated mtDNA variants. VCF files were processed into a comma separated file (CSV) for analysis of heteroplasmy.
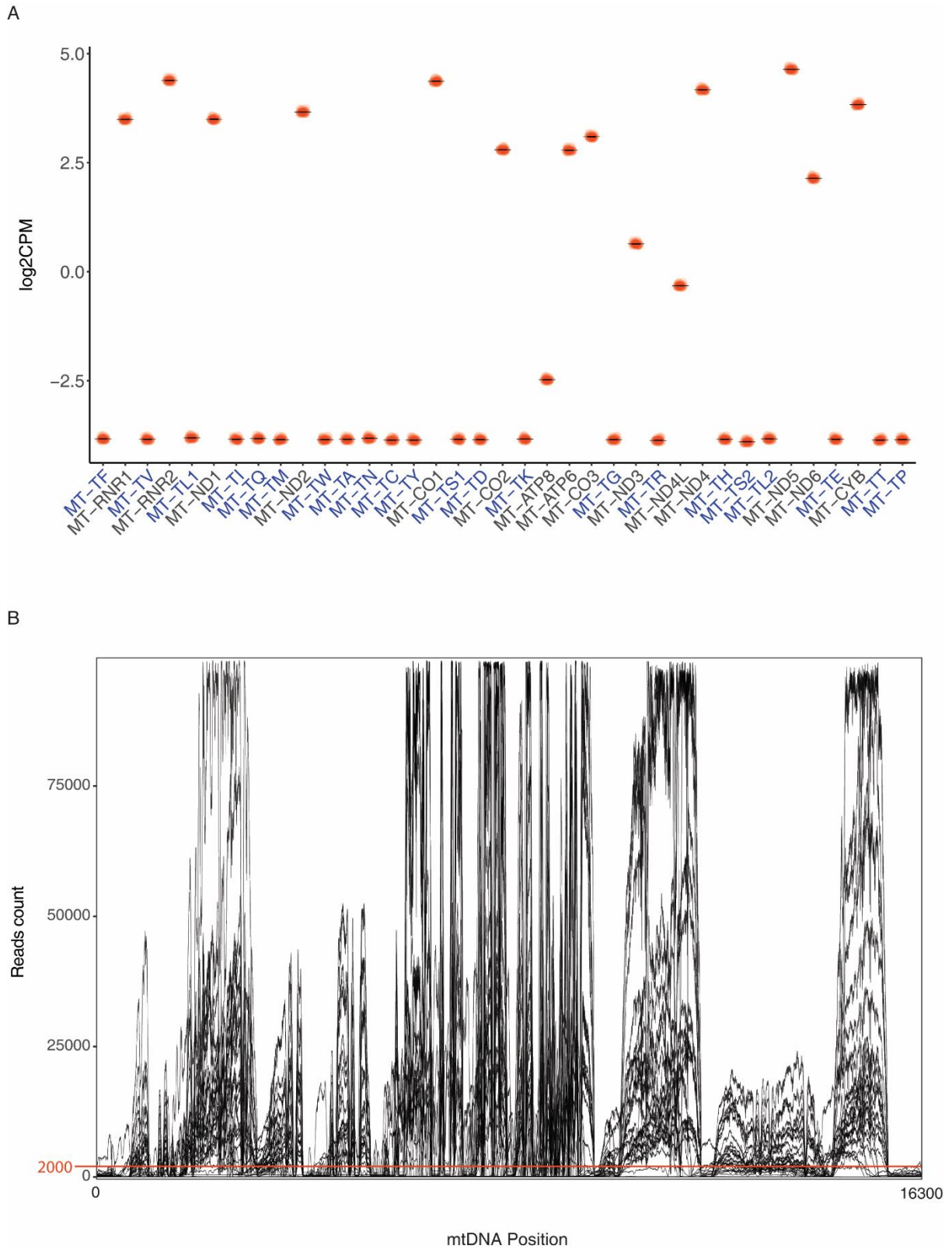
Figure 5.13. mtDNA genome expression and coverage in human PNT blastocyst scRNAseq data.

(A) A total of 54 PNT blastocyst cells underwent scRNAseq. Expression of tRNA genes (light blue on x-axis) was near negligible, whereas mitochondrial protein (black) and rRNA (blue) genes showed variable expression. (B) Coverage of the mtDNA genome across 54 PNT blastocyst single cells. X-axis represents the mitochondrial genome. Orange line represents cut-off value for variant calling. 27 samples had sufficient coverage to undergo variant calling at key positions.

144

Despite their low coverage, one *tRNA* variant surpassed the 2000 reads threshold for analysis (Table 5.5). In addition to scRNAseq data, Hyslop *et al* reported pyrosequencing of mtDNA from cell clumps collected from the same embryos. Pyrosequencing is regarded as a rigorous method of quantifying heteroplasmy (Sobenin et al., 2014), and comparison of this data to my own scRNAseq analysis allows assessment of the accuracy of scRNAseq variant calling (Figure 5.14). One embryo showed significantly different average heteroplasmy between the methodologies (2.73±0.41% pyrosequencing versus 6.06±1.32% scRNAseq, two-tailed t-test, P<0.01), but clear trends towards diverging results were apparent in all other cases. Given that the pyrosequencing method has been more rigorously tested and controlled (Hyslop et al., 2016), this suggests analysis of heteroplasmy via scRNA seq has significant caveats which must be considered conducting analysis. Noticeable variation between variants even within scRNAseq samples (Figure 5.15).

However, the possible existence of exaggerated segregation of mtDNA heteroplasmy may compromise this comparison. Compared to the naturally arising heteroplamsy of the *tRNAala* mouse, intercellular variation of heteroplasmy was wider in human PNT blastocysts when measured via scRNAseq (11.94% compared to 56.72%, Table 5.6, Figure 5.16). This suggests that, even when only a small volume of cytoplasm is co-transferred in a karyoplast, intercellular heteroplasmy in the blastocyst is exaggerated immediately following procedures including transfer of cytoplasm, such as those of Lee *et al* (Lee et al., 2012). Consistent with this, GFP-tagging of the mitochondria from the nuclear donor zygote shows asymmetric distributions of karyoplast (co-transferred) mitochondria following PNT and subsequent enrichment in a subset of cells (Y. Takeda, unpublished).

This extreme intercellular variation limits the extent to which I can compare previous pyrosequencing of human PNT blastocyst cell clumps to scRNAseq analysis of single cells from the same embryo to measure the accuracy of scRNAseq mtDNA variant calling. The elevated intercellular variation in scRNAseq analysis relative to pyrosequencing of clumps likely cannot be entirely accounted for by disaggregation into single cells, reaffirming the drawbacks of my scRNAseq analysis. It is unclear what extent performing total RNAseq, without poly-A selection, might improve on these results. Furthermore, true comparison of methods would require both DNA and RNA sequencing of the same samples, so that background intercellular variation of the blastocyst does not compromise comparisons. Accurate measurement of heteroplasmy using scRNAseq would have the advantage of being able to measure heteroplasmy directly in the epiblast, which could be identified based on

expression of lineage specific genes. Unfortunately, cellular lineage could not be identified in the PNT dataset, presumably because the vast majority of ICM cells were directed towards pyrosequencing.

1PNT		3PNT		4PNT		9PNT	
Variant	Gene	Variant	Gene	Variant	Gene	Variant	Gene
A2706G	TL1	T8473C	ATP6	G3010A	ND1	A2706G	TL1
C6371T	CO1			T8473C	ATP6	C6371T	CO1
T8705C	CO3					C12705T	ND5
C12705T	ND5					G13708A	ND6
						A13966G	ND6

Table 5.5. Variants measurable within each human PNT blastocyst.

Position, base change and gene harbouring the variants are displayed. ATP6, ATP synthase membrane subunit 6; CO1, Cytochrome c oxidase subunit I; CO2, Cytochrome c oxidase subunit II; ND1, NADH-ubiquinone oxidoreductase chain 1; ND5, NADH-ubiquinone oxidoreductase chain 5; ND6, NADH-ubiquinone oxidoreductase chain 6; TL1, tRNAleucine.
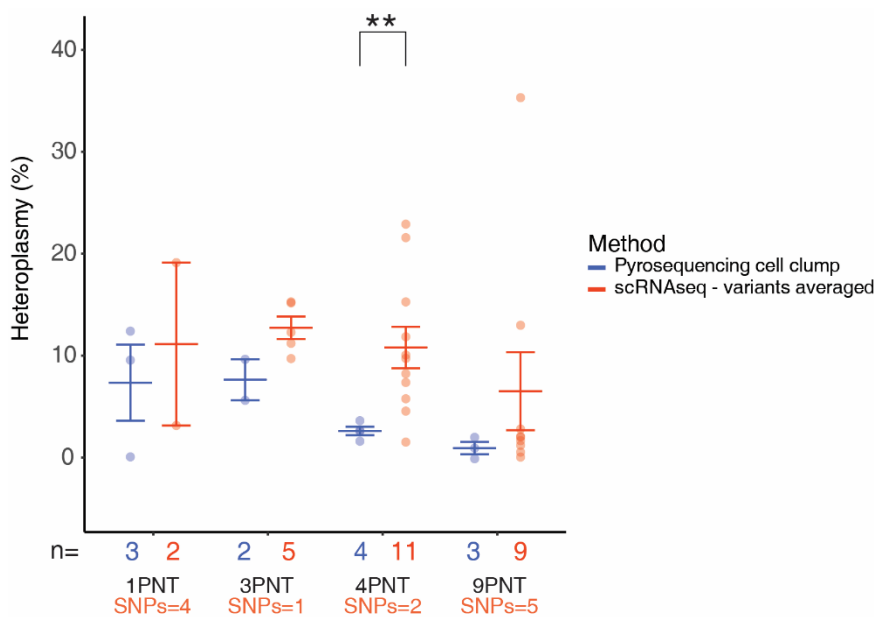
Figure 5.14. Comparison of mtDNA heteroplasmy in human PNT blastocysts as measured by pyrosequencing or scRNAseq.

Pyrosequencing was used to analyse cell clumps, scRNAseq single cells. Differences are apparent in mostly embryos, but statistically significant in only one. Central bar represents mean, outer bar standard error. Statistical significance was measure via two-tailed t-test. $** = P \leq 0.01$.

Source	Methodology	Sample type	Variation (%)	Standard deviation (%)	Range (%)
tRNA[ala] mouse blastocysts	Pyrosequencing	Cells	11.94 (3.46)	2.95	9.75 (1.85)
Human PNT blastocysts	scRNAseq	Cells	56.72 (40.70)	7.91	19.54 (10.70)
Human PNT blastocysts	Pyrosequencing	Cell clumps	8.29 (11.34)	2.92	5.12 (4.24)

Table 5.6. Summary of intercellular variation across different models and methodologies.

Data are expressed as mean with standard deviation.
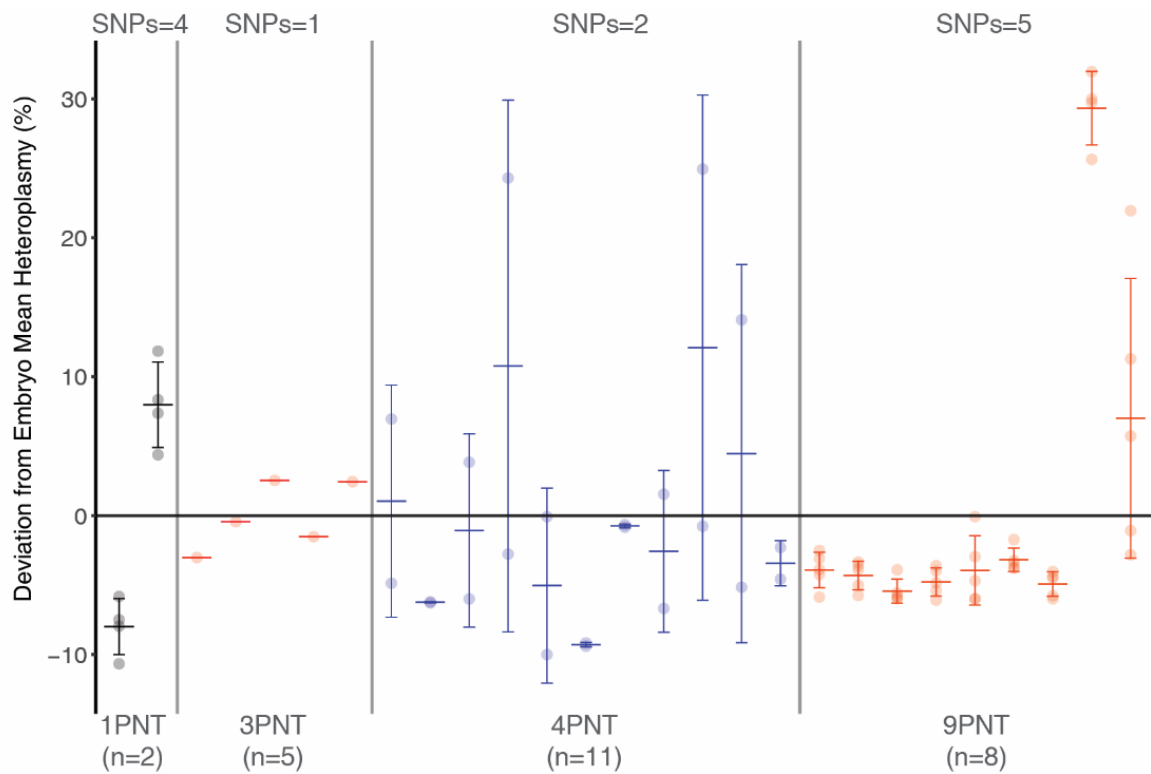
Figure 5.15. Heteroplasmy of human PNT blastocysts as measured by scRNAseq.

Divergence of cell heteroplasmy from mean of each embryo. Each dot represents a cell, averaged from a variable number of SNPS in each embryo (top).
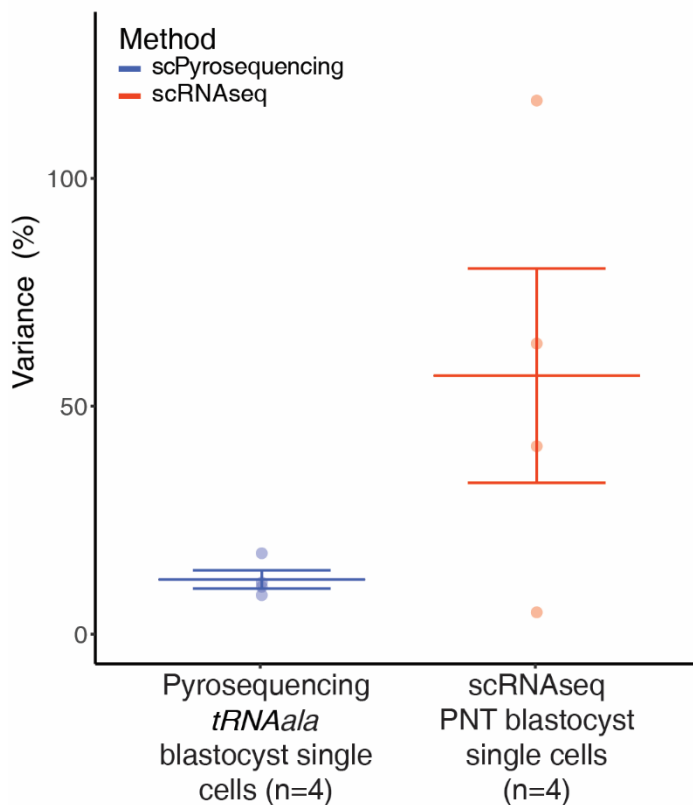
Figure 5.16. Comparison of coefficient of variation measured by the pyrosequencing of *tRNAala* mice blastocyst single cells, and human PNT blastocyst single cells measured by scRNAseq.

Central bar represents mean, outer bar standard error.

5.5. Discussion

Diseases caused by pathogenic variants in mtDNA currently have no curative treatments, and as such the understanding inheritance and optimisation of methods to prevent it are paramount. While maternal inheritance has been well documented, the question of whether heteroplasmy levels are further modulated during preimplantation development has not been explored. In support of this possibility, we have recently discovered that mammalian embryos exhibit a wave of mitophagy that commences at the morula stage and increases as the embryo developed to the blastocyst stage. In this chapter, I investigated the possibility that mitophagy might induce a shift in heteroplasmy levels during progression towards implantation. In addition, I asked whether the heterplasmy levels at the preimplantation stage can best be predicted by a blastomere from an 8 cell embryo or by samples of cells taken from the TE at the blastocyst stage. Finally, I determined whether heteroplasmy levels could be inferred from scRNAseq data from human blastocysts. My findings shed light on the physiological relevance of mitophagy and address the long-standing clinical question of whether an 8 cell or blastocyst biopsy is best for PGD.

My analysis reveals a lower level of intercellular variation of heteroplasmy in 8-cell embryos of the *tRNAala* mouse compared to the blastocyst. Earlier work examining intercellular variation in 8-cell embryos utilised heteroplasmic BALB/OlaHsd mice, with heteroplasmy generated via cytoplast transfer of two mouse lines carrying wildtype mtDNA genomes, but bred across at least one generation. Initial reports indicated a tight spread of heteroplasmy between cell of 8-cell embryos with a mean range of 3.3% heteroplasmy, similar to my own analysis (Dean et al., 2003). Later, expanded analysis of the same model reported a similar mean range of 4% heteroplasmy across 8-cell embryos, but an average CoV of 5.6% and with intercellular variation across some 8-cell embryos reaching a maximum range of 17.3%, both higher than in my analysis (Neupane et al., 2014). Discrepancies may have arisen due to differences in technical approach. It is also unclear to what extent the genotype of the BALB/OlaHsd mice, harbouring 101 mtDNA variants generally at >40% heteroplasmy (Neupane et al., 2014), replicates the behaviour of a pathogenic variant. My own analysis from a model with a small number of biologically arising variants, including a single pathogenic mutation, supports that intercellular variation in the 8-cell is minimal.

Work analysing the intercellular variation of heteroplasmy in human embryos has the advantage of analysing pathogenic mtDNA variants directly. In work examining human 8-cell embryos carrying the m.3243A>G variant the intercellular variation of heteroplasmy was largely tight, with an average range of 2.2% across two biopsied blastomeres (Monnot et al., 2011), bearing strong resemblance to my own measurements. Further work on m.3243A>G heteroplasmy in single cells of cleavage stage embryos showed average standard deviation was 2.03% across individual embryos (excluding embryos with fewer than 6 blastomeres sampled) slightly higher than my data (Treff et al., 2012). Further work examined human cleavage stage embryos carrying either m.3234A>G or m.8994T>G. Most verifiable single cells of cleavage embryos showed little variation within embryos, generally under 10%, but with a few instances of heteroplasmy range extending higher (Sallevelt et al., 2013). A later study expanding on segregation of m.3243A>G in human cleavage embryos again showed limited variation of heteroplasmy between blastomeres, generally under 10% and often as low as around 5%, but again with sporadic outliers (Sallevelt et al., 2017a). Such outliers were not apparent in my analysis, which was also showed an even more narrow spread of heteroplasmy than human embryos. Discrepancies may have arisen due to differences in technical approach, differences in the nature of models or pathogenic variants, or the wider diversity of cleavage stages and embryo morphologies examined by Sallevelt *et al* (2013/2017).

Intercellular variation of heteroplasmy in the blastocyst has been less thoroughly explored, and previous work was conducted at the level of either a biopsy or clumps of cells, thus masking a level of variation. In the BALB/OlaHsd mouse model, Neupane *et al* reported a slightly wider prediction interval in heteroplasmy between a TE biopsy and the remaining embryo compared to that between the cells of an 8-cell embryo, although this did not manifest a meaningful change in the CoV (Neupane et al., 2014). In a human carrier of m.3234A>G Treff *et al* reported average standard deviation of 3.23% across individual cells, slightly higher than 8-cell embryos of the same study (2.03%) and similar to that reported here in blastocyst cell clumps and single cells (Treff et al., 2012). Therefore, between the cleavage and blastocyst stages, heteroplasmy of pathogenic mtDNA variants in human embryos appears to behave similarly to the mouse *tRNAala* pathogenic variant I have analysed in mice, with intercellular variation of heteroplasmy increasing in the blastocyst. This pattern of segregation requires confirmation in human embryos.

The above data strongly suggest that the 8-cell embryo is the optimal stage of development for PGD biopsy. Furthermore, blastocyst mitophagy occurring during blastocyst development

did not represent purifying selection against the m.5024C>T pathogenic variant, and the heteroplasmy of an 8-cell biopsy reflected the average heteroplasmy of a whole blastocyst. However, it remains unclear exactly to what extent heteroplasmy of an 8-cell embryo reflects that of specific epiblast cells. The intercellular variation of heteroplasmy I report in the *tRNAala* mouse 8-cell embryo is lower than that of previous reports in mouse and human, likely because previous reports rely on restriction fragment length polymorphism methods, whereas I utilised pyrosequencing (Sobenin et al., 2014). This suggests that with sufficiently powerful analytical methods, only one 8-cell biopsy need be collected. Based on the range of heteroplasmy in blastocysts of the *tRNAala* mouse, a TE biopsy may misestimate an embryo by as much as 9.33%. This broadly corroborates human data on the m.3243A>G data (Heindryckx et al., 2014). TE biopsy carries benefits to fetal health due to the sampling of only cells that give rise to the placenta (Vermeesch et al., 2016, Cimadomo et al., 2016). However, given a threshold of 15-18% heteroplasmy for safe PGD, the risk of misestimating embryo heteroplasmy by 9.33% represents a considerable risk to the success of the procedure.

Upregulation of mitophagy had no detectable impact on the segregation of mtDNA heteroplasmy in the late morula of *tRNAala* mice. Based on the above, mitophagy in the preimplantation embryo has no impact on the inheritance of mtDNA variants. Instead, intercellular variation likely increases in the blastocyst and morula due to the uneven inheritance of mitochondria during cell division events.

The mechanics of mitochondrial inheritance in mitosis of symmetrically dividing cells were recently characterised through high resolution microscopy (Moore et al., 2021). Imaging revealed that the actin network which regulates organelle distribution in mitosis can rapidly transport mitochondria across a cell, leading to a more even distribution of mitochondrial network components with variable functional profiles in daughter cells. In Hela cells, mitochondria with photo-induced damaged were split more evenly across two daughter cells in comparison to when the actin network was inhibited. If the above mechanism occurred in the cleavage stage preimplantation embryo of the *tRNAala* mouse, the m.5024C>T variant (as well as others) would be would remain similar between cells of the morula and blastocyst.

The absence of this mechanism may be underlined by fundamental differences between mitosis in embryos and other models; a cleavage embryo blastomere does not increase cytoplasm content before a division event thus cells become progressively smaller (Prados et

al., 2012), and mitochondria exist in a more punctuate state comparative to Hela cells (Seo et al., 2018, Moore et al., 2021). Whilst the mechanisms detailed by Moore *et al* (2021) occurred in cells containing ostensibly healthy mitochondria, it is not clear if the incidence of these translocation events were increased by the presence of damaged mitochondria, and it is plausible the outcomes detailed in the context of photo induced toxicity would be different in the context of pathogenic mtDNA variants.

The mtDNA variants of the *tRNAala* are assumedly interspersed throughout the mitochondrial network, and given that all cells of the 32-cell morula maintain totipotency changes in mtDNA segregation cannot be explained by asymmetric stem cell division geared towards differentiation of a daughter cell (Morrison and Kimble, 2006). Thus it is unclear exactly how mtDNA comes to be unevenly inherited at the compaction stage. However differential size between daughter cells has been noted in the cleavage embryo (Prados et al., 2012), and the onset of morphological changes in the embryo may alter symmetry of cell division events, explaining why the diverging heteroplasmy of cells does not reveal itself earlier. Further work is needed to explore this phenomenon in the cleavage stage embryo.

Intercellular variation in m.5024C>T heteroplasmy increased rapidly between the 8-cell and 32-cell late morula stage, demonstrating that intercellular variation between blastomeres can change rapidly in 24 h. Some studies so far in human embryos have at times compared biopsies of cleavage stage embryos to disaggregated embryos after a delay for diagnostic sequencing of an initial blastomere biopsy and associated clinical procedures (Sallevelt et al., 2013, Sallevelt et al., 2017b). It is plausible that the potential for a rapid change in the segregation of mtDNA heteroplasmy may have some impact on some samples in such analyses.

Measurement of mtDNA copy number will be important to further characterisation of mitophagy in the blastocyst. Preliminary analysis so far suggests mitophagy is accompanied by a modest decrease in copy number at the level of the whole blastocyst compared to the whole 8-cell embryo (Dr. Magomet Aushev, data not shown). Measurement of copy number at the level of single cells of the embryo may also prove valuable. Importantly, measurement of copy number following pBNIP3L overexpression shows a profound reduction in copy number at the blastocyst stage (Dr. Magomet Aushev, Dr. Yuko Takeda, data not shown), offering validation of mitophagy upregulation.

Analysis of heteroplasmy via variant calling of scRNAseq data benefits from being able to measure the heteroplasmy of a number of variants within each sample. Nonetheless, heteroplasmy measured via scRNAseq data showed a trend of diverging from measurements made by pyrosequencing of a single variant in cell clumps of the same embryo. This difference was significant in one instance. Pyrosequencing is regarded as a highly robust method of measuring heteroplasmy (Sobenin et al., 2014), suggesting that measuring heteroplasmy via scRNAseq has significant drawbacks. This is largely in agreement with earlier attempts using RNAseq (Zhang et al., 2016a, Ludwig et al., 2019), but my analysis of the accuracy of RNAseq variant calling is compromised by the background intercellular variation of the embryo. My analysis was also compromised by loss of sequencing coverage, particularly in non-protein coding areas of mtDNA, suggesting that future attempts to analyse heteroplasmy via scRNAseq would benefit from the use of total-RNAseq, as opposed to poly-A selected RNAseq. Accurate measurements of analysis scRNAseq data to measure heteroplasmy in blastocysts would also carry the benefit of being able to measure heteroplasmy directly in the blastocyst.

My analysis of scRNAseq data from human PNT blastocysts revealed a higher level of variation of heteroplasmy between cells of PNT blastocysts than was apparent in blastocysts of the *tRNAala* mouse. It is likely that the drawbacks of my scRNAseq analysis relative to pyrosequencing contributed to the increased intercellular variation of heteroplasmy relative to *tRNAala* mouse blastocysts, but this increased variation is in large part likely due to heteroplasmy being produced by karyoplst transfer in the zygote during PNT. In this context the two mitochondrial genomes have little opportunity to fuse, thus skewing their segregation in cell divisions. This level of intercellular variation arose despite PNT blastocysts harbouring a low level of heteroplasmy (<13%, Hyslop et al., 2016), which likely leaves less opportunity for variation to arise across cell divisions. In a similar primate model generated via cytoplast transfer of two wildtype genomes, variation across cells of the 8-cell embryo was reported to range from 10% to 70%. When primate blastocysts were separated into TE and ICM portions, intercellular ranged from 4% to 31% (Lee et al., 2012). The severity of segregation in this primate model in far higher than that which I report, likely because primate zygotes were generated with ~50% heteroplasmy. The PNT blastocysts I analysed where produced with the aim of achieving minimum heteroplasy. Together this evidence suggests intercellular variation immediately following cytoplast transfer is exaggerated and does not reflect the true segregation of mtDNA in this period of development. Data from such models cannot be

extrapolated to draw conclusions on the segregation of a naturally arising heteroplasmy in the blastocyst, or on wider mechanisms of mtDNA inheritance. The BALB/OlaHsd mouse model was originally produced via the same means. The extent to which this skewed pattern of mtDNA segregation is inherited in offspring is unclear, as is the number of generations bred produced before analysis is unclear (Neupane et al., 2014), but may give rise to variation between different organ systems and embryos.

Amplification of mtDNA from single cells of the blastocyst for NGS was successful using a 5-amplicon format. Although larger amplicons are preferred to avoid nuclear encoded mitochondrial segment contamination in sequencing (Santibanez-Koref et al., 2019), PCR strategies using 2-amplicon and 3-amplicon formats were unsuccessful. This confirms the limitations of currently available technologies in amplification of mtDNA from low template blastomeres, and provides a framework for further analysis. In the process of optimisation, a total of 5 unreported mtDNA variants were identified in ear biopsies of the *tRNAala* mouse model. Two of these variants are non-synonymous variants and are located in protein-coding regions, thus it is possible these variants manifest a metabolic dysfunction at sufficiently high levels of heteroplasmy. Furthermore, it remains unclear if these new variants affect the dynamics of mitochondrial inheritance.

Following blastocyst implantation, the fetus arises from a small number of epiblast cells within the ICM. Therefore, intercellular variation across cells of the blastocyst could have wide-ranging implications for the inheritance of mtDNA. If epiblast cells stochastically inherit a lower or higher heteroplasmy level relative to other cells of the blastocyst, this may skew the inheritance of a mtDNA variant. A similar mechanism may underlie the reversion of mtDNA in PNT hESCs, where a small number of epiblasts carrying karyoplast mtDNA at a higher level of heteroplasmy may come to dominate a colony across passages.

The data above make it clear that a single cell biopsy isolated from an 8-cell embryo accurately reflects the average heteroplasmy of the subsequently developing blastocyst. This would suggest that purifying selection against pathogenic mtDNA mutations occurs at other stages (Floros et al., 2018, Wallace and Chalkia, 2013). However, not all patterns of inheritance can be explained by mechanisms in this period (Freyer et al., 2012). Analysis of the m.5024C>T mutation must be interpreted in the context of the associated pathological phenotype, which is mild and only manifests disease in advanced age (Kauppila et al., 2016). It is plausible that

a more severe metabolic dysfunction is necessary to expose dysfunctional mitochondria to mitophagy preferentially and thus purifying selection. Therefore, the m.5024C>T variant may escape elimination in this stage. A repeat of this analysis with other mouse models harbouring a severely pathogenic mtDNA mutations would clarify this question.

Efforts to inhibit mitophagy using CsA and MRT68921 were unsuccessful. No changes in the level of mitophagy were detected as measured by analysis of the matrix-mito-QC probe. Analysis of scRNAseq data (**Chapter 3**) and the effect of pBNIP3L upregulation suggests that the BNIP3/BNIP3L protein interactions are key to mitophagy in the blastocyst. Due to the mechanism of action of CsA, it is possible BNIP3/BNIP3L mediated mitophagy is able to continue. CsA inhibits mitochondrial membrane depolarisation (Osman et al., 2011), and thus may be more likely to inhibit PINK/PRKN mediated mitophagy. However this relies on the assumption that there is little to no cross-talk between mitophagy pathways, the extent of which is unclear (Zimmermann and Reichert, 2017). Successful inhibition of mitophagy/autophagy by CsA and MRT68921 is evidenced in a limited range of tissues *in vitro* and not in the context of physiological autophagy, with most evidence relying on the induction of autophagy via other pharmaceutical agents (Rodriguez-Enriquez et al., 2009, Petherick et al., 2015, Wei et al., 2015, Liu et al., 2020). Furthermore, in my analysis the action of these compounds on embryos could not be verified beyond evident toxicity at higher concentrations. These factors more likely explain the lack of mitophagy inhibition apparent in analysis of the matrix-mito-QC signal. Inhibition of mitophagy will be a useful tool in characterisation of embryonic mitophagy, but will likely have to rely on targeted methods of inhibition such as genome editing technologies.

In conclusion, intercellular variation of heteroplasmy increases between the 8-cell and blastocyst stage. The segregation of mtDNA heteroplasmy in epiblast cells may influence inheritance of mtDNA heteroplasmy. Furthermore, it is appareant that the 8-cell embryo is the optimal phase of development for PGD biopsy to predict average blastocyst heteroplasmt, but it is not clear if the 8-cell biopsy reflects heteroplasmy of the epiblast. Mitophagy had no detectable influence of the segregation or inheritance of heteroplasmy in this period, as upregulation of mitophagy did not influence intercellular variation, and no selection against a mutation was apparent in the same period. However, methods of inhibiting mitophagy are required to properly characterise its impact in the preimplantation embryo, and more severely pathogenic mutations may behave differently. More thorough analysis also requires a larger sample size. Analysis of scRNAseq from human PNT embryos, despite significant drawbacks,

suggests heteroplasmy generated through karyoplast linked transfer of cytoplasm does not replicate the dynamics of naturally occurring heteroplasmies, and analysis of similar models should be interpreted cautiously.

5.6. Future work

Differing inheritance patterns of different mitochondrial mutations has been noted (Otten et al., 2018), likely dependant on their variable pathogenicity and the specifics of related biochemical dysfunction. The *tRNAala* mouse represents progress in the establishment of mice stably transmitting a single pathogenic mutation, but analysis must be considered with consideration to the mild phenotype of the mutation. As such a repetition of some of the analysis above with a variant causing a more severely pathogenic phenotype has value. Most likely this would utilise a model derived from the mtDNA mutator mouse (Trifunovic et al., 2004), assuming such a model can be maintained without elimination of mtDNA variants. In the absence of a mouse line stably transmitting such a variant, mouse models shown to rapidly eliminate a mutation could be used, as few generations of mice would be required to harvest embryos. A model carrying a severe ND6 mutation serves as an example (Fan et al., 2008).

The mtDNA mutator mouse itself rapidly generated mtDNA mutations due to a polymerase mutation , and eliminates those in protein-encoding regions across a few generations (Stewart et al., 2008a). By sequencing the mtDNA of these mice in embryonic tissues, I could explore whether the profile of these variants changes during preimplantation development, including at the time when mitophagy occurs. By backcrossing the mtDNA mutator mouse with mice carrying wildtype nuclear genomes (Yang et al., 2020), the mutations carried could be embedded in somatic tissues without rapid accumulation of *de novo* variants.

Analysis of blastocyst intercellular variation in the context of heteroplasmies induced through transfer of cytoplasm can be expanded on through analysis of mouse PNT samples, allowing use of more reliable sequencing formats. In testing strategies to prevent carryover, PNT blastocysts will be produced with large karooplasts. Blastocysts will be disaggregated to cells or cell clumps and heteroplasmy measured via NGS. The variation across these tissues can then be compared to variation in tissues of the *tRNAala* mouse. The same protocols could be applied in human tissue as well.

Downregulation of mitophagy will be an important tool for assessing the impact of mitophagy on heteroplasmy, but also elucidating mechanisms of mitophagy. Genome editing technologies such as CAS9 or CAS13 could be utilised to target a specific gene in a mitophagy

pathway, or several. The application of these methods in preimplantation embryos has already been demonstrated (Fogarty et al., 2017). If a method of inhibiting or preventing mitophagy can be established without lethality to the embryo, this would more clearly identify the mechanism by which mitophagy is activated, and would allow analysis of intercellular variation in the context of reduced or absent mitophagy, better characterising its impact.

Analysis of why intercellular variation increased at the morula stage could be explored though similar methods to those employed to explore in the inheritance of mitochondria in Hela cells (Moore et al., 2021); super resolution time laps live cell imaging. However, access to necessary technology would be a hindrance. First, establishing whether actin filaments act to translocate mitochondria in blastomeres would be necessary. Inhibitors could then be utilised to explore its effect on intercellular variation.

Whilst evidence indicates that scRNAseq analysis of heteroplasmy has limitations, I did not directly compare different methodologies in the same samples. It is also possible that total RNAseq will improve analysis. If this proved true, analysis of scRNAseq data could also be used to directly identify the epiblast cells of the blastocyst on the basis of lineage specific gene expression (Chapter 4). Epiblast heteroplasmy could then be compared to that of other cells or clumps/biopsies, improving analysis of the predictive value of different PGD protocols. Additionally, heteroplasmy could be measured at a range of positions, rather than at one position as is the case in pyrosequencing. Alternatively, genes expressed specifically in the epiblast (NANOG, OCT4, FGF4) could be visualised by co-expression of a fluorescent protein (Yang et al., 2013), allowing identification of epiblast cells at the stage of cell isolation. Heteroplasmy of those cells could then be compared to others of the blastocyst.

6. Effect on oocyte ageing on the accumulation of mitochondrial DNA variants and inheritance of somatic pathogenic variants

6.1. Introduction

Ageing has a profound impact on the success rate of female mammalian reproduction. In humans, as well as a decrease in female fertility, an increase in miscarriages and neonatal chromosomal abnormalities in widely reported (Herbert et al., 2015), and a reduction in the capacity of zygotes to form blastocysts (Ubaldi et al., 2017). This occurs in large part due to a decline in the ability of oocytes to faithfully segregate chromosomes in preparation for fertilisation resulting in aneuploidy – the presence of an abnormal number of chromosomes (Pellestor et al., 2003). While this is associated with a deterioration of chromosome architecture (Herbert et al., 2015), the underlying causes are unclear.

In the oocytes of older women, changes to mitochondrial morphology have been reported (Müller-Höcker et al., 1996) and membrane potential is reported to change progressively (Wilding et al., 2001), consistent with impaired mitochondrial function. Similarly, in mice, aged oocytes have been shown to be deficient in energy metabolism, have a lower membrane potential, and develop to blastocyst at a lower rate compared to controls (Thouas et al., 2005). A reduction in stored Ca^{2+}, and a dysregulation of Ca^{2+} signalling and the oscillation of intracellular Ca^{2+} fluctuations has been reported.

In somatic cells the accumulation of mitochondrial (mtDNA) variants is implicated in age-related defects (Larsson, 2010). Oocytes are subject to a long quiescent period beginning in fetal development and lasting until ovulation, and thus are amongst the oldest cells in the body (Pan and Li, 2019), providing a long time period for mtDNA variants to accumulate. It has been shown in aged human oocytes that mitochondrial morphology and membrane potential are altered (Müller-Höcker et al., 1996, Wilding et al., 2001). In mice, deficiencies in energy metabolism and a reduced rate of blastocyst development are reported (Thouas et al., 2005), and changes to Ca^{2+} metabolism have also been reported (Haverfield et al., 2016, Szpila et al., 2019). Given the central role of mitochondria in energy metabolism and Ca^2+ signalling, as well as ROS management and proteostasis, it is conceivable that impaired mitochondrial function, potentially arising from accumulating mtDNA mutations, may contribute to age-related defects in oocytes (Cimadomo et al., 2018).

It has been shown that in children born to older mothers harbour an increased number of acquired mtDNA variants (Rebolledo-Jaramillo et al., 2014), and later that aged women undergoing IVF harbour a higher number of variants in their oocytes (Yang et al., 2020). Conducting further studies in mice has a number of advantages; it allows the analysis of a relatively larger number of oocytes from mice in a narrow age range, and means oocytes undergoing analysis are not discarded from a clinical IVF setting, where an early reproductive issue would already be guaranteed. Importantly, the phenotype of aged oocytes resembles that of human (Herbert et al., 2015). A recent study in mice has found an accumulation of mtDNA variants in oocytes of aged mice (Arbeithuber et al., 2020), but the impact of this has not been explored in the context of the inheritance of a pre-established pathogenic variant.

If acquired oocyte mtDNA variants contribute to progressive decline of oocyte health in ageing, so too may a pre-existing germline variant. If declining health of an oocyte manifests as premature cell death, the presence of a pre-established mutation may accelerate the process, manifesting a level of selection against the inheritance of dysfunctional mtDNA variants, and further suggesting a role for oocyte mitochondrial dysfunction in age-related impairment of reproduction. If this were true, oocytes with the highest heteroplasy of the pre-existing mutation would be eliminated first. Selection against high levels of m.3243A>G has been demonstrated in human oocytes from women of unclear age (Otten et al., 2018). Furthermore, such a mechanism has been demonstrated in mouse models of ageing; in mice carrying a 4,696 bp mtDNA deletion (Sato et al., 2007), and in heteroplasmic mice carrying a mix of two wildtype mtDNA genomes generated by cytoplast transfer (Latorre-Pellicer et al., 2019), but without concurrent measurements of acquired mtDNA variants. The *tRNAalanine* (*tRNAala*) mouse (Kauppila et al., 2016), carrying a pathogenic mutation in its mtDNA (m.5024C>T), provides the opportunity to explore this paradigm. It has already been demonstrated that this mouse exhibits selection against the m.5024C>T when heteroplasmy surpasses 80% (Kauppila et al., 2016)

To elucidate the incidence of mtDNA variant acquisition in ageing *tRNAala* mouse oocytes, I sequenced the mtDNA of oocytes harvested from m.5024C>T heteroplasmy-matched young and aged *tRNAala* mice. In addition, I measured the distribution of m.5024C>T heteroplasmy in oocyte*s* of these two age groups to determine whether oocytes carrying higher mutation load are eliminated during ageing.

6.2. Aims and hypotheses

Somatic ageing has been suggested to feature an accumulation of mtDNA variants. If the same occurs in oocytes this may compromise oocyte viability. I hypothesise that the oocytes from aged females will harbour increased mtDNA variation. In addition, I hypothesise that aging alters the distribution of heteroplasmic variation the oocytes mice.

To address these hypotheses:

1. I determined the frequency and nature of acquired mtDNA variants in oocytes of younger and aged *tRNAala* mice mice using next generation sequencing (NGS) of mtDNA.

2. I compared m.5024C>T heteroplasmy distribution across oocytes of young and aged *tRNAala* mice.

6.3. Results

6.3.1. Study groups, oocyte harvests and PCR amplification of mtDNA

I analysed oocytes from the *tRNAala* mouse strain to determine whether they accumulate new mtDNA sequence variants during ageing, and to determine whether selection against oocytes with higher levels of m.5024C>T heteroplasmy is associated with ageing.

Fully-grown germinal vesicle (GV) stage oocytes (n=86) were harvested from the ovaries of *tRNAala females. mtDNA of individual oocytes was sequenced by NGS* (Table 5.3.1). This included oocytes from females aged around 16 months (range = 4 weeks, n = 58 oocytes from 7 mice) and oocytes from females approximately 2 months old (range = 2 weeks, n = 36 oocytes from 3 mice). I amplified sample mtDNA via PCR of two overlapping mtDNA fragments and sequenced their mtDNA genome. In addition, I amplified mtDNA of ear biopsies sampled from 7 mice at 3 weeks of age and measured m.5024C>T via both NGS and pyrosequencing to compare both methods. I collected a further ear biopsy from a subset of these mice (n=4) mice at culling, and compared m.5024C>T heteroplasmy, allowing comparison of biopsied collected at ~3 weeks (pyrosequencing) and ~16 months (NGS) analysed by different methods. Mice in young and aged *tRNAala* groups were matched for m.5024C>T heteroplasmy as measured by pyrosequencing of ear tissue at three weeks of age. No sample showed evidence of large-scale deletions (i.e. evidence of shorter amplicons when visualising long-range PCR products by agarose gel electrophoresis).

	Young *tRNAala*	**Aged** *tRNAala*
n	3	7
Age (weeks, with SD)	11.57 (0.53)	71.96 (1.31)
Three week heteroplasmy (ear biopsy,%, with SD)	63.66 (0.03)	61.29 (0.03)
Average oocyte yield (n, SD)	24.00 (3.59)	6.29 (3.65)
Total oocytes analysed	36	50
Number of oocytes passing quality control	35	47

Table 6.2 Characteristics of *tRNAala* mice undergoing NGS.

Not all oocytes collected underwent NGS due to time limitations. SD; standard deviation.

6.3.2. Acquired mtDNA variants in young and aged mice

Four oocyte samples failed quality control analysis; one young and three aged oocytes. Known mtDNA variants of the mouse model were disregarded from further analysis (Chapter 5). Between both groups, a total of 991 variants were detected above 1% heteroplasmy (Figure 6.1.B). Any variants appearing 3 or more times across littermates were excluded from analysis to exclude any variants which may have been inherited (372 variants across 61 positions), leaving a total of 626 variants across both groups.
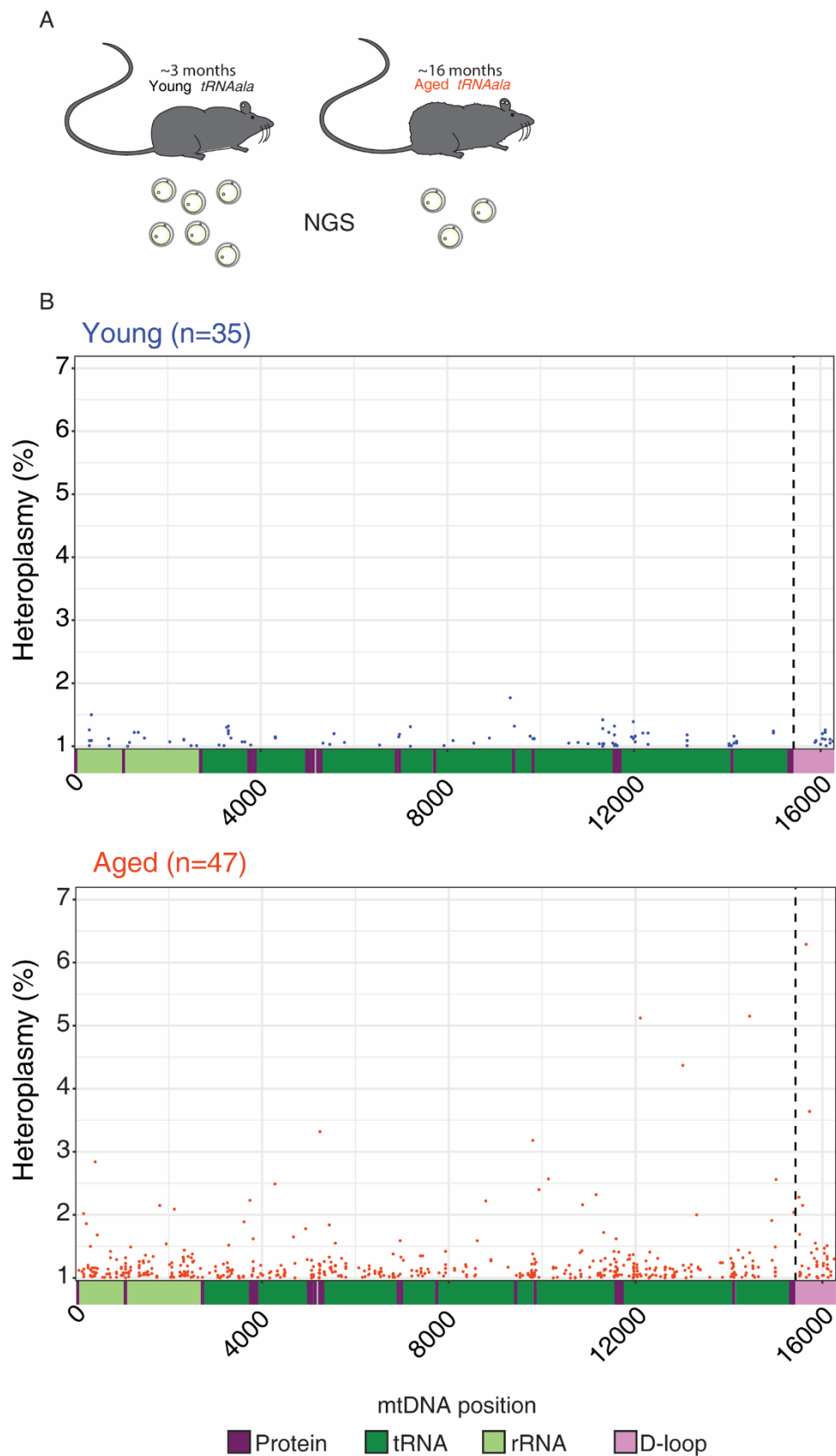
Figures 6.1. Variants analysed in *tRNAala* oocytes.

(A) Summary of experimental design. (B) All variants detected in young and aged *tRNAala* oocytes. X-axis represents the mtDNA genome sequence and its regions; purple = protein-coding, dark green = tRNA, light green = rRNA, pink = d-loop. Dots represent a variant at that position. Dashed line represents beginning of the D-loop.

For calculation of mtDNA mutation frequency, heteroplasmic positions were considered acquired variants at two thresholds (Figure 6.2.A); variants between 1% and 98%, and between 2% and 98% heteroplasmy, which has been used elsewhere to prevent analysis of false positives (Boucret et al., 2017). Known heteroplasmic positions of the model (Chapter 4) were disregarded from analysis.

Aged *tRNAala* mice showed a 3.8-fold increase in mean mutation rate compared to young mice using the >1%/<98% threshold (young=$0.00018\pm8.35\times10^{-5}$ versus aged= 0.00068 ± 0.00018, Wilcoxon rank sum test, P<0.001). The difference, although measurable across a smaller number of variants (n=22), remained statistically significant when applying the more stringent threshold (young=0 versus aged=$3.13\times10^{-5}\pm1.71\times10^{-5}$, Wilcoxon rank sum test, P<0.001). Of 47 aged oocytes analysed at the more stringent threshold (excluding one outlier), 11 carried a variant between 2% and 98% heteroplasmy, whereas no variants were detected above 2% in young oocytes. Three variants in the aged oocytes surpassed 5% heteroplasmy. These findings suggest that the mouse oocyte acquires mtDNA variants during ageing. For comparison, a specific subset (n=4) of the aged mice had corresponding ear tissue collected at the time of culling. NGS of extracted mtDNA showed no evidence of the heteroplasmies identified in the oocytes (data not shown). This suggests that the variants in the oocytes are truly acquired variants. However, it is possible that the variants may be present at undetectable levels in homogenate ear tissue. Furthermore, variation of mtDNA heteroplasmy levels has been reported across tissues (Samuels et al., 2013).

I next profiled the acquired variants within the 1% and 98% heteroplasmy threshold. I first stratified heteroplasmic mutational burden (>1% and <99%) by mtDNA locus type, grouping mutation counts into protein coding regions (combining OXPHOS subunit genes), tRNA (combining all tRNA genes), rRNA (combining 16s and 12s rRNA) and D-loop (m.15423 to m.16.300) (Figure 6.2B). A comparison of each region revealed significantly higher mutational burdens in the protein coding (young=$0.00016\pm7.58\times10^{-5}$ versus aged=$0.00055\pm1.54\times10^{-4}$, Wilcoxon rank sum test, P<0.01) and rRNA (young=$0.00026\pm1.28\times10^{-4}$ versus aged=$0.00094\pm2.44\times10^{-4}$, Wilcoxon rank sum test, P<0.05) regions of aged mice when compared to young mice. Mutation rate also increased in other regions but not significantly. In young oocytes mutation rate was similarly low in all regions.

A total of 100 mutations were detected in young oocytes across 71 positions (86 of these mutations occurred across only three oocytes). Of these, 57 were in protein encoding regions

(39 positions), of which 49 were non-synonymous (49.00% of total mutations) In contrast, a total of 526 mutations were detected in aged oocytes across a total of 314 positions. Of these 300 (187 positions) were in protein coding regions, of which 260 were non-synonymous (49.43% of total mutations).
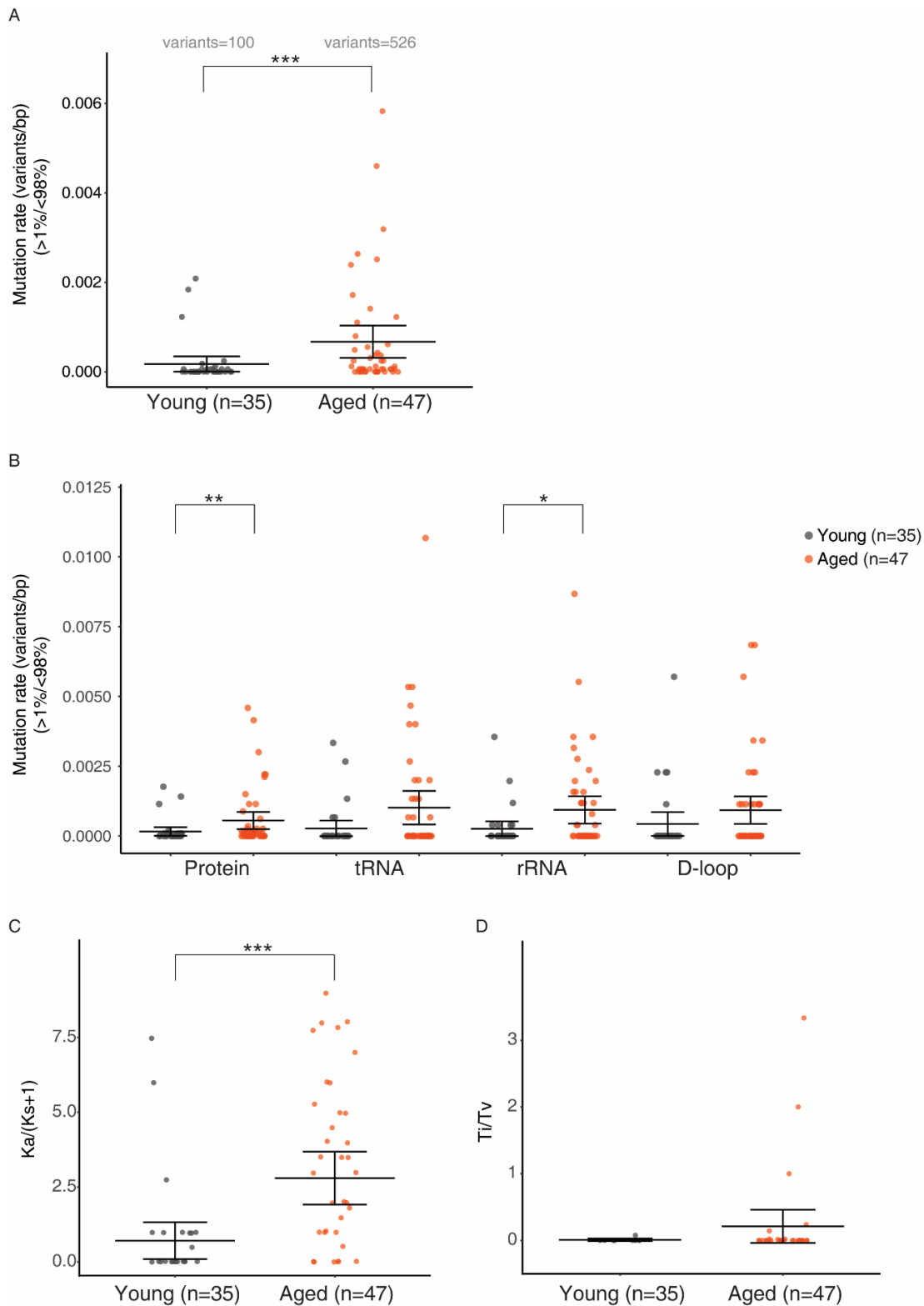
Figure 6.2. Variant acquisition rate and profile of variants.

(A) mtDNA mutation rate of variants between 1% and 98% in young and aged oocytes. Known heteroplasmic positions of the model were disregarded from calculation. (B) Mutation rate with variants designated as heteroplasmies above 1% and below 98% across different mtDNA regions; D-loop (877 bp), tRNA (1,499 bp), rRNA (2,536 bp) and protein-coding (11,331 bp). (C) Ka/Ks ratio for variants in protein coding regions of young and aged mice. Dots correspond to individual oocytes. (D) Ti/Tv ratio for variants in protein coding regions of young and aged mice. Dots correspond to individual oocytes. Central bars represent means, outer bars confidence intervals. Statistical significance was measured via Mann-Whitney test. *=P$\leq$0.05, ***=P$\leq$0.001.

I subsequently calculated the Ka/Ks ratio for young and aged groups. The Ka/Ks ratio measures the ratio nonsynonymous substitutions per nonsynonymous site (*Ka*) synonymous substitutions per synonymous site (*Ks*) (Hurst, 2002), and is a commonly used assessment of mutational neutrality and purifying selection. It has been adapted for use in mitochondrial genetics previously (Mishmar et al., 2003), with a constant of 1 added to Ks to avoid dividing by 0. Mean Ka/Ks ratio was significantly higher in aged oocytes compared to young oocytes (young=0.72$\pm$0.30 versus aged=3.77$\pm$0.58, t-test, P<0.001, Figure 6.2.C). This suggest that variants acquired in oocyte ageing are not influenced by purifying selection, as nonsynonymous variants appear at a higher rate than do synonomous.

Variants in the first or second codon positions are more likely to result in an amino acid change, and previous work has shown codon mutational bias in mouse models of mtDNA disease (Stewart et al., 2008b). Codon bias was also similar between the young and aged groups (1:1.82:0.73 and 1:1.05:0.73 respectively), with a reduced number of mutations in the third position. Next, to further investigate the prevalence of transversion as opposed to transition variants I calculated the transition/transversion (Ti/Tv) ratio (Belle et al., 2005) for young and aged groups (Figure 6.2.D). Although the ratio was not significantly different between the young and aged oocytes (0.009 and 0.211 respectively), analysis was hampered by the scarcity of variants in young oocytes. Nonetheless, both groups appeared prone to develop transversion mutations.

6.3.3. Factors in the development of acquired variants

It is clear that the acquisition of mtDNA variants is not a feature of every oocyte with large variation of mutation rate across aged *tRNAala* oocytes (aged oocyte mutation rate coefficient of variation=1.57x10^{-6}), raising the question of why some oocytes acquire variants but not others. To explore whether the acquisition of mtDNA variants (>1%/<98% heteroplasmy) could be linked to a low level background dysfunction of mitochondria, I correlated mutation rate with m.5024C>T heteroplasmy of an oocyte (Figure 6.3.A), but no significant correlation was detected. To further characterise this relationship I stratified oocytes by their m.5024C>T heteroplasmy into groups above and below 65% heteroplasmy (Figure 6.3.B), the threshold at which defects in mitochondrial biology have been reported (Kauppila et al., 2016). Despite a trend towards higher mutation rate in the higher m.5024C>T heteroplasmy group, mutation

rate was not significantly higher amongst oocytes harbouring higher m.5024C>T heteroplasmy. A larger sample size may allow more convincing exploration of this relationship. Measuring copy number oocytes concurrently to mtDNA heteroplasmy would allow the exploration of the relationship between mtDNA copy number and heteroplasmy. It is plausible that the reduced mtDNA copy number reported in mouse oocyte ageing (Pasquariello et al., 2019) could play a role in the emergence of mtDNA mutations at higher heteroplasmy I report.

To explore whether a higher mutation rate could be linked to maternal factors, I analysed the spread of oocyte mutation rate in the oocytes of specific females (Figure 6.3.C). Although analysis is impeded by variable sample sizes between mice, it is apparent that some mice produced oocytes with a higher acquired variant frequency. To further investigate this I correlated the maternal m.5024C>T heteroplasmy in ear biopsies to the mutation rate in the oocytes of the same mouse (Figure 6.3.D), but no significant correlation was detected. Whilst no trends emerge between maternal factors and an oocytes acquisition of mtDNA variants emerge in the above analysis, it would be interesting to determine if other characteristics of aged mice could influence oocyte mutation rate.
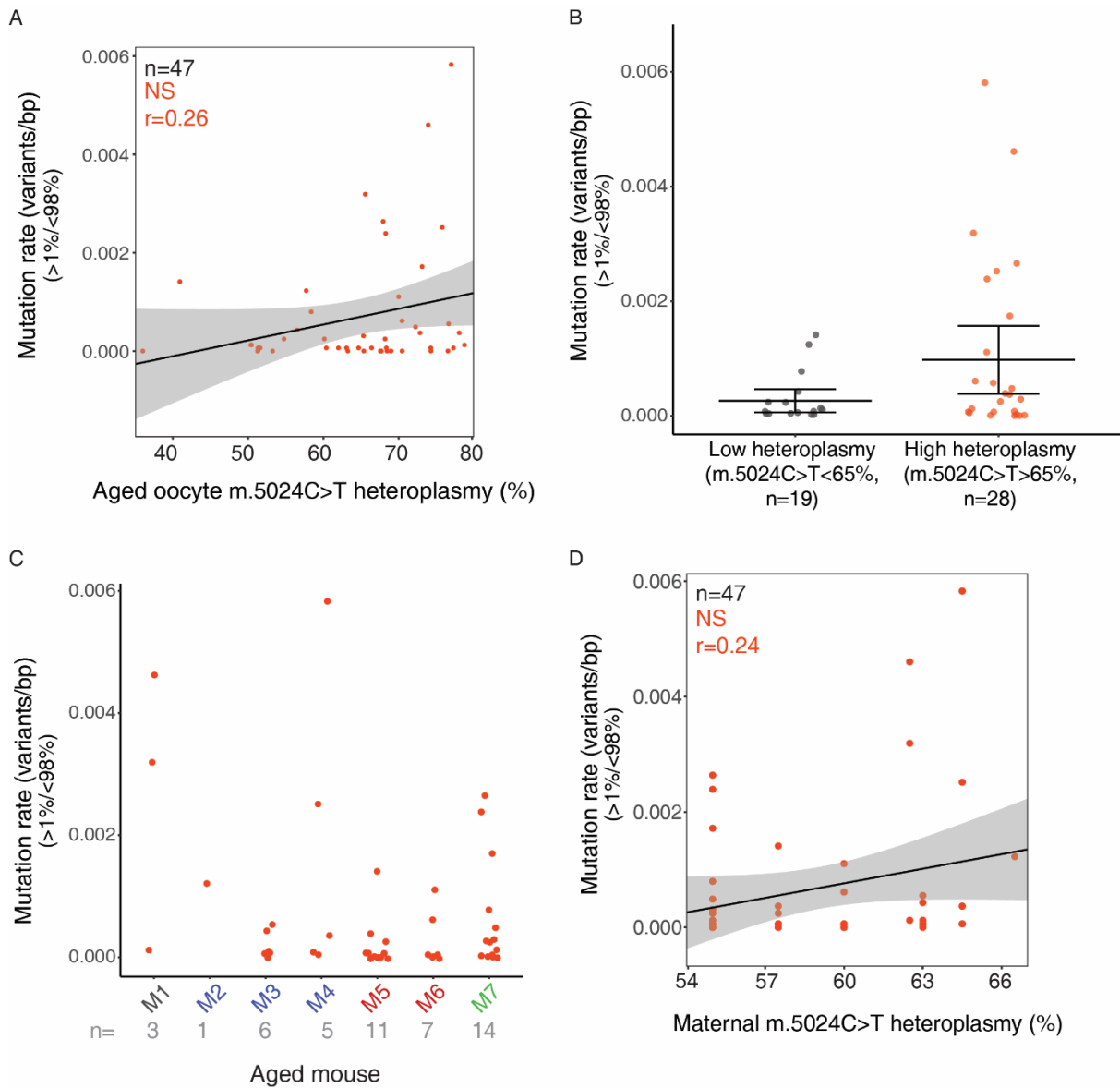
Figure 6.3. Factors influencing the variant acquisition rate (>1%/<98%) in aged *tRNAala* mice.

(A) Pearson correlation between variant rate and m.5024C>T heteroplasmy in oocytes of aged *tRNAala* mice. Grey area represents confidence interval. (B) Distribution of variant rate between aged mouse oocytes carrying <65% (low) and >65% (high) m.5024C>T heteroplasmy. Central bar represents mean, outer bars confidence intervals. (C) Distribution of variant rate in individual oocytes of each aged *tRNAala* mouse. Colour of x-axis label denotes litter mates. (D) Pearson correlation between variant rate in individual oocytes and maternal m.5024C>T heteroplasmy of aged *tRNAala* mice. Grey area represents confidence interval.

6.3.4. Distribution of m.5024C>T heteroplasmy in young and aged *tRNAala mice*

Having confirmed the acquisition of mtDNA variants in aged oocytes of the *tRNAala* mouse, I explored the possibility that underlying dysfunction of m.5024C>T heteroplasmy could act in conjunction with accumulating variants to impair mitochondrial functions, promoting selection against those oocytes. To do so I measured the distribution of oocyte m.5024C>T heteroplasmy in oocytes of young and aged *tRNAala* mice. If the above were true, the spread of m.5024C>T heteroplasmy in aged oocytes would be lower than that of young oocytes. This was not the case (Figure 6.4.A), suggesting m.5024C>T heteroplasmy has no profound impact on the health of the aged oocyte, at least up to the GV stage. This may be because the m.5024C>T variant is phenotypically weak (Kauppila et al., 2016).

I also examined the correlation between the number of oocytes collected from a particular mouse, a measure of ovarian ageing, and m.5024C>T heteroplasmy of that mouse (Figure 6.4.B/C), and the average mutation rate across oocytes of that mouse (Figure 6.4.D/E). While no significant correlation emerged between oocyte yield and maternal m.5024C>T heteroplasmy in young mice, likely due to low sample size, a strong negative correlation emerged between maternal ear tissue heteroplasmy and the number of oocytes collected (r=-0.94, Pearson correlation, P<0.01). This may suggest higher levels of m.5024C>T heteroplasmy manifest an inhospitable environment in the ovaries of aged mice, promoting ovarian ageing and presenting a barrier to oocyte survival in ageing. No significant correlation emerged between maternal heteroplasmy and average oocyte mutation rate.
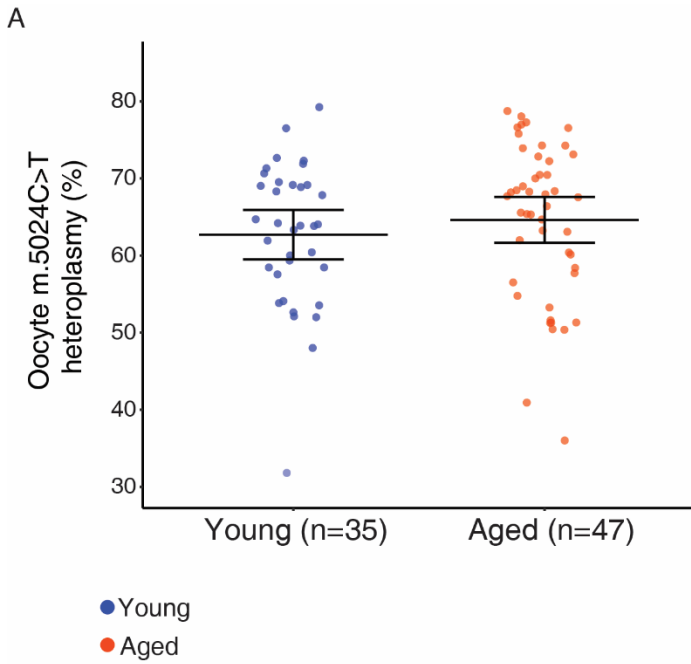
Figure 6.4. Relationship between m.5024C>T heteroplasmy and oocyte survival.

(A) Distribution of m.5024C>T heteroplasmy in oocytes of young and aged tRNAala mice. Central bar represents mean, outer bars confidence intervals. (B) Correlation between number of oocytes collected from a young mouse and the ear tissue heteroplasmy of the same mouse. Grey area represents confidence interval. (C) As in (B) but for aged mice. (D) Correlation between number of oocytes collected from a young mouse and the average mutation rate (>1%/≤98%) across all oocytes of the same mouse. Grey area represents confidence interval. (E) As in (D) but for aged mice.
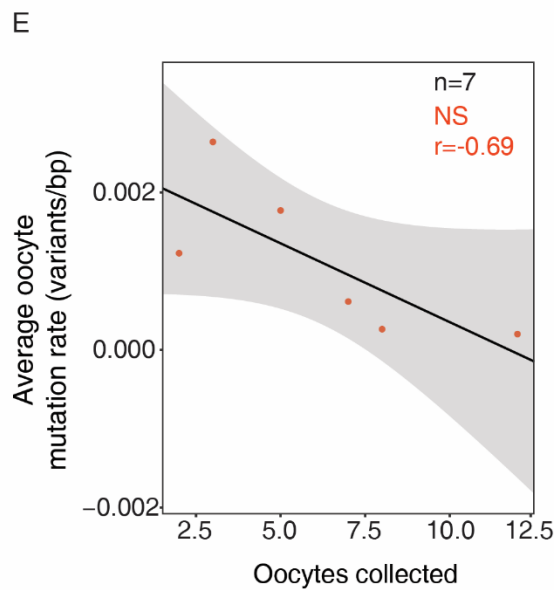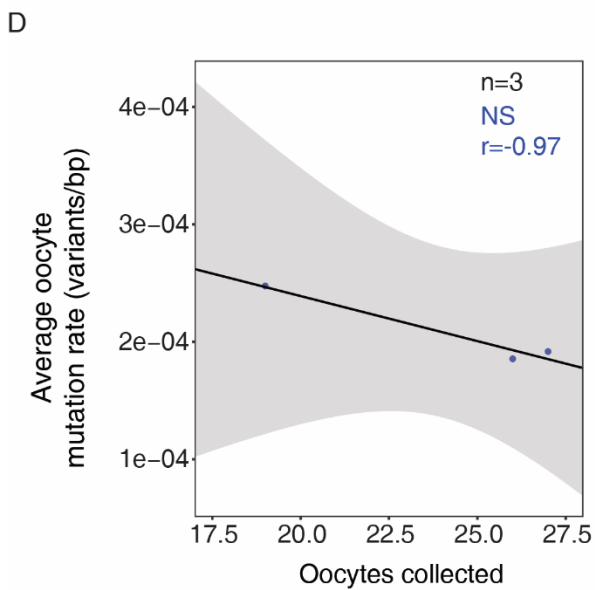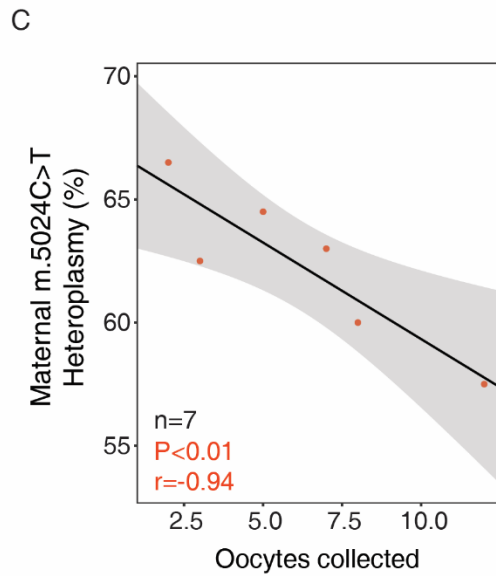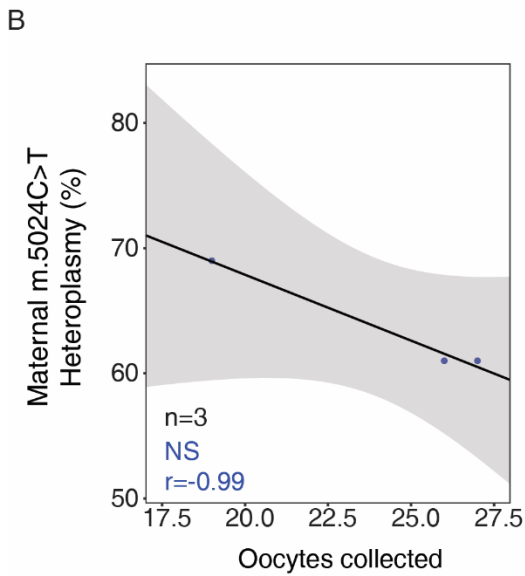
6.3.5. Impact of ageing on m.5024C>T heteroplasmy in somatic tissues

In comparing heteroplasmy measurements of the same ear biopsies measured via pyrosequencing and NGS a strong correlation emerged (2=0.98, Pearson correlation, P<0.001, Figure 6.4.A). Using a small number of ear biopsies taken from aged mice at culling, I re-analysed m.5024C>T heteroplasmy using NGS and compared this to the same measurement taken at 3 weeks of age via pyrosequencing (Figure 6.5.B). While one sample remained roughly unchanged, three others showed a decrease in heteroplasmy. Whilst it must be considered that sample size is severely restricted, this suggests an elimination of m.5024C>T heteroplasmy in ageing of somatic tissues.
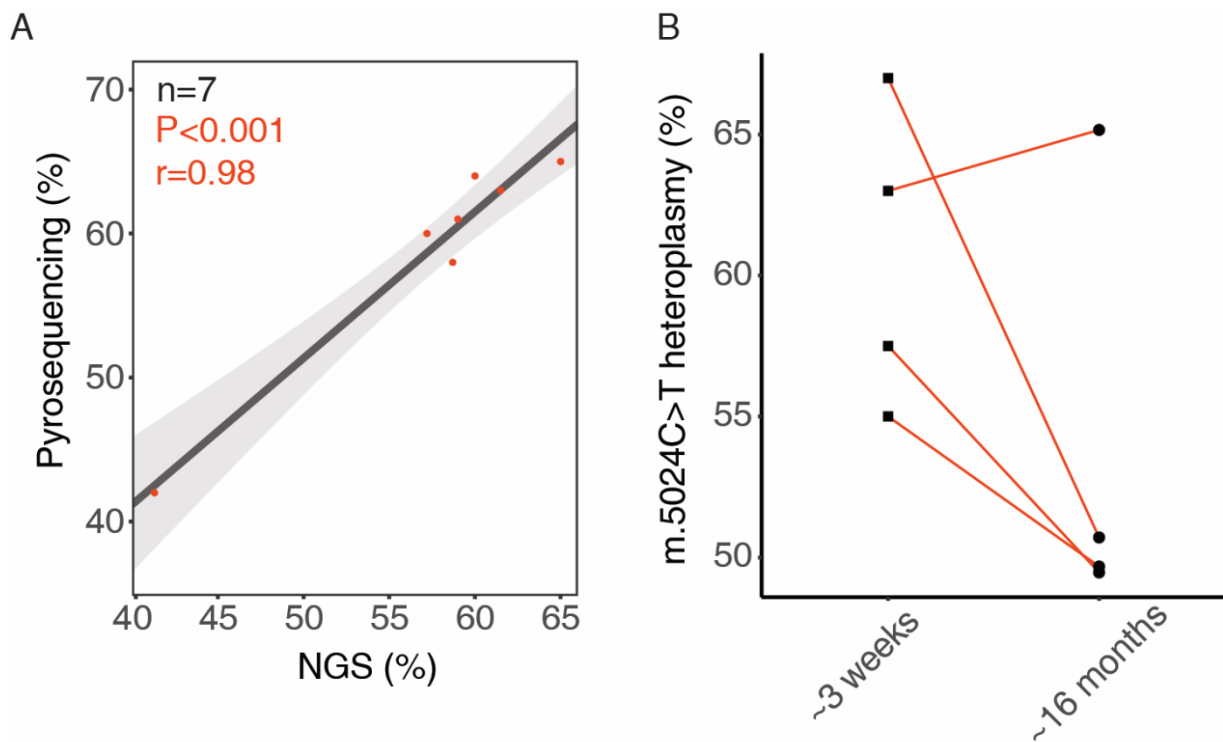
Figure 6.15. Changing somatic m.5024C>T heteroplasmy in aged *tRNAala* mice.

(A) Pearson correlation between pyrosequencing and NGS measurements in ear biopsies of 3 week old mice. Grey area represents confidence interval. (B) Change in m.5024C>T heteropasmy in ear tissue of aged *tRNAala* mice between 3 weeks of age and 16 months. Heteroplasmy at 3 weeks was measured by pyrosequencing (squares), and at 16 months by NGS (circles).

6.4. Discussion

Normal mitochondrial function is likely key to oocyte viability. Oocyte mitochondrial regulation of CA2+ signalling, ROS management and efficient energy metabolism is vital for several key processes of the oocyte; GV breakdown, and microtubule assembly and disassembly (Cimadomo et al., 2018). In the older women, changes to mitochondrial morphology have been reported (Müller-Höcker et al., 1996) and membrane potential is reported to change progressively (Wilding et al., 2001), consistent with impaired mitochondrial function. Similarly, in mice, aged oocytes have been shown to be deficient in energy metabolism, have a lower membrane potential, and develop to blastocyst at a lower rate compared to controls (Thouas et al., 2005). A reduction in stored Ca^{2+}, and a dysregulation of Ca^{2+} signalling and the oscillation of intracellular Ca^{2+} fluctuations have also been reported (Haverfield et al., 2016, Szpila et al., 2019). These impairments in mitochondrial function could be explained by the presence of mtDNA variants.

Here I show that the *tRNAala* mouse model accumulates mtDNA variants in the oocyte in the process of ageing. Oocytes undergo a long period of quiescence beginning in the fetus and ending with ovulation on a particular oocyte (Pan and Li, 2019), giving oocytes of aged mice a prolonged period to acquire mtDNA variants. While variants in younger oocytes never exceeded 2% heteroplasmy, 23 oocytes in aged oocytes did with 3 exceeding 5%, suggesting the capacity for expansion of variants during quiescence. Metrics including codon bias and Ka/Ks ratio suggest these variants could have an effect on mitochondrial function due to elevated numbers of non-synonomous mutations, assuming heteroplasmy surpasses a sufficient threshold. Furthermore, elevated mutation rate was most severe in protein encoding regions, suggesting no purifying mechanism act against these low-level heteroplasmies in more potentially severe variant positions.

The Ts/Tv ratio of oocytes I analysed suggested a bias towards the accumulation of transversion mutations. Most previous reports suggest the age-related accumulation of mtDNA variants in somatic tissues is attributable to mtDNA polymerase γ (POLG) errors during mtDNA replication (Larsson, 2010), though it is unclear to what extent this also occurs in mice (Greaves et al., 2011). POLG errors show a bias for accumulation of transition variants in ageing somatic tissues (Zheng et al., 2006, Ameur et al., 2011, Kauppila et al., 2018). My analysis of the Ti/Tv ratio was severely hampered by the lack of variants detected, but suggests other causes for the accumulation of mtDNA variants during oocyte quiescence.

173

Evidence from zebra fish models suggests that oogenesis is accompanied by increase in mtDNA copy number preceding the oocyte extended arrest (Otten et al., 2016), which would provide the opportunity for POLG errors to introduce variants. Assuming this mechanism is conserved in mammals; given that both aged and young mice of my study underwent oogenesis in early development, it is unlikely this process could generate a different quantity of mtDNA variants in oocytes of the two groups. However, it remains possible that mtDNA quality control mechanisms are impaired in ageing, leading to introduction of mtDNA variants or the expansion of variants introduced during oogenesis. Indeed, unlike aged oocytes, oocytes of young mice showed a slight tendency toward synonomous variants, perhaps suggesting that mechanisms act to remove non-synonomous variants, but become less effective in oocyte ageing. The generation of ROS over this extended arrest could also be a cause of mtDNA variants.

My analysis broadly supports a recent study using CD1 mice where mice at 10 months of age accumulated a higher level oocyte mtDNA variants relative to mice of 1 month (Arbeithuber et al., 2020). In comparison to my analysis a number of other discrepancies arise. The oocytes of Arbeithuber *et al* (2020) display a lower incidence of mtDNA variant acquisition in aged oocytes and higher rate in young oocytes. Furthermore, the aged oocytes of Arbeithuber *et al* (2020) show an increase in mutation rate across all regions of mtDNA when measured individually. The incidence of variant acquisition in the young mice of Arbeithuber *et al* (2020) was elevated in the D-loop relative to other regions, which was not evident in my analysis. Arbeithuber *et al* (2020) reported a similar Ka/Ks ratio between young and aged oocytes (1.69 and 1.32 respectively). Whereas my analysis featured predominantly transversion mutations, oocytes of Arbeithuber *et al* (2020) accumulated transition mutations, more in keeping with POLG errors as a source of mtDNA variants. These discrepancies likely reflect the different sequencing strategy employed by Arbeithuber *et al* (2020) which allows mutations below my 1% threshold to be reported, differences in processing of NGS data, or strain differences. Given that ear tissue in my sequencing showed no variants, it is unlikely the variants I report constitute noise, and that these mutations were acquired within the oocyte. However, given the larger number of cells and tissue types within ear clips, it is possible variants are masked in those samples. Differences may also arise because the aged mice of Arbeithuber *et al* (2020) are younger in comparison to the corresponding group I used, and had been used in breeding to produce litters for the same study (mice I analysed were not used in breeding at any point). Furthermore, mice I analysed are of a different strain, and carry a pathogenic mutation which may influence oocyte metabolism in unidentified ways.

My data also corroborates a report in human oocytes where mtDNA variants accumulated at low levels of heteroplasmy (Yang et al., 2020). Whereas I found a modest increase in mtDNA variants above 2% heteroplasmy in aged oocytes based on a small number of variants, other work has evidenced no increase in variants above 2% heteroplasmy in oocytes in human women at 36 year of age (Boucret et al., 2017). This discrepancy could be due to differences in technical approach, or because aged human oocytes were defined as such based on hormone measurements, and as such chronological age and thus length of oocyte arrest was similar to controls. Similarly, no increase in variants above 2% heteroplasmy variants was reported in a bovine model (Hammond et al., 2016), possibly because of limited sample numbers or more modest chronological age of the aged bovine oocytes.

In contrast to other studies, I did not detect an increase in the prevalence of large scale deletions. Hammond *et al* reported this phenomenon in bovine oocytes from aged females, but relied on a cloned model which featured coexistence of two mtDNA genomes, raising questions of its generalisability (Hammond et al., 2016). Meanwhile, a study of human oocytes encompassed only women presenting with infertility and thus undergoing IVF, and focused on a known common deletion, which was only marginally different between young and aged groups (Keefe et al., 1995).

The extent to which my analysis of variant acquisition can be extrapolated to wildtype mouse models and humans is questionable given the presence of a pathogenic germline mutation in the mouse model, as well as other mtDNA variants (Chapter 5), despite the fact that no relationship between the weakly pathogenic m.5024C>T variant and number of acquired variants was apparent. It is plausible the dysfunction arising from the m.5024C>T variant gives rise to increased ROS prompting more DNA damage (Hahn and Zuryn, 2019).

Consistent with age-related depletion of the ovarian pool of oocytes (Amanvermez and Tosun, 2016), I obtained fewer oocytes from aged females compared to young. I detected no evidence of the elimination of aged oocytes carrying elevated m.5024C>T heteroplasmy alongside an accumulation of mtDNA variants. Therefore, my analysis indicates no evidence of impaired oocyte survival in aged *tRNAala mouse* oocytes attributable to mtDNA variants. It has previously been shown that an inherited 4,696 bp deletion in mouse mtDNA, generated via electro-fusion of embryos, lead to a lower spread of heteroplasmy across the oocytes of aged mice, which was not a feature of somatic tissues. This suggested that a selection mechanism exists in oocyte development to eliminate oocytes with more severe mtDNA variants (Sato et

al., 2007). It has also been evidenced that mice with heteroplasmic mtDNA arising from a mix of two wild-type mtDNA genomes appear to undergo accelerated loss of oocytes with higher heteroplasmy (Latorre-Pellicer et al., 2019). It remains possible that, instead of undergoing premature cell death, oocytes harbouring a higher level of mtDNA variant heteroplasmy are those which undergo ovulation earlier thus are unavailable for analysis in aged animals. Alternatively, selection against pathogenic variants may occur within the oocyte itself at a molecular level. The weak phenotype of the pathogenic m.5024C>T variant and relatively few number of pre-existing mtDNA variants in the mouse model (Chapter 5) likely explain why no such mechanisms are apparent in my analysis.

Using the mtDNA mutator mouse, which rapidly acquires mtDNA variants and provides a model of premature ageing (Trifunovic et al., 2004), it was shown that the number of oocyte ovarian follicles in the ovary is reduced in the presence of higher levels of mtDNA variants throughout mouse tissues, including oocytes (Yang et al., 2020). It must be noted that other tissues of this model accumulate mtDNA variants similarly to oocytes themselves, thus it is not clear to whether this reduction of follicles can be attributed to mitochondrial dysfunction in oocytes, ovaries or multiple systems. Yang *et al* (2020) also demonstrated a disruption in oocyte NADH/NAD$^+$ metabolism of oocytes harbouring high levels of mtDNA variants. It is not clear if oocytes being selected against are those with higher levels of mtDNA variants and thus metabolic dysfunction, or if fewer oocytes are produced in early development. Similar follicle counts and metabolic analyses in aged wildtype mice would allow confirmation of whether this is characteristic of genuine mouse ageing, especially as the rate of mtDNA variant acquisition in oocytes of mtDNA mutator mice is unclear and may differ from that of chronological ageing.

It appears the acquired variants I report here cannot manifest a dysfunctional phenotype strong enough to drive a selective mechanism in combination with the m.5024C>T mutation, likely due to their low heteroplasmy. However, Sato *et al* (2007) and Latorre-Pellicer *et al* (2019) each analysed ovulated oocytes, whereas I analysed GV oocytes during their arrest, so the possibility of a selective mechanism that acts during oocyte maturation. Thus it appears the acquisition of mtDNA variants is unlikely to impact oocyte survivability severely. It is unclear to what extent mitochondrial turnover is active during an oocyte's prolonged arrest, and whether mechanisms may act to constrain these acquired variants at low heteroplasmy.

The strong negative correlation I report between the m.5024C>T heteroplasmy of an aged mouse and the number of oocytes harvested suggests that instead of inducing a metabolic defect in the oocyte which acts as a barrier to oocyte survival, the m.5024C>T pathogenic mutation might influence oocyte survivability by compromising the environment of the ovary. Thus the survivability of the oocytes within would be irrespective of their own m.5024C>T heteroplasmy. It must be noted that analysis of oocyte numbers is based on a very limited number of samples, and the quantity of oocytes collected is highly operator dependant as oocytes can be missed in a collection dish. Further study would be required with more stringent quantification. It is possible that oocytes with higher mutation loads have an increased incidence of chromosome segregation errors upon resumption of meiosis., but further study is required to determine whether this is the case. Alternatively, it is possible that mitochondria can contribute to oocyte ageing and dysfunction by other means. For example, reduced mtDNA copy number has been evidenced in aged oocytes of mice (Pasquariello et al., 2019), while reduced copy number has been linked to failure to fertilise in humans (Santos et al., 2006).

Measurements of heteroplasmy by pyrosequencing and NGS of the same tissue were strongly correlated. As such, measurements of peripheral heteroplasmy at young and aged time points are comparable. The m.5024C>T variant declined with ageing in peripheral tissues of mice in 3 of 4 cases, remaining virtually the same in the final case. This would suggest selection against this variant occurs in somatic tissues, though it is not clear to what extent this can be extrapolated to other pathogenic mtDNA variants or other organisms, especially given limited sample size. A larger sample size and more expansive study of variants is required.

In conclusion, mtDNA variants accumulate in the oocytes of *tRNAala* mice at low levels of heteroplasmy. A high proportion of these variants are non-synonymous and are found in protein-encoding regions, but this is not a feature of every oocyte. The presence of the m.5024C>T variant in combination with these acquired variants did not present a barrier to the survival of aged oocytes during the prolonged arrest period, as the spread of oocyte m.5024C>T heteroplasmy remained the same in young and aged mice. Although ear tissue of a subset of mice showed none of the variants identified in oocytes, it must be acknowledged that the sample size of aged mice is small and arise from a narrow pedigree, some being direct litter mates. In no instance was a variant detected in every oocyte of a given mouse. If variants were filtered to only those occurring in a single oocyte, my conclusions remain the same, but this may exclude mutation hotspots. While further work is needed to characterise the role of

mitochondrial function in the decline of oocyte viability with age, the data presented here indicates that the acquisition of acquired mtDNA sequence variants in ageing is not a barrier to oocyte survival and growth. However, further work is required to determine whether age-related errors in chromosome segregation during the subsequent meiotic divisions are exacerbated by accumulation of mtDNA variants.

6.5. Future Work

Whilst it is apparent that the m.5024C>T mutation and its associated phenotype do not induce any level of selection in aged oocytes, it remains to be seen if more severely pathogenic substitutions do so. Further analysis would be limited be availability and suitability of mouse models, given the strong purifying selection in the inheritance of suitable models (Chapter 5.6).

The effects of an accumulation of mtDNA variants should be explored. Ideally this would be performed in chronologically aged mice of at least 10 months of age, despite the impracticality and expense of maintaining mice for extended periods. The mtDNA mutator mouse could be used as a model of ageing (Yang et al., 2020), but the extent to which this replicates all key features of ageing is unclear. The validation of metabolic NADH/NAD+ redox defects shown in mtDNA mutator mice (Yang et al., 2020) in chronologically aged mice would be an important step. Imaging protocols could also be employed to study mitochondrial membrane potential in aged oocytes(Farkas et al., 1989); mitochondrial membrane depolarisation has been linked to compromised cellular health (Zorova et al., 2018).

Defects of chromosome segregation could be analysed via live-cell imaging and chromosome spreads (Hwang et al., 2018), then oocytes sequenced and segregation defects correlated with mtDNA variant accumulation.

The impact of changes in nuclear gene expression and the acquisition of nuclear DNA (nDNA) variants could both have a profound impact on the ageing phenotype of oocytes. Changes in nuclear gene expression have been reported for an array of genes, including some relating to mitochondrial functions, in mice (Hamatani et al., 2004, Lee et al., 2019, Hou and Sun, 2020), and humans (Zhang et al., 2020). A first-step could be validating protein expression of genes of interest, which could also be analysed in relation to their localisation to mitochondria. Germline nDNA mutations have been reported to increase with age in humans (Wong et al., 2016, Rahbari et al., 2016, Jónsson et al., 2017), but based on analysis of parents and offspring. Analysis of nDNA variant acquisition in oocytes could be conducted using whole exome sequencing.

Measurements in children born to aged mothers has suggested aged-related acquired mtDNA variants can be inherited (Rebolledo-Jaramillo et al., 2014). This has not yet been explored in mice, which would allow easier examination of the phenomenon and the potential impacts of these variants *in vivo*. However, this would rely on mothers with a younger age than the mice I analyse above, and would require better profiling of when acquired mtDNA mutations arise at sufficient enough numbers to facilitate both variant accumulation and successful breeding.

My analysis suggests the m.5024C>T variant has an impact on the ovary of aged mice, with a number of caveats in mind. Using chronologically age-matched mice, hormone measurements (follicle stimulating hormone, lutenising hormone, anti-Müllerian hormone) or follicle counts could be used to asses ovarian ageing (Amanvermez and Tosun, 2016). This would then be interpreted in relation to wider m.5024C>T heteroplasmy, and may provide better insights on any impact the m.5024C>T variant has. This analysis would avoid the high dependency on an operator which compromises my analysis.

Given the occurrence of mitophagy in the preimplantation embryo (Chapter 1), it would be interesting to examine whether the accumulated mtDNA variants in the oocyte persist in the embryo. This would require successful mating of aged mice, which may pose a challenge, before sequencing of the entire mtDNA, potentially at the single cell level. Alternatively, using backcrossed mtDNA mutator mice to generate a model carrying numerous inherited somatic mtDNA variants (Yang et al., 2020), and embryos of younger mice examined.

7. Final Discussion

Mitochondrial DNA (mtDNA) is inherited exclusively through the maternal germline, and is subject to a genetic bottleneck giving rise to unpredictable heteroplasmy across the oocytes of a woman (Burr et al., 2018). The lack of curative treatments for diseases caused by pathogenic mtDNA variants and difficulty in predicting the inheritance of these diseases, has given rise to methods used to prevent the inheritance of the associated variants; preimplantation genetic diagnosis (PGD, Dean et al., 2003) and pronuclear transfer (PNT, Hyslop et al., 2016). Recent work within our lab using the mito-QC probe (Allen et al., 2013) revealed mitophagy occurring in the preimplantation embryo, beginning in the morula stage. This may have implications for the inheritance of mtDNA disease and methods to prevent transmission.

The central aim of this thesis was to characterise the previously unreported mitophagy occurring in the preimplantation embryo, identifying key genes which explain its onset and explore the wider impact or role of mitophagy. Analysis of a large single cell RNA sequencing (scRNAseq) dataset from human preimplantation embryos (Petropoulos et al., 2016) suggested that BNIP3 family genes and the associated mechanisms of mitophagy were responsible for preimplantation embryo mitophagy. Attempts to inhibit mitophagy via an inhibitor of mitochondrial membrane depolarisation and thus *PINK1/PRKN* mitophagy, cyclosporine A (CsA, Osman et al., 2011), failed, as measured by confocal imaging and quantification of the mito-QC probe signal. This further supports the argument that preimplantation embryo mitophagy is attributable to receptor-mediated mechanisms such as the BCL2 Interacting Protein 3/BNIP3-Like Protein 3 XL (*BNIP3/BNIP3L*) pathway. Upregulation of a serine 34/35 phosphorylated BNIP3L (pBNIP3L) succeeded in upregulating mitophagy. The utility of this intervention in eradicating karyoplast mitochondria in the PNT procedure is currently being tested in mice.

Analysis of the same scRNAseq dataset allowed better characterisation of other processes which could be related to wider mitochondrial metabolism, and mitophagy. At the level of relevant gene ontologies (GOs) and specific promoters of apoptosis, the expression of apoptosis genes was elevated in the blastocyst relative to the 8-cell embryo, and in the inner cell mass (ICM) relative to the trophectoderm (TE). This is largely in agreement with imaging studies from human and mouse embryos, which suggest onset of apoptosis in the blastocyst

and at a higher rate in the ICM (Hardy et al., 1989, Hardy and Handyside, 1996). Gene expression patterns of some apoptotic genes suggested a key role for those genes in apoptosis in the blastocyst, primarily PMAIP1. The above requires verification in *in vitro* cultured mouse embryos and functional studies. Mitophagy has been linked to apoptosis in some contexts (Kubli and Gustafsson, 2012, Wanderoy et al., 2021), but no correlations emerged between genes of the two processes in the day 6 and 7 blastocyst.

Expression of genes relating to the production of ATP, specifically the processes of oxidative phosphorylation (OXPHOS) and glycolysis, suggested the blastocyst is broadly more metabolically active compared to cleavage stage embryos. Similarly, biosynthetic pathways were elevated in the blastocyst stage. The mirrors the metabolic profile of the embryo has largely been characterised through metabolomics studies, but only in mouse and bovine models (Thompson et al., 1996, Houghton et al., 1996, Sturmey and Leese, 2003, Chi et al., 2020). This represents significant progress in confirming these mechanisms are conserved in the human embryo. Despite the possibility that remodelling of the mitochondria is required to facilitate a higher level of glycolysis (Montava-Garriga and Ganley, 2020), no significant correlations were apparent between mitophagy and glycolysis genes in the day 6 and 7 blastocyst.

Instead, correlations emerged between mitophagy genes (hypoxia inducible factor 1 subunit alpha, *BNIP3*, and *BNIP3L*) and the expression of genes which drive specification of blastocyst cellular lineages in days 5 and 6 of development. In the Day 5 TE, mitophagy genes negatively correlated with *GATA2/3*, which drive TE specification in the early blastocyst (Krendl et al., 2017). In the day 6 primitive endoderm (PE), mitophagy genes positively correlated with genes driving PE specification, *GATA4/6* (Cai et al., 2008, Rojas et al., 2010). In the pluripotent day 6 epiblast mitophagy genes correlated negatively with markers of pluripotency such as *FGF4* (Kang et al., 2013) and *POUF51* (Nichols et al., 1998). Mitophagy has previously been demonstrated to have a role in regulating the differentiation or maintenance of stem cells (Krendl et al., 2017, Cairns et al., 2020), but not until now in the blastocyst. This potential role of mitophagy in regulating the establishment of blastocyst lineages requires confirmation and further characterisation in *in vitro* cultured mouse and human embryos.

In addition to the role of mitophagy in regulating physiological processes of the blastocyst, I explored its role in shaping the inheritance and/or segregation of heteroplasmy through

preimplantation development using the *tRNAalanine* (*tRNAala*) mouse model (Kauppila et al., 2016), carrying a single pathogenic mtDNA variant (m.5024C>T). Purifying selection acts to reduce the heteroplasmy of some pathogenic mtDNA variants at unidentified stages of development and through unknown mechanisms, but potentially involving mitophagy (Burr et al., 2018). Therefore, using the *tRNAala* mouse I collected a single cell biopsy at the 8-cell embryo stage and cultured the same embryo to blastocyst. Comparison of heteroplasmy between the two, measured by pyrosequencing, suggested that mitophagy in the preimplantation embryo did not constitute any selection against the pathogenic m.5024C>T variant.

In the period of development when mitophagy is occurring, an increase in the intercellular variation of mtDNA heteroplasmy had been demonstrated in the BALB/OlaHsd mouse carrying heteroplasmy generated by cytoplast transfer (Neupane et al., 2014), and in human embryos carrying pathogenic mtDNA mutations (Treff et al., 2012). I confirmed this pattern of segregation is consistent with that of *tRNAala* mouse embryos using pyrosequencing, providing a model to explore this mechanism in a mouse model carrying a single pathogenic mtDNA mutation. This model likely more faithfully replicates inheritance of human pathogenic mtDNA variants than does the BALB/OlaHsd mouse, owing to its single pathogenic variant and fewer number of variants. Upregulation of mitophagy by overexpression of pBNIP3L had no detectable influence on the segregation of mtDNA in the late morula stage measured using Illumina NGS. This suggests that instead the increase in intercellular variation of heteroplasy, which appeared rapidly over 24 h as the 8-cell embryo developed into a late morula, occurs due to random segregation of mitochondria during cell divisions occurring as the embryo compacts. However, a number of caveats must be considered; sample size was small, it is unclear how long it takes for mtDNA to be degraded within a lysosome and engulfed genomes may still have been sequenced, and the level of mitophagy induced via microinjection of pBNIP3L is likely variable.

A means of inhibiting mitophagy will be required for more definitive characterisation of mitophagy as well as its impact on the segregation of mtDNA heteroplasmy and wider metabolism in the embryo. My attempts to inhibit mitophagy by the addition of pharmacological agents to culture media were unsuccessful. In the case of CsA, this may be due to the specificity of its mechanisms, which likely inhibit *PINK1/PRKN* mitophagy specifically (Osman et al., 2011). However, both CsA and MRT68921, an inhibitor of ULK1 and thus broad autophagy including mitophagy (Petherick et al., 2015), have only been demonstrated to inhibit

mitophagy in limited models, most often in cell lines. Furthermore, they have only been shown to inhibit mitophagy induced by other interventions (Rodriguez-Enriquez et al., 2009, Petherick et al., 2015, Wei et al., 2015, Liu et al., 2020). Therefore, it may be the case that these agents do not inhibit physiological mitophagy. Methods of ablating or inhibiting mitophagy through genome editing technologies would allow further exploration of mitophagy in the embryo, and would also allow confirmation of the role of *BNIP3L* in its regulation.

The increase in intercellular variation of heteroplasmy in blastocyst formation could have implications for the application of PGD to prevent the inheritance of mtDNA diseases. My analysis, through biopsy or disaggregation of 8-cell embryos, shows that the heteroplasmy of an 8-cell biopsy accurately reflects that of the wider 8-cell as well as that of the subsequently-developing whole blastocyst. Meanwhile disaggregation of a blastocysts into single cells or cell clumps suggested that biopsy of the TE has potential to misrepresent the average heteroplasmy of a blastocyst by a small margin.

Compared to analysis of the BALB/OlaHsd mouse model (Dean et al., 2003, Neupane et al., 2014), I report a tighter spread of heteroplasmy in the 8-cell embryo in *tRNAala* mice. This supports some human studies reporting little variation between cells of cleavage embryos carrying pathogenic mtDNA variants(Monnot et al., 2011, Treff et al., 2012, Sallevelt et al., 2013). Some human embryos have been shown to carry a wider spread of heteroplasmy compared to my analysis (Sallevelt et al., 2013, Sallevelt et al., 2017a), suggesting confirmation of the segregation dynamics of more pathogenic mtDNA variants in human embryos will be an important next step. It remains unclear to what extent intercellular variation of such variants increased in the human blastocyst.

Furthermore, whereas blastocysts of the BALB/OlaHsd mouse model showed only a marginal increase in intercellular variation of heteroplasmy in the blastocyst (Neupane et al., 2014), *tRNAala* mice showed significantly increased intercellular variation, more comparable to human blastocysts (Treff et al., 2012). Differences in the segregation of mtDNA between mouse models may be explained by fundamental differences in heteroplasmy within; the BALB/OlaHsd mouse model carries a far greater number of variants but no pathogenic variants. Alternatively, differences in technical approach may have led to discrepancies. Importantly, Neupane *et al* (2004) analysed blastocyst variation only at the level of a single TE biopsy and remaining whole embryo.

Despite this increase in intercellular variation of heteroplasmy, the margin of error of a TE biopsy in predicting ICM heteroplasmy remained modest (maximally 9.33%) and is unlikely to impact clinical decisions in the PGD process. However, it will be important for clinicians to be aware of this when weighing the advantages of disadvantages of biopsies at cleavage and blastocyst stages. Confidence in the ability of a biopsy to predict the eventual heteroplasmy of a child could be improved by analysing the extent to which they reflect the heteroplasmy of epiblast cells which give rise to the fetus.

Studies have suggested that following transfer of a cytoplast or karyoplast and the mitochondria within to a second zygote, the dynamics of mtDNA heteroplasmy segregation through preimplantation development are altered (Meirelles and Smith, 1998, Lee et al., 2012). To better understand this segregation following PNT, which requires a karyoplast transfer, I analysed a scRNAseq dataset drawn from human PNT blastocysts (Hyslop et al., 2016). Compared to pyrosequencing of cell clumps collected from the same blastocysts, measurements of heteroplasmy from scRNAseq were more variable across cells of blastocysts, and across multiple SNPs measured within the same cell. This suggests flaws in heteroplasmy measurements from scRNAseq, supporting previous attempts (Ludwig et al., 2019). However, my analysis of the accuracy of scRNAseq measurements is compromised due to an inability to measure heteroplasmy by both methods in the same cell, as well as background variation across samples of the blastocyst. Nonetheless, this provides the groundwork to improve this approach. My analysis was conducted on poly-A selected RNA libraries, leading to compromised coverage across tRNA genes of mtDNA which lack poly-A tails, and resulting in the inability to accurately analyse large amounts of SNPS which could have expanded heteroplasmy measurements. Utilising total RNAseq may improve analysis, and combined with approaches to target epiblast cells *in vitro* or *in situ*, it may be possible to test whether biopsies accurately reflect the epiblast.

The variation of heteroplasmy across cells as measured by scRNAseq was far wider than that across cells of the *tRNAala* mouse blastocyst measured via pyrosequencing, supporting evidence that mtDNA segregates more sharply after karyoplast transfer (Meirelles and Smith, 1998). This will be an important consideration in verifying the success of the PNT procedure clinically.

The segregation of mtDNA during blastocyst development could have long-ranging implications given that only a small number of epiblast cells give rise to the fetus. If epiblast cells stochastically inherit a lower or higher level of heteroplasmy, this may further modulate the genetic bottleneck of mtDNA in the female germ line. Furthermore, it has been reported that 15% of hESC cell lines generated from mitochondrial replacement blastocysts show a reversion to the karyoplast mtDNA genotype across passages (Hudson et al., 2019). A similar mechanism may underlie this phenomenon, where a small number of epiblast cells carrying a higher level of karoyplast mtDNA may come to dominate colonies across passages.

In the course of sequencing tissues of the *tRNAala* mouse, I discovered 5 unexpected mtDNA variants in the mtDNA of the mouse model. Whilst previous work characterising this mouse model has shown strong correlations between only the pathogenic m.5024C>T variant and metabolic deficiencies (Kauppila et al., 2016), the impact these variants might have on the inheritance of mtDNA is unclear.

I also explored the impact the m.5024C>T had on the health of aged oocytes in *tRNAala* mice. First, using Illumina NGS, I revealed an accumulation of mtDNA variants at low levels of heteroplasmy in aged oocytes of the *tRNAala* mouse. The variants acquired in aged oocytes occurred in protein coding genes and show a high Ka/Ks ratio, suggesting the potential for biochemical defects at sufficiently high levels of heteroplasmy. This supports a recent study which also revealed an accumulation of mtDNA variants in mice at 10 months (Arbeithuber et al., 2020). However, the detected variants of Arbeithuber *et al* (2020) showed different Ti/Tv ratios suggesting, more in keeping with mtDNA polymerase γ errors as a source of variants. These differences were likely due to differences in technical approach differences in processing of NGS data, or strain differences.

Interestingly, aged oocytes carried a similar distribution of m.5024C>T heteroplasmy as young oocytes, suggesting that in combination these mtDNA variants do not present a barrier to survival of oocytes in ageing. Furthermore, the acquisition of mtDNA variants likely has a modest effect on oocyte health. It has been shown that in mice carrying a 4,696 bp mtDNA deletion that across oocytes of aged mice, heteroplasmy of the deletion is reduced, suggesting oocytes carrying higher mutation loads die prematurely (Sato et al., 2007). I likely did not detect a similar mechanism as the m.5024C>T variant produces a relatively weak phenotype. Instead, significant correlations emerge between maternal ear biopsy m.5024C>T

heteroplasmy and the number of oocytes collected from an aged mouse, a measure of ovarian ageing. It must be remembered that this quantification method is highly operator dependant as oocytes can be missed during collection and more stringent quantification would be beneficial, encompassing measuring ovarian reserve and horomone levels as a guide to ovarian ageing. Furthermore, sample size too small for definitive conclusions.

It has been shown that different pathogenic variants segregate differently during inheritance (Brown et al., 2001, Otten et al., 2018). Therefore, analysis of the inheritance of mtDNA variants must be interpreted in the context of specific mtDNA variants. The *tRNAala* mouse mat better reflect the inheritance and segregation of pathogenic mtDNA variants than does the BALB/OlaHsd mouse, owing to having far fewer variants in its mtDNA genome, and a single pathogenic mutation subject to both a bottleneck and purifying selection (Kauppila et al., 2016). However, this pathogenic variant is phenotypically weak, and thus the extent to which conclusions can be extrapolated to inheritance of more deleterious or pathogenic mutations may be limited. In particular, this limited my ability to detect signs of selection mechanisms. It would be informative to continue much of my analysis in the context of a more severely pathogenic mutation, which may show a differing pattern of segregation or present a barrier to survival in oocyte ageing.

In conclusion my thesis presents the first steps in characterising mitophagy in the preimplantation embryo. I have identified *BNIP3/BNIP3L* family genes as likely mediators of this mitophagy. Using overexpression of pBNIP3L to upregulate mitophagy in the morula stage, I showed that mitophagy has no detectable influence on the segregation of mtDNA in preimplantation development, with intercellular variation of heteroplasmy remaining unchanged. The utility of pBNIP3L upregulation in reducing carryover of mutated mtDNA genomes in PNT will be tested. I also report an increase in intercellular variation of heteroplasmy in the blastocyst stage relative to the 8-cell, which may have implications for PGD biopsy. Finally, the m.5024C>T mtDNA variant did not cause premature oocyte death in aged oocytes carrying increased levels of acquired mtDNA variants, suggesting mtDNA mutations have a modest effect on the health of aged oocytes. These key findings advance our understanding of mitophagy in the preimplantation embryo and the ways mtDNA is inherited in early development. However, my analysis relates to only one mtDNA variant, and wider characterisation of mtDNA mutations in these tissues is required.

Appendices

Appendix 1: Gene ontologies analysed. Gene numbers and those not detected in the dataset are indicated.

GO	mitophagy	negative regulation of mitophagy	positive regulation of mitophagy	apoptotic process	execution phase of apoptosis	negative regulation of execution phase of apoptosis	positive regulation of execution phase of apoptosis
No. of genes in GO	25	7	10	2015	94	22	15
No. of genes detected	25	7	10	1628	78	19	14
Genes not detected	N/A	N/A	N/A	n=387	CASP12	CIDEA	FAP
					CASP5	GCG	
					CASP1	MIR146A	
					ERN2		
					CIDEA		
					CASP14		
					GCG		
					FAP		
					XKR7		
					AIFM3		
					FOXL2		
					MIR146A		
					GPER1		
					XKR5		
					CDKN2A		
					DNASE2B		

GO	oxidative phosphorylation	negative regulation of oxidative phosphorylation	positive regulation of oxidative phosphorylation	glycolytic process	pentose-phosphate shunt	UDP-N-acetylglucosamine metabolic process
No. of genes in GO	149	8	11	118	16	16
No. of genes detected	143	6	9	103	15	16
Genes not detected	MYOG	MIR210	MYOG	PKLR	RPEL1	N/A
	MIR210	SNCA	PGK2	MYOG		
	AP000721.1			INS		
	COX6A2			IFNG		
	SNCA			GAPDHS		
	PGK2			PRKAG3		
				PPARGC1A		
				SLC4A4		
				HK3		
				PGK2		
				PGAM2		
				ALDOB		
				SLC2A6		
				PFKFB1		
				PGAM4		

GO	mitochondrial DNA replication	mitochondrial transcription	mitochondrial translation
No. of genes in GO	14	16	137
No. of genes detected	13	16	136
Genes not detected	MIR155	N/A	AC011455.2

Appendix 2: List of List of genes analysed in relation to mitophagy.

AMBRA1, ATG5, ATG9A, BECN1, BNIP3, BNIP3L, CITED2, FUNDC1, GABARAPL1, GABARAPL2, HIF1A, MARCHF5, NBR1, NRAS, OPTN, PGAM5, PINK1, PRKN, SQSTM1, UBB, ULK1, USP30, VPS13D.

Appendix 3: List of List of genes analysed in relation to intrinsic apoptosis.

APAF1, BAD, BAG1, BAK1, BAX, BBC3, BCL2, BCL2A1, BCL2L1, BCL2L11, BCL2L2, BID, BMP4, CASP10, CASP2, CASP3, CASP6, CASP7, CASP8, CASP9, CYCS, DIABLO, HRK, MCL1, PMAIP1, SIRT1, TP53, XIAP.

Appendix 4: List of List of genes analysed in relation to extrinsic apoptosis.

FADD, FASLG, TNF, TNFRSF10B, TNFRSF1A, TNFRSF25, TNFSF10, TRADD.

Appendix 5: List of List of genes analysed in relation to extrinsic apoptosis.

LDHA, LDHB, LDHC, LDHD, PGAM1, SLC16A1, SLC16A3, SLC16A7.

Appendix 6: List of genes analysed in relation to mitochondrial network maintenance.

DNA2, DNM1L, ESRRA, ESRRG, FEN1, FIS1, LIG1, LIG3, MFF, MFN1, MFN2, MGME1, NFE2L2, OPA1, PIF1, POLG, POLG2, POLRMT, PPARGC1B, PPRC1, PRDM16, RAD51, RECQL4, RELA, SIN3A, SIRT1, SSBP1, TEFM, TFAM, TOMM20, TOP1MT, TOP2B, TOP3A, TWNK.

References

Aerbajinai, W., Giattina, M., Lee, Y. T., Raffeld, M. & Miller, J. L. 2003. The proapoptotic factor Nix is coexpressed with Bcl-xL during terminal erythroid differentiation. *Blood,* 102**,** 712.

Akella, N. M., Ciraku, L. & Reginato, M. J. 2019. Fueling the fire: emerging role of the hexosamine biosynthetic pathway in cancer. *BMC Biology,* 17**,** 52.

Allen, G. F. G., Toth, R., James, J. & Ganley, I. G. 2013. Loss of iron triggers PINK1/Parkin-independent mitophagy. *EMBO reports,* 14**,** 1127-1135.

Amanvermez, R. & Tosun, M. 2016. An Update on Ovarian Aging and Ovarian Reserve Tests. *International journal of fertility & sterility,* 9**,** 411-415.

Ameur, A., Stewart, J. B., Freyer, C., Hagström, E., Ingman, M., Larsson, N. G. & Gyllensten, U. 2011. Ultra-deep sequencing of mouse mitochondrial DNA: mutational patterns and their origins. *PLoS Genet,* 7**,** e1002028.

Arbeithuber, B., Hester, J., Cremona, M. A., Stoler, N., Zaidi, A., Higgins, B., Anthony, K., Chiaromonte, F., Diaz, F. J. & Makova, K. D. 2020. Age-related accumulation of de novo mitochondrial mutations in mammalian oocytes and somatic tissues. *PLOS Biology,* 18**,** e3000745.

Avilion, A. A., Nicolis, S. K., Pevny, L. H., Perez, L., Vivian, N. & Lovell-Badge, R. 2003. Multipotent cell lineages in early mouse development depend on SOX2 function. *Genes & development,* 17**,** 126-140.

Bakker, W. J., Harris, I. S. & Mak, T. W. 2007. FOXO3a Is Activated in Response to Hypoxic Stress and Inhibits HIF1-Induced Apoptosis via Regulation of CITED2. *Molecular Cell,* 28**,** 941-953.

Barchiesi, A. & Vascotto, C. 2019. Transcription, Processing, and Decay of Mitochondrial RNA in Health and Disease. *Int J Mol Sci,* 20.

Barritt, J. A., Cohen, J. & Brenner, C. A. 2000. Mitochondrial DNA point mutation in human oocytes is associated with maternal age. *Reprod Biomed Online,* 1**,** 96-100.

Belle, E. M. S., Piganeau, G., Gardner, M. & Eyre-Walker, A. 2005. An investigation of the variation in the transition bias among various animal mitochondrial DNA. *Gene,* 355**,** 58-66.

Benard, G., Bellance, N., Jose, C., Melser, S., Nouette-Gaulain, K. & Rossignol, R. 2010. Multi-site control and regulation of mitochondrial energy production. *Biochimica et Biophysica Acta (BBA) - Bioenergetics,* 1797**,** 698-709.

Bhattacharya, S., Michels, C. L., Leung, M. K., Arany, Z. P., Kung, A. L. & Livingston, D. M. 1999. Functional role of p35srj, a novel p300/CBP binding protein, during transactivation by HIF-1. *Genes & development,* 13**,** 64-75.

Bingol, B., Tea, J. S., Phu, L., Reichelt, M., Bakalarski, C. E., Song, Q., Foreman, O., Kirkpatrick, D. S. & Sheng, M. 2014. The mitochondrial deubiquitinase USP30 opposes parkin-mediated mitophagy. *Nature,* 510**,** 370-375.

Blakeley, P., Fogarty, N. M. E., del Valle, I., Wamaitha, S. E., Hu, T. X., Elder, K., Snell, P., Christie, L., Robson, P. & Niakan, K. K. 2015. Defining the three cell lineages of the human blastocyst by single-cell RNA-seq. *Development,* 142**,** 3151.

Borowski, L. S., Szczesny, R. J., Brzeźniak, L. K. & Stepien, P. P. 2010. RNA turnover in human mitochondria: More questions than answers? *Biochimica et Biophysica Acta (BBA) - Bioenergetics,* 1797**,** 1066-1070.

Boucret, L., Bris, C., Seegers, V., Goudenège, D., Desquiret-Dumas, V., Domin-Bernhard, M., Ferré-L'Hotellier, V., Bouet, P. E., Descamps, P., Reynier, P., Procaccio, V. & May-Panloup, P. 2017. Deep sequencing shows that oocytes are not prone to accumulate mtDNA heteroplasmic mutations during ovarian ageing. *Human Reproduction,* 32**,** 2101-2109.

Boumela, I., Assou, S., Haouzi, D., Déchaud, H., Aït-Ahmed, O. & Hamamah, S. 2014. Developmental regulated expression of anti- and pro-apoptotic BCL-2 family genes during human early embryonic development. *Curr Med Chem,* 21**,** 1361-9.

Brison, D. R. & Schultz, R. M. 1997. Apoptosis during mouse blastocyst formation: evidence for a role for survival factors including transforming growth factor alpha. *Biol Reprod,* 56**,** 1088-96.

Broekemeier, K. M., Dempsey, M. E. & Pfeiffer, D. R. 1989. Cyclosporin A is a potent inhibitor of the inner membrane permeability transition in liver mitochondria. *J Biol Chem,* 264**,** 7826-30.

Brown, D. T., Samuels, D. C., Michael, E. M., Turnbull, D. M. & Chinnery, P. F. 2001. Random Genetic Drift Determines the Level of Mutant mtDNA in Human Primary Oocytes. *American Journal of Human Genetics,* 68**,** 533-536.

Brown, J. J. & Whittingham, D. G. 1991. The roles of pyruvate, lactate and glucose during preimplantation development of embryos from F1 hybrid mice in vitro. *Development,* 112**,** 99-105.

Burr, S. P., Pezet, M. & Chinnery, P. F. 2018. Mitochondrial DNA Heteroplasmy and Purifying Selection in the Mammalian Female Germ Line. *Dev Growth Differ,* 60**,** 21-32.

Cai, K. Q., Capo-Chichi, C. D., Rula, M. E., Yang, D.-H. & Xu, X.-X. 2008. Dynamic GATA6 expression in primitive endoderm formation and maturation in early mouse embryogenesis. *Developmental dynamics : an official publication of the American Association of Anatomists,* 237**,** 2820-2829.

Cairns, G., Thumiah-Mootoo, M., Burelle, Y. & Khacho, M. 2020. Mitophagy: A New Player in Stem Cell Biology. *Biology,* 9**,** 481.

Cao, L., Shitara, H., Horii, T., Nagao, Y., Imai, H., Abe, K., Hara, T., Hayashi, J.-I. & Yonekawa, H. 2007. The mitochondrial bottleneck occurs without reduction of mtDNA content in female mouse germ cells. *Nature Genetics,* 39**,** 386.

Cao, L., Shitara, H., Sugimoto, M., Hayashi, J., Abe, K. & Yonekawa, H. 2009. New evidence confirms that the mitochondrial bottleneck is generated without reduction of mitochondrial DNA content in early primordial germ cells of mice. *PLoS Genet,* 5**,** e1000756.

Chaban, Y., Boekema, E. J. & Dudkina, N. V. 2014. Structures of mitochondrial oxidative phosphorylation supercomplexes and mechanisms for their stabilisation. *Biochimica et Biophysica Acta (BBA) - Bioenergetics,* 1837**,** 418-426.

Chan, C. C. W., Liu, V. W. S., Lau, E. Y. L., Yeung, W. S. B., Ng, E. H. Y. & Ho, P. C. 2005. Mitochondrial DNA content and 4977 bp deletion in unfertilized oocytes. *Molecular Human Reproduction,* 11**,** 843-846.

Chazaud, C., Yamanaka, Y., Pawson, T. & Rossant, J. 2006. Early Lineage Segregation between Epiblast and Primitive Endoderm in Mouse Blastocysts through the Grb2-MAPK Pathway. *Developmental Cell,* 10**,** 615-624.

Chen, G., Han, Z., Feng, D., Chen, Y., Chen, L., Wu, H., Huang, L., Zhou, C., Cai, X., Fu, C., Duan, L., Wang, X., Liu, L., Liu, X., Shen, Y., Zhu, Y. & Chen, Q. 2014. A regulatory signaling loop comprising the PGAM5 phosphatase and CK2 controls receptor-mediated mitophagy. *Molecular cell,* 54**,** 362-377.

Chen, H., Detmer, S. A., Ewald, A. J., Griffin, E. E., Fraser, S. E. & Chan, D. C. 2003. Mitofusins Mfn1 and Mfn2 coordinately regulate mitochondrial fusion and are essential for embryonic development. *J Cell Biol,* 160**,** 189-200.

Chen, Z., Liu, L., Cheng, Q., Li, Y., Wu, H., Zhang, W., Wang, Y., Sehgal, S. A., Siraj, S., Wang, X., Wang, J., Zhu, Y. & Chen, Q. 2017. Mitochondrial E3 ligase MARCH5 regulates FUNDC1 to fine-tune hypoxic mitophagy. *EMBO reports,* 18**,** 495-509.

Chi, F., Sharpley, M. S., Nagaraj, R., Roy, S. S. & Banerjee, U. 2020. Glycolysis-Independent Glucose Metabolism Distinguishes TE from ICM Fate during Mammalian Embryogenesis. *Dev Cell,* 53**,** 9-26.e4.

Chinnery, P. F. & Hudson, G. 2013. Mitochondrial genetics. *Br Med Bull,* 106**,** 135-59.

Chourasia, A. H., Tracy, K., Frankenberger, C., Boland, M. L., Sharifi, M. N., Drake, L. E., Sachleben, J. R., Asara, J. M., Locasale, J. W., Karczmar, G. S. & Macleod, K. F. 2015. Mitophagy defects arising from BNip3 loss promote mammary tumor progression to metastasis. *EMBO reports,* 16**,** 1145-1163.

Cimadomo, D., Capalbo, A., Ubaldi, F. M., Scarica, C., Palagiano, A., Canipari, R. & Rienzi, L. 2016. The Impact of Biopsy on Human Embryo Developmental Potential during Preimplantation Genetic Diagnosis. *BioMed Research International,* 2016**,** 10.

Cimadomo, D., Fabozzi, G., Vaiarelli, A., Ubaldi, N., Ubaldi, F. M. & Rienzi, L. 2018. Impact of Maternal Age on Oocyte and Embryo Competence. *Frontiers in Endocrinology,* 9**,** 327.

Conaghan, J., Hardy, K., Handyside, A. H., Winston, R. M. & Leese, H. J. 1993. Selection criteria for human embryo transfer: a comparison of pyruvate uptake and morphology. *J Assist Reprod Genet,* 10**,** 21-30.

Craven, L., Tuppen, H. A., Greggains, G. D., Harbottle, S. J., Murphy, J. L., Cree, L. M., Murdoch, A. P., Chinnery, P. F., Taylor, R. W., Lightowlers, R. N., Herbert, M. & Turnbull, D. M. 2010. Pronuclear transfer in human embryos to prevent transmission of mitochondrial DNA disease. *Nature,* 465**,** 82.

Cree, L. M., Samuels, D. C., de Sousa Lopes, S. C., Rajasimha, H. K., Wonnapinij, P., Mann, J. R., Dahl, H.-H. M. & Chinnery, P. F. 2008. A reduction of mitochondrial DNA molecules during embryogenesis explains the rapid segregation of genotypes. *Nature Genetics,* 40**,** 249.

de Laat, P., Koene, S., Heuvel, L. P. W. J. V., Rodenburg, R. J. T., Janssen, M. C. H. & Smeitink, J. A. M. 2013. Inheritance of the m.3243A>G mutation. *JIMD reports,* 8**,** 47-50.

De Paepe, C., Aberkane, A., Dewandre, D., Essahib, W., Sermon, K., Geens, M., Verheyen, G., Tournaye, H. & Van de Velde, H. 2019. BMP4 plays a role in apoptosis during human preimplantation development. *Mol Reprod Dev,* 86**,** 53-62.

Dean, N. L., Ao, A., Battersby, B. J., Shoubridge, E. A., Gosden, R. G. & Tan, S. L. 2003. Prospect of preimplantation genetic diagnosis for heritable mitochondrial DNA diseases. *MHR: Basic science of reproductive medicine,* 9**,** 631-638.

Dimmer, K. S., Friedrich, B., Lang, F., Deitmer, J. W. & Bröer, S. 2000. The low-affinity monocarboxylate transporter MCT4 is adapted to the export of lactate in highly glycolytic cells. *The Biochemical journal,* 350 Pt 1**,** 219-227.

Dobin, A., Davis, C. A., Zaleski, C., Schlesinger, F., Drenkow, J., Chaisson, M., Batut, P., Jha, S. & Gingeras, T. R. 2012. STAR: ultrafast universal RNA-seq aligner. *Bioinformatics,* 29**,** 15-21.

Dobson, A. T., Raja, R., Abeyta, M. J., Taylor, T., Shen, S., Haqq, C. & Pera, R. A. 2004. The unique transcriptome through day 3 of human preimplantation development. *Hum Mol Genet,* 13**,** 1461-70.

Edfors, F., Danielsson, F., Hallström, B. M., Käll, L., Lundberg, E., Pontén, F., Forsström, B. & Uhlén, M. 2016. Gene-specific correlation of RNA and protein levels in human cells and tissues. *Molecular systems biology,* 12**,** 883-883.

Elliott, H. R., Samuels, D. C., Eden, J. A., Relton, C. L. & Chinnery, P. F. 2008. Pathogenic Mitochondrial DNA Mutations Are Common in the General Population. *The American Journal of Human Genetics,* 83**,** 254-260.

Epping, M. T., Wang, L., Edel, M. J., Carlée, L., Hernandez, M. & Bernards, R. 2005. The human tumor antigen PRAME is a dominant repressor of retinoic acid receptor signaling. *Cell,* 122**,** 835-47.

Esteban-Martínez, L., Sierra-Filardi, E., McGreal, R. S., Salazar-Roa, M., Mariño, G., Seco, E., Durand, S., Enot, D., Graña, O., Malumbres, M., Cvekl, A., Cuervo, A. M., Kroemer, G. & Boya, P. 2017. Programmed mitophagy is essential for the glycolytic switch during cell differentiation. *The EMBO journal,* 36**,** 1688-1706.

Fan, W., Waymire, K. G., Narula, N., Li, P., Rocher, C., Coskun, P. E., Vannan, M. A., Narula, J., Macgregor, G. R. & Wallace, D. C. 2008. A mouse model of mitochondrial disease reveals germline selection against severe mtDNA mutations. *Science,* 319**,** 958-62.

Farkas, D. L., Wei, M. D., Febbroriello, P., Carson, J. H. & Loew, L. M. 1989. Simultaneous imaging of cell and mitochondrial membrane potentials. *Biophys J,* 56**,** 1053-69.

Floros, V. I., Pyle, A., Dietmann, S., Wei, W., Tang, W. C. W., Irie, N., Payne, B., Capalbo, A., Noli, L., Coxhead, J., Hudson, G., Crosier, M., Strahl, H., Khalaf, Y., Saitou, M., Ilic, D., Surani, M. A. &

Chinnery, P. F. 2018. Segregation of mitochondrial DNA heteroplasmy through a developmental genetic bottleneck in human embryos. *Nat Cell Biol,* 20**,** 144-151.

Flusberg, D. A. & Sorger, P. K. 2015. Surviving apoptosis: life-death signaling in single cells. *Trends in cell biology,* 25**,** 446-458.

Fogarty, N. M. E., McCarthy, A., Snijders, K. E., Powell, B. E., Kubikova, N., Blakeley, P., Lea, R., Elder, K., Wamaitha, S. E., Kim, D., Maciulyte, V., Kleinjung, J., Kim, J. S., Wells, D., Vallier, L., Bertero, A., Turner, J. M. A. & Niakan, K. K. 2017. Genome editing reveals a role for OCT4 in human embryogenesis. *Nature,* 550**,** 67-73.

Freyer, C., Cree, L. M., Mourier, A., Stewart, J. B., Koolmeister, C., Milenkovic, D., Wai, T., Floros, V. I., Hagstrom, E., Chatzidaki, E. E., Wiesner, R. J., Samuels, D. C., Larsson, N. G. & Chinnery, P. F. 2012. Variation in germline mtDNA heteroplasmy is determined prenatally but modified during subsequent transmission. *Nat Genet,* 44**,** 1282-5.

Friedman, J. R. & Nunnari, J. 2014. Mitochondrial form and function. *Nature,* 505**,** 335.

Gardner, D. K. & Harvey, A. J. 2015. Blastocyst metabolism. *Reproduction, Fertility and Development,* 27**,** 638-654.

Gardner, D. K. & Leese, H. J. 1990. Concentrations of nutrients in mouse oviduct fluid and their effects on embryo development and metabolism in vitro. *Reproduction,* 88**,** 361-368.

Gardner, D. K., Wale, P. L., Collins, R. & Lane, M. 2011. Glucose consumption of single post-compaction human embryos is predictive of embryo sex and live birth outcome. *Human Reproduction,* 26**,** 1981-1986.

Ge, T., Yang, J., Zhou, S., Wang, Y., Li, Y. & Tong, X. 2020. The Role of the Pentose Phosphate Pathway in Diabetes and Cancer. *Frontiers in Endocrinology,* 11**,** 365.

Ghosh, S. S., Fahy, E., Bodis-Wollner, I., Sherman, J. & Howell, N. 1996. Longitudinal study of a heteroplasmic 3460 Leber hereditary optic neuropathy family by multiplexed primer-extension analysis and nucleotide sequencing. *American Journal of Human Genetics,* 58**,** 325-334.

Gong, G., Song, M., Csordas, G., Kelly, D. P., Matkovich, S. J. & Dorn, G. W. 2015. Parkin-mediated mitophagy directs perinatal cardiac metabolic maturation in mice. *Science (New York, N.Y.),* 350**,** aad2459.

Gorman, G. S., Chinnery, P. F., DiMauro, S., Hirano, M., Koga, Y., McFarland, R., Suomalainen, A., Thorburn, D. R., Zeviani, M. & Turnbull, D. M. 2016. Mitochondrial diseases. *Nature Reviews Disease Primers,* 2**,** 16080.

Gorman, G. S., Schaefer, A. M., Ng, Y., Gomez, N., Blakely, E. L., Alston, C. L., Feeney, C., Horvath, R., Yu-Wai-Man, P., Chinnery, P. F., Taylor, R. W., Turnbull, D. M. & McFarland, R. 2015. Prevalence of nuclear and mitochondrial DNA mutations related to adult mitochondrial disease. *Ann Neurol,* 77**,** 753-9.

Gott, A. L., Hardy, K., Winston, R. M. L. & Leese, H. J. 1990. Non-invasive measurement of pyruvate and glucose uptake and lactate production by sigle human preimplantation embryos. *Human Reproduction,* 5**,** 104-108.

Greaves, L. C., Barron, M. J., Campbell-Shiel, G., Kirkwood, T. B. & Turnbull, D. M. 2011. Differences in the accumulation of mitochondrial defects with age in mice and humans. *Mech Ageing Dev,* 132**,** 588-91.

Gureev, A. P., Shaforostova, E. A. & Popov, V. N. 2019. Regulation of Mitochondrial Biogenesis as a Way for Active Longevity: Interaction Between the Nrf2 and PGC-1α Signaling Pathways. *Frontiers in Genetics,* 10**,** 435.

Hafner, A., Bulyk, M. L., Jambhekar, A. & Lahav, G. 2019. The multiple mechanisms that regulate p53 activity and cell fate. *Nature Reviews Molecular Cell Biology,* 20**,** 199-210.

Hahn, A. & Zuryn, S. 2019. Mitochondrial Genome (mtDNA) Mutations that Generate Reactive Oxygen Species. *Antioxidants (Basel, Switzerland),* 8**,** 392.

Hamatani, T., Falco, G., Carter, M. G., Akutsu, H., Stagg, C. A., Sharov, A. A., Dudekula, D. B., VanBuren, V. & Ko, M. S. H. 2004. Age-associated alteration of gene expression patterns in mouse oocytes. *Human Molecular Genetics,* 13**,** 2263-2278.

Hammond, E. R., Green, M. P., Shelling, A. N., Berg, M. C., Peek, J. C. & Cree, L. M. 2016. Oocyte mitochondrial deletions and heteroplasmy in a bovine model of ageing and ovarian stimulation. *Molecular Human Reproduction,* 22**,** 261-271.

Haouzi, D., Boumela, I., Chebli, K. & Hamamah, S. 2018. Global, Survival, and Apoptotic Transcriptome during Mouse and Human Early Embryonic Development. *BioMed Research International,* 2018**,** 5895628.

Hardy, K. & Handyside, A. H. 1996. Metabolism and cell allocation during parthenogenetic preimplantation mouse development. *Molecular Reproduction and Development,* 43**,** 313-322.

Hardy, K., Handyside, A. H. & Winston, R. M. 1989. The human blastocyst: cell number, death and allocation during late preimplantation development in vitro. *Development,* 107**,** 597-604.

Hashimoto, M. & Sasaki, H. 2019. Epiblast Formation by TEAD-YAP-Dependent Expression of Pluripotency Factors and Competitive Elimination of Unspecified Cells. *Dev Cell,* 50**,** 139-154.e5.

Haverfield, J., Nakagawa, S., Love, D., Tsichlaki, E., Nomikos, M., Lai, F. A., Swann, K. & FitzHarris, G. 2016. Ca2+ dynamics in oocytes from naturally-aged mice. *Scientific Reports,* 6**,** 19357.

He, X., Sun, C., Wang, F., Shan, A., Guo, T., Gu, W., Cui, B. & Ning, G. 2012. Peri-implantation lethality in mice lacking the PGC-1-related coactivator protein. *Dev Dyn,* 241**,** 975-83.

Heindryckx, B., Neupane, J., Vandewoestyne, M., Christodoulou, C., Jackers, Y., Gerris, J., Van den Abbeel, E., Van Coster, R., Deforce, D. & De Sutter, P. 2014. Mutation-free baby born from a mitochondrial encephalopathy, lactic acidosis and stroke-like syndrome carrier after blastocyst trophectoderm preimplantation genetic diagnosis. *Mitochondrion,* 18**,** 12-17.

Hellebrekers, D. M., Wolfe, R., Hendrickx, A. T., de Coo, I. F., de Die, C. E., Geraedts, J. P., Chinnery, P. F. & Smeets, H. J. 2012. PGD and heteroplasmic mitochondrial DNA point mutations: a systematic review estimating the chance of healthy offspring. *Hum Reprod Update,* 18**,** 341-9.

Heo, J.-M., Ordureau, A., Paulo, J. A., Rinehart, J. & Harper, J. W. 2015. The PINK1-PARKIN Mitochondrial Ubiquitylation Pathway Drives a Program of OPTN/NDP52 Recruitment and TBK1 Activation to Promote Mitophagy. *Molecular cell,* 60**,** 7-20.

Herbert, M., Kalleas, D., Cooney, D., Lamb, M. & Lister, L. 2015. Meiosis and maternal aging: insights from aneuploid oocytes and trisomy births. *Cold Spring Harb Perspect Biol,* 7**,** a017970.

Herbert, M. & Turnbull, D. 2018. Progress in mitochondrial replacement therapies. *Nature Reviews Molecular Cell Biology,* 19**,** 71.

Hou, G. & Sun, Q.-Y. 2020. Maternal ageing causes changes in DNA methylation and gene expression profiles in mouse oocytes. *Zygote,* 28**,** 360-366.

Houghton, F. D., Thompson, J. G., Kennedy, C. J. & Leese, H. J. 1996. Oxygen consumption and energy metabolism of the early mouse embryo. *Mol Reprod Dev,* 44**,** 476-85.

Hudson, G., Takeda, Y. & Herbert, M. 2019. Reversion after replacement of mitochondrial DNA. *Nature,* 574**,** E8-E11.

Hurst, L. D. 2002. The Ka/Ks ratio: diagnosing the form of sequence evolution. *Trends Genet,* 18**,** 486.

Hwang, G. H., Hopkins, J. L. & Jordan, P. W. 2018. Chromatin Spread Preparations for the Analysis of Mouse Oocyte Progression from Prophase to Metaphase II. *Journal of visualized experiments : JoVE***,** 56736.

Hyslop, L. A., Blakeley, P., Craven, L., Richardson, J., Fogarty, N. M., Fragouli, E., Lamb, M., Wamaitha, S. E., Prathalingam, N., Zhang, Q., O'Keefe, H., Takeda, Y., Arizzi, L., Alfarawati, S., Tuppen, H. A., Irving, L., Kalleas, D., Choudhary, M., Wells, D., Murdoch, A. P., Turnbull, D. M., Niakan, K. K. & Herbert, M. 2016. Towards clinical application of pronuclear transfer to prevent mitochondrial DNA disease. *Nature,* 534**,** 383-6.

Ilicic, T., Kim, J. K., Kolodziejczyk, A. A., Bagger, F. O., McCarthy, D. J., Marioni, J. C. & Teichmann, S. A. 2016. Classification of low quality cells from single-cell RNA-seq data. *Genome Biology,* 17**,** 29.

Ishihara, N., Nomura, M., Jofuku, A., Kato, H., Suzuki, S. O., Masuda, K., Otera, H., Nakanishi, Y., Nonaka, I., Goto, Y., Taguchi, N., Morinaga, H., Maeda, M., Takayanagi, R., Yokota, S. & Mihara, K. 2009. Mitochondrial fission factor Drp1 is essential for embryonic development and synapse formation in mice. *Nat Cell Biol,* 11**,** 958-66.

Israel, S., Ernst, M., Psathaki, O. E., Drexler, H. C. A., Casser, E., Suzuki, Y., Makalowski, W., Boiani, M., Fuellen, G. & Taher, L. 2019. An integrated genome-wide multi-omics analysis of gene expression dynamics in the preimplantation mouse embryo. *Scientific Reports,* 9**,** 13356.

Israelsen, W. J. & Vander Heiden, M. G. 2015. Pyruvate kinase: Function, regulation and role in cancer. *Semin Cell Dev Biol,* 43**,** 43-51.

Jansen, S., Pantaleon, M. & Kaye, P. L. 2008. Characterization and Regulation of Monocarboxylate Cotransporters Slc16a7 and Slc16a3 in Preimplantation Mouse Embryos1. *Biology of Reproduction,* 79**,** 84-92.

Javaeed, A. & Ghauri, S. K. 2019. MCT4 has a potential to be used as a prognostic biomarker - a systematic review and meta-analysis. *Oncology reviews,* 13**,** 403-403.

Jónsson, H., Sulem, P., Kehr, B., Kristmundsdottir, S., Zink, F., Hjartarson, E., Hardarson, M. T., Hjorleifsson, K. E., Eggertsson, H. P., Gudjonsson, S. A., Ward, L. D., Arnadottir, G. A., Helgason, E. A., Helgason, H., Gylfason, A., Jonasdottir, A., Jonasdottir, A., Rafnar, T., Frigge, M., Stacey, S. N., Th Magnusson, O., Thorsteinsdottir, U., Masson, G., Kong, A., Halldorsson, B. V., Helgason, A., Gudbjartsson, D. F. & Stefansson, K. 2017. Parental influence on human germline de novo mutations in 1,548 trios from Iceland. *Nature,* 549**,** 519-522.

Jurisicova, A., Antenos, M., Varmuza, S., Tilly, J. L. & Casper, R. F. 2003. Expression of apoptosis-related genes during human preimplantation embryo development: potential roles for the Harakiri gene product and Caspase-3 in blastomere fragmentation. *Mol Hum Reprod,* 9**,** 133-41.

Jurisicova, A., Varmuza, S. & Casper, R. F. 1996. Programmed cell death and human embryo fragmentation. *Mol Hum Reprod,* 2**,** 93-8.

Kageyama, Y., Zhang, Z., Roda, R., Fukaya, M., Wakabayashi, J., Wakabayashi, N., Kensler, T. W., Reddy, P. H., Iijima, M. & Sesaki, H. 2012. Mitochondrial division ensures the survival of postmitotic neurons by suppressing oxidative damage. *J Cell Biol,* 197**,** 535-51.

Kamjoo, M., Brison, D. R. & Kimber, S. J. 2002. Apoptosis in the preimplantation mouse embryo: effect of strain difference and in vitro culture. *Mol Reprod Dev,* 61**,** 67-77.

Kandul, N. P., Zhang, T., Hay, B. A. & Guo, M. 2016. Selective removal of deletion-bearing mitochondrial DNA in heteroplasmic Drosophila. *Nature Communications,* 7**,** 13100.

Kang, E., Wu, J., Gutierrez, N. M., Koski, A., Tippner-Hedges, R., Agaronyan, K., Platero-Luengo, A., Martinez-Redondo, P., Ma, H., Lee, Y., Hayama, T., Van Dyken, C., Wang, X., Luo, S., Ahmed, R., Li, Y., Ji, D., Kayali, R., Cinnioglu, C., Olson, S., Jensen, J., Battaglia, D., Lee, D., Wu, D., Huang, T., Wolf, D. P., Temiakov, D., Belmonte, J. C., Amato, P. & Mitalipov, S. 2016. Mitochondrial replacement in human oocytes carrying pathogenic mitochondrial DNA mutations. *Nature,* 540**,** 270-275.

Kang, M., Piliszek, A., Artus, J. & Hadjantonakis, A.-K. 2013. FGF4 is required for lineage restriction and salt-and-pepper distribution of primitive endoderm factors but not their initial expression in the mouse. *Development,* 140**,** 267-279.

Kauppila, Johanna H. K., Baines, Holly L., Bratic, A., Simard, M.-L., Freyer, C., Mourier, A., Stamp, C., Filograna, R., Larsson, N.-G., Greaves, Laura C. & Stewart, James B. 2016. A Phenotype-Driven Approach to Generate Mouse Models with Pathogenic mtDNA Mutations Causing Mitochondrial Disease. *Cell Reports,* 16**,** 2980-2990.

Kauppila, J. H. K., Bonekamp, N. A., Mourier, A., Isokallio, M. A., Just, A., Kauppila, T. E. S., Stewart, J. B. & Larsson, N. G. 2018. Base-excision repair deficiency alone or combined with increased

oxidative stress does not increase mtDNA point mutations in mice. *Nucleic Acids Res,* 46**,** 6642-6669.

Ke, F. F. S., Vanyai, H. K., Cowan, A. D., Delbridge, A. R. D., Whitehead, L., Grabow, S., Czabotar, P. E., Voss, A. K. & Strasser, A. 2018. Embryogenesis and Adult Life in the Absence of Intrinsic Apoptosis Effectors BAX, BAK, and BOK. *Cell,* 173**,** 1217-1230.e17.

Keefe, D. L., Niven-Fairchild, T., Powell, S. & Buradagunta, S. 1995. Mitochondrial deoxyribonucleic acid deletions in oocytes and reproductive aging in women. *Fertil Steril,* 64**,** 577-83.

Killackey, S. A., Philpott, D. J. & Girardin, S. E. 2020. Mitophagy pathways in health and disease. *Journal of Cell Biology,* 219.

Klein, R., Nagy, O., Tóthová, C. & Chovanová, F. 2020. Clinical and Diagnostic Significance of Lactate Dehydrogenase and Its Isoenzymes in Animals. *Veterinary medicine international,* 2020**,** 5346483-5346483.

Kowalik, M. A., Columbano, A. & Perra, A. 2017. Emerging Role of the Pentose Phosphate Pathway in Hepatocellular Carcinoma. *Frontiers in Oncology,* 7**,** 87.

Koyano, F., Okatsu, K., Kosako, H., Tamura, Y., Go, E., Kimura, M., Kimura, Y., Tsuchiya, H., Yoshihara, H., Hirokawa, T., Endo, T., Fon, E. A., Trempe, J.-F., Saeki, Y., Tanaka, K. & Matsuda, N. 2014. Ubiquitin is phosphorylated by PINK1 to activate parkin. *Nature,* 510**,** 162-166.

Krendl, C., Shaposhnikov, D., Rishko, V., Ori, C., Ziegenhain, C., Sass, S., Simon, L., Müller, N. S., Straub, T., Brooks, K. E., Chavez, S. L., Enard, W., Theis, F. J. & Drukker, M. 2017. GATA2/3-TFAP2A/C transcription factor network couples human pluripotent stem cell differentiation to trophectoderm with repression of pluripotency. *Proceedings of the National Academy of Sciences,* 114**,** E9579-E9588.

Krisher, R. L., Lane, M. & Bavister, B. D. 1999. Developmental competence and metabolism of bovine embryos cultured in semi-defined and defined culture media. *Biol Reprod,* 60**,** 1345-52.

Krisher, R. L. & Prather, R. S. 2012. A role for the Warburg effect in preimplantation embryo development: metabolic modification to support rapid cell proliferation. *Molecular reproduction and development,* 79**,** 311-320.

Kubli, D. A. & Gustafsson, Å. B. 2012. Mitochondria and mitophagy: the yin and yang of cell death control. *Circulation research,* 111**,** 1208-1221.

Lampert, M. A., Orogo, A. M., Najor, R. H., Hammerling, B. C., Leon, L. J., Wang, B. J., Kim, T., Sussman, M. A. & Gustafsson, Å. B. 2019. BNIP3L/NIX and FUNDC1-mediated mitophagy is required for mitochondrial network remodeling during cardiac progenitor cell differentiation. *Autophagy,* 15**,** 1182-1198.

Lane, M. & Gardner, D. K. 1996. Fertilization and early embryology: Selection of viable mouse blastocysts prior to transfer using a metabolic criterion. *Human Reproduction,* 11**,** 1975-1978.

Lane, M. & Gardner, D. K. 1998. Amino acids and vitamins prevent culture-induced metabolic perturbations and associated loss of viability of mouse blastocysts. *Hum Reprod,* 13**,** 991-7.

Lane, M. & Gardner, D. K. 2005. Understanding cellular disruptions during early embryo development that perturb viability and fetal development. *Reprod Fertil Dev,* 17**,** 371-8.

Larsson, N. G. 2010. Somatic mitochondrial DNA mutations in mammalian aging. *Annu Rev Biochem,* 79**,** 683-706.

Larsson, N. G., Tulinius, M. H., Holme, E., Oldfors, A., Andersen, O., Wahlström, J. & Aasly, J. 1992. Segregation and manifestations of the mtDNA tRNA(Lys) A-->G(8344) mutation of myoclonus epilepsy and ragged-red fibers (MERRF) syndrome. *American Journal of Human Genetics,* 51**,** 1201-1212.

Latorre-Pellicer, A., Lechuga-Vieco, A. V., Johnston, I. G., Hämäläinen, R. H., Pellico, J., Justo-Méndez, R., Fernández-Toro, J. M., Clavería, C., Guaras, A., Sierra, R., Llop, J., Torres, M., Criado, L. M., Suomalainen, A., Jones, N. S., Ruíz-Cabello, J. & Enríquez, J. A. 2019. Regulation of Mother-to-Offspring Transmission of mtDNA Heteroplasmy. *Cell Metabolism,* 30**,** 1120-1130.e5.

Lazarou, M., Sliter, D. A., Kane, L. A., Sarraf, S. A., Wang, C., Burman, J. L., Sideris, D. P., Fogel, A. I. & Youle, R. J. 2015. The ubiquitin kinase PINK1 recruits autophagy receptors to induce mitophagy. *Nature,* 524**,** 309-314.

Lee, H.-S., Ma, H., Juanes, Rita C., Tachibana, M., Sparman, M., Woodward, J., Ramsey, C., Xu, J., Kang, E.-J., Amato, P., Mair, G., Steinborn, R. & Mitalipov, S. 2012. Rapid Mitochondrial DNA Segregation in Primate Preimplantation Embryos Precedes Somatic and Germline Bottleneck. *Cell Reports,* 1**,** 506-515.

Lee, J. W., Park, S., Takahashi, Y. & Wang, H.-G. 2010. The Association of AMPK with ULK1 Regulates Autophagy. *PLOS ONE,* 5**,** e15394.

Lee, T. L., Qian, Y., Cao, Q., Liao, J., Lee, A. W. T., Yip, Y. L., Leung, T. Y., Zhao, M. P., Chan, D. Y., Lee, T. C. & Chan, W. Y. 2019. The landscape of aging and maturation signatures of mouse oocyte development. *The FASEB Journal,* 33**,** 474.8-474.8.

Leese, H. J. 2002. Quiet please, do not disturb: a hypothesis of embryo metabolism and viability. *Bioessays,* 24**,** 845-9.

Leese, H. J., Sturmey, R. G., Baumann, C. G. & McEvoy, T. G. 2007. Embryo viability and metabolism: obeying the quiet rules. *Human Reproduction,* 22**,** 3047-3050.

Lima, A., Lubatti, G., Burgstaller, J., Hu, D., Green, A., Gregorio, A. D., Zawadzki, T., Pernaute, B., Mahammadov, E., Montero, S. P., Dore, M., Sanchez, J. M., Bowling, S., Sancho, M., Karimi, M., Carling, D., Jones, N., Srinivas, S., Scialdone, A. & Rodriguez, T. A. 2021. Cell competition acts as a purifying selection to eliminate cells with mitochondrial defects during early mouse development. *bioRxiv***,** 2020.01.15.900613.

Liu, K., Zhan, Z., Gao, W., Feng, J. & Xie, X. 2020. Cyclosporine attenuates Paraquat-induced mitophagy and pulmonary fibrosis. *Immunopharmacol Immunotoxicol,* 42**,** 138-146.

Ludwig, L. S., Lareau, C. A., Ulirsch, J. C., Christian, E., Muus, C., Li, L. H., Pelka, K., Ge, W., Oren, Y., Brack, A., Law, T., Rodman, C., Chen, J. H., Boland, G. M., Hacohen, N., Rozenblatt-Rosen, O., Aryee, M. J., Buenrostro, J. D., Regev, A. & Sankaran, V. G. 2019. Lineage Tracing in Humans Enabled by Mitochondrial Mutations and Single-Cell Genomics. *Cell,* 176**,** 1325-1339.e22.

Lunt, S. Y. & Vander Heiden, M. G. 2011. Aerobic Glycolysis: Meeting the Metabolic Requirements of Cell Proliferation. *Annual Review of Cell and Developmental Biology,* 27**,** 441-464.

Ma, H., Hayama, T., Van Dyken, C., Darby, H., Koski, A., Lee, Y., Gutierrez, N. M., Yamada, S., Li, Y., Andrews, M., Ahmed, R., Liang, D., Gonmanee, T., Kang, E., Nasser, M., Kempton, B., Brigande, J., McGill, T. J., Terzic, A., Amato, P. & Mitalipov, S. 2020a. Deleterious mtDNA mutations are common in mature oocytes. *Biology of Reproduction,* 102**,** 607-619.

Ma, H., Lee, Y., Hayama, T., Van Dyken, C., Marti-Gutierrez, N., Li, Y., Ahmed, R., Koski, A., Kang, E., Darby, H., Gonmanee, T., Park, Y., Wolf, D. P., Jai Kim, C. & Mitalipov, S. 2018. Germline and somatic mtDNA mutations in mouse aging. *PLoS One,* 13**,** e0201304.

Ma, L.-N., Huang, X.-B., Muyayalo, K. P., Mor, G. & Liao, A.-H. 2020b. Lactic Acid: A Novel Signaling Molecule in Early Pregnancy? *Frontiers in Immunology,* 11.

Martinez, F., Rienzi, L., Iacobelli, M., Ubaldi, F., Mendoza, C., Greco, E. & Tesarik, J. 2002. Caspase activity in preimplantation human embryos is not associated with apoptosis. *Human Reproduction,* 17**,** 1584-1590.

Matsuda, N., Sato, S., Shiba, K., Okatsu, K., Saisho, K., Gautier, C. A., Sou, Y.-S., Saiki, S., Kawajiri, S., Sato, F., Kimura, M., Komatsu, M., Hattori, N. & Tanaka, K. 2010. PINK1 stabilized by mitochondrial depolarization recruits Parkin to damaged mitochondria and activates latent Parkin for mitophagy. *The Journal of cell biology,* 189**,** 211-221.

McGrath, J. & Solter, D. 1984. Completion of mouse embryogenesis requires both the maternal and paternal genomes. *Cell,* 37**,** 179-83.

Meirelles, F. V. & Smith, L. C. 1998. Mitochondrial genotype segregation during preimplantation development in mouse heteroplasmic embryos. *Genetics,* 148**,** 877-83.

Melser, S., Chatelain, Etienne H., Lavie, J., Mahfouf, W., Jose, C., Obre, E., Goorden, S., Priault, M., Elgersma, Y., Rezvani, Hamid R., Rossignol, R. & Bénard, G. 2013. Rheb Regulates Mitophagy Induced by Mitochondrial Energetic Status. *Cell Metabolism,* 17**,** 719-730.

Mishmar, D., Ruiz-Pesini, E., Golik, P., Macaulay, V., Clark, A. G., Hosseini, S., Brandon, M., Easley, K., Chen, E., Brown, M. D., Sukernik, R. I., Olckers, A. & Wallace, D. C. 2003. Natural selection shaped regional mtDNA variation in humans. *Proceedings of the National Academy of Sciences,* 100**,** 171.

Mitalipov, S., Amato, P., Parry, S. & Falk, M. J. 2014. Limitations of Preimplantation Genetic Diagnosis for Mitochondrial DNA Diseases. *Cell reports,* 7**,** 935-937.

Mitsui, K., Tokuzawa, Y., Itoh, H., Segawa, K., Murakami, M., Takahashi, K., Maruyama, M., Maeda, M. & Yamanaka, S. 2003. The homeoprotein Nanog is required for maintenance of pluripotency in mouse epiblast and ES cells. *Cell,* 113**,** 631-42.

Monnot, S., Gigarel, N., Samuels, D. C., Burlet, P., Hesters, L., Frydman, N., Frydman, R., Kerbrat, V., Funalot, B., Martinovic, J., Benachi, A., Feingold, J., Munnich, A., Bonnefont, J.-P. & Steffann, J. 2011. Segregation of mtDNA throughout human embryofetal development: m.3243A>G as a model system. *Human Mutation,* 32**,** 116-125.

Montava-Garriga, L. & Ganley, I. G. 2020. Outstanding Questions in Mitophagy: What We Do and Do Not Know. *Journal of Molecular Biology,* 432**,** 206-230.

Montava-Garriga, L., Singh, F., Ball, G. & Ganley, I. G. 2020. Semi-automated quantitation of mitophagy in cells and tissues. *Mechanisms of ageing and development,* 185**,** 111196-111196.

Moore, A. S., Coscia, S. M., Simpson, C. L., Ortega, F. E., Wait, E. C., Heddleston, J. M., Nirschl, J. J., Obara, C. J., Guedes-Dias, P., Boecker, C. A., Chew, T.-L., Theriot, J. A., Lippincott-Schwartz, J. & Holzbaur, E. L. F. 2021. Actin cables and comet tails organize mitochondrial networks in mitosis. *Nature*.

Morris, S. A., Teo, R. T. Y., Li, H., Robson, P., Glover, D. M. & Zernicka-Goetz, M. 2010. Origin and formation of the first two distinct cell types of the inner cell mass in the mouse embryo. *Proceedings of the National Academy of Sciences,* 107**,** 6364-6369.

Morrison, S. J. & Kimble, J. 2006. Asymmetric and symmetric stem-cell divisions in development and cancer. *Nature,* 441**,** 1068-1074.

Müller-Höcker, J., Schäfer, S., Weis, S., Münscher, C. & Strowitzki, T. 1996. Morphological-cytochemical and molecular genetic analyses of mitochondria in isolated human oocytes in the reproductive age. *Mol Hum Reprod,* 2**,** 951-8.

Naik, P. P., Birbrair, A. & Bhutia, S. K. 2019. Mitophagy-driven metabolic switch reprograms stem cell fate. *Cell Mol Life Sci,* 76**,** 27-43.

Narendra, D. P., Jin, S. M., Tanaka, A., Suen, D. F., Gautier, C. A., Shen, J., Cookson, M. R. & Youle, R. J. 2010. PINK1 is selectively stabilized on impaired mitochondria to activate Parkin. *PLoS Biol,* 8**,** e1000298.

Neupane, J., Vandewoestyne, M., Heindryckx, B., Ghimire, S., Lu, Y., Qian, C., Lierman, S., Van Coster, R., Gerris, J., Deroo, T., Deforce, D. & De Sutter, P. 2014. A systematic analysis of the suitability of preimplantation genetic diagnosis for mitochondrial diseases in a heteroplasmic mitochondrial mouse model. *Hum Reprod,* 29**,** 852-9.

Niakan, K. K., Han, J., Pedersen, R. A., Simon, C. & Pera, R. A. R. 2012. Human pre-implantation embryo development. *Development (Cambridge, England),* 139**,** 829-841.

Nichols, J., Zevnik, B., Anastassiadis, K., Niwa, H., Klewe-Nebenius, D., Chambers, I., Schöler, H. & Smith, A. 1998. Formation of pluripotent stem cells in the mammalian embryo depends on the POU transcription factor Oct4. *Cell,* 95**,** 379-91.

Nishimura, T. & Tooze, S. A. 2020. Emerging roles of ATG proteins and membrane lipids in autophagosome formation. *Cell Discovery,* 6**,** 32.

Niu, Y.-J., Nie, Z.-W., Shin, K.-T., Zhou, W. & Cui, X.-S. 2019. PINK1 regulates mitochondrial morphology via promoting mitochondrial fission in porcine preimplantation embryos. *The FASEB Journal,* 33**,** 7882-7895.

Okatsu, K., Oka, T., Iguchi, M., Imamura, K., Kosako, H., Tani, N., Kimura, M., Go, E., Koyano, F., Funayama, M., Shiba-Fukushima, K., Sato, S., Shimizu, H., Fukunaga, Y., Taniguchi, H., Komatsu, M., Hattori, N., Mihara, K., Tanaka, K. & Matsuda, N. 2012. PINK1 autophosphorylation upon membrane potential dissipation is essential for Parkin recruitment to damaged mitochondria. *Nature communications,* 3**,** 1016.

Olivo, P. D., Van de Walle, M. J., Laipis, P. J. & Hauswirth, W. W. 1983. Nucleotide sequence evidence for rapid genotypic shifts in the bovine mitochondrial DNA D-loop. *Nature,* 306**,** 400.

Osman, M. M., Lulic, D., Glover, L., Stahl, C. E., Lau, T., van Loveren, H. & Borlongan, C. V. 2011. Cyclosporine-A as a neuroprotective agent against stroke: its translation from laboratory research to clinical application. *Neuropeptides,* 45**,** 359-68.

Osorio, D. & Cai, J. 2020. Systematic determination of the mitochondrial proportion in human and mice tissues for single-cell RNA sequencing data quality control. *bioRxiv***,** 2020.02.20.958793.

Otten, A. B. C., Sallevelt, S., Carling, P. J., Dreesen, J., Drüsedau, M., Spierts, S., Paulussen, A. D. C., de Die-Smulders, C. E. M., Herbert, M., Chinnery, P. F., Samuels, D. C., Lindsey, P. & Smeets, H. J. M. 2018. Mutation-specific effects in germline transmission of pathogenic mtDNA variants. *Hum Reprod,* 33**,** 1331-1341.

Otten, Auke B. C., Theunissen, Tom E. J., Derhaag, Josien G., Lambrichs, Ellen H., Boesten, Iris B. W., Winandy, M., van Montfoort, Aafke P. A., Tarbashevich, K., Raz, E., Gerards, M., Vanoevelen, Jo M., van den Bosch, Bianca J. C., Muller, M. & Smeets, Hubert J. M. 2016. Differences in Strength and Timing of the mtDNA Bottleneck between Zebrafish Germline and Non-germline Cells. *Cell Reports,* 16**,** 622-630.

Pampfer, S. & Donnay, I. 1999. Apoptosis at the time of embryo implantation in mouse and rat. *Cell Death & Differentiation,* 6**,** 533-545.

Pan, B. & Li, J. 2019. The art of oocyte meiotic arrest regulation. *Reproductive Biology and Endocrinology,* 17**,** 8.

Pasquariello, R., Ermisch, A. F., Silva, E., McCormick, S., Logsdon, D., Barfield, J. P., Schoolcraft, W. B. & Krisher, R. L. 2019. Alterations in oocyte mitochondrial number and function are related to spindle defects and occur with maternal aging in mice and humans†. *Biol Reprod,* 100**,** 971-981.

Patro, R., Duggal, G., Love, M. I., Irizarry, R. A. & Kingsford, C. 2017. Salmon provides fast and bias-aware quantification of transcript expression. *Nat Methods,* 14**,** 417-419.

Pellestor, F., Andréo, B., Arnal, F., Humeau, C. & Demaille, J. 2003. Maternal aging and chromosomal abnormalities: new data drawn from in vitro unfertilized human oocytes. *Human Genetics,* 112**,** 195-203.

Petherick, K. J., Conway, O. J. L., Mpamhanga, C., Osborne, S. A., Kamal, A., Saxty, B. & Ganley, I. G. 2015. Pharmacological inhibition of ULK1 kinase blocks mammalian target of rapamycin (mTOR)-dependent autophagy. *The Journal of biological chemistry,* 290**,** 11376-11383.

Petropoulos, S., Edsgard, D., Reinius, B., Deng, Q., Panula, S. P., Codeluppi, S., Plaza Reyes, A., Linnarsson, S., Sandberg, R. & Lanner, F. 2016. Single-Cell RNA-Seq Reveals Lineage and X Chromosome Dynamics in Human Preimplantation Embryos. *Cell,* 165**,** 1012-26.

Pikó, L., Hougham, A. J. & Bulpitt, K. J. 1988. Studies of sequence heterogeneity of mitochondrial DNA from rat and mouse tissues: evidence for an increased frequency of deletions/additions with aging. *Mech Ageing Dev,* 43**,** 279-93.

Ploner, C., Kofler, R. & Villunger, A. 2008. Noxa: at the tip of the balance between life and death. *Oncogene,* 27 Suppl 1**,** S84-S92.

Pocaterra, A., Romani, P. & Dupont, S. 2020. YAP/TAZ functions and their regulation at a glance. *Journal of Cell Science,* 133**,** jcs230425.

Prados, F. J., Debrock, S., Lemmen, J. G. & Agerholm, I. 2012. The cleavage stage embryo. *Human Reproduction,* 27**,** i50-i71.

Rahbari, R., Wuster, A., Lindsay, S. J., Hardwick, R. J., Alexandrov, L. B., Turki, S. A., Dominiczak, A., Morris, A., Porteous, D., Smith, B., Stratton, M. R. & Hurles, M. E. 2016. Timing, rates and spectra of human germline mutation. *Nat Genet,* 48**,** 126-133.

Rahman, S. & Islam, R. 2011. Mammalian Sirt1: insights on its biological functions. *Cell Communication and Signaling,* 9**,** 11.

Rebolledo-Jaramillo, B., Su, M. S.-W., Stoler, N., McElhoe, J. A., Dickins, B., Blankenberg, D., Korneliussen, T. S., Chiaromonte, F., Nielsen, R., Holland, M. M., Paul, I. M., Nekrutenko, A. & Makova, K. D. 2014. Maternal age effect and severe germ-line bottleneck in the inheritance of human mitochondrial DNA. *Proceedings of the National Academy of Sciences,* 111**,** 15474.

Redel, B. K., Brown, A. N., Spate, L. D., Whitworth, K. M., Green, J. A. & Prather, R. S. 2012. Glycolysis in preimplantation development is partially controlled by the Warburg Effect. *Mol Reprod Dev,* 79**,** 262-71.

Rhinn, M. & Dollé, P. 2012. Retinoic acid signalling during development. *Development,* 139**,** 843-858.

Riedl, S. J. & Shi, Y. 2004. Molecular mechanisms of caspase regulation during apoptosis. *Nature Reviews Molecular Cell Biology,* 5**,** 897-907.

Rinkenberger, J. L., Horning, S., Klocke, B., Roth, K. & Korsmeyer, S. J. 2000. Mcl-1 deficiency results in peri-implantation embryonic lethality. *Genes & development,* 14**,** 23-27.

Ritchie, M. E., Phipson, B., Wu, D., Hu, Y., Law, C. W., Shi, W. & Smyth, G. K. 2015. limma powers differential expression analyses for RNA-sequencing and microarray studies. *Nucleic Acids Research,* 43**,** e47-e47.

Rodger, C. E., T.G., M. & I., G. 2017. Mammalian mitophagy – from in vitro molecules to in vivo models. *The FEBS Journal,* 285**,** 1185-1202.

Rodriguez-Enriquez, S., Kai, Y., Maldonado, E., Currin, R. T. & Lemasters, J. J. 2009. Roles of mitophagy and the mitochondrial permeability transition in remodeling of cultured rat hepatocytes. *Autophagy,* 5**,** 1099-106.

Rogov, V. V., Suzuki, H., Marinković, M., Lang, V., Kato, R., Kawasaki, M., Buljubašić, M., Šprung, M., Rogova, N., Wakatsuki, S., Hamacher-Brady, A., Dötsch, V., Dikic, I., Brady, N. R. & Novak, I. 2017. Phosphorylation of the mitochondrial autophagy receptor Nix enhances its interaction with LC3 proteins. *Scientific reports* [Online], 7.

Rojas, A., Schachterle, W., Xu, S.-M., Martín, F. & Black, B. L. 2010. Direct transcriptional regulation of Gata4 during early endoderm specification is controlled by FoxA2 binding to an intronic enhancer. *Developmental biology,* 346**,** 346-355.

Rossant, J. & Tam, P. P. L. 2009. Blastocyst lineage formation, early embryonic asymmetries and axis patterning in the mouse. *Development,* 136**,** 701.

Russell, R. C., Tian, Y., Yuan, H., Park, H. W., Chang, Y.-Y., Kim, J., Kim, H., Neufeld, T. P., Dillin, A. & Guan, K.-L. 2013. ULK1 induces autophagy by phosphorylating Beclin-1 and activating VPS34 lipid kinase. *Nature Cell Biology,* 15**,** 741.

Safra, M., Sas-Chen, A., Nir, R., Winkler, R., Nachshon, A., Bar-Yaacov, D., Erlacher, M., Rossmanith, W., Stern-Ginossar, N. & Schwartz, S. 2017. The m1A landscape on cytosolic and mitochondrial mRNA at single-base resolution. *Nature,* 551**,** 251-255.

Sallevelt, S. C. E. H., Dreesen, J. C. F. M., Coonen, E., Paulussen, A. D. C., Hellebrekers, D. M. E. I., de Die-Smulders, C. E. M., Smeets, H. J. M. & Lindsey, P. 2017a. Preimplantation genetic diagnosis for mitochondrial DNA mutations: analysis of one blastomere suffices. *Journal of Medical Genetics,* 54**,** 693.

Sallevelt, S. C. E. H., Dreesen, J. C. F. M., Drüsedau, M., Hellebrekers, D. M. E. I., Paulussen, A. D. C., Coonen, E., van Golde, R. J. T., Geraedts, J. P. M., Gianaroli, L., Magli, M. C., Zeviani, M., Smeets, H. J. M. & de Die-Smulders, C. E. M. 2017b. PGD for the m.14487 T>C mitochondrial DNA mutation resulted in the birth of a healthy boy. *Human Reproduction,* 32**,** 698-703.

Sallevelt, S. C. E. H., Dreesen, J. C. F. M., Drüsedau, M., Spierts, S., Coonen, E., van Tienen, F. H. J., van Golde, R. J. T., de Coo, I. F. M., Geraedts, J. P. M., de Die-Smulders, C. E. M. & Smeets, H. J. M. 2013. Preimplantation genetic diagnosis in mitochondrial DNA disorders: challenge and success. *Journal of Medical Genetics,* 50**,** 125.

Samuels, D. C., Li, C., Li, B., Song, Z., Torstenson, E., Boyd Clay, H., Rokas, A., Thornton-Wells, T. A., Moore, J. H., Hughes, T. M., Hoffman, R. D., Haines, J. L., Murdock, D. G., Mortlock, D. P. & Williams, S. M. 2013. Recurrent tissue-specific mtDNA mutations are common in humans. *PLoS genetics,* 9**,** e1003929-e1003929.

Sánchez-Martín, P. & Komatsu, M. 2018. p62/SQSTM1 – steering the cell through health and disease. *Journal of Cell Science,* 131**,** jcs222836.

Sandoval, H., Thiagarajan, P., Dasgupta, S. K., Schumacher, A., Prchal, J. T., Chen, M. & Wang, J. 2008. Essential role for Nix in autophagic maturation of erythroid cells. *Nature,* 454**,** 232.

Santibanez-Koref, M., Griffin, H., Turnbull, D. M., Chinnery, P. F., Herbert, M. & Hudson, G. 2019. Assessing mitochondrial heteroplasmy using next generation sequencing: A note of caution. *Mitochondrion,* 46**,** 302-306.

Santos, T. A., El Shourbagy, S. & St John, J. C. 2006. Mitochondrial content reflects oocyte variability and fertilization outcome. *Fertil Steril,* 85**,** 584-91.

Sato, A., Kono, T., Nakada, K., Ishikawa, K., Inoue, S.-I., Yonekawa, H. & Hayashi, J.-I. 2005. Gene therapy for progeny of mito-mice carrying pathogenic mtDNA by nuclear transplantation. *Proceedings of the National Academy of Sciences of the United States of America,* 102**,** 16765.

Sato, A., Nakada, K., Shitara, H., Kasahara, A., Yonekawa, H. & Hayashi, J.-I. 2007. Deletion-mutant mtDNA increases in somatic tissues but decreases in female germ cells with age. *Genetics,* 177**,** 2031-2037.

Schaaf, M. B. E., Keulers, T. G., Vooijs, M. A. & Rouschop, K. M. A. 2016. LC3/GABARAP family proteins: autophagy-(un)related functions. *The FASEB Journal,* 30**,** 3961-3978.

Schultz, R. M. 1993. Regulation of zygotic gene activation in the mouse. *Bioessays,* 15**,** 531-8.

Schulz, K. N. & Harrison, M. M. 2019. Mechanisms regulating zygotic genome activation. *Nature Reviews Genetics,* 20**,** 221-234.

Schwanhäusser, B., Busse, D., Li, N., Dittmar, G., Schuchhardt, J., Wolf, J., Chen, W. & Selbach, M. 2011. Global quantification of mammalian gene expression control. *Nature,* 473**,** 337-342.

Schweers, R. L., Zhang, J., Randall, M. S., Loyd, M. R., Li, W., Dorsey, F. C., Kundu, M., Opferman, J. T., Cleveland, J. L., Miller, J. L. & Ney, P. A. 2007. NIX is required for programmed mitochondrial clearance during reticulocyte maturation. *Proceedings of the National Academy of Sciences,* 104**,** 19500.

Seo, B. J., Yoon, S. H. & Do, J. T. 2018. Mitochondrial Dynamics in Stem Cells and Differentiation. *International Journal of Molecular Sciences,* 19.

Shibue, T., Takeda, K., Oda, E., Tanaka, H., Murasawa, H., Takaoka, A., Morishita, Y., Akira, S., Taniguchi, T. & Tanaka, N. 2003. Integral role of Noxa in p53-mediated apoptotic response. *Genes Dev,* 17**,** 2233-8.

Shyh-Chang, N. & Ng, H.-H. 2017. The metabolic programming of stem cells. *Genes & development,* 31**,** 336-346.

Singh, R., Letai, A. & Sarosiek, K. 2019. Regulation of apoptosis in health and disease: the balancing act of BCL-2 family proteins. *Nature Reviews Molecular Cell Biology,* 20**,** 175-193.

Smith, D. G. & Sturmey, R. G. 2013. Parallels between embryo and cancer cell metabolism. *Biochem Soc Trans,* 41**,** 664-9.

Smits, A. H., Lindeboom, R. G. H., Perino, M., van Heeringen, S. J., Veenstra, G. J. C. & Vermeulen, M. 2014. Global absolute quantification reveals tight regulation of protein expression in single Xenopus eggs. *Nucleic acids research,* 42**,** 9880-9891.

Sobenin, I. A., Mitrofanov, K. Y., Zhelankin, A. V., Sazonova, M. A., Postnov, A. Y., Revin, V. V., Bobryshev, Y. V. & Orekhov, A. N. 2014. Quantitative assessment of heteroplasmy of

mitochondrial genome: perspectives in diagnostics and methodological pitfalls. *Biomed Res Int,* 2014**,** 292017.

Spikings, E. C., Alderson, J. & John, J. C. S. 2007. Regulated Mitochondrial DNA Replication During Oocyte Maturation Is Essential for Successful Porcine Embryonic Development. *Biology of Reproduction,* 76**,** 327-335.

St John, J. 2014. The control of mtDNA replication during differentiation and development. *Biochim Biophys Acta,* 1840**,** 1345-54.

Steffann, J., Frydman, N., Gigarel, N., Burlet, P., Ray, P. F., Fanchin, R., Feyereisen, E., Kerbrat, V., Tachdjian, G., Bonnefont, J. P., Frydman, R. & Munnich, A. 2006. Analysis of mtDNA variant segregation during early human embryonic development: a tool for successful NARP preimplantation diagnosis. *Journal of Medical Genetics,* 43**,** 244.

Stewart, J. B. & Chinnery, P. F. 2015. The dynamics of mitochondrial DNA heteroplasmy: implications for human health and disease. *Nature Reviews Genetics,* 16**,** 530.

Stewart, J. B., Freyer, C., Elson, J. L. & Larsson, N.-G. 2008a. Purifying selection of mtDNA and its implications for understanding evolution and mitochondrial disease. *Nature Reviews Genetics,* 9**,** 657.

Stewart, J. B., Freyer, C., Elson, J. L., Wredenberg, A., Cansu, Z., Trifunovic, A. & Larsson, N. G. 2008b. Strong purifying selection in transmission of mammalian mitochondrial DNA. *PLoS Biol,* 6**,** e10.

Stirparo, G. G., Boroviak, T., Guo, G., Nichols, J., Smith, A. & Bertone, P. 2018. Integrated analysis of single-cell embryo data yields a unified transcriptome signature for the human preimplantation epiblast. *Development*.

Stokes, P. J., Hawkhead, J. A., Fawthrop, R. K., Picton, H. M., Sharma, V., Leese, H. J. & Houghton, F. D. 2007. Metabolism of human embryos following cryopreservation: Implications for the safety and selection of embryos for transfer in clinical IVF. *Human Reproduction,* 22**,** 829-835.

Strumpf, D., Mao, C.-A., Yamanaka, Y., Ralston, A., Chawengsaksophak, K., Beck, F. & Rossant, J. 2005. Cdx2 is required for correct cell fate specification and differentiation of trophectoderm in the mouse blastocyst. *Development,* 132**,** 2093-2102.

Sturmey, R. G. & Leese, H. J. 2003. Energy metabolism in pig oocytes and early embryos. *Reproduction,* 126**,** 197-204.

Suen, D.-F., Narendra, D. P., Tanaka, A., Manfredi, G. & Youle, R. J. 2010. Parkin overexpression selects against a deleterious mtDNA mutation in heteroplasmic cybrid cells. *Proceedings of the National Academy of Sciences,* 107**,** 11835-11840.

Szpila, M., Walewska, A., Sabat-Pośpiech, D., Strączyńska, P., Ishikawa, T., Milewski, R., Szczepańska, K. & Ajduk, A. 2019. Postovulatory ageing modifies sperm-induced Ca2+ oscillations in mouse oocytes through a conditions-dependent, multi-pathway mechanism. *Scientific Reports,* 9**,** 11859.

Tachibana, M., Sparman, M., Sritanaudomchai, H., Ma, H., Clepper, L., Woodward, J., Li, Y., Ramsey, C., Kolotushkina, O. & Mitalipov, S. 2009. Mitochondrial gene replacement in primate offspring and embryonic stem cells. *Nature,* 461**,** 367-372.

Tang, F., Barbacioru, C., Wang, Y., Nordman, E., Lee, C., Xu, N., Wang, X., Bodeau, J., Tuch, B. B., Siddiqui, A., Lao, K. & Surani, M. A. 2009. mRNA-Seq whole-transcriptome analysis of a single cell. *Nat Methods,* 6**,** 377-82.

Tanhauser, S. M. & Laipis, P. J. 1995. Multiple Deletions Are Detectable in Mitochondrial DNA of Aging Mice (∗). *Journal of Biological Chemistry,* 270**,** 24769-24775.

Taylor, D. M., Ray, P. F., Ao, A., Winston, R. M. & Handyside, A. H. 1997. Paternal transcripts for glucose-6-phosphate dehydrogenase and adenosine deaminase are first detectable in the human preimplantation embryo at the three- to four-cell stage. *Mol Reprod Dev,* 48**,** 442-8.

Taylor, R. W. & Turnbull, D. M. 2005. Mitochondrial DNA mutations in human disease. *Nat Rev Genet,* 6**,** 389-402.

Thompson, J. G., Partridge, R. J., Houghton, F. D., Cox, C. I. & Leese, H. J. 1996. Oxygen uptake and carbohydrate metabolism by in vitro derived bovine embryos. *J Reprod Fertil,* 106**,** 299-306.

Thorburn, D., Wilton, L. & Stock-Myer, S. Healthy baby girl born following pre-implantation Genetic diagnosis for mitochondrial DNA m. 8993t> g Mutation. Molecular Genetics and Metabolism, 2009. ACADEMIC PRESS INC ELSEVIER SCIENCE 525 B ST, STE 1900, SAN DIEGO, CA 92101-4495 USA, 5-6.

Thouas, G. A., Trounson, A. O. & Jones, G. M. 2005. Effect of Female Age on Mouse Oocyte Developmental Competence Following Mitochondrial Injury1. *Biology of Reproduction,* 73**,** 366-373.

Treff, N. R., Campos, J., Tao, X., Levy, B., Ferry, K. M. & Scott, R. T., Jr. 2012. Blastocyst preimplantation genetic diagnosis (PGD) of a mitochondrial DNA disorder. *Fertil Steril,* 98**,** 1236-40.

Trifunovic, A., Wredenberg, A., Falkenberg, M., Spelbrink, J. N., Rovio, A. T., Bruder, C. E., Bohlooly, Y. M., Gidlöf, S., Oldfors, A., Wibom, R., Törnell, J., Jacobs, H. T. & Larsson, N. G. 2004. Premature ageing in mice expressing defective mitochondrial DNA polymerase. *Nature,* 429**,** 417-23.

Trimarchi, J. R., Liu, L., Porterfield, D. M., Smith, P. J. S. & Keefe, D. L. 2000. Oxidative Phosphorylation-Dependent and -Independent Oxygen Consumption by Individual Preimplantation Mouse Embryos1. *Biology of Reproduction,* 62**,** 1866-1874.

Turner, K., Martin, K. L., Woodward, B. J., Lenton, E. A. & Leese, H. J. 1994. Comparison of pyruvate uptake by embryos derived from conception and non-conception natural cycles. *Hum Reprod,* 9**,** 2362-6.

Twig, G., Elorza, A., Molina, A. J. A., Mohamed, H., Wikstrom, J. D., Walzer, G., Stiles, L., Haigh, S. E., Katz, S., Las, G., Alroy, J., Wu, M., Py, B. F., Yuan, J., Deeney, J. T., Corkey, B. E. & Shirihai, O. S. 2008. Fission and selective fusion govern mitochondrial segregation and elimination by autophagy. *The EMBO journal,* 27**,** 433-446.

Twig, G. & Shirihai, O. S. 2011. The interplay between mitochondrial dynamics and mitophagy. *Antioxidants & redox signaling,* 14**,** 1939-1951.

Ubaldi, F. M., Cimadomo, D., Capalbo, A., Vaiarelli, A., Buffo, L., Trabucco, E., Ferrero, S., Albani, E., Rienzi, L. & Levi Setti, P. E. 2017. Preimplantation genetic diagnosis for aneuploidy testing in women older than 44 years: a multicenter experience. *Fertil Steril,* 107**,** 1173-1180.

Upholt, W. B. & Dawid, I. B. 1977. Mapping of mitochondrial DNA of individual sheep and goats: Rapid evolution in the D loop region. *Cell,* 11**,** 571-583.

Valente, E. M., Abou-Sleiman, P. M., Caputo, V., Muqit, M. M. K., Harvey, K., Gispert, S., Ali, Z., Del Turco, D., Bentivoglio, A. R., Healy, D. G., Albanese, A., Nussbaum, R., González-Maldonado, R., Deller, T., Salvi, S., Cortelli, P., Gilks, W. P., Latchman, D. S., Harvey, R. J., Dallapiccola, B., Auburger, G. & Wood, N. W. 2004. Hereditary early-onset Parkinson's disease caused by mutations in PINK1. *Science (New York, N.Y.),* 304**,** 1158-1160.

Van Blerkom, J. 2008. Mitochondria as regulatory forces in oocytes, preimplantation embryos and stem cells. *Reproductive BioMedicine Online,* 16**,** 553-569.

Van der Auwera, G. A., Carneiro, M. O., Hartl, C., Poplin, R., del Angel, G., Levy-Moonshine, A., Jordan, T., Shakir, K., Roazen, D., Thibault, J., Banks, E., Garimella, K. V., Altshuler, D., Gabriel, S. & DePristo, M. A. 2013. From FastQ Data to High-Confidence Variant Calls: The Genome Analysis Toolkit Best Practices Pipeline. *Current Protocols in Bioinformatics,* 43**,** 11.10.1-11.10.33.

van Oven, M. 2015. PhyloTree Build 17: Growing the human mitochondrial DNA tree. *Forensic Science International: Genetics Supplement Series,* 5**,** e392-e394.

Vander Heiden, M. G., Cantley, L. C. & Thompson, C. B. 2009. Understanding the Warburg effect: the metabolic requirements of cell proliferation. *Science (New York, N.Y.),* 324**,** 1029-1033.

Vander Heiden, M. G., Locasale, J. W., Swanson, K. D., Sharfi, H., Heffron, G. J., Amador-Noguez, D., Christofk, H. R., Wagner, G., Rabinowitz, J. D., Asara, J. M. & Cantley, L. C. 2010. Evidence for an alternative glycolytic pathway in rapidly proliferating cells. *Science,* 329**,** 1492-9.

Vanneste, E., Voet, T., Melotte, C., Debrock, S., Sermon, K., Staessen, C., Liebaers, I., Fryns, J.-P., D'Hooghe, T. & Vermeesch, J. R. 2009. What next for preimplantation genetic screening? High mitotic chromosome instability rate provides the biological basis for the low success rate. *Human reproduction (Oxford, England),* 24**,** 2679-2682.

Vermeesch, J. R., Voet, T. & Devriendt, K. 2016. Prenatal and pre-implantation genetic diagnosis. *Nature Reviews Genetics,* 17**,** 643.

Wadelin, F., Fulton, J., McEwan, P. A., Spriggs, K. A., Emsley, J. & Heery, D. M. 2010. Leucine-rich repeat protein PRAME: expression, potential functions and clinical implications for leukaemia. *Molecular Cancer,* 9**,** 226.

Wai, T., Teoli, D. & Shoubridge, E. A. 2008. The mitochondrial DNA genetic bottleneck results from replication of a subpopulation of genomes. *Nature Genetics,* 40**,** 1484.

Wakabayashi, J., Zhang, Z., Wakabayashi, N., Tamura, Y., Fukaya, M., Kensler, T. W., Iijima, M. & Sesaki, H. 2009. The dynamin-related GTPase Drp1 is required for embryonic and brain development in mice. *J Cell Biol,* 186**,** 805-16.

Wallace, D. C. & Chalkia, D. 2013. Mitochondrial DNA genetics and the heteroplasmy conundrum in evolution and disease. *Cold Spring Harbor perspectives in biology,* 5**,** a021220-a021220.

Wanderoy, S., Hees, J. T., Klesse, R., Edlich, F. & Harbauer, A. B. 2021. Kill one or kill the many: interplay between mitophagy and apoptosis. *Biological Chemistry,* 402**,** 73-88.

Wang, L., Ye, X. & Zhao, T. 2019. The physiological roles of autophagy in the mammalian life cycle. *Biological Reviews,* 94**,** 503-516.

Wang, Z., Gerstein, M. & Snyder, M. 2009. RNA-Seq: a revolutionary tool for transcriptomics. *Nature Reviews Genetics,* 10**,** 57-63.

Wear, H. M., McPike, M. J. & Watanabe, K. H. 2016. From primordial germ cells to primordial follicles: a review and visual representation of early ovarian development in mice. *Journal of ovarian research,* 9**,** 36-36.

Wei, X., Qi, Y., Zhang, X., Gu, X., Cai, H., Yang, J. & Zhang, Y. 2015. ROS act as an upstream signal to mediate cadmium-induced mitophagy in mouse brain. *Neurotoxicology,* 46**,** 19-24.

Weil, M., Jacobson, M. D., Coles, H. S., Davies, T. J., Gardner, R. L., Raff, K. D. & Raff, M. C. 1996. Constitutive expression of the machinery for programmed cell death. *J Cell Biol,* 133**,** 1053-9.

Weissensteiner, H., Pacher, D., Kloss-Brandstatter, A., Forer, L., Specht, G., Bandelt, H. J., Kronenberg, F., Salas, A. & Schonherr, S. 2016. HaploGrep 2: mitochondrial haplogroup classification in the era of high-throughput sequencing. *Nucleic Acids Res,* 44**,** W58-63.

Wilding, M., Dale, B., Marino, M., di Matteo, L., Alviggi, C., Pisaturo, M. L., Lombardi, L. & De Placido, G. 2001. Mitochondrial aggregation patterns and activity in human oocytes and preimplantation embryos. *Human Reproduction,* 16**,** 909-917.

Wong, W. S., Solomon, B. D., Bodian, D. L., Kothiyal, P., Eley, G., Huddleston, K. C., Baker, R., Thach, D. C., Iyer, R. K., Vockley, J. G. & Niederhuber, J. E. 2016. New observations on maternal age effect on germline de novo mutations. *Nat Commun,* 7**,** 10486.

Wu, H., Xue, D., Chen, G., Han, Z., Huang, L., Zhu, C., Wang, X., Jin, H., Wang, J., Zhu, Y., Liu, L. & Chen, Q. 2014a. The BCL2L1 and PGAM5 axis defines hypoxia-induced receptor-mediated mitophagy. *Autophagy,* 10**,** 1712-1725.

Wu, W., Tian, W., Hu, Z., Chen, G., Huang, L., Li, W., Zhang, X., Xue, P., Zhou, C., Liu, L., Zhu, Y., Zhang, X., Li, L., Zhang, L., Sui, S., Zhao, B. & Feng, D. 2014b. ULK1 translocates to mitochondria and phosphorylates FUNDC1 to regulate mitophagy. *EMBO reports,* 15**,** 566-575.

Xiang, G., Yang, L., Long, Q., Chen, K., Tang, H., Wu, Y., Liu, Z., Zhou, Y., Qi, J., Zheng, L., Liu, W., Ying, Z., Fan, W., Shi, H., Li, H., Lin, X., Gao, M., Liu, J., Bao, F., Li, L., Duan, L., Li, M. & Liu, X. 2017. BNIP3L-dependent mitophagy accounts for mitochondrial clearance during 3 factors-induced somatic cell reprogramming. *Autophagy,* 13**,** 1543-1555.

Yagi, R., Kohn, M. J., Karavanova, I., Kaneko, K. J., Vullhorst, D., DePamphilis, M. L. & Buonanno, A. 2007. Transcription factor TEAD4 specifies the trophectoderm lineage at the beginning of mammalian development. *Development,* 134**,** 3827.

Yamano, K. & Youle, R. J. 2013. PINK1 is degraded through the N-end rule pathway. *Autophagy,* 9**,** 1758-1769.

Yang, H., Wang, H., Shivalila, C. S., Cheng, A. W., Shi, L. & Jaenisch, R. 2013. One-step generation of mice carrying reporter and conditional alleles by CRISPR/Cas-mediated genome engineering. *Cell,* 154**,** 1370-9.

Yang, L., Lin, X., Tang, H., Fan, Y., Zeng, S., Jia, L., Li, Y., Shi, Y., He, S., Wang, H., Hu, Z., Gong, X., Liang, X., Yang, Y. & Liu, X. 2020. Mitochondrial DNA mutation exacerbates female reproductive aging via impairment of the NADH/NAD+ redox. *Aging Cell,* 19**,** e13206.

Yang, Y., Ouyang, Y., Yang, L., Beal, M. F., McQuibban, A., Vogel, H. & Lu, B. 2008. Pink1 regulates mitochondrial dynamics through interaction with the fission/fusion machinery. *Proceedings of the National Academy of Sciences,* 105**,** 7070.

Zamaraeva, M. V., Sabirov, R. Z., Maeno, E., Ando-Akatsuka, Y., Bessonova, S. V. & Okada, Y. 2005. Cells die with increased cytosolic ATP during apoptosis: a bioluminescence study with intracellular luciferase. *Cell Death & Differentiation,* 12**,** 1390-1397.

Zhang, J.-J., Liu, X., Chen, L., Zhang, S., Zhang, X., Hao, C. & Miao, Y.-L. 2020. Advanced maternal age alters expression of maternal effect genes that are essential for human oocyte quality. *Aging,* 12**,** 3950-3961.

Zhang, J., Liu, H., Luo, S., Lu, Z., Chávez-Badiola, A., Liu, Z., Yang, M., Merhi, Z., Silber, S. J., Munné, S., Konstantinidis, M., Wells, D., Tang, J. J. & Huang, T. 2017. Live birth derived from oocyte spindle transfer to prevent mitochondrial disease. *Reprod Biomed Online,* 34**,** 361-368.

Zhang, P., Samuels, D. C., Lehmann, B., Stricker, T., Pietenpol, J., Shyr, Y. & Guo, Y. 2016a. Mitochondria sequence mapping strategies and practicability of mitochondria variant detection from exome and RNA sequencing data. *Briefings in Bioinformatics,* 17**,** 224-232.

Zhang, R., Nakahira, K., Choi, A. M. K. & Gu, Z. 2019. Heteroplasmy concordance between mitochondrial DNA and RNA. *Scientific Reports,* 9**,** 12942.

Zhang, T., Xue, L., Li, L., Tang, C., Wan, Z., Wang, R., Tan, J., Tan, Y., Han, H., Tian, R., Billiar, T. R., Tao, W. A. & Zhang, Z. 2016b. BNIP3 Protein Suppresses PINK1 Kinase Proteolytic Cleavage to Promote Mitophagy. *The Journal of biological chemistry,* 291**,** 21616-21629.

Zhao, J.-F., Rodger, C. E., Allen, G. F. G., Weidlich, S. & Ganley, I. G. 2020. HIF1α-dependent mitophagy facilitates cardiomyoblast differentiation. *Cell stress,* 4**,** 99-113.

Zhao, N., Zhang, Y., Liu, Q. & Xiang, W. 2015. Mfn2 Affects Embryo Development via Mitochondrial Dysfunction and Apoptosis. *PLOS ONE,* 10**,** e0125680.

Zheng, W., Khrapko, K., Coller, H. A., Thilly, W. G. & Copeland, W. C. 2006. Origins of human mitochondrial point mutations as DNA polymerase gamma-mediated errors. *Mutat Res,* 599**,** 11-20.

Zimmermann, M. & Reichert, A. S. 2017. How to get rid of mitochondria: crosstalk and regulation of multiple mitophagy pathways. *Biol Chem,* 399**,** 29-45.

Zorova, L. D., Popkov, V. A., Plotnikov, E. J., Silachev, D. N., Pevzner, I. B., Jankauskas, S. S., Zorov, S. D., Babenko, V. A. & Zorov, D. B. 2018. Functional Significance of the Mitochondrial Membrane Potential. *Biochemistry (Moscow), Supplement Series A: Membrane and Cell Biology,* 12**,** 20-26.